

The Functional Role of VEGF Secretion During Neuronal Development

Dissertation

zur Erlangung des Doktorgrades
der Naturwissenschaften

vorgelegt beim Fachbereich Biowissenschaften
der Johann Wolfgang Goethe-Universität

in Frankfurt am Main

von

LaShae Kavita Nicholson,
aus Alabama, USA

Frankfurt am Main 2023

(D30)

Vom Fachbereich Biowissenschaften der Johann Wolfgang Goethe - Universität Frankfurt am Main
als Dissertation angenommen.

Dekan: Prof. Dr. Sven Klimpel

Gutachter: Prof. Dr. Amparo Acker-Palmer

Prof. Dr. Jasmin Hefendehl

Datum der Disputation: _____

Zusammenfassung

Die Entwicklung des Gehirns ist ein komplexer und hochorganisierter Prozess, der auf einer koordinierten Interaktion von Neuronen und Gefäßen beruht. Diese Zellsysteme bilden eine neurovaskuläre Verbindung, die den Austausch von Sauerstoff, Ionen und anderen physiologischen Komponenten ermöglicht, die für eine reguläre neuronale und vaskuläre Funktion notwendig sind. Dieser physiologisch aneinander gekoppelte Prozess wird durch analoge, strukturelle und molekulare Signalmechanismen gesteuert, die beiden Zelltypen gemeinsam sind. An der neurovaskulären Schnittstelle ermöglicht der zelluläre Austausch über diese gemeinsamen Signalmechanismen die synchronisierte Expansion und Integration von Neuronen und Gefäßen in komplexe zelluläre Netzwerke. Die hier durchgeführte Studie untersuchte die Rolle von VEGFR2, einem Rezeptor des vaskulären endothelialen Wachstumsfaktors (VEGF), während der postnatalen neuronalen Entwicklung im Hippocampus der Maus. Frühere Studien haben physiologische Rollen von VEGF, einem proangiogenen Morphogen, bei der Entwicklung des Nervensystems untersucht. Es war jedoch bisher nicht bekannt, ob die VEGF-Signalübertragung über neuronale exprimierende Rezeptoren einen direkten Einfluss auf die neuronale Physiologie und Funktion hat.

In dieser Dissertation habe ich die VEGF-induzierte Signalübertragung identifiziert, die die Entwicklung und Integration von CA3-Pyramidenneuronen im frühen postnatalen Hippocampus der Maus koordiniert - eine bisher unbekannte Funktion von VEGFR2. Weiterhin habe ich auf dem mechanistischen Level gezeigt, dass die VEGFR2-basierte Signalübertragung eine Rezeptorendozytose erfordert, was einen durch ephrinB2 vermittelten Prozess darstellt. Ich fand zudem heraus, dass die VEGF-induzierte kooperative Signalübertragung zwischen VEGFR2 und ephrinB2 funktionell für die dendritische Verzweigung und Reifung dendritischer Dornenfortsätze sich entwickelnder CA3-Neuronen während der ersten Wochen nach der Geburt erforderlich ist.

Darüber hinaus haben wir im Rahmen einer Zusammenarbeit mit der Arbeitsgruppe von Carmen Ruiz de Almodovar, ehemals an der Universität Heidelberg, die VEGF-induzierte VEGFR2-Signalübertragung in der axonalen Entwicklung von CA3 untersucht. Das Ziel dieser Kooperation war, gemeinsam ein umfassendes Verständnis des komplexen Zusammenspiels zwischen VEGF- und VEGFR2-Signalen während der frühen postnatalen Entwicklung von CA3-Neuronen zu erreichen. Die Arbeitsgruppe von Ruiz de Almodovar fand dabei heraus, dass die VEGF-VEGFR2-Signalübertragung im Gegensatz zur Entwicklung von dendritischer Verzweigung und der Entwicklung der Dornenfortsätze von CA3-Dendriten, die axonale Entwicklung durch Mechanismen fördert, die von der ephrinB2-Funktion unabhängig sind. Unsere Ergebnisse zur CA3-Dendritenentwicklung (Harde et al., 2019), sowie die ergänzende Arbeit von Ruiz de Almodovars Arbeitsgruppe zur axonalen Entwicklung von CA3 (Luck et al., 2019), wurden mittlerweile beide veröffentlicht. Obwohl die Gesamtheit der Arbeiten von Ruiz de Almodovars Gruppe zu CA3-Axonon hier nicht vollständig diskutiert wird, wird an den entsprechenden Stellen darauf verwiesen, um den biologischen Kontext für unsere Ergebnisse zur dendritischen CA3-Entwicklung darzulegen.

Während der Embryonalentwicklung spielt die VEGFR2-gesteuerte Signalübertragung in neurovaskulären Nischen eine wichtige Rolle für die Neurogenese neuronaler Vorläuferzellen. Eine ähnliche Rolle wird diesem Mechanismus auch im erwachsenen Gehirn zugeschrieben. Die genaue Lokalisierung neuronaler VEGFR2-Expression, sowie deren funktionelle Bedeutung im Nervensystem während der postnatalen Gehirnentwicklung, war jedoch bisher unbekannt. Um diese Rolle näher zu untersuchen, verwendete ich Methoden der Immunhistochemie, dies im Spezifischen um die räumliche Expression von VEGFR2 im Hippocampus der Maus in den ersten Wochen nach der Geburt zu identifizieren. Die Ergebnisse zeigten, dass VEGFR2 überwiegend im Gefäßsystem des Hippocampus exprimiert, was mit früheren Studien übereinstimmt. Ich beobachtete jedoch auch eine lokalisierte VEGFR2-Expression in Pyramidenzellen der Hippocampus-CA3-Region am postnatalen Tag 10 (P10). Diese lokalisierte postnatale Expression von VEGFR2 in CA3-Neuronen zwischen P1 und P10 deutet auf eine mögliche Rolle dieses Rezeptors bei der Entwicklung dieser Neuronen in diesem Entwicklungsstadium hin.

Die ersten zwei Wochen nach der Geburt stellen eine kritische Phase für die Entwicklung neuronaler Schaltkreise im Hippocampus der Maus dar, weil in diesem Zeitraum Neuronen eine umfassende dendritische Verzweigung durchlaufen und sich dendritische Dornenfortsätze innerhalb dieses sich entwickelnden Netzwerks bilden. Um die Rolle von VEGFR2 im postnatalen Nervensystem zu untersuchen, verwendete ich eine Nes-cre VEGFR2^{lox/-} Mauslinie, die keine VEGFR2-Expression im Nervensystem zeigt. Die normale Rezeptorexpression in allen anderen Zelltypen ist in dieser genetischen Variante jedoch aufrechterhalten und ich habe zusätzlich entsprechende Nes-cre-negative Kontrollmäuse generiert. Durch die Kreuzung dieser Tiere mit einer Thy1-GFP-Reporter Mauslinie konnte ich die funktionellen Konsequenzen von VEGFR2 analysieren. Diese Analyse beruhte auf einem morphologischen Vergleich der dendritischen CA3-Verzweigungen, sowie die Dichte der Dornenfortsätze und deren Reifung in P10 bzw. P15 Tieren. Meine Analyse zeigte, dass CA3-Neuronen in Nes-cre VEGFR2^{lox/-} Mäusen im Vergleich zu Kontrollmäusen weniger komplexe dendritische Dornenfortsätze aufwiesen. Es kam zu erheblichen Verkürzungen der Gesamtlänge und der Verzweigungspunkte, insbesondere in Bereichen, die 100–250 µm entfernt von den Zellsomata innerhalb der Schicht des *stratum radiatum* liegen. Darüber hinaus zeigten Nes-cre VEGFR2^{lox/-} Mäuse eine signifikante Reduktion der Dornenfortsatzdichte, begleitet von einem erhöhten Anteil unreifer Dornenfortsätze. Diese Ergebnisse legen nahe, dass VEGFR2 in den ersten Wochen nach der Geburt eine entscheidende Rolle für die normale Entwicklung von CA3-Dendriten und -Dornenfortsätze spielt.

VEGFR2 ist eine Typ-IV-Rezeptor-Tyrosinkinase, die Signale an der Zelloberfläche übertragen und sowohl eine Rezeptorinternalisierung als auch Rezeptortransport gesteuert durch Co-Rezeptoren durchlaufen kann, wodurch wiederum verschiedene intrazelluläre Signalwege aktiviert werden. In früheren Arbeiten haben wir über die Funktion von VEGFR2 in retinalen Endothelspitzenzellen berichtet und gezeigt, dass die Rezeptorinternalisierung für die nachgeschaltete Signalübertragung der Akt notwendig ist, was zur Erweiterung dieser spezialisierten Strukturen beitrug (Sawamiphak

et al., 2010). Es wurde festgestellt, dass VEGF in Netzhautgefäßen die Aktivierung und Internalisierung von VEGFR2 durch einen durch ephrinB2 vermittelten Prozess induziert. In Anbetracht der Tatsache, dass viele Signalmechanismen sowohl in Gefäßen als auch in Neuronen vorkommen, postulierten wir, dass ephrinB2 in VEGFR2-exprimierenden Neuronen co-exprimiert werden könnte, was möglicherweise die VEGFR2-Rezeptorsignalisierung erleichtert. Um die mögliche funktionelle Rolle von ephrinB2 und VEGFR2 bei der postnatalen Entwicklung von Hippocampus-Neuronen zu untersuchen, verglichen wir die räumliche Expression dieser Proteine im Hippocampus der P10-Maus. Es wurde festgestellt, dass ephrinB2 in allen CA-Hippocampusfeldern exprimiert wird, jedoch nicht im Gefäßsystem, während es in CA3-Pyramidenneuronen zu einer co-lokalisierten Expression von ephrinB2 mit VEGFR2 kam.

Die Expression von VEGFR2 und seine Co-Lokalisierung mit ephrinB2 in CA3-Pyramidenneuronen ließen auf eine mögliche funktionelle Rolle dieser beiden Proteine bei der postnatalen Entwicklung dieser Neuronen schließen. Folglich untersuchten wir, ob es eine mechanistisch analoge Signalinteraktion zwischen VEGFR2 und ephrinB2 in Neuronen gibt, ähnlich dem Phänomen, welches wir in den vaskulären Endothelzellen beobachteten. In kultivierten Primärneuronen wurde nach VEGF-Stimulation eine verstärkte Immunpräzipitation sowohl von phosphoryliertem VEGFR2 als auch von ephrinB2 beobachtet, was auf eine Signalwechselwirkung zwischen diesen beiden Proteinen hinweist. Um dies zu bestätigen, wurden Nes-cre ephrinB2^{lox/lox} Mäuse verwendet, und es wurde gezeigt, dass die VEGF-induzierte Phosphorylierung von ephrinB2 und VEGFR2 in neuronalen Zellkulturen dieser Mäuse im Vergleich zu nicht stimulierten Nes-cre-Negativkontrollen verringert war. Darüber hinaus wurde festgestellt, dass die Internalisierung von VEGFR2 durch ephrinB2 in Neuronen vermittelt wird, wobei die Internalisierung von VEGFR2 bei VEGF-Stimulation um das Doppelte zunahm, was in Nes-cre ephrinB2^{lox/lox} Neuronen nicht der Fall war. In neuronaler Zellkultur löst VEGF-Stimulation normalerweise VEGFR2-Internalisierung aus, die wiederum für die nachgeschaltete Aktivierung von Src und Akt erforderlich ist. Wenn Neuronen von Wildtypmäusen in Zellkultur mit Dynasore, einem Inhibitor der Clathrin-vermittelten Endozytose, behandelt wurden, konnten weder VEGFR2 noch die nachgeschalteten Signalpartner Src und Akt phosphoryliert werden. Insgesamt zeigen meine hier dargestellten Ergebnisse, dass VEGF einen interaktiven Signalkomplex zwischen VEGFR2 und ephrinB2 induziert und dass dessen Internalisierung für die Aktivierung nachgeschalteter Signalpartner erforderlich ist. Dieser Prozess der VEGFR2-Endozytose wird zudem durch ephrinB2 an neuronalen Zelloberflächen moduliert.

Weitere Untersuchungen zeigten, dass eine Interaktion von VEGFR2 und ephrinB2 *in vivo* während der CA3-Entwicklung funktionell erforderlich war. Mäuse aus Nes-cre VEGFR2^{lox/+} ephrinB2^{lox/+} Kreuzungen zeigten Defekte in der dendritischen Verzweigung und der Dornenfortsatzreifung, die denen ähnelten, die bereits bei Nes-cre VEGFR2^{lox/-} Mäusen beobachtet wurden. Umgekehrt zeigten einzelne heterozygote Nes-cre VEGFR2^{lox/+} und Nes-cre ephrinB2^{lox/+} Mäuse im Vergleich zu ihren entsprechenden Kontrollen keine Defekte in CA3 Dornenfortsätzen (Daten hier nicht gezeigt). Diese Ergebnisse bestätigen, dass die phänotypischen Defekte, die bei Nes-cre

VEGFR2^{lox/+} ephrinB2^{lox/+} Mäusen beobachtet wurden, auf eine genetische Interaktion zwischen VEGFR2 und ephrinB2 zurückzuführen sind und nicht auf einem reduzierten VEGFR2-Spiegel allein beruhen.

VEGF wird in die extrazelluläre Umgebung abgesondert, wo durch alternative Spleißung Liganden mit unterschiedlichen Bindungsaffinitäten zur extrazellulären Matrix (ECM) entstehen. Die Bioverfügbarkeit und räumliche Verteilung von VEGF innerhalb der ECM moduliert einen Teil der Stimulationssignale, die ein breites Spektrum zellulärer Reaktionen auslösen können. Für die normale Entwicklung des hippocampalen Netzwerks ist eine strikte Regulierung der VEGF-Signalübertragung auf verschiedenen zellulären Ebenen, einschließlich der Quelle der zellulären Freisetzung in das ECM, erforderlich. Die drei wichtigsten VEGF-Spleißvarianten (VEGF₁₂₁, VEGF₁₆₄ und VEGF₁₆₄ bei Mäusen) sind im Hippocampus der P10-Maus global hochreguliert und weisen unterschiedliche Expressionsmuster rund um Astrozyten, Gefäßen und Neuronen auf. Die nächste Phase dieser Studie hatte das Ziel den zellulären Ursprung von VEGF zu identifizieren, der die Verschaltung und Schaltkreisintegration von CA3-Neuronen koordinieren könnte. Unter Verwendung verschiedener Maus-Modelle für die gezielte zellspezifische VEGF-Deletion haben wir die Mauslinien CaMKIIa-cre, GLAST-creERT2 und Cdh5-creERT2 etabliert, die die Cre-Rekombinase-Expression jeweils in Neuronen, Astrozyten und Gefäßen selektiv steuern. Dies ermöglichte eine systematische Analyse der neurovaskulären, neuroglialen und neuroautokrinen Signalübertragung von VEGF während der Entwicklung von CA3-Neuronen. Bei der Kreuzung mit der (ROSA26)EYFP-Reportermauslinie war die induzierte YFP-Expression eine direkte Reaktion auf die räumliche und zeitliche Aktivierung von Cre und zwar nur im entsprechenden Zelltyp. Dieses Modell eröffnet das Potenzial, VEGF-Verfügbarkeit zeitlich und räumlich präzise zu steuern, sowie den Zelltyp zu identifizieren der VEGF-Signale an sich entwickelnde CA3-Neuronen weiterleitet.

Abstract

Brain development is a complex and highly organized process that relies on the coordinated interaction between neurons and vessels. These cell systems form a neurovascular link that involves the exchange of oxygen, ions, and other physiological components necessary for proper neuronal and vascular function. This physiologically coupled process is executed through analogous structural and molecular signaling mechanisms shared by both cell types. At the neurovascular interface, the cellular crosstalk via these shared signaling mechanisms allows for the synchronized expansion and integration of neurons and vessels into complex cellular networks. This study investigated the role of VEGFR2, a receptor for vascular endothelial growth factor (VEGF), during postnatal neuronal development in the mouse hippocampus. Prior studies have revealed physiological roles of VEGF, a pro-angiogenic morphogen, in nervous system development. However, it was unclear if VEGF signaling had a direct effect on neuronal physiology and function through neuronal-expressing receptors. In this investigative work, we identified a previously unknown function of VEGFR2, whereby VEGF-induced signaling coordinates the development and circuitry integration of CA3 pyramidal neurons in the early postnatal mouse hippocampus. Mechanistically, we found that VEGFR2 signaling requires receptor endocytosis, a process mediated by ephrinB2. We also found that VEGF-induced cooperative signaling between VEGFR2 and ephrinB2 is functionally required for the dendritic arborization and spine maturation of developing CA3 neurons during the first few postnatal weeks. Moreover, in a collaborative effort with the research group of Carmen Ruiz de Almodovar, formerly at the University of Heidelberg, we simultaneously studied VEGF-induced VEGFR2 signaling in CA3 axonal development. Together, we aimed to gain a comprehensive understanding of the complex interplay between VEGF and VEGFR2 signaling during the early postnatal development of CA3 neurons. Ruiz de Almodovar's research group found that, unlike the branch and spine development of CA3 dendrites, VEGF-VEGFR2 signaling promotes axonal development through mechanisms that are independent of ephrinB2 function. Our findings on CA3 dendritic development are reported in the published manuscript, Harde et al. (2019), and the complementary work on CA3 axonal development from Ruiz de Almodovar's group is presented in the co-published manuscript, Luck et al. (2019). Although the totality of Ruiz de Almodovar's group's work on CA3 axons is not fully discussed here, it is referenced where noted to provide biological context for our findings on CA3 dendritic development.

VEGFR2 signaling within neurovascular niches is known to play a role in the neurogenesis of neural progenitor cells during embryonic development and within the adult brain. However, the precise localization of neuronal VEGFR2 expression and functional role within the nervous system during postnatal brain development was unknown. To investigate this, we used immunohistochemistry to identify the spatial expression of VEGFR2 within the mouse hippocampus during the first few weeks after birth. Our results showed that VEGFR2 was predominantly expressed within the hippocampal vasculature, consistent with prior studies. However, we also observed localized VEGFR2 expression in pyramidal cell neurons of the hippocampal CA3 region by postnatal day 10 (P10). This spatially restricted postnatal expression of VEGFR2 in CA3 neurons suggested a potential role in the development of these neurons during this developmental stage.

The first two weeks after birth in the mouse hippocampus is a critical period for the development of neuronal circuits, as neurons undergo extensive dendritic arborization and spine formation. To explore the role of VEGFR2 in the postnatal nervous system, we used a Nes-cre VEGFR2^{lox/-} mouse line to target the deletion of VEGFR2 expression within the nervous system while preserving normal receptor expression in all other cell types. We also generated corresponding control mice that were negative for Nes-cre. By breeding these mice with Thy1-GFP reporter mice, we could analyze the functional consequences of VEGFR2 by assessing the morphologies of CA3 dendritic trees and spine density and maturation at P10 and P15, respectively. Our analysis showed that CA3 neurons in Nes-cre VEGFR2^{lox/-} mice had less complex dendritic arbors compared to control mice. There were significant reductions in total length and branch points, particularly in areas located 100-250 μm from the cell soma within the *stratum radiatum* layer. Additionally, Nes-cre VEGFR2^{lox/-} mice exhibited a significant decrease in spine density accompanied by an increased proportion of immature spines. These findings suggest that VEGFR2 plays a crucial role in the proper development of CA3 dendrites and spines during the early postnatal weeks.

VEGFR2 is a type III receptor tyrosine kinase that can transduce signals at the cell surface and undergo receptor internalization and trafficking by co-receptors, thereby activating various intracellular signaling pathways. Previously, we reported on VEGFR2 function in retinal endothelial tip cells and demonstrated that receptor internalization was necessary for downstream signaling of Akt, which contributed to the extension of these specialized structures (Sawamiphak et al., 2010). In retinal vessels, VEGF was found to induce VEGFR2 activation and internalization through a process mediated by ephrinB2. Considering that many signaling mechanisms are common to both vessels and neurons, we postulated that

ephrinB2 could be co-expressed in VEGFR2-expressing neurons, potentially facilitating VEGFR2 receptor signaling. To investigate the potential functional role of ephrinB2 and VEGFR2 in the postnatal development of hippocampal neurons, we compared the spatial expression of these proteins in the P10 mouse hippocampus. ephrinB2 was found to be expressed in all CA hippocampal fields, but not in the vasculature, while there was colocalized expression of ephrinB2 with VEGFR2 in CA3 pyramidal neurons.

The expression of VEGFR2 and its co-localization with ephrinB2 in CA3 pyramidal neurons suggested a potential functional role of these two proteins in the postnatal development of these neurons. Consequently, we investigated if there was a mechanistically analogous signaling interaction between VEGFR2 and ephrinB2 in neurons, similar to what we observed in vascular endothelial cells. An enhanced immunoprecipitation of both phosphorylated VEGFR2 and ephrinB2 was observed in primary cultured neurons following VEGF stimulation, indicating a signaling interaction between these two proteins. To confirm this, Nes-cre ephrinB2^{lox/lox} mice were used, and it was found that the VEGF-induced phosphorylation of both ephrinB2 and VEGFR2 was reduced in cultured neurons from these mice compared to non-stimulated Nes-cre negative controls. Additionally, the internalization of VEGFR2 was found to be mediated by ephrinB2 in neurons, with a two-fold increase in the internalization of VEGFR2 upon VEGF stimulation, which was abolished in Nes-cre ephrinB2^{lox/lox} neurons. In cultured neurons, VEGF stimulation triggers the VEGFR2 internalization, which is required for the downstream activation of Src and Akt. When wild-type culture neurons were treated with Dynasore, an inhibitor of clathrin-mediated endocytosis, VEGFR2 as well as downstream signaling partners Src and Akt failed to be phosphorylated. Collectively our results show that VEGF induces an interactive signaling complex between VEGFR2 and ephrinB2, of which its internalization is required for the activation of downstream signaling partners. This process of VEGFR2 endocytosis is modulated by ephrinB2 at neuronal cell surfaces.

Further investigation showed that an interaction between VEGFR2 and ephrinB2 was functionally required during CA3 development *in vivo*. Compound Nes-cre VEGFR2^{lox/+} ephrinB2^{lox/+} mice displayed defects in dendritic arborization and spine maturation resembling those observed in Nes-cre VEGFR2^{lox/-} mice. Conversely, single heterozygous Nes-cre VEGFR2^{lox/+} and Nes-cre ephrinB2^{lox/+} mice showed no defects in CA3 dendritic arbors when compared to their corresponding control (data not shown). These findings confirm that the phenotypical defects observed in Nes-cre VEGFR2^{lox/+} ephrinB2^{lox/+} mice were due to a genetic interaction between VEGFR2 and ephrinB2, rather than reduced VEGFR2 levels alone. Furthermore, while dendritic development is impaired, CA3 axons of

Nestin-cre VEGFR2^{lox/+} ephrinB2^{lox/+} mice develop normally (Luck et al., 2019). Our findings show that VEGF signaling coordinates the development and circuitry formation of CA3 neurons through a differential trafficking mechanism of VEGFR2 within the axonal and somatodendritic compartments.

VEGF is secreted into the extracellular environment, of which alternative splice produces ligands with different binding affinities to the extracellular matrix (ECM). The bioavailability and spatial distribution of VEGF within the ECM in part modulates the stimulatory signals that can trigger a wide range of cellular responses. Tight regulation of VEGF signaling at various cellular levels, including the source of cellular release into the ECM, is necessary for the proper orchestration of hippocampal development. We found that the three major VEGF splice variants (VEGF₁₂₁, VEGF₁₆₄, and VEGF₁₆₄ in mice) are globally upregulated in the P10 mouse hippocampus, with distinct expression patterns surrounding astrocytes, vessels, and neurons. In the next phase of this study, we aimed to identify the cellular source of VEGF, which could coordinate the wiring and circuitry integration of CA3 neurons. Using a multi-mouse model for targeted cell-specific VEGF deletion, we established CaMKIIa-cre, GLAST-creERT2, and Cdh5-creERT2 mouse lines, which selectively drive Cre-recombinase expression in neurons, astrocytes, and vessels, respectively. This allows for the systematic analysis of neuro-vascular, neuroglial, and neuronal autocrine signaling of VEGF during the development of CA3 neurons. When crossed with (ROSA26)EYFP reporter mouse line, the induced YFP expression was in direct response to the spatial and temporal activation of Cre, only in the appropriate cell type. Accordingly, this opens up the potential to precisely control the timing and location of VEGF availability as an investigative tool for identifying which cell type titrates VEGF signals to developing CA3 neurons.

Table of Contents

1	Abbreviations	1
2	Introduction	6
2.1	The hippocampus.....	6
2.1.1	The architectural arrangement of the hippocampal formation	6
2.2	Development of the Hippocampus: The Collaborative Roles of Neurons, Glia, and Blood Vessels	8
2.2.1	Neurogenesis	8
2.2.2	Gliogenesis	10
2.2.3	Vasculogenesis and angiogenesis	12
2.3	Neuronal development and plasticity	14
2.3.1	Axon specification and dendritogenesis	14
2.3.2	Spine morphogenesis and synaptogenesis.....	17
2.3.3	Synaptic plasticity.....	19
2.4	Molecular links between neuronal and vascular development.....	20
2.4.1	Spatial scales of neurovascular patterning.....	21
2.4.2	Neurovascular guidance molecules and receptors.....	21
2.5	Eph receptors, ligands, and signaling	24
2.5.1	Eph receptors and ephrin ligands	24
2.5.2	Bi-directional signaling	26
2.6	Vascular endothelial growth factor signaling system.....	26
2.6.1	Molecular function and structure of VEGF receptors.....	27
2.6.2	Structure and function of VEGF	29
2.6.3	Spatial and gene expression regulation of VEGF bioavailability	31
2.6.4	VEGF-induced activation of VEGFR2	34
2.6.5	VEGFR2 signaling: Insights from vascular physiology	34
2.6.6	Endocytic trafficking and signaling of VEGFR2.....	37
3	Results	40
3.1	VEGF-induced VEGFR2 signaling in neurons requires ephrinB2	40

3.1.1	VEGFR2 colocalizes with ephrinB2 in CA3 hippocampal neurons <i>in vivo</i> .	40
3.1.2	VEGF induces VEGFR2-ephrinB2 interaction in neurons <i>in vitro</i>	42
3.2	ephrinb2 modulates VEGFR2 function <i>in vivo</i> to promote the morphological development of CA3 pyramidal cells.....	46
3.2.1	Neuronal-specific VEGFR2 deletion impairs the dendritic arborization and spine formation of CA3 neurons.....	47
3.2.2	VEGFR2 and ephrinB2 genetic interaction is functionally required for the dendritic arborization and spine morphogenesis of CA3 hippocampal neurons. . .	50
3.3	VEGF is expressed by multiple cell types in the early postnatal hippocampal.....	53
3.3.1	Multiple VEGF mRNA splice variants were detected in the postnatal mouse hippocampus	53
3.3.2	VEGF mRNA expression colocalizes with vessels, astrocytes, and neurons in mouse hippocampus.....	54
3.3.3	Astrocytes secrete VEGF in response to cellular stimulation <i>in vitro</i>	55
3.4	A mouse model for the targeted ablation of cell type-specific VEGF expression..	58
4	Discussion	63
4.1	VEGF induces VEGFR2-ephrinB2 cooperative signaling in neurons	64
4.2	VEGF signaling promotes the development and circuitry formation of CA3 pyramidal neurons.....	67
4.3	Future directions: A comparative mouse model strategy to identify the cellular source of VEGF guidance cues coordinating the wiring of CA3 neurons.....	73
4.4	Clinical implications	79
4.5	Concluding remarks.....	82
5	Materials & Methods	83
5.1	Materials.....	83
5.1.1	Chemicals & reagents	83
5.1.2	Reagents for tri-color fluorescent <i>in situ</i> (FISH)	86
5.1.3	Commercial kits.....	87
5.1.4	Consumables	87

5.1.5	Equipment	89
5.1.6	Surgical tools	90
5.1.7	Drugs, injectable probes, and stimulants.....	91
5.1.8	Primary Antibodies.....	91
5.1.9	Secondary Antibodies	92
5.1.10	Primer sequences for genotyping	93
5.1.11	Primers & Probes for Quantitative Real-Time PCR.....	94
5.1.12	Riboprobes	95
5.1.13	Mouse lines.....	95
5.1.14	Standard solutions	96
5.1.15	Solutions for genotyping and agarose gel electrophoresis.....	96
5.1.16	Media and supplements for primary cell culture	97
5.1.17	Solutions for VEGF biotinylation assay	100
5.1.18	Solutions for animal perfusion and tissue fixation	100
5.1.19	Solutions for immunohistochemistry and immunocytochemistry.....	101
5.1.20	Solutions and buffers for western blot.....	102
5.1.21	Solutions for fluorescent <i>in situ</i> hybridization (FISH).....	104
5.2	Methods.....	106
5.2.1	Mouse care and husbandry.....	106
5.2.2	Strategy for generating a cell-type specific Rosa26 reporter mice.....	107
5.2.3	Tamoxifen applications of inducible knockout mouse lines.....	107
5.2.4	Breeding for embryonic neuronal cultures	107
5.2.5	Coverslip pre-treatment for primary cell cultures	108
5.2.6	Coating of coverslips and culture dishes	108
5.2.7	Isolation of primary hippocampal neuron cultures.....	108
5.2.8	Isolation of primary Astrocytic cultures.....	109
5.2.9	Plasmid DNA preparations.....	110
5.2.10	Genomic DNA extraction	110
5.2.11	Genotyping PCR.....	110
5.2.12	DNA size discrimination by agarose gel electrophoresis.....	111
5.2.13	RNA extraction from primary tissue and cell samples.....	112
5.2.14	Reverse transcriptase PCR	113
5.2.15	Quantitative Real-Time PCR.....	113
5.2.16	VEGF stimulation assay of primary neuronal cultures	115
5.2.17	KCl stimulation assay of primary astrocytic cultures.....	115

5.2.18	VEGFR2 receptor internalization assay	115
5.2.19	Protein concentration measurements of cell lysates.....	116
5.2.20	Immunoprecipitation and pull-down assays	117
5.2.21	SDS polyacrylamide gel electrophoresis and Immunoblotting	118
5.2.22	Stripping and re-blotting.....	118
5.2.23	Perfusion and fixations	119
5.2.24	Immunocytochemistry	119
5.2.25	Embedding and cutting of vibratome sections.....	119
5.2.26	Immunohistochemistry of free-floating sections.....	120
5.2.27	<i>In situ</i> hybridization probe design	121
5.2.28	Fluorescence <i>In situ</i> hybridization (FISH)	121
5.3	Data analysis	122
5.3.1	bodyweight measurements of endothelial-specific VEGF deletion mice .	122
5.3.2	Image acquisition.....	122
5.3.3	Dendrite branching and Sholl analysis.....	123
5.3.4	Dendritic spine density and morphology analysis	123
5.3.5	Quantification of mRNA levels using qRT-PCR.....	123
5.3.6	Statistical analysis.....	123
6	References	125
7	Appendix.....	152
7.1	Publications	152
7.2	Acknowledgment.....	154
7.3	Curriculum Vitae.....	158

1 Abbreviations

α	anti
∞	Infinity or indefinitely
μ	Micro
$^{\circ}\text{C}$	Degree Celsius
Aldh1l1	Aldehyde Dehydrogenase 1 Family Member L1
Akt	Synonym PKB (protein kinase B)
AMPA(R)	α -amino-3-hydroxy-5-methyl-4-isoxazole propionic acid (Receptor)
APS	Ammonium persulfate
ATP	Adenosine-e5'-triphosphate
B2M	Beta-2-microglobulin
BCA	Bicinchoninic acid assay
BBB	Blood-brain barrier
BDNF	Brain-derived neurotrophic factor
bp	Base pairs
BSA	Bovine serum albumin
CA	<i>Cornu Ammonis</i>
Ca	Calcium
CamKIIa	Ca ²⁺ /calmodulin-dependent kinase II
cAMP	Cyclic adenosine monophosphate
Cdh5	VE-cadherin
cGMP	Cyclic guanosine monophosphate
CNS	Central nervous system
Cre	Cyclization recombinase
DAPI	4',6-Diamidino-2-phenylindole
DCC	Deleted in colorectal cancer
DG	Dentate gyrus
DIV	Days in vitro
DM	Dissection medium
DMEM	Dulbecco's modified Eagle's medium
DMSO	Dimethyl sulfoxide
DNA	Deoxyribonucleic acid
dNTP	Deoxynucleoside triphosphate

1 Abbreviations

DTT	Dithiothreitol
E	Embryonic day
EC	Endothelial cells
ECL	Enhanced chemiluminescence
(E)GFP	(Enhanced) Green fluorescent protein
(E)YFP	(Enhanced) Yellow fluorescent protein
ECM	Extracellular matrix
ECKO	Endothelial conditional knockout
EDTA	Ethylenediamine-tetra acetic acid
EEA1	Early endosome antigen 1
ELISA	Enzyme-linked immunosorbent assay
Eph	Erythropoietin-producing hepatocellular (receptor)
ephrin	Eph receptor-interacting
ERT2	Tamoxifen-inducible estrogen receptor
FBS	Fetal bovine serum
Fc	Constant Fragment (Fc-receptor fragment)
FISH	Fluorescence in situ hybridization
Flk-1	Fetal liver kinase 1 (synonym VEGFR2)
Flt-1	Fms-like tyrosine kinase 1 (synonym VEGFR1)
g	Gram
GABA	Gamma-aminobutyric acid
GFAP	Glial fibrillary acidic protein
GLAST	Glutamate aspartate transporter (SLC1A3)
GluR	Glutamate receptor subunit
GLUT-1	Glutamine
GS	Glutamine synthetase
GTP	Guanosine triphosphate
h	hour
HBSS	Hank's balanced salt solution
HC	Hippocampus
HEPES	2-[4-(2-hydroxyethyl)piperazin-1-yl]ethane-1-sulfonic acid
HIF-1a	Hypoxia-inducible transcription factor 1a
HRE	Hypoxia-response element
HRP	Horseradish peroxidase
IB4	Griffonia Simplicifolia isolectin B4

ICC	Immunocytochemistry
IgG	Immunoglobulin G
IHC	Immunohistochemistry
INVP	Interneural vascular plexus
i.p.	Intraperitoneal
IP	Immunoprecipitation
K	Potassium
Kb	Kilo base
Kg	Kilogram
kDa	Kilo Dalton
KDR	Kinase insert-domain containing receptor (synonym VEGFR2)
KO	Knockout
L	Liter
lox, <i>loxP</i>	LoxP sequence
LTD	Long-term depression
LTP	Long-term potentiation
M	Molar
m	meter
min	minutes
mm	millimeter
ms	millisecond
MAPK	Mitogen-activated protein kinase (synonym ERK)
Mg	Magnesium
Min	Minutes
MLEC	Mouse lung endothelial cells
MPI	Max-Planck Institute
mOSm	milliosmole
mRNA	Messenger ribonucleic acid
N	normal
n	nano
n.s.	Not significant
Na	Sodium
NaCL	Sodium chloride
NB	Neurobasal
NeuN	Neuronal nuclei (Antibody)

1 Abbreviations

NMDA(R)	N-methyl-D-aspartate (receptor)
OD	Optical density
p	Phospho, phosphorylated
P	Postnatal day
PBS	Phosphate Buffer Saline
PCR	Polymerase chain reaction
PDGF(R)	Platelet-derived growth factor (receptor)
PDL	Poly-D-lysine
PDx	Podocalyxin
PFA	Paraformaldehyde
pH	Potential hydrogen
PI3K	Phosphatidylinositol 3 kinase
PKC	Protein Kinase C
PLC- γ	Phospholipase C- γ
PNVP	Perineural vascular plexus
qPCR	Quantitative Realtime-PCR
q.s.	quantum sufficit (Required quantity)
Rab	Ras-associated binding
ROI	Region of interest
Robo	Roundabout guidance receptor
Rosa26	ROSA β geo26
RT	Room temperature
RTK	Receptor tyrosine kinase
S100 β	Calcium binding protein β
SC	Schaffer-collateral
SDS	Sodium dodecyl sulfate
Sec	Seconds
SEM	Standard error of the mean
Sema	Semaphorin
SFK	Src family kinase
SFM	Serum free media
SG	<i>Stratum granulare</i>
S.L-M	<i>Stratum lacunosum moleculare</i>
SL	<i>Stratum lucidum</i>
SO	<i>Stratum oriens</i>

SP	<i>Stratum pyramidales</i>
SR	<i>Stratum radiatum</i>
Src	Sarcoma (Schmidt-Ruppin A-2) viral oncogene homolog
TAE	Tris-acetate-EDTA
Taq	Thermus aquaticus
TBS	Tris-buffered saline
TBST	Tris-buffered saline + Tween20
TEMED	Tetramethyl ethylenediamine
Tg	Transgene
Thy1	Thermocyte differentiation antigen 1
Tuji1	Neuron-specific class III beta-tubulin
Tyr	Tyrosine residue
Unc5	Uncoordinated-5
uPA	Urokinase-type plasminogen activator
v/v	Volume per volume
VE	Vascular endothelial
VEGF	Vascular endothelial growth factor
VEGFR	Vascular endothelial growth factor receptor 2
w/v	weight per volume
WB	Western blot
Wnt	Wingless/Integrated (Refers to Drosophila wing development gene)
WT	Wildtype

2 Introduction

2.1 The hippocampus

2.1.1 The architectural arrangement of the hippocampal formation

In the rodent brain, the hippocampus is positioned along the septal-temporal axis directly beneath each cortical hemisphere, beginning at the dorsal parietal lobe and ending in the medial temporal lobe. The architectural structure of the hippocampus is defined by the spatial arrangement and circuitry connections of its excitatory neurons, depicted in Figure 2.1. There are several distinct regions within the hippocampal formation: the dentate gyrus (DG) and *cornu Ammonis* (CA, or hippocampus proper), subiculum (SB), and entorhinal cortex (EC).

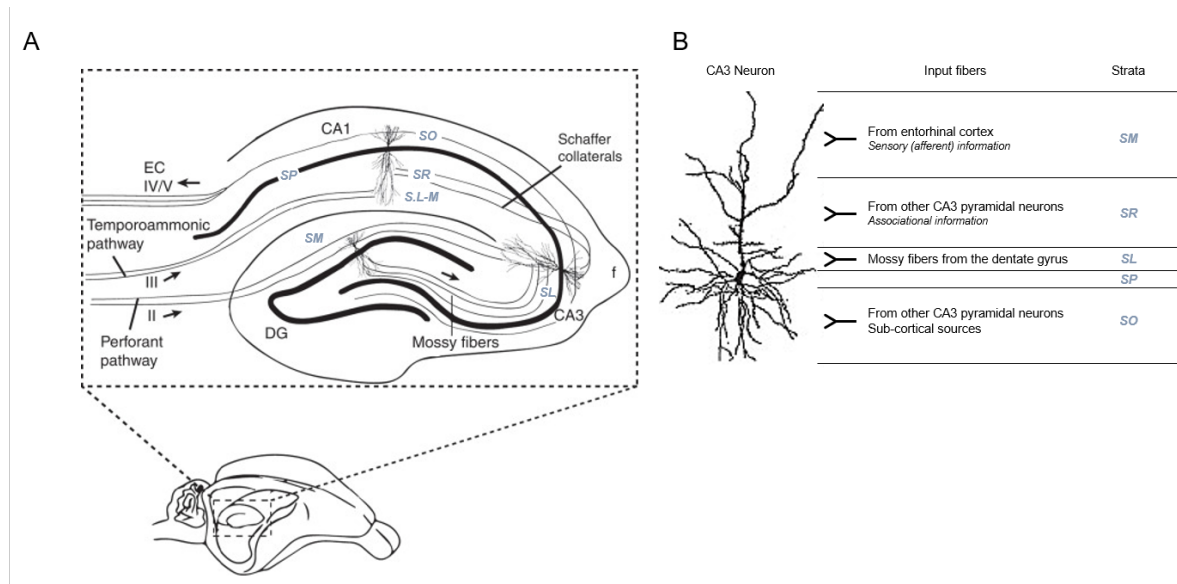


Figure 2.1 Cellular organization and circuitry of the hippocampal formation. **A)** Schematic diagram of a transverse slice through the hippocampus showing the input of the entorhinal cortex (EC), to the DG fields, CA3, and CA1. Each of the primary fields can be further subdivided into strata. The apical dendrites of DG granule cells extend into *stratum moleculare* (SM). Pyramidal cell somas are positioned in the *stratum pyramidales* (SP). The apical dendrites of CA3 and CA1 pyramidal cells extend into *stratum lacunosum-moleculare* (S.L-M), *stratum radiatum* (SR), and *stratum lucidum* (SL; CA3 only), whereas the basal dendrites extend into *stratum oriens* (SO). The fornix (f) is a bundle of fibers that carry information from the hippocampus to the hypothalamus. **B)** Laminar specificity of information flow in the hippocampus is organized along the main axis of pyramidal cells. For simplicity, only a single CA3 pyramidal cell is shown. Adapted from (Vago et al., 2014).

The cytoarchitecture of each hippocampal region is due to the organized stratification of cell bodies and the cellular connections of densely packed neurons (Figure 2.1A). The hooked-shaped blade, or *stratum granulare* (SG) of the DG harbors the somata of granule cell neurons whose dendrites are in the *stratum moleculare* (SM) (Vago et al., 2014). Mossy fibers, the axons of the DG granule cell, exit the SG via the hilus (H). The hippocampus

proper is further divided into the subfields of CA3, CA2, and CA1 excitatory pyramidal cell neurons, oriented proximally to distally from the DG (Grove & Tole, 1999). Pyramidal cells of the hippocampus have “pyramid-shaped” somata positioned in the *stratum pyramidales* (SP) with their apical dendrites making up the *stratum oriens* (SO) and basal dendrites spanning the *stratum lucidum* (SL), *stratum radiatum* (SR), and the deeper *stratum lacunosum moleculare* (S.L-M) layer (Figure 2.1B). The stratified organization of hippocampal neurons also extends to their axonal fibers, with axons forming circuitry connections originating from distinct somatic locations and projecting to similar dendritic termination points (Ishizuka et al., 1990). The axonal projections themselves are thin and myelinated, forming *en passant* synaptic connections (Ishizuka et al., 1990).

The main neuronal circuitry formation of the hippocampus is the “trisynaptic circuit” (Figure 2.1A, (Vago et al., 2014). Axonal fibers of the EC extend their projections through the perforant pathway, innervating the dendrites of the DG granule cells within the SM (Vago et al., 2014). The mossy fibers of the DG project to CA3 neurons, forming synapses within the SL region of CA3 basal dendrites (Li et al., 1994). CA3 neurons send axonal projections, also known as Schaffer collaterals, which originate from the SO and terminate within the SR of proximal CA1 neurons (Szirmai et al., 2012). The SL region of distal CA1 dendrites is also directly innervated by the EC axonal fibers along the perforant pathway. In turn, CA1 neurons send projections back to the EC, which completes the tri-synaptic circuit (Vago et al., 2014). The functional role of the tri-synaptic circuit is the consolidation of newly learned tasks into short- and long-term memory (Vago et al., 2014).

CA3 neurons also form a highly interconnected neuronal network, of which their axons branch into associational and commissural fibers projections (Figure 2.1B) (Ishizuka et al., 1990). The associational fiber track of CA3 neurons form synaptic connections within the SO and SR of neighboring ipsilateral CA3 neurons (Ishizuka et al., 1990). Conversely, CA3 commissural fibers form synaptic connections within the SO and SR region of CA3 neurons of the contralateral hippocampus (Ishizuka et al., 1990; Vago et al., 2014). Thus, associational fibers coordinate the intra-hippocampal network function of adjacent neuronal cells while commissural fibers coordinate inter-hippocampal network activity between brain hemispheres (Vago et al., 2014). Dendrites of the hippocampal neurons are covered with thousands of spines. Individual spine morphologies can range from filopodia-like or thin spines to stubby and mushroom-shaped spines, depending on the strength of the synaptic connection (Ishizuka et al., 1990). Unique to CA3 pyramidal neurons, are the complex dendritic spines called ‘thorny excrescences’, also known as branched or thorny spines, resulting from synaptic connections with mossy fibers of the DG (Sorra & Harris, 2000).

These 'thorny excrescences' are individual multi-branching spines originating from a single dendritic branch point (Sorra & Harris, 2000). Section 2.3.2 provides a more detailed description of spine morphogenesis and the classification of spine morphologies.

2.2 Development of the Hippocampus: The Collaborative Roles of Neurons, Glia, and Blood Vessels

2.2.1 Neurogenesis

The brain is a highly complex organ that undergoes defined, coordinated phases of development, resulting in its highly organized structure and function (Walchli, Wacker, et al., 2015). These developmental processes occur at the level of individual cells as well as at the gross anatomical level of tissues. The development of the mouse hippocampal formation begins at embryonic day 10 (E10) when the medial cortex invaginates to form the cortical hem and choroid plexus (Figure 2.2) (Grove & Tole, 1999; Supèr et al., 1998). These structures act as signaling centers that initiate the formation of the preplate, a transient layer of cells that lies below the developing cortical plate (Grove & Tole, 1999; Supèr et al., 1998). The neuroepithelium is adjacent to the preplate and gives rise to radial glia cells, which provide a scaffold for the migration of neurons to their final positions in the hippocampus (Hatami et al., 2018; Vasistha & Khodosevich, 2021). Between E12-E14, the dense cell layer of the preplate expands to form the subplate, which lies between the cortical plate and the intermediate zone, a layer of proliferating cells (Grove & Tole, 1999; Supèr et al., 1998). During this stage, the specification of the hippocampal CA fields begins with neurogenesis at the neuroepithelium (Figure 2.2B) (Paridaen & Huttner, 2014). Neuroblasts in the neuroepithelium migrate along radial glial cells into the intermediate zone, of which their cell bodies will form the SP (Figure 2.2A) (Götz et al., 2002; Supèr et al., 1998). Upon arrival at their appropriate position within the hippocampus, neuroblasts begin the development of their dendritic and axonal processes (Götz et al., 2002; Supèr et al., 1998).

CA3 neurons are generated around E14.5 and CA1 neurons one day later at E15.5 (Figure 2.2B) (Grove & Tole, 1999). The genesis of the dentate gyrus granule cell starts shortly before birth and peaks in the first postnatal week (Hatami et al., 2018). By E16.5, CA neurons become innervated by perforant pathway axonal projections from the EC (Grove & Tole, 1999). Directly after birth, CA3 neurons begin to receive mossy fiber input from the DG as well as project their own CA3-CA1 Schaffer collaterals and CA3-CA3 associational

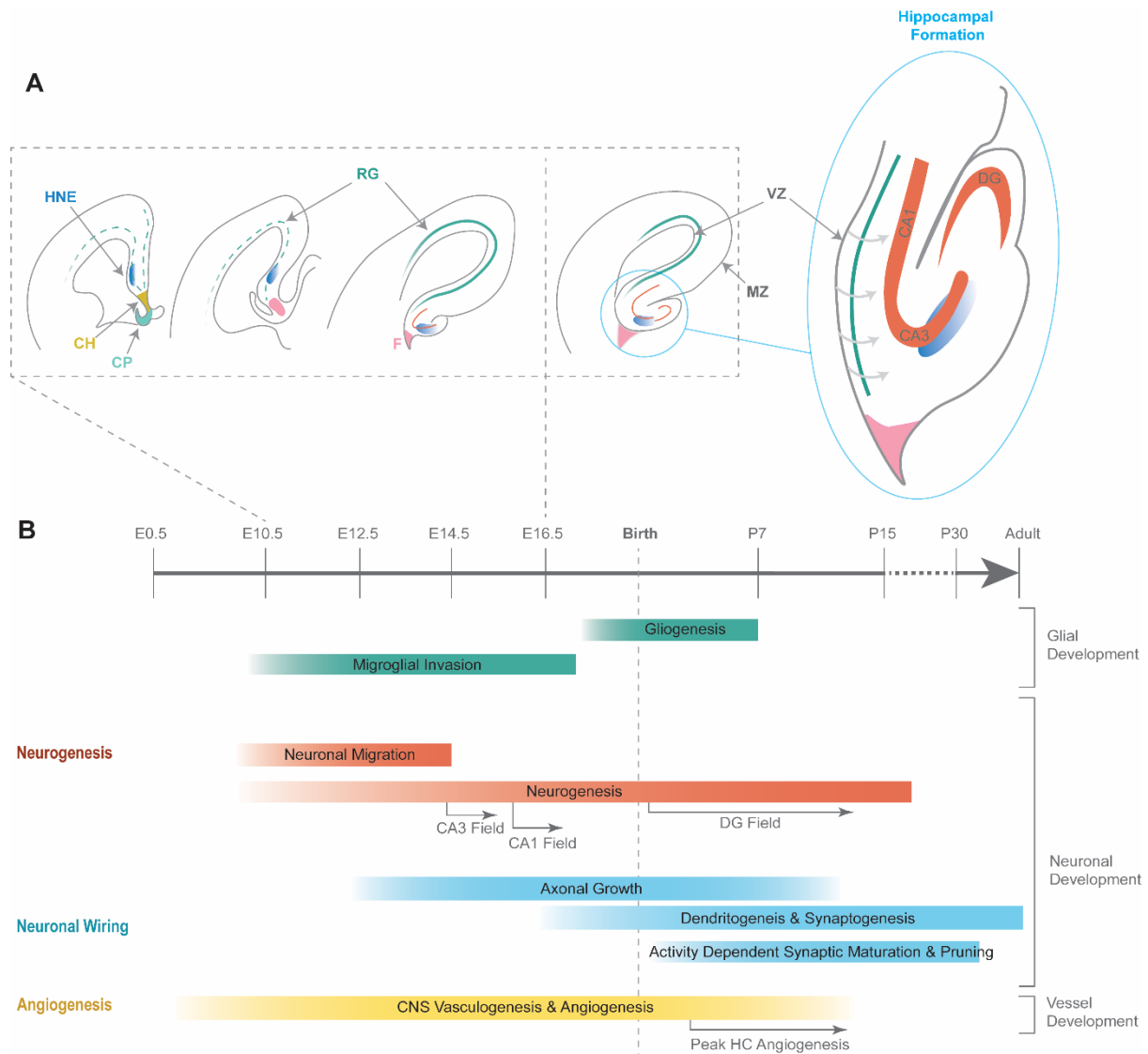


Figure 2.2 Developmental stages of the mouse hippocampus. **A)** Schematic diagram showing the development of the mouse hippocampus from E10 to the postnatal stage. Hippocampal development begins with field patterning followed by the invagination of the medial cortex to form the cortical hem (CH) and choroid plexus (CP). Formation of the hippocampal preplate ends by E14, becoming subdivided into the dentate gyrus (DG) and CA (orange), and fimbria (pink) regions of the hippocampus. During this time, the development of neuroblasts begins within the neuroepithelium, with cell migration (grey arrows) and differentiation occurring along glia scaffolds formed by radial glial (RG). At E14 neurogenesis of CA3 neurons (blue) begins within the hippocampus neuroepithelium (HNE) subzone of the neuroepithelium. F, Fimbria; VZ; Ventricular zone; MZ, Marginal zone. **B)** Developmental milestones of the hippocampus and major cell types. Adapted from (Hatami et al., 2018; Mody et al., 2001; Thion & Garel, 2017; Vasistha & Khodosevich, 2021).

/commissural fibers (Szirmai et al., 2012). Synapse formation coincides with the later stages of dendritic development, with the maturation of neuronal dendrites resulting from an activity-dependent increase of innervating synaptic connections and transmission (Echegoyen et al., 2007). This is a dynamic process in which the integration and remodeling of neuronal networks occur through the first weeks after birth (Grove & Tole, 1999). Overall, the neuronal development of the hippocampus is a complex and highly regulated process

that involves the interplay of multiple cell types, including glia, and blood vessels. The proper development of the hippocampus is crucial for the functional processes of memory and learning in the adult brain.

2.2.2 Gliogenesis

Neurons develop in close coordination with vessels (detailed below) and glia, non-neuronal cells, which both provide instructive guidance cues for proper neuronal placement and function (Fellin, 2009; Götz et al., 2002). Glial cells, or “nerve glue,” were first discovered by Rudolph Virchow who mistakenly identified these cells as passive cellular elements that serve as neuronal connective tissue within the brain (Kettenmann & Ransom, 2004). Central nervous system (CNS) glial cells include radial glia, astrocytes, oligodendrocytes, and microglia, which collectively account for nearly 50% of total brain volume (Kettenmann & Ransom, 2004). These cells are highly dynamic with complex and diverse functional roles during nervous system development, including synaptic plasticity and the maintenance of neuronal circuits, oxygen exchange, and pathogenic clearance (Araque et al., 1999; Bushong et al., 2004; Fellin, 2009; Götz et al., 2002).

Radial glial cells, pericytes, astrocytes, and oligodendrocytes are derived from the ectoderm, thus sharing a similar cellular lineage with neurons. Microglia, on the other hand, are derived from the endoderm and are considered “first wave” cells as they are the first cells to invade the developing CNS (Swinnen et al., 2013). In mice, microglia are initially located in the pia surface, only beginning to colonize the brain between E11.5-E17.5 as amoeboid progenitor cells (Figure 2.2B)(Ashwell, 1991; Swinnen et al., 2013). Vascular capillaries start to sprout into the neuroepithelium at E9.5, followed by the extravascular invasion of microglia progenitors at E11.5 (Ashwell, 1991). It is believed that apoptotic signals may trigger the onset of migration as high levels of proliferating microglia are also found in areas of cell death (Ashwell, 1991; Swinnen et al., 2013). Between E14-E16, a second massive wave of peripheral microglia progenitors migrate into the brain parenchyma. Invading microglia proliferate and become ramified then, by E17.5, they begin to scatter throughout the brain. Throughout this process, microglia undergo continuous development and maturation, becoming fully mature approximately a few weeks after birth (Thion & Garel, 2017).

During hippocampal development, radial glia cells are derived from neuroepithelium progenitor cells during neurogenesis, appearing at E9 (Figure 2.2) (Götz et al., 2002). These cells undergo asymmetrical cell division, generating a radial glial cell and a postmitotic neuron or an intermediate progenitor daughter cell (Kamei et al., 1998). Radial glial cells

are so named as they extend elongated processes from their cell bodies, located in the ventricular zone, with the expansion of the OMZ from the preplate (Götz et al., 2002). Throughout hippocampal development, radial glial fibers act as a scaffold for newly born neurons as they migrate to their final position (Götz et al., 2002; Paridaen & Huttner, 2014). Astrogenesis begins at the end of the neurogenesis wave, around E18, lasting approximately until postnatal day 7 (P7) (Figure 2.2). Simultaneously, radial glial cells can detach themselves from the ventricular zone and retract their fibers (Kamei et al., 1998). During this time, astrocytes can either differentiate directly from radial glial cells or intermediate progenitor cells (Kamei et al., 1998). Migrating radial glia cells are also thought to be the source of oligodendrocyte progenitor cells, which further differentiate into myelinating oligodendrocytes (Kettenmann & Ransom, 2004). Functionally, oligodendrocytes ensheath projecting axons with myelin, allowing for the more efficient circuit propagation of action potentials across neuronal networks.

Astrocytes are highly ramified “star-like” cells with encapsulating processes that can surround both the developing vasculature and synapses (Abbott, 2002; Araque et al., 1999; Dorrell et al., 2002; Stone et al., 1995). These cells are involved in neurovascular coupling as they provide a functional link between the metabolic requirements of neurons and vascular flow (Abbott, 2002; McCaslin et al., 2011; Stackhouse & Mishra, 2021). Of all glial cells within the brain, astrocytes are the most abundant, varying greatly in their diversity as indicated by the lack of a general astrocytic marker (Bushong et al., 2002; Farmer et al., 2016; Jurga et al., 2021). Glial fibrillary acidic protein (GFAP) and vimentin have both been identified as intermediate filamentary proteins expressed by astrocytes (Jurga et al., 2021; Regan et al., 2007). Within the neonatal rodent brain, GFAP⁺ and vimentin⁺ astrocytes are equally distributed across the brain (Jurga et al., 2021). Despite their diversity, similarities in the cellular distribution of astrocytes in the early postnatal and adult brain indicate that astrocytes migrate to their final location during their gliogenic window, then proliferate “in place” (Molofsky & Deneen, 2015). However, there can also be a developmental shift from vimentin toward GFAP expression in maturing astrocytes (Bushong et al., 2004; Bushong et al., 2002). In addition to vimentin and GFAP, sub-populations of astrocytes can also express one or more of the following proteins: calcium-binding protein β (S100 β), glutamine synthetase (GS), aldehyde dehydrogenase one family, member L1 (Aldh1L1), and glutamate aspartate transporter (GLAST) (Jurga et al., 2021; Molofsky & Deneen, 2015; Regan et al., 2007). However, beginning at E11, GLAST mRNA is highly expressed in the cell bodies of neuroepithelial cells and then later within cells located in the ventricular zone, following radial glial progenitor cell differentiation and development (Shibata et al., 1997). As the

hippocampus continues to develop, migrating neurons, radial glia, and astrocytes all express GLAST mRNAs (Shibata et al., 1997). From E18-P7, the temporal window for astrogenesis, GLAST expression is downregulated in both radial glia and neurons, but the persistent expression is maintained in astrocytes (Shibata et al., 1997).

2.2.3 Vasculogenesis and angiogenesis

Blood vessels are a complex network of cellular conduits which are responsible for the circulation of oxygen and nutrients to all brain tissues and body organs. Endothelial cells in the CNS form a specialized cellular complex with astrocytes, pericytes, and neurons referred to as the neurovascular unit (NVU), and their dynamic interactions help to regulate the proper brain function (Paredes et al., 2018; Sweeney et al., 2018; Tam & Watts, 2010; Zlokovic, 2008). The vasculature in the CNS has two specialized primary functions: acting as a blood-brain barrier (BBB) and facilitating neurovascular coupling. The BBB is the physical and biochemical barrier between the blood and CNS formed by the tight junctions between endothelial cells (Zhao et al., 2015). Functionally, the BBB acts as an immunological filter for pathogens and toxic substances, while simultaneously titrating essential molecules such as glucose and amino acids to CNS tissues (Abbott, 2002; Zlokovic, 2008). The physiological mechanism of neurovascular coupling adapts local changes in neuronal activity to changes in blood flow to meet the metabolic demands of active neurons (Paredes et al., 2018; Zlokovic, 2008). Neurons undergo continuous metabolic turnover, requiring a continuous replenishment of glucose and oxygen which is critical for driving cognitive function. Disruption in the metabolic homeostasis of neurons can lead to a build-up of toxic byproducts and oxidative imbalances, causing cellular stress (Zhao et al., 2015). Thus, due to coordinated neuronal and vascular development, most neurons are ~10-20 μm from their vascular counterparts (Blinder et al., 2010; Tsai et al., 2009). This proximity to the circulating vasculature allows for the efficient homeostatic exchange of oxygen, ions, and other physiological components required for proper neuronal and vascular function (Blinder et al., 2010). Blood vessels themselves are derived from angioblasts or endothelial precursor cells (EPCs). Through a process called vasculogenesis, EPCs differentiate into proliferating endothelial cells (EC) which directly assemble themselves into a complex cellular network (Goldie et al., 2008). Established blood vessels can undergo continuous angiogenesis: the sprouting, outgrowth, and splitting of new vessel branches from pre-existing ones in response to physiological perturbations.

Vasculogenesis begins at E7.5-E8.5 with the establishment of the perineural vascular plexus (PNVP), a cellular enrichment of angioblasts along the surface of the neural tube

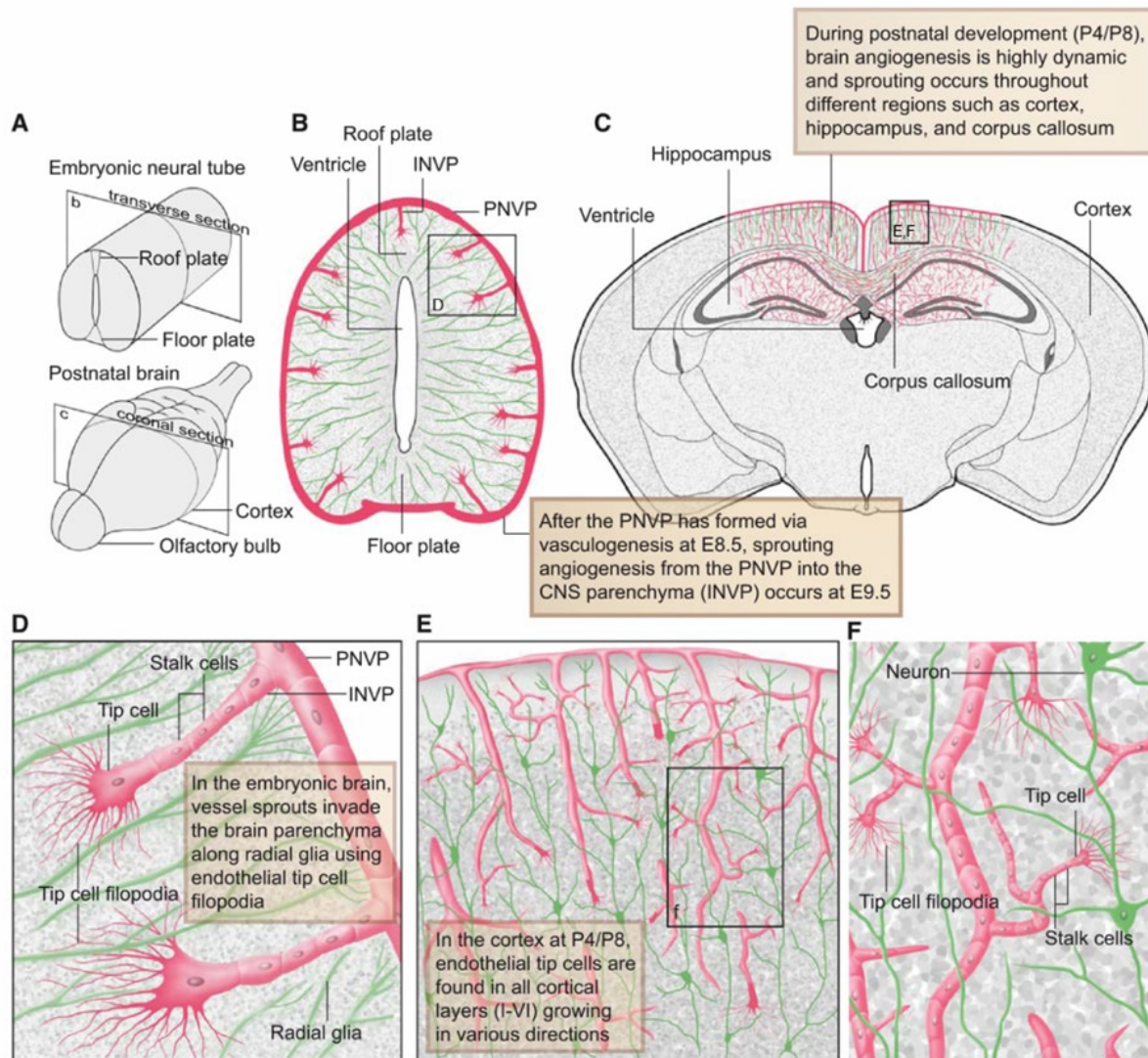


Figure 2.3 Embryonic and Postnatal Vascularization of the CNS. **A)** Schematic diagram of an embryonic mouse neural tube (top) and postnatal mouse brain (bottom). The transverse (embryonic neural tube) and coronal (postnatal brain) cutting planes are indicated. **B)** Schematic representation of sprouting angiogenesis into the neural tube during mouse embryogenesis. The boxed area is enlarged in **(D)**. **C)** Schematic representation of a coronal section of a mouse brain during postnatal development. Blood vessels (red) and nerves (green) are indicated in the cortex, corpus callosum, and hippocampus (blood vessels only). Schematic enlargements are shown in **(E, F)**. **D)** Vessels undergo sprouting angiogenesis into the CNS parenchyma in response to chemoattractive cues presumably acting on endothelial tip cell filopodia: endothelial sprouts invading the CNS parenchyma from E9.5 onward grow along radial glia fibers towards the ventricle. **E)** Postnatal (e.g., at P4/P8) angiogenesis in the CNS is highly dynamic with the complex vessel network mainly established via sprouting angiogenesis. The boxed area is enlarged in **(F)**. **F)** At the forefront of vascular sprouts, endothelial tip cells guide the growing vessel, thereby further expanding the vascular network **(F)**. By P4/P8, endothelial tip cells can be found in all cortical layers (I–VI) and within the hippocampus. Adapted from (Walchli, Mateos, et al., 2015; Walchli, Wacker, et al., 2015).

(Figure 2.3A-B) (Mancuso et al., 2008; Quaegebeur et al., 2011; Risau & Wolburg, 1990). Within the neural tube, there is an enrichment of vascular endothelial growth factor alpha (VEGF-A), a pro-angiogenic guidance molecule secreted by neuronal progenitor cells (Hogan et al., 2004; James & Mukoyama, 2011). Angioblasts expressing vascular

endothelial growth factor receptor 2 (VEGFR2) are recruited to the pia surface in response to the chemoattractive gradients of VEGF molecules (Hogan et al., 2004). As angioblasts differentiate into ECs, specialized sprouting stalk and tip cells are produced (Figure 2.3B) (Gerhardt et al., 2003; Walchli, Mateos, et al., 2015). Tip cells have multiple environment-sensing filopodia expressing concentrated levels of VEGFR2, of which the activation promotes the sprout elongation and vessel growth (Figure 2.3D) (Gerhardt et al., 2003; Hogan et al., 2004). VEGF-A signaling from the neuronal tube also leads to the subsequent angiogenic blood vessel ingression from the PNVP at around E9.5, forming the intraneural vascular plexus (INVP) (Figure 2.3B) (Daneman et al., 2009; Liebner et al., 2008; Stenman et al., 2008). With the onset of neurogenesis, blood vessel sprouts continue to invade the brain parenchyma by migrating along the radial glia towards the central ventricle (Tata & Ruhrberg, 2018). This angiogenic expansion and remodeling of the vascular network continues throughout the embryogenesis phase and into postnatal development of the CNS. By P4-P8, the expanding vascular network has sprouted throughout various cortical regions, including the hippocampus (Figure 2.3C, E-F) (Walchli, Wacker, et al., 2015).

Maturation of the vasculature is a cumulative process in which ECs transition from an active proliferation state into a fully assembled NVU and established BBB (Paredes et al., 2018; Zhao et al., 2015; Zlokovic, 2008). While VEGF/VEGFR2 signaling is essential to vascular development and patterning, Wnts (wingless/integrated) and other molecules are required for lumen formation and maturation of the vasculature (Daneman et al., 2009; Stenman et al., 2008). Endothelial cell Wnt signaling also induces the upregulation of tight-junctions and trans-membrane transport proteins specific to BBB function (Liebner et al., 2008). Sprouting tip cells also secrete PDGF-B (platelet-derived growth factor B) to recruit mural cells, pericytes, and vascular smooth muscle cells, which provide the coverage and stabilization of the cell-cell contacts between ECs (Sweeney et al., 2016). With the onset of gliogenesis, differentiating astrocytes extend end-feet projections that encircle the vascular conduits, further reinforcing and stabilizing the BBB (Stackhouse & Mishra, 2021). Astrocytes simultaneously form connections with developing neuronal synapses, a cellular link completing the formation of the NVU (Zhao et al., 2015; Zlokovic, 2008).

2.3 Neuronal development and plasticity

2.3.1 Axon specification and dendritogenesis

Neurons are specialized cells that usually have a single projecting axon and many dendrites arising from the cell soma. Axonal projections can reach 300 μm or much longer in length,

while the length of dendritic neurites ranges between 100-400 μm (Craig & Banker, 1994). Overall, neurons are much larger when compared to the average length (10-50 μm) of other mammalian cells. Varying highly in their complexity, neuronal diversity occurs at different spatial scales, from the level of a single synapse to the global morphology of a given cell (Bączyńska et al., 2021; Dailey & Smith, 1996; Peters & Kaiserman-Abramof, 1970; Sorra & Harris, 2000). At the global cellular level, dendritic neurites form tree-like structures with very complex branching patterns. The dendritic trees of individual neurons receive inputs via synaptic connections with the projecting axons of other neuronal cells.

Newborn neurons pass through stages of development characterized by specific morphological features, protein expression levels, and distribution patterns (Craig & Banker, 1994). Neuronal morphology is not static in nature as it evolves during neuronal development and, in some instances, can be plastic in mature cells (Bourne & Harris, 2011; De Roo et al., 2008; Okamoto et al., 2004). Neuronal polarity is the result of selective sorting, trafficking, and segregation of axonal and dendritic proteins into their respective compartments (Al-Bassam et al., 2012; Song et al., 2009). Prior to axonal specification, proteins normally preferentially expressed in axons or dendrites are evenly distributed across the cell (Craig & Banker, 1994; Goslin & Banker, 1989). However, upon the specialization of the axon, protein expression is spatially restricted to either the axon or somatodendritic compartments by the formation of the axonal initial segment (Craig & Banker, 1994; Petersen et al., 2014; Song et al., 2009). For example, Song et al. (2009) found that the dendritic protein, N-methyl-D aspartate receptor subunit 2B or NR2B, is preferentially expressed in dendrites, and not axons, following cytoskeletal rearrangements that restrict the movement of this protein into the axon. Cytoskeletal rearrangements and differential trafficking of membrane proteins in neurons direct the specificity, growth patterns, and membrane dynamics of the axon and dendritic neurites (Kennedy et al., 1994; Petersen et al., 2014; Ye et al., 2007). This is the underlying molecular and structural basis for the directional functionality of neurons.

Axonal specification denotes the establishment of neural polarization, a process in which neurons adopt the bipolar morphological segregation of the axonal versus somatodendritic compartment (Craig & Banker, 1994; Goslin & Banker, 1989). The cell bodies of new neurons form lamellipodia, short projections or outgrowths around the cell, which play a role in cell placement and positioning (Parker et al., 2002). Some lamellipodia outgrowths transition into minor processes called filopodia, which elongate and retract spontaneously (Goslin & Banker, 1989). These processes are indistinguishable from each other until intrinsic cellular signaling cues promote the rapid growth and extension of a single neurite,

which will become the axon (Goslin & Banker, 1989). Migrating neuroblasts become polarized neurons before reaching their final somatic position. For example, migrating cortical neurons extend trailing and leading processes, which respectively become the axon and dendritic tree (Barnes et al., 2007).

Projecting axons navigate toward their targets in response to molecular guidance cues (Carmeliet & Tessier-Lavigne, 2005; Kennedy et al., 2006; Ruiz de Almodovar et al., 2011). At the tip of the axons, there is a specialized region called the axonal growth cone, a highly dynamic and actin-rich structure. The growth cone consists of bundled F-actin containing filopodial protrusion with interconnected flattened lamellipodia region containing actin meshes (Dent & Gertler, 2003; Lowery & Vactor, 2009). This structure is also enriched with membrane-bound receptors and adhesion molecules that respond to diffusion gradients of repulsive and attractive molecules within the extracellular space (Dent et al., 2011). The axon extends, elongates, and collapses via cytoskeletal reorganization at the axonal growth cone until its target region is reached (Adams & Eichmann, 2010; Dent & Gertler, 2003; Dent et al., 2011; Lowery & Vactor, 2009). Innervating axons can also undergo extensive branching when they navigate towards their postsynaptic counterparts, including the bifurcation of the axonal growth cone to reach divergent, distal targets (Kalil & Dent, 2014; Szebenyi et al., 1998). Axons can also undergo interstitial branching at filopodia or lamellipodia protrusions located along the axonal shaft (Kalil & Dent, 2014). The elongation and pruning of axonal branches enable localized alterations of synaptic connections, an underlying mechanism of synaptic plasticity within a neuronal network (Bagri et al., 2003; Liu et al., 2005; Luo & O'Leary, 2005).

Like axons, dendritic neurites are dynamic and responsive to extracellular cues. Following the specification of the axon, dendritic neurites increase in size and number with the overall tree structure undergoing continuous alterations in its shape and branch complexity (Dailey & Smith, 1996). Along the dendritic arbors, synaptic spines are also established as the cell differentiates and develops (Figure 2.4) (Bączyńska et al., 2021; Mel, 1993; Sorra & Harris, 2000; Yang et al., 2009). The dendritic trees of individual neurons receive inputs via connections with the projecting axons of other neuronal cells. Because of selective trafficking, the molecular composition of proteins in dendrites is distinctly different compared to that of the axon (Al-Bassam et al., 2012; Song et al., 2009). Connectivity between neurons occurs at chemical synapses, localized functional domains where the pre-synapse of the axon contacts the post-synaptic partners located along the branches of dendrites (P. Vetter et al., 2001). Synapse formation promotes the stabilization of both dendritic and axonal branches, while the inability to form synaptic connections leads to

their destabilization and retraction (Bagri et al., 2003; Goslin & Banker, 1989; Yoshihara et al., 2009). Activation of synapses occurs in a protein-dependent manner, in which the strength of activation depends on the receptor density and composition of individual synapses (Dumas, 2005; Takahashi et al., 2003). As neurons mature, the overall geometries of their dendritic trees contribute to the integration of synaptic inputs and the propagation efficacy of action potentials across the cell (Mel, 1993; Valnegri et al., 2015; Philipp Vetter et al., 2001). Thus, the formation of synaptic connections is essential to the maturation process of neurons as well as the wiring of neuronal circuits.

2.3.2 Spine morphogenesis and synaptogenesis

Synaptic connections are adjustable, undergoing molecular and structural changes, which is the physiological basis of learning and memory (De Roo et al., 2008; Li et al., 2011; Malenka, 1994; Mel, 1993; Turrigiano, 2017). Thus, neuronal networks are hardwired yet flexible in their excitability, a result of an adaptive cellular response of individual neurons to changing inputs (Ho et al., 2011). This response includes changes in axonal (Demas et al., 2012; Yasuda et al., 2011) and dendritic structure (Mel, 1993; P. Vetter et al., 2001), the number of synaptic connections (Li et al., 2011; Majewska et al., 2006), the morphology of individual synapses (Bourne & Harris, 2011; Fischer et al., 1998; Tønnesen et al., 2014), and number of receptors (Dumas, 2005; Takahashi et al., 2003). Thus, individual neurons can alter specific cellular structures to improve information processing within the brain. Non-functional connections between neurons are removed; while active or weak connections are preserved and strengthened (De Roo et al., 2008; Malenka, 1994). For example, in the *Xenopus* tadpole, the axonal branches of the retinotectal projection extend and retract in an activity-dependent manner at synaptic connections in response to chromatic cues during visual learning (Demas et al., 2012). Therefore, the adaptive nature of individual neurons represents the "plasticity" within the neuronal connectivity of the brain.

Synapses are F-actin-enriched specialized compartments located along the shafts of axonal (pre-synapse) and dendritic (post-synapse) neurites (Fischer et al., 1998; Majewska et al., 2006; Okamoto et al., 2004). Structurally, pre- and post-synapses form a functional synaptic unit that is tens of nanometers apart. The pre-synapse contains synaptic vesicles, typically filled with neurotransmitters, which fuse and are recycled from the pre-synaptic membrane. Localized at dendritic spines, the post-synapse is comprised of a dense formation of receptors and other functional proteins involved in synaptic transmission, held in place by cytoskeletal arrangements (Okamoto et al., 2004). Dendritic spines can be classified as either inhibitory (GABAergic) or excitatory (glutamatergic) depending on the post-synaptic response to its pre-synaptic input (Jinno et al., 2007; Sorra & Harris, 2000;

Turrigiano et al., 1998). Inhibitory synapses become hyperpolarized upon binding of the neurotransmitter GABA (gamma-aminobutyric acid) at their post-synaptic receptors, while the binding of glutamate leads to a depolarizing response at excitatory synapses (Jinno et al., 2007; Turrigiano et al., 1998). Glutamate signaling at excitatory synapses mainly is mediated by two neurotransmitter-gated ion channels, the AMPA (α -amino-3-hydroxy-5-methyl-4-isoxazole propionic acid) and NMDA (N-methyl-D-aspartate) receptors (Mel, 1993; Sorra & Harris, 2000; Takahashi et al., 2003). In most mammals, excitatory post-synapses are located on spines that protrude radially from the dendritic shaft (Figure 2.4C) (Sorra & Harris, 2000). Conversely, inhibitory synapses tend to be located on or near the soma, either directly on the dendritic shaft in clusters with other inhibitory or excitatory synapses (Bourne & Harris, 2011).

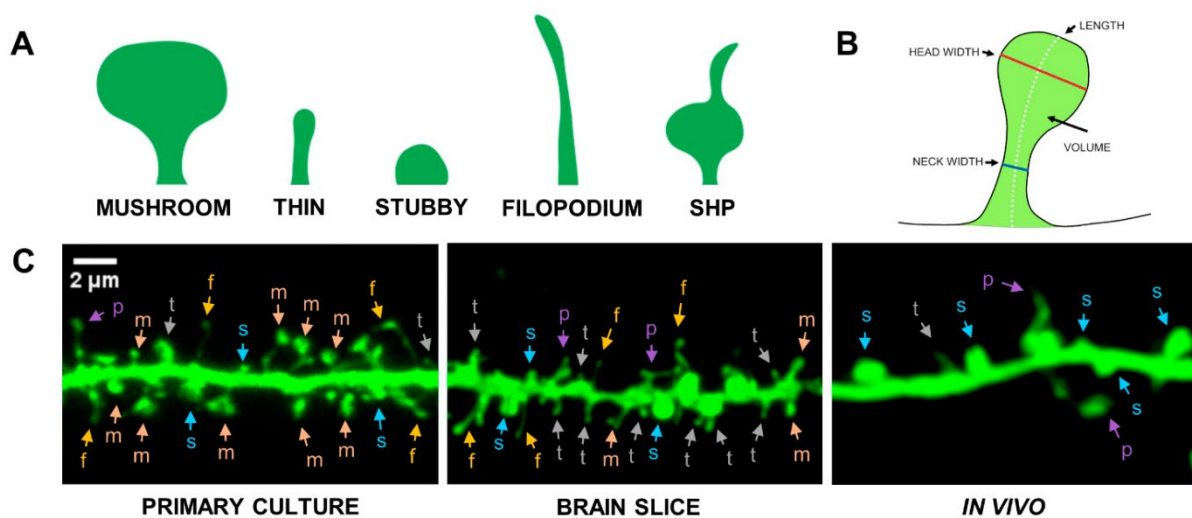


Figure 2.4 Morphological diversity of dendritic spines. **A**) Spine shape classification: mushroom (m); thin (t); stubby (s); filopodium (f); SHP, spine head protrusion (p). **B**) Definition of morphometric parameters; **C**) Microscopic images of dendrites covered with dendritic spines obtained from in vitro (primary culture), ex vivo (brain slice), and in vivo (cranial window) imaging. Scale bar: 2 μ m. Adopted from (Bączyńska et al., 2021).

Dendritic spines are highly dynamic and motile (Dailey & Smith, 1996; Yuste & Bonhoeffer, 2004). The formation and remodeling of spines can be regulated by extrinsic and intrinsic factors, such as guidance cues and their receptors, scaffolding molecules, or molecular regulators of the cytoskeleton (Yoshihara et al., 2009). On younger dendrites, elongated filopodia (>2 μ m) function as exploratory spine precursors (Dailey & Smith, 1996; Yuste & Bonhoeffer, 2004). The transformation of a filopodium into a maturing spine is initiated upon its successful contact with a pre-synaptic axonal terminal, while unsuccessful synaptic contact formation leads to the retraction of the filopodium (Yoshihara et al., 2009). Mature excitatory spines are typically between 0.5-2 μ m long and possess a thin neck emerging from the dendritic shaft and with a spine head bouton serving as the site of synaptic contact

(Tsay & Yuste, 2004). Spine neck and head features can vary in length, shape, and volume, of which they are broadly categorized as thin, stubby, or mushroom-shaped (Figure 2.4 A-B) (Peters & Kaiserman-Abramof, 1970). Total synaptic densities can vary along neurites as synaptic connections can be transient or stabilized by synaptic activity (Vlachos et al., 2013; Yang et al., 2009). The stabilization and strengthening of newly formed synapses are the result of an increase in membrane insertion of AMPA and NMDA receptors as well as cytoplasmic signaling in response to pre-synaptic neurotransmitter release (Bourne & Harris, 2011; Fischer et al., 1998; Okamoto et al., 2004). Furthermore, the increase of molecular content within spines directly correlates with the expansion of the post-synaptic density and volumetric increase in spine head size (Bourne & Harris, 2011; Malinow, 2003; Mel, 1993; Takahashi et al., 2003; Turrigiano et al., 1998). Thus, the morphological and functional characteristics of individual spines are directly linked to their molecular composition.

2.3.3 Synaptic plasticity

Plasticity in the brain represents the nervous system's ability to modulate its neuronal circuits through changes in synaptic strength and connectivity (Bortolotto et al., 2001; Takahashi et al., 2003; Turrigiano et al., 1998). Information transfer across synapses is a complex process involving the chemical release of neurotransmitters at multiple synaptic connections that are integrated into a sequence of post-synaptic potentials by voltage-gated ion channels (Feldman, 2012). Nearly every phase of this process can exhibit activity-dependent plasticity, the morphology, molecular, and physiological alterations of synaptic connections. There are two established forms of neuronal plasticity in the nervous system: correlation-based Hebbian plasticity which mediates changes in synaptic connections of neuronal circuits, and homeostatic plasticity, which is required for stabilizing the firing in neuronal networks (Echegoyen et al., 2007; Turrigiano et al., 1998).

Hebbian synaptic plasticity is a feed-forward mechanism that describes the coincident firing of excitatory neurons (Turrigiano, 2017). When neuron 'B' fires in direct response to neuron 'A', the synaptic strength between the two excitatory neurons is potentiated, where the level of chronic excitation leads to either long-term potential (LTP) or depression (LTD) at individual synapses (Feldman, 2012). A well-studied example of Hebbian plasticity is the regulation of AMPAR at excitatory synapses (Malenka, 1994; Malinow, 2003). LTP is exhibited when electrical stimulation of NMDARs induces a Ca^{2+} influx-mediated increase in the protein synthesis and insertion of post-synaptic AMPARs (Bliss & Collingridge, 1993; De Roo et al., 2008). During low-frequency stimulation protocol, AMPARs are internalized resulting in LTD of synaptic activity (Malenka, 1994; Malinow, 2003). Another form of

plasticity is scaling, a feedback mechanism where prolonged changes in synaptic activity lead to compensatory changes in synaptic strength (Turrigiano et al., 1998). During homeostatic synaptic plasticity expression levels of receptors and ion channels are scaled up or down to maintain a set level of synaptic activity (Echevoyen et al., 2007). Both Hebbian and homeostatic synaptic plasticity depend on the exchange and metabolic turnover of proteins (Turrigiano, 2017).

2.4 Molecular links between neuronal and vascular development

From the embryonic stage until adulthood, neuronal cells expand to form a multi-cellular network with the brain alone consisting of ~70 million neurons and trillions of synaptic connections (Herculano-Houzel et al., 2006). Nervous system development is a dynamic and metabolically demanding process requiring a continuous oxygen and nutrient supply from the vascular system. Co-development of vessels alongside neurons is a biological adaptation to hypoxia-induced oxidative stress during CNS development, in which localized increases in CNS blood flow and vessel angiogenesis occur in the presence of low oxygen tension (Oosthuyse et al., 2001; Paredes et al., 2018; Ramakrishnan et al., 2014; Stone et al., 1995). Low oxygen levels promote the pathway activation of hypoxia-inducible factor (HIF), of which HIF-1 α regulates a broad spectrum of pro-angiogenic genes involved in vessel tube formation, sprouting, migration, and other angiogenic processes modulating vascular patterning (Ramakrishnan et al., 2014; Stone et al., 1995). Genes upregulated by HIF-1 α include angiopoietin-1/-2, PDGF, and VEGF, a key pro-angiogenic mitogen with physiological links to nervous system development (De Almodovar et al., 2009; Mackenzie & Ruhrberg, 2012). The spatial proximity of neuronal and vascular cell systems has been associated with extracellular signaling molecules at the neurovascular interface, coordinating their development (Hogan et al., 2004; Oosthuyse et al., 2001; Paredes et al., 2018). In the peripheral nervous system, VEGF is secreted by Schwann cells and projecting nerve fibers, which promote and guide the outgrowth of following vessels (Sondell et al., 2000). VEGF-secreting neurons also direct vascular patterning and layer ingrowth during the early stages of retinal development (Haigh et al., 2003; Okabe et al., 2014; Stone et al., 1995). Despite having delineated biological functions, the structural patterning and spatial proximity of neuronal and vascular cell systems is a result of the close functional relationship between neurons and vessels (Quaegebeur et al., 2011; Walchli, Wacker, et al., 2015).

2.4.1 Spatial scales of neurovascular patterning

The co-development of neurons and vessels is exemplified by their structural similarities, of which neurovascular patterning is seen at different spatial scales (Carmeliet & Tessier-Lavigne, 2005; Elorza Ridaura et al., 2021; Paredes et al., 2018; Tam & Watts, 2010). At the gross anatomical level, neurons and vessels exhibit similar structurally complex multicellular networks, which innervate nearly every tissue and organ of the body, as first described by Andreas Vesalius in the 16th century, and extensively reviewed by (Carmeliet & Tessier-Lavigne, 2005; Tam & Watts, 2010). This structural link extends from similarities in specialized cellular structures and molecular signaling mechanisms shared by neuronal and endothelial cells, thus, allowing for the co-migration and navigation of cellular projections through their extracellular environments (Adams & Eichmann, 2010; Carmeliet & Tessier-Lavigne, 2005; Elorza Ridaura et al., 2021). The cellular extension machinery differs between neurons and vessels. Neurons have a subcellular specialization, the axonal growth cone, whereas a tip cell is a morphologically distinct leader cell at the forefront of a multi-endothelial cell unit of elongating vessels (Carmeliet & Tessier-Lavigne, 2005). However, both axonal growth cone and endothelial tip cells have structurally similar filopodial extensions enriched with actin and microtubule filaments (Carmeliet & Tessier-Lavigne, 2005; Dent et al., 2011; Elorza Ridaura et al., 2021; Lowery & Vactor, 2009). These highly motile finger-like extensions express similar receptors that can sense attractive and repulsive cues (Adams & Eichmann, 2010; Carmeliet & Tessier-Lavigne, 2005). Upon receptor stimulation, intracellular signals induce the rearrangement of actin and microtubule filaments (Dent et al., 2011; Lowery & Vactor, 2009). Filopodia can retract, elongate, and turn as projecting cells extend toward target regions along the extracellular gradients of molecular guidance cues. Analogous cellular structures and signaling mechanism results in parallel patterning and expansion as neurons and vessels are wired into complex cellular circuits (Carmeliet & Tessier-Lavigne, 2005; Tam & Watts, 2010).

2.4.2 Neurovascular guidance molecules and receptors

Studies focused on the molecular mechanisms driving neuronal connectivity, have led to the discovery of several signaling molecules (Adams & Eichmann, 2010; Segura et al., 2009; Walchli, Wacker, et al., 2015). Initially identified for their pathfinding role in axons projecting toward target tissues, these canonical guidance cues are now known to also have a functional role in vascular system development and function (Elorza Ridaura et al., 2021). These neurovascular signaling molecules fall into four major categories: Slits, Netrins, Semaphorins, and Ephs/ephrins (Figure 2.5) (Adams & Eichmann, 2010). These ligands and their corresponding receptor targets are categorized into sub-families based on their

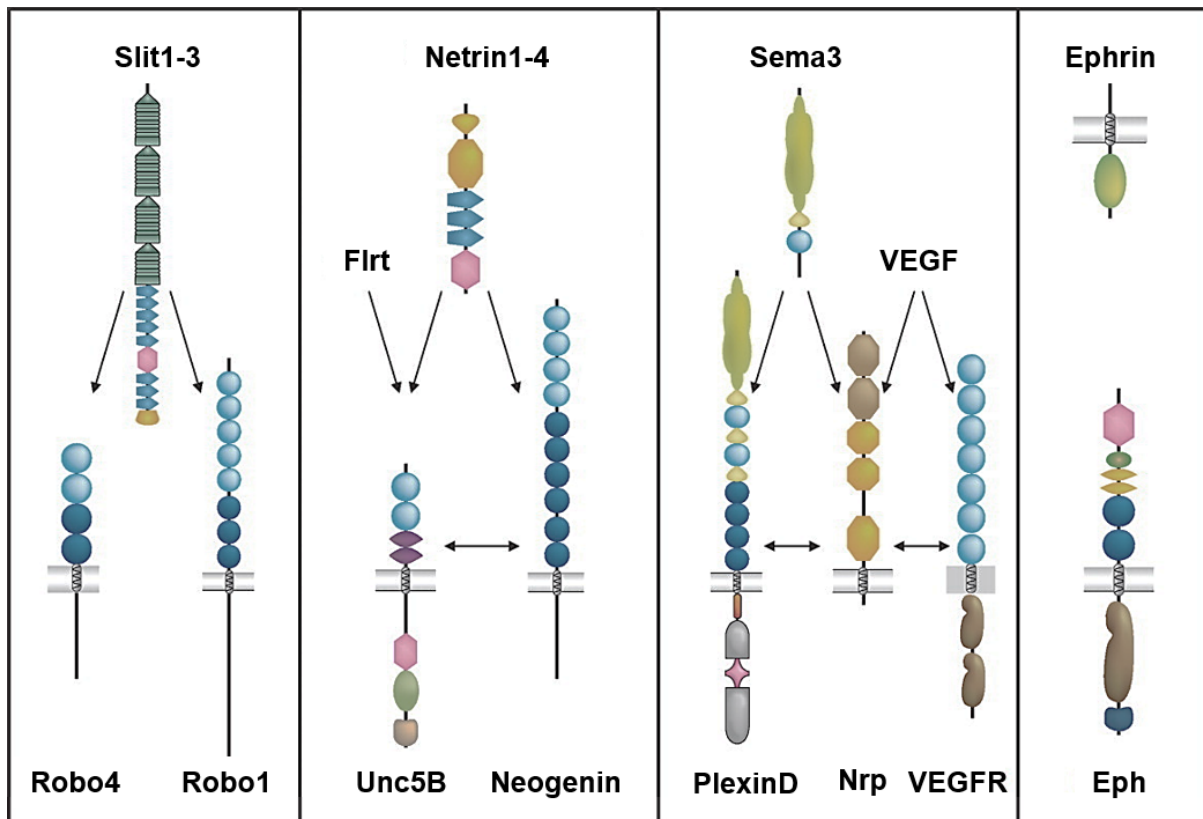


Figure 2.5 Molecular guidance cues with shared roles in neuronal and vascular development. Schematic representation of the four families of neurovascular guidance cues and their receptors. Initially described for their respective roles in either axonal or endothelial tip cell guidance, these cell guidance molecules are now known to have diverse functional roles in both the vasculature and nervous system. Adapted from (Adams & Eichmann, 2010).

signaling mechanism and evoked cellular responses. The physiological context and receptor composition are determinates of the attractive and repulsive effects these guidance cues will have on developing vessels and neurons (Adams & Eichmann, 2010; Elorza Ridaura et al., 2021). In many cases, signaling molecules participate in neuronal-vascular crosstalk to coordinate network formation and the patterning of either or both cell systems (Elorza Ridaura et al., 2021; Paredes et al., 2018; Segura et al., 2009). Some of these biological effects are highlighted below. Notably, however, these same molecules have some functional aspects linked to VEGF signaling, modulating VEGF binding affinity and signal transduction at VEGF receptors (VEGFRs) (Segura et al., 2009). For example, crosstalk between Slit/Robo and VEGF/VEGFR signaling between neurons and endothelial cells mechanistically coordinate vascular patterning in the retina (Rama et al., 2015). Slits, a class of glycoproteins, have also been shown to regulate VEGFR signaling by both inhibiting or synergistically enhancing VEGF binding, although the underlying physiological context remains to elucidate (Segura et al., 2009).

Netrins are a family of laminin-like secreted and membrane-bound proteins that bind to DCC (deleted in colorectal cancer), UNC5 (Uncoordinated-5), and Neogenin-1 receptors

(Rajasekharan & Kennedy, 2009). Netrin-1 and Netrin-4 have both attractive and repulsive effects on both neurons and vessels (Castets & Mehlen, 2010). In nervous system development, Netrin-1 expression at the midline is a chemoattractive cue for DCC/Neogenin-1 expressing spinal commissural axons, promoting midline crossing (Kennedy et al., 1994; Kennedy et al., 2006). Conversely, Netrin-1 repels UNC5-expressing axons away from the midline (Keleman & Dickson, 2001). In vessels, UNC5 receptor function also exhibits repulsive anti-angiogenic properties, restricting vessel branching and outgrowth in response to Netrin-1 (Lu et al., 2004). Netrin-1 and Netrin-4 binding at DCC receptors can also promote the recruitment of either UNC5 or Neogenin-1, down-regulating or enhancing DCC chemoattractive activity, respectively (Rajasekharan & Kennedy, 2009). In endothelial cells, the pro-angiogenic and cell proliferative effects of Netrin-4 signals become inhibitory in the presence of VEGF (Castets et al., 2009). Thus, elicited attractive and repulsive responses, through the modulation of Netrin receptor dynamics, can lead to localized modifications of neuronal and vascular cell networks.

Semaphorins are a super-class of large membrane-bound and secrete proteins that bind to holoreceptor complexes, of which Plexins and Neuropilins (NRPs) receptor families are the major ligand binding partners (Tillo et al., 2012). Class 3 Semaphorins (Sema3) are predominately expressed in mammals and can directly bind to Plexin receptors (Adams & Eichmann, 2010; Elorza Ridaura et al., 2021; Segura et al., 2009). However, signal transduction occurs when Plexins form an active holoreceptor complex with either NRP1 or NRP2 as co-receptors (Janssen et al., 2012). Besides Sema3, NRP1 and NRP2 are modular co-receptors that also bind VEGF, either simultaneously or independently, to mechanistically modify cellular signaling (Tillo et al., 2012). In vessels, NRPs can enhance VEGF signaling by clustering and increasing VEGFR stability at endothelial cell membranes (Horowitz & Seerapu, 2012; Sarabipour et al., 2023; Teran & Nugent, 2015). Functionally, Semaphorins participate in neuronal and vascular circuit formation through repellent signaling. Thus, the biological consequence of impaired Semaphorin expression is hyperproliferation, unstable vessel formation within the vasculature system, or the mistargeting of axonal projects in the nervous system, resulting in disorganized cellular networks (Oosthuyse et al., 2001; Schwarz et al., 2004). In the vasculature, SEMA3-Plexin signaling inhibits endothelial cell proliferation, vascular growth, and branching by mechanistically restricting VEGF signaling (Yang et al., 2015). In the nervous system, secreted Sema3 surrounds axonal fiber bundles, guiding their distal target trajectories through repulsive signaling (Chauvet et al., 2007). Following axonal upregulation of transmembrane Semaphorin, individual axons are repelled away from projecting axonal fiber bundles toward

specific tissue targets. This is facilitated through the bi-directional signaling capabilities of transmembrane Semaphorins, which serve as receptors for holoreceptor complexes to regulate axonal targeting (Adams & Eichmann, 2010).

Eph/ephrins are a family of cell surface receptors and corresponding ligands that regulate cell-cell communication and tissue patterning during development and throughout adulthood (Egea & Klein, 2007; Grunwald et al., 2004; Kania & Klein, 2016; Salvucci & Tosato, 2012). Besides structural differences, they have functional features that are distinct from the Slit, Netrin, and Semaphorin families of guidance cues. Unlike Eph/ephrins, Slit, Netrin, and Semaphorin receptors often require co-receptors for signaling, and their ligands are typically secreted proteins that bind to receptors on the surface of other cells (Adams & Eichmann, 2010; Kania & Klein, 2016). Functionally, Eph/ephrins also act as repulsive or attractive cues, depending on the context, and can regulate a wide range of cellular processes, including angiogenesis, axon guidance, synapse formation, and plasticity (Bochenek et al., 2010; Essmann et al., 2008; Sawamiphak et al., 2010; Takeuchi et al., 2015). In the following chapter, further details regarding the structural and functional features of the Eph/ephrin protein family are further discussed.

2.5 Eph receptors, ligands, and signaling

2.5.1 Eph receptors and ephrin ligands

Ephs are the largest group of receptor-interacting protein tyrosine kinase (RTKs), in which both Eph receptors and their ligands, ephrins, are membrane-bound (Figure 2.6) (Darling & Lamb, 2019). There are two sub-classes of the Eph receptor family of which there are nine EphA and five EphB receptors (Darling & Lamb, 2019). RTKs are known for their intrinsic enzymatic activity resulting in cross-phosphorylation of receptor tyrosine residues which can activate various intracellular signaling cascades (Kania & Klein, 2016). Structurally, Eph receptors have an extracellular ephrin binding domain, a cysteine-rich EGF-like motif, and FGF binding domain with an intracellular kinase domain linked to a sterile alpha motif (SAM) followed by a PDZ-binding motif (Figure 2.6A) (Darling & Lamb, 2019; Kania & Klein, 2016). The extracellular and intracellular portion of Eph receptors is linked by a juxtamembrane region which mediates the autophosphorylation at its two tyrosine residues upon receptor activation. EphAs and EphBs are structurally similar with the capacity to bind either ephrinA or ephrinB ligands, only differing in receptor-ligand binding affinities (Himanen et al., 1998). In contrast, ephrin ligands are structurally distinct as ephrinAs are a glycosylphosphatidylinositol (GPI)-anchored membrane protein without a cytoplasmic tail, while ephrinBs have

a transmembrane domain with a short cytoplasmic tail containing a PDZ-binding motif (Figure 2.6A) (Darling & Lamb, 2019; Kania & Klein, 2016).

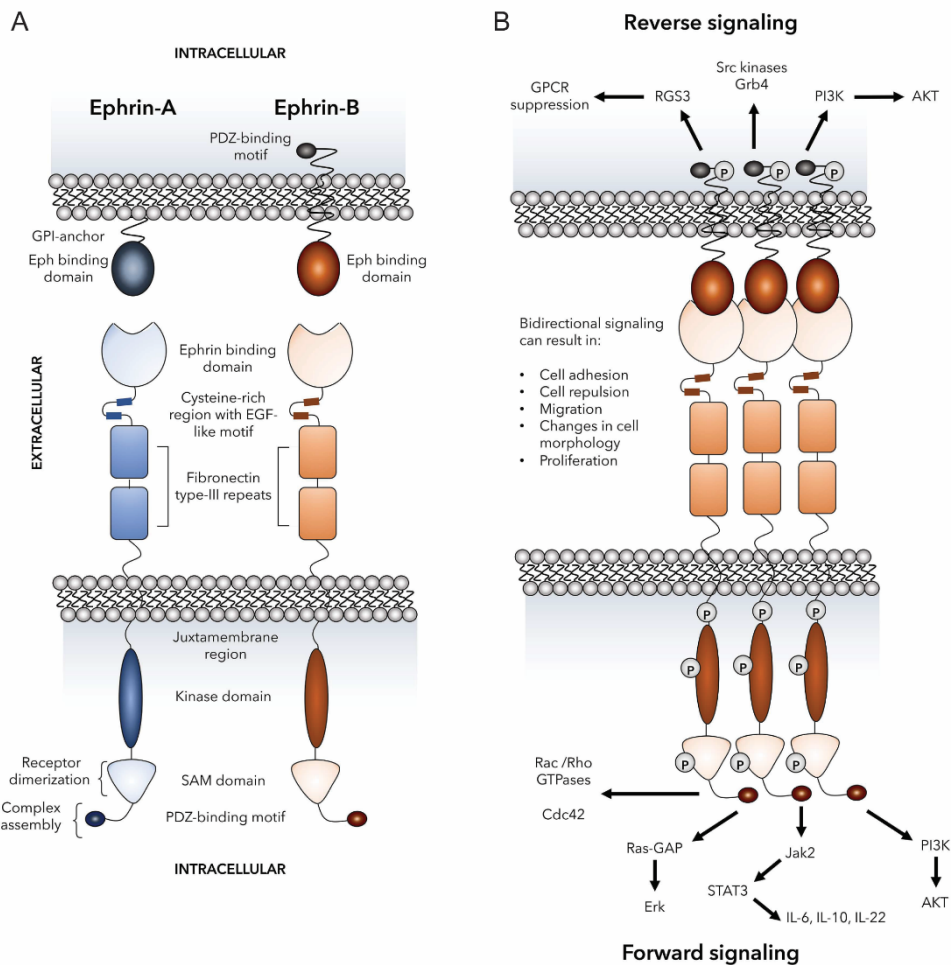


Figure 2.6 Eph receptor and Ephrin ligand structure and signaling pathways. **A)** The structure of ephrin ligands (top) and their receptors (bottom). Eph receptors have an extracellular structure consisting of an ephrin binding domain connected to two fibronectin type-III repeats followed by a cysteine-rich EGF-like motif. The juxtamembrane region connects the extracellular portion of the receptor to the intracellular kinase domain that is linked to a sterile alpha motif (SAM) domain and PDZ-binding motif. Two tyrosine residues on the juxtamembrane region mediate autophosphorylation. Eph receptors bind to ephrin ligands via an extracellular Eph binding domain. ephrin-A ligands are GPI-anchored to the plasma membrane and signal through co-receptors. ephrin-B ligands are transmembrane and are linked to an intracellular PDZ-binding motif via a linker containing five tyrosine residues for autophosphorylation. **B)** Dimerization of Eph receptors is regulated by various processes including SAM domain interactions, ligand clustering, and interactions between cysteine-rich regions and ephrin binding domains on neighboring receptors. Receptor dimerization mediates the formation of heterocomplexes that are required for signaling and are assembled via the Eph receptor PDZ-binding motif. Formation of the heterocomplex mediates bi-directional signaling. Both ephrin “reverse” and Eph “forward” signaling can induce several downstream signaling events, including the activation of Rho GTPases, MAP kinases, PI3 kinase, Src family kinases, Jak-STAT molecules, and RGS3 that has been shown to suppress G-protein coupled receptors including chemokine receptors. P, representative of tyrosine phosphorylation sites; GPCRs, G-protein coupled receptors; RGS3, regulator of G-protein signaling 3; Grb4, cytoplasmic protein NCK2; PI3K, phosphatidylinositol 3-kinase; AKT, protein kinase B; Cdc42, cell division control protein 42 homolog; Ras-GAP, Ras-GTPase-activating protein; Erk, extracellular signal-regulated kinases; Jak, Janus kinase; STAT, signal transducer and activator of transcription; IL, interleukin. Adopted from (Darling & Lamb, 2019).

2.5.2 Bi-directional signaling

The chimeric activation and signaling dynamics of Eph receptors and ephrin ligands facilitate a wide range of cell contact-mediated processes including cell repulsion and adhesion, patterning, and spatial organization (Bochenek et al., 2010; Takeuchi et al., 2015; Wang et al., 2010). As both are membrane-bound, Eph receptor and ephrin ligand signaling interactions can occur *in cis* (same cells) or *in trans* (neighboring cells) (Kania & Klein, 2016). Due to structural similarities, Eph receptor activation can lead to the cross-phosphorylation of multiple receptors to form homo-, hetero-, and even oligomeric receptor clusters (Himanen et al., 1998). Eph receptor signaling complexes can have inner *cis-trans* orientations, incorporating bound and unbound Eph receptors into bi-directional cell-cell interactions via cross-phosphorylation (Kania & Klein, 2016). Eph-ephrin binding interactions also elicit a bi-directional forward-signaling response in Eph-receptor expressing cells and a reverse-signaling response in ephrin-ligand expressing cells (Figure 2.6B) (Klein, 2009; Murai & Pasquale, 2011; Takeuchi et al., 2015). As ephrinA ligands lack a transmembrane domain, reverse-signal transduction occurs through complex formation and activation of other transmembrane proteins (Kania & Klein, 2016). Reverse signaling through ephrinB ligands leads to the recruitment of adaptor proteins at its cytoplasmic domain, resulting in the activation of downstream signaling proteins (Segura et al., 2007; Su et al., 2004; Takeuchi et al., 2015). This is best exemplified by ephrinB2 ligands and EphB4 receptors, which have distinct functional roles in vascular development. In the vascular system, ephrinB2 becomes enriched within arterials whereas EphB4 enrichment occurs within veins (Kania & Klein, 2016; Salvucci & Tosato, 2012). While ephrinB2 and EphB4 signaling respectively repel arterial vessels away from veins, both also play a respective dynamic role in arterial and venous specification and development (Salvucci & Tosato, 2012). Forward and reverse signaling at ephrinB2 ligands and EphB4 receptors promote endothelial cell sprouting, elongation, migration, and adhesion via the activation of Src, PI3-Kinase, and Akt signaling pathways (Figure 2.6B) (Palmer et al., 2002; Sawamiphak et al., 2010; Wang et al., 2010).

2.6 Vascular endothelial growth factor signaling system

The vascular endothelial growth factor (VEGF) ligands and receptors (VEGFRs) are key regulators of vasculogenesis, the *de novo* generation of new vessels, and angiogenesis (Favia et al., 2014; Hogan et al., 2004; Millauer et al., 1993; Ogunshola et al., 2000). VEGF signaling is critical during embryonic development, with direct and indirect effects on multiple cell types (Greenberg et al., 2008; Hayakawa et al., 2011; Lee et al., 2007; Ogunshola et al., 2002; Zhang et al., 2003). During development, expanding tissues

become locally hypoxic, inducing the expression and secretion of VEGF to initiate the chemoattractive recruitment of VEGFR-expressing endothelial cells (Hogan et al., 2004; Tata & Ruhrberg, 2018). Subsequently, the vascular network expands and is locally remodeled to support organ development and growth (Hogan et al., 2004; Li et al., 2013; Paredes et al., 2018; Zhang et al., 2003). Thus, VEGF is a tightly regulated secreted protein essential for physiological vascular homeostasis. Pathogenic VEGF signaling stems from imbalances in extracellular VEGF levels resulting in neoangiogenic diseases such as tumors, ischemia, and diabetic retinopathies (Carmeliet & Storkebaum, 2002; Just et al., 2007; Lee et al., 2012; Nagata et al., 2007; Raz et al., 2016; K. Wada et al., 2006).

2.6.1 Molecular function and structure of VEGF receptors

VEGFs are a ligand family of secreted proteins composed of VEGF-A, VEGF-B, VEGF-C, VEGF-D, and placental growth factor (PlGF) (Figure 2.7) (Mac Gabhann & Popel, 2008). These ligands can elicit a wide range of physiological cellular responses through the distinct binding specificities to three types of receptor tyrosine kinases (RTKs): VEGFR1, VEGFR2, and VEGFR3, in addition to the non-RTKs co-receptors, NRP1/2 (Koch & Claesson-Welsh, 2012; Simons et al., 2016). The cell surface expression of VEGFRs is essential for the coordinated establishment and maturation of the vascular, CNS, and lymphatic systems during embryonic development (Hicklin & Ellis, 2005). Ligands VEGF-B and PlGF uniquely bind and activate VEGFR-1 (also known as fms-like tyrosine kinase1 or Flt1), of which receptor signaling is physiologically involved in both angiogenic and hematopoietic processes during early stages of development (Goldie et al., 2008). Embryos of VEGFR1 null mice are reported to die between 8.5 to 9.5 days *in utero*, exhibiting excessive hematopoietic progenitor cell and endothelial cell proliferation and poorly developed vascular tube formation (Hicklin & Ellis, 2005). VEGF-C and VEGF-D both bind to VEGFR3 (also known as fms-like tyrosine kinase 4 or Flt4), a receptor involved in embryonic cardiovascular and lymphatic development (Koch & Claesson-Welsh, 2012; Singh et al., 2013; Wang et al., 2010). VEGFR3 is initially expressed in both blood and lymphatic endothelial cells with expression becoming mostly limited to lymphatic endothelial cells during later stages of postnatal development and in the adult (Kaipainen et al., 1995; Tammela et al., 2008). Therefore, VEGFR3 is indispensable for lymphangiogenesis during later stages of development as altered receptor function critically impacts lymphatic architecture (Bower et al., 2017; Hicklin & Ellis, 2005). VEGFR2, also known as fetal liver kinase (murine Flk1) or kinase insert-domain containing receptor (human KDR), is highly expressed in vascular endothelial cells (Millauer et al., 1993). However, it is also expressed in other cell types such as the embryonic precursors of lymphatic cells as well as in neurons

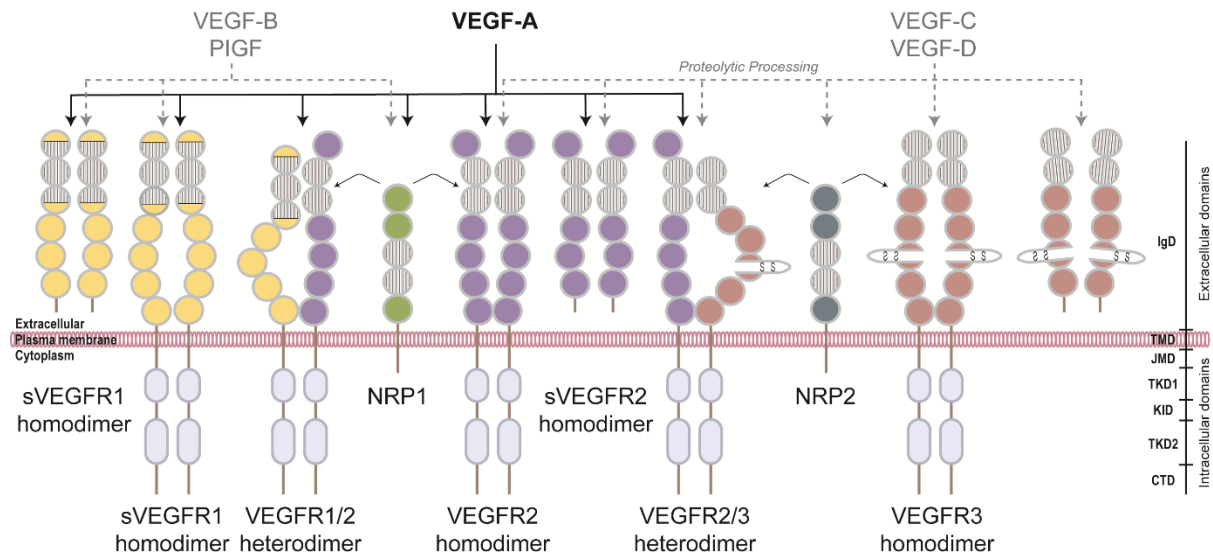


Figure 2.7 VEGF binding specificities and VEGFR signaling complexes. Five vascular endothelial growth factors, VEGFA, VEGFB, VEGFC, VEGFD, and PIGF, bind with different affinities to three VEGF receptor tyrosine kinases (VEGFR) and two NRP coreceptors initiating homo- and heterodimer formations. Proteolytic processing of VEGFC and VEGFD allows binding to VEGFR2. Extracellular domains of VEGFRs and NRPs involved in VEGF binding are indicated by hatched circles. PIGF, placenta growth factor; sVEGFR1, soluble VEGFR1; sVEGFR2, soluble VEGFR2; TMD, transmembrane domain; JMD, juxtamembrane domain; TKD1, ATP binding domain; KID, kinase insert domain; TKD2, phosphotransferase domain; CTD, carboxy-terminal domain. Adapted from (Koch & Claesson-Welsh, 2012; Singh et al., 2013).

(Bower et al., 2017; Jin et al., 2002; Ruiz de Almodovar et al., 2011). VEGFR2 can bind to VEGF-A, VEGF-C, and VEGF-D. Whilst VEGF-C and VEGF-D can directly bind to VEGFR3, facilitating its functional participation in lymphangiogenic signaling pathways, proteolytic processing of these ligands is required for activated VEGFR2 signaling (Koch & Claesson-Welsh, 2012).

VEGFRs are membrane-bound receptors comprised of a 750 amino acid (aa) long extracellular region structurally organized into seven immunoglobulin-like (Ig) domains (Lemmon & Schlessinger, 2010). Of these receptors, VEGFR1 and VEGFR2 have less sequence similarity to VEGFR3 which has a disulfide bridge in place of a fifth Ig domain (Figure 2.7) (Hicklin & Ellis, 2005; Lemmon & Schlessinger, 2010). The extracellular domain is followed by a single short transmembrane domain and intracellular region consisting of a juxtamembrane domain (JMD), tyrosine kinase domain (TKD) split by a kinase insert domain (KID), and C-terminal tail. Within the extracellular domain, the second and third Ig-domains are the binding region for VEGF ligands of which the third Ig-domain determines ligand binding specificity (Holmes et al., 2007; Koch & Claesson-Welsh, 2012; Wang et al., 2020). Soluble forms of VEGFRs have also been identified by which alternative splicing generates a truncated receptor lacking an intracellular domain (Koch & Claesson-Welsh, 2012; Singh

et al., 2013). These functionally behave as endogenous inhibitors, trapping VEGF ligands to limit the activated signaling of VEGFRs at cellular membranes.

Cell surface anchored VEGFRs can form both homodimers as well as heterodimers of which their functional properties are guided by binding interactions with VEGFs ligands and NRPs (Bellon et al., 2010; Dixelius et al., 2003; Koch & Claesson-Welsh, 2012; Sarabipour et al., 2023). NRPs have an extracellular domain with binding sites for VEGF ligands along with a 40 amino acid-long intracellular domain containing a PDZ-binding motif (Koch & Claesson-Welsh, 2012). The intracellular domain of NRPs is too short to allow for sufficient, independent signal transduction upon ligand binding. Serving as a co-receptor, NRPs interact with VEGFRs to strengthen their functional activity by enhancing their binding affinity to VEGF ligands, as well as amplifying receptor phosphorylation and intracellular signaling (Janssen et al., 2012; Sarabipour et al., 2023; Teran & Nugent, 2015). VEGF-A binds VEGFR1 homodimers and heterodimeric VEGFR1-VEGFR2 complexes with a 10-fold higher binding affinity than to homodimeric VEGFR2. Yet strong signal transduction occurs when VEGF-A binds to VEGFR2 as compared to VEGFR1, which has a weaker kinase activity (Koch & Claesson-Welsh, 2012). Furthermore, studies have shown that the functional consequence of PlGF binding to VEGFR1 is the displacement of VEGF-A, increasing its bioavailability for VEGFR2 activation (Gabhann & Popel, 2004). PlGF-VEGFR1 signaling was also found to trigger the intercellular transphosphorylation of VEGFR2 (Gabhann & Popel, 2004). Another study has shown that mutated VEGFR1 with a truncated TKD region resulted in normal vascular development in *VEGFR1(TK)^{-/-}* mice (Hiratsuka et al., 1998). Conversely, both hetero- and homozygous VEGF-A knockout mice die *in utero* due to impaired vessel and hematopoietic cell development (Ferrara et al., 1996; Hiratsuka et al., 2005). Therefore, VEGFR1 functions as a negative regulator of angiogenesis, acting primarily as a decoy receptor for VEGF-A to modulate the activity of VEGFR2.

2.6.2 Structure and function of VEGF

VEGF-A is the primary binding partner of VEGFR2, of which VEGF-A/VEGFR2 signaling plays a dominant role in developmental angiogenesis (Hicklin & Ellis, 2005; Hogan et al., 2004; A.-K. Olsson et al., 2006; Paredes et al., 2018). VEGF-A ligands (from here referred to as VEGF), are structurally related to the PDGFs, a subgroup of extracellular signaling molecules within the cysteine-knot superfamily characterized by their conserved presence of eight cysteine residues (Peach et al., 2018; Takahashi & Shibuya, 2005; Wang et al., 2020). VEGF was initially designated as Factor-X in the 1950s, an unknown soluble pro-angiogenic molecule (Apte et al., 2019). It was then independently identified in 1983 as the vascular permeability factor (VPF) found in

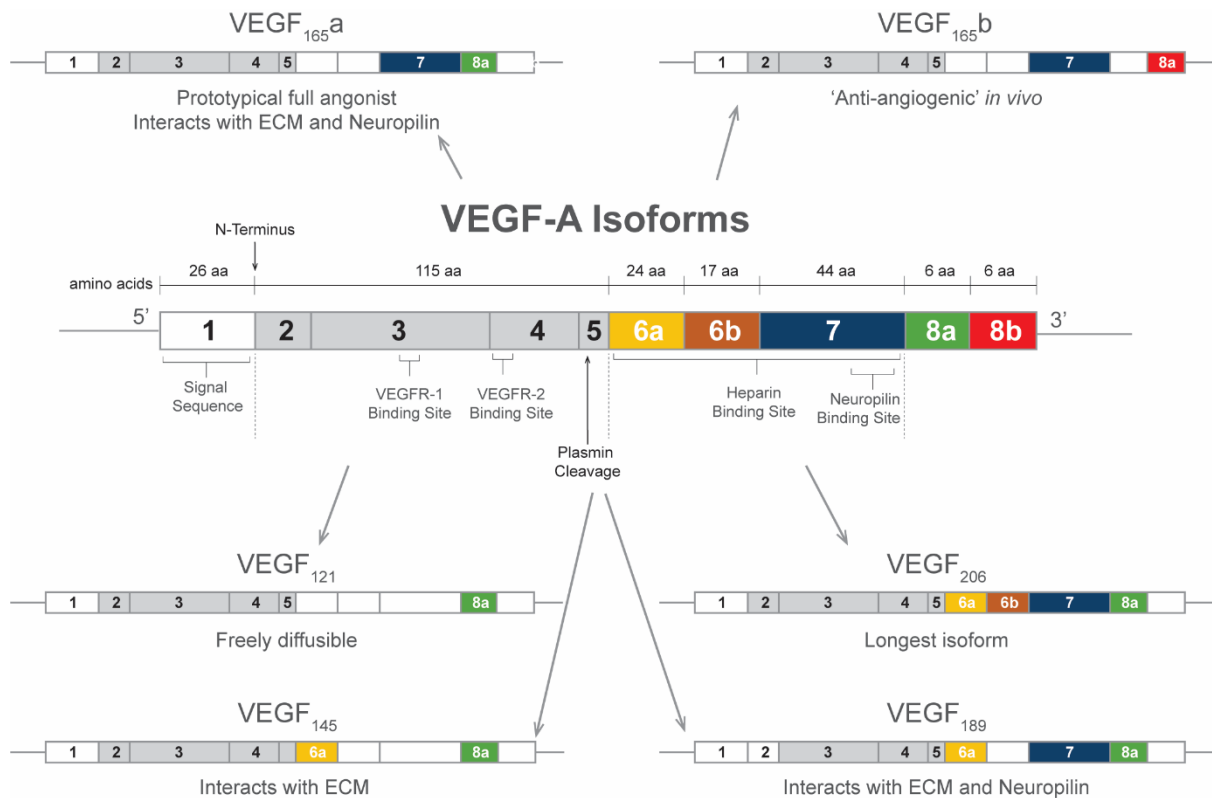


Figure 2.8 Genetic structure of human vascular endothelial growth factor A (VEGF-A) isoforms. The VEGF-A gene consists of eight exons, which can be alternatively spliced to generate a range of VEGF-A isoforms. These isoforms differ in length and have been designated VEGFxxx, where xxx represents the number of amino acids present. Each exon contains residues conferring distinct properties if included in the resultant isoform, including VEGFR1/2, extracellular matrix (ECM), and Neuropilin (NRP) binding. A major site of alternative splicing occurs at exon 8, whereby proximal splicing results in the prototypical VEGFxxx_a forms whereas distal splicing produces the “anti-angiogenic” VEGFxxx_b containing exon 8b. VEGF isoforms in the mouse have one less amino acid than human VEGF isoforms. Adapted From (Peach et al., 2018).

tumor-secreted fluids and in 1990 as a heparin-binding endothelial cell mitogen termed VEGF (Apte et al., 2019). As a pro-angiogenic factor, VEGF is functionally linked to increased vascular permeability as well as endothelial cell proliferation, motility and morphology changes, and survival (Chow et al., 2001; Gerhardt et al., 2003; Lee et al., 2007; Ogunshola et al., 2000; T. Wada et al., 2006). VEGF is encoded by a single gene from which alternative splicing generates physiologically distinct variants ranging in length from 121 to 209 amino acids (Figure 2.8). Of the VEGF isoforms, the most abundant splice variants are VEGF_{120/121}, VEGF_{164/165}, and VEGF_{188/189}, which are predominantly expressed in both mice and humans (Holmes et al., 2007; Peach et al., 2018; Takahashi & Shibuya, 2005). Mammalian VEGF is genetically conserved across all vertebrate species with human VEGF being one amino acid longer than that of mouse (Holmes & Zachary, 2005). Unless specifically noted, murine VEGF is used for the remainder of this text.

All VEGF transcripts contain exons 1-5, regionally encoding a cellular secretion signal and VEGFR binding domains, and exon 8 (Peach et al., 2018; Takahashi & Shibuya, 2005). The isoform

diversity amongst VEGF ligands is due to the alternative splicing of exons 6 and 7 (Peach et al., 2018; Takahashi & Shibuya, 2005). Exon 6 encodes a heparin-binding domain (HBD), while exon 7 and a portion of exon 8 encode a separate heparin/NRP-binding domain (Ambesi & McKeown-Longo, 2014; Peach et al., 2018; Takahashi & Shibuya, 2005; Tillo et al., 2015). Secreted VEGF molecules interact with heparan sulfate proteoglycans (HSPGs) at the cell surface and/or extracellular matrix (ECM) via their HBD sites (Ng et al., 2001; Teran & Nugent, 2015). This differential binding affinity of VEGF ligands to HSPGs produces diffusion gradients surrounding VEGF-expressing endothelial cells (Gerhardt et al., 2003; Ng et al., 2001; Teran & Nugent, 2015). VEGF₁₂₀ is highly diffusible through the ECM with no binding affinity to heparin as it lacks both exons 6 and 7 (Peach et al., 2018; Takahashi & Shibuya, 2005). Conversely, VEGF₁₈₈ has both exon 6 and 7, thus is strongly sequestered to cell membranes and local ECM by its dual HBDs (Ng et al., 2001). The VEGF₁₆₄ contains exon 7 but lacks exon 6. Therefore, while VEGF₁₆₄ can bind NRPs, it is only partially diffusible within the ECM with up to 70% of VEGF₁₆₄ molecules remaining bound to HSPGs (Peach et al., 2018; Takahashi & Shibuya, 2005; Teran & Nugent, 2015).

2.6.3 Spatial and gene expression regulation of VEGF bioavailability

All isoforms of VEGF are secreted as head-to-tail homodimeric proteins covalently cross-linked at the cysteines of two monomers by disulfide bond bridges (Ferrara, 2001; Wang et al., 2020). The mitogenic potential of VEGF is spatially modulated by HSPG-binding interactions, of which VEGF₁₆₄ is the most abundant as well as the most biologically active form of the VEGF splice variants (Ng et al., 2001; Yamamoto et al., 2016). Although VEGF₁₆₄ can activate both VEGFR2 and NRP, VEGF₁₆₄ can only bind NRP when bound to extracellular HSPGs (Bergantino et al., 2015; Horowitz & Seerapu, 2012; Sarabipour et al., 2023; Teran & Nugent, 2015). Furthermore, VEGFR2 signal transduction is enhanced by VEGF₁₆₄-induced receptor interaction with NRP as compared to VEGF₁₆₄ binding to VEGFR2 alone (Teran & Nugent, 2015). Comparatively, VEGF₁₆₄ is more biologically active than VEGF₁₂₀ due to its inability to bind neither HSPGs nor NRPs (Ambesi & McKeown-Longo, 2014; Bergantino et al., 2015; Ng et al., 2001). HSPGs also regulate VEGF bioavailability of which proteolytic processing is required to release sequestered VEGF molecules from the cell surface and ECM (Ruhrberg et al., 2002; Teran & Nugent, 2015). VEGF₁₆₄ can be sequentially cleaved at the COOH terminus of either subunit of the homodimeric molecule by proteases such as plasminogen and various matrix metalloproteinases (MMPs) (Figure 2.9) (Ferrara, 2010). Cleavage of VEGF₁₆₄ removes the amino acid sequences encoding part of exon 5, and all of exons 7 and 8, generating a final proteolytic fragment that is freely diffusible and biochemically equivalent to VEGF₁₂₀

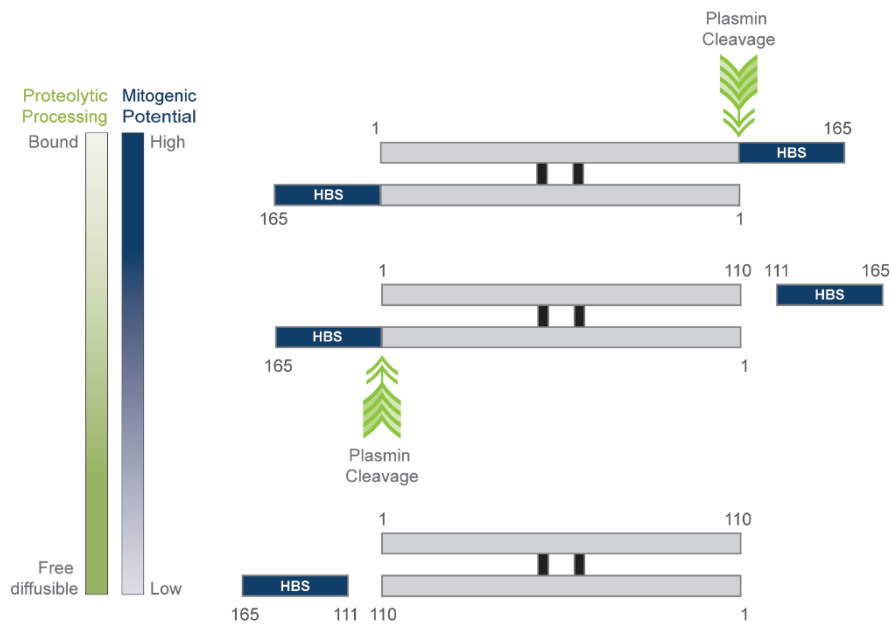


Figure 2.9 Plasmin-mediated cleavage of VEGF₁₆₅. VEGF undergoes sequential cleavage, generating first the heterodimer VEGF_{165/110}. The final product is VEGF₁₁₀, lacking the sequences encoded by exons 7 and 8 and part of exon 5, and is biologically and biochemically similar to alternatively spliced VEGF₁₂₁. Adopted from (Ferrara, 2010).

(Ferrara, 2001). VEGF₁₆₄ is also biologically more active than VEGF₁₈₈ which requires proteolytic processing to reach its full mitogenic potential (Ng et al., 2001; Yamamoto et al., 2016). Like all other VEGF splice variants, HSPG-bound VEGF₁₈₈ can bind to but not induce VEGFR1 signaling (Koch & Claesson-Welsh, 2012). The VEGFR2 binding site of VEGF₁₈₈ is masked by protein folding, which can only be unveiled by proteolytic enzymes, such as plasmin or urokinase-type plasminogen activator (uPA) (Ferrara, 2010). Enzymatic cleavage of VEGF₁₈₈ occurs at the C-terminal end of its exon 6 coding region, generating a truncated form that is still HSPG-bound yet biochemically equivalent to VEGF₁₆₄ (Arcondeguy et al., 2013; Ng et al., 2001; Peach et al., 2018). Consequently, both HSPG-binding VEGF₁₈₈ and VEGF₁₆₄ elicit a mitogenic effect on endothelial cells 50 times higher than that of VEGF₁₂₀ (Ambesi & McKeown-Longo, 2014; Bergantino et al., 2015; Fearnley et al., 2015; Ng et al., 2001). Differential binding of HSPGs to VEGFs, either through alternative splicing or proteolytic processing, directly translates to the gradient angiogenic signaling of these molecules. Shorter VEGF molecules diffuse through the ECM providing weaker stimulatory cues at distal sites to promote endothelial cell proliferation and migration. In contrast, longer and intermediate VEGF molecules provide enhanced signaling closer to endothelial cell membrane surfaces promoting vascular extension and branching. Evidence of this is supported by several vascular studies involving the targeted expression of VEGF splice variants (Ng et al., 2001; Ruhrberg et al., 2002; Ruiz de Almodovar et al., 2009; Yamamoto et al., 2016). The full genetic deletion of VEGF is embryonically lethal

(Carmeliet et al., 1996). Embryos of homozygous VEGF knockout mice die by E9, while heterozygous knockouts can only survive until E11 due to severe defects in vessel formation and cardiovascular dysfunction (Carmeliet et al., 1996; Haigh et al., 2003; Li et al., 2013). This indicates that the spatial-temporal expression of VEGF is tightly regulated during early embryonic development. Transgenic mice solely expressing VEGF₁₂₀ exhibit an altered distribution of vascular endothelial cells caused by the disruption of VEGF diffusion gradients due to the lack of longer VEGF isoforms (Ruhrberg et al., 2002). In VEGF₁₂₀-only mice, VEGF-stimulated endothelial cells were incorporated into existing vessels, producing vessels with larger caliber lumens and vascular networks with an overall reduce branch complexity (Carmeliet & Tessier-Lavigne, 2005; Ruhrberg et al., 2002; Zelzer et al., 2002). Subsequently, these mice die within two weeks of birth due to ischemic cardiomyopathy caused in part by impaired angiogenesis in multiple organs and vascular hemorrhaging (Carmeliet & Tessier-Lavigne, 2005; Ruhrberg et al., 2002). VEGF₁₈₈-only expressing mice display the direct opposite phenotype, exhibiting a highly disorganized vascular network with excessive branching and thin vessels (Carmeliet & Tessier-Lavigne, 2005; Zelzer et al., 2002). Unlike VEGF₁₂₁ mice, VEGF₁₈₈-only mice grow into adulthood and exhibit numerous skeletal defects resulting in delayed development and stunted growth (Zelzer et al., 2002). Conversely, mice expressing only the VEGF₁₆₄ isoform develop normally as do heterozygous VEGF_{164/188} mice (Zelzer et al., 2002). Collectively, these studies show that the spatial restriction of VEGF isoforms within the ECM is required to initiate vessel branching and promote vascular network expansion.

In addition to endothelial cells, VEGF is expressed by many cell types including neurons, pericytes, and glial cells which work in concert to coordinate organ development (Chow et al., 2001; Hogan et al., 2004; Sennino et al., 2009). The genetic expression and cellular secretion of VEGF are regulated by ischemia/hypoxia-induced genes such as PDGF, hypoxia-inducible factor-1 (HIF-1), and epidermal growth factor (EGF) (Gianni-Barrera et al., 2016; Greenberg et al., 2008; Sennino et al., 2009). Direct transcriptional regulation occurs via a hypoxia response element (HRE) within the VEGF promoter, which contains a consensus binding sequence for HIF-1 (Marti et al., 2000; Ramakrishnan et al., 2014; Zhang et al., 2002). Hypoxic conditions drive the post-translational elevation and nuclear translocation of HIF-1, increasing its binding affinity to the HRE sequence to enhance VEGF expression (Ramakrishnan et al., 2014). In turn, the vessel outgrowth induced by the pro-angiogenic signaling of VEGF supports the oxygenation of hypoxic tissues (Stone et al., 1995). Low oxygen tension leads to a sharp increase in VEGF mRNAs, but not that of the other VEGF ligand family members, highlighting the role of VEGF as the primary mediator

for hypoxia-induced vascularization (Koch & Claesson-Welsh, 2012; A. K. Olsson et al., 2006; Zhang et al., 2002).

2.6.4 VEGF-induced activation of VEGFR2

Surface-bound, murine VEGFR2 is genetically translated as a 1367 amino acid monomeric protein, with a molecular weight of 220 kDa post glycosylation maturation (Koch & Claesson-Welsh, 2012; Wang et al., 2020). Murine VEGFR2 shares 83% sequence homology with the mature human KDR protein, which is 2 amino acids shorter with a molecular weight of 230 kDa (Koch & Claesson-Welsh, 2012). VEGFR2 activation starts with the binding of a dimeric VEGF ligand to the second and third Ig-domains of one VEGFR2 monomer (Figure 2.7) (Peach et al., 2018; Wang et al., 2020). As dimeric VEGFs are ECM-linked, ligand binding to one monomer increases the probability of binding a second VEGFR2 monomer (Koch & Claesson-Welsh, 2012). The simultaneous interaction of two VEGFR2 monomers with a dimeric VEGF ligand correctly orients their transmembrane domains to cross-link and stabilize the receptors (King & Hristova, 2019; Stutfeld & Ballmer-Hofer, 2009). The proximity of dually bound VEGFR2 monomers allows for the exact positioning of their intracellular kinase domains to induce their autophosphorylation (Holmes et al., 2007; Simons et al., 2016; Wang et al., 2020). It is important to note that the overall cell surface concentration of VEGFR2 is very low, with less than 10^2 receptors/ μm^2 detected in endothelial cells (Simons, 2012). Instead of being homogeneously distributed across cell surfaces, VEGFR2 is enriched within membrane domains such as cell-cell junctions, focal adhesions, and lipid rafts, which is permissive to ligand-induced dimerization (Horowitz & Seerapu, 2012; Sarabipour et al., 2023; Simons, 2012; Smith et al., 2015; Tahir et al., 2009). A recent study observed that even within VEGF gradients, only 1% of all expressed VEGFR2 was found in a ligand-bound state (King & Hristova, 2019). Therefore, VEGFR2 is exceptionally sensitive to small amounts of VEGF ligands, of which receptor activation can induce robust cellular responses.

2.6.5 VEGFR2 signaling: Insights from vascular physiology

VEGFR2 signaling mediates the various VEGF-stimulated physiological responses of vascular endothelial cells, mainly the angiogenic processes (Figure 2.10) (Holmes et al., 2007; Sivaraman Siveen et al., 2017). Cellular responses are highly dependent on the cell type and its surrounding microenvironment. VEGF-induced dimerization of VEGFR2 results in the cross (auto)phosphorylation of specific tyrosine residues within the VEGFR2 intracellular domains (Koch & Claesson-Welsh, 2012; Wang et al., 2020). Adjacent to tyrosine phosphorylation sites are unique amino-acid binding sequences for Src homology 2 (SH2) domains (Koch & Claesson-Welsh, 2012). Tyrosine phosphorylation creates a

consensus sequence for the recruitment and signal transduction to specific intercellular proteins via their SH2-domains (Koch & Claesson-Welsh, 2012). This leads to the activation of specific signaling cascades to produce distinct, cell-type-specific, biological responses some of which are detailed below.

Cell migration is a key attribute of sprouting angiogenesis and vascular patterning, which relies on actin cytoskeleton dynamics. This process is regulated in part by the phosphorylation of tyrosine residue Y949 (human Y951), located in the C-terminal tail of VEGFR2, in the binding site for the signaling molecule VRAP (VEGFR-associated protein, also known as T-cell-specific adaptor molecule, TSAAd) (Simons et al., 2016; Wang et al., 2020). Inhibition of Y949 phosphorylation prevents VEGF-mediated cytoskeletal reorganization by blocking VRAP/TSAAd complex formation with Src, impairing cell migration (Simons et al., 2016). Phosphorylation sites Y1212 (human Y1214) also regulate key aspects of cell migration (Koch & Claesson-Welsh, 2012). The adaptor protein Nck binds Y1212, which associates with the Src family kinase Fyn leading to the activation of Cdc42, p38/MAPK (mitogen-activated protein kinase), and subsequent phosphorylation of heat-shock protein 27 (HSP27) to also trigger actin polymerization and cell motility (Bjorge et al., 2000; Holmes et al., 2007).

Tyrosine residue Y1173 (KDR Y1175), within the C-terminal tail of VEGFR2, is involved in cell migration, proliferation, and permeability by regulating the ShB-FAK-paxillin, ShB-PI3K-Rac, PLC γ -PKC-MAPK/ERK pathways (Holmes et al., 2007). Y1173 is phosphorylated in a Src-dependent manner by the binding of Shb, an adaptor protein for the binding partner, focal adhesion kinase (FAK), an enzyme important for cellular spreading and attachment (Holmqvist et al., 2003). The formation of FAK-Src signaling complex recruits and phosphorylates other adaptor proteins such as paxillin (Bjorge et al., 2000; Holmes et al., 2007). This assembly complex stimulates PI3K catalytic conversion of PIP₂ to PIP₃ (phosphatidylinositol (4,5)-bisphosphate and phosphatidylinositol (3,4,5)-trisphosphate, respectively) to regulate lamellipodia formation and cell motility through the activation of Rac then Rho GTPases (Bjorge et al., 2000; Holmes et al., 2007; Wang et al., 2020). Generated PIP₃ molecules also activate the protein kinase B (PKB/Akt) signaling pathway to promote cell survival (Downward, 2004). Activated Akt phosphorylates the pro-apoptosis proteins, Bcl-2 associated death promoter (BAD) and Caspase 9, to inhibit their apoptotic activity (Bjorge et al., 2000; Holmes et al., 2007). Binding of PLC γ to Y1173 results in the hydrolysis of PIP₂ to generate the second messengers, diacylglycerol (DAG) and inositol 1,4,5-trisphosphate (IP3) (Bjorge et al., 2000; Holmes et al., 2007; Wang et al., 2020). Working in concert, DAG is the physiological activator of protein kinase C (PKC), whilst IP3

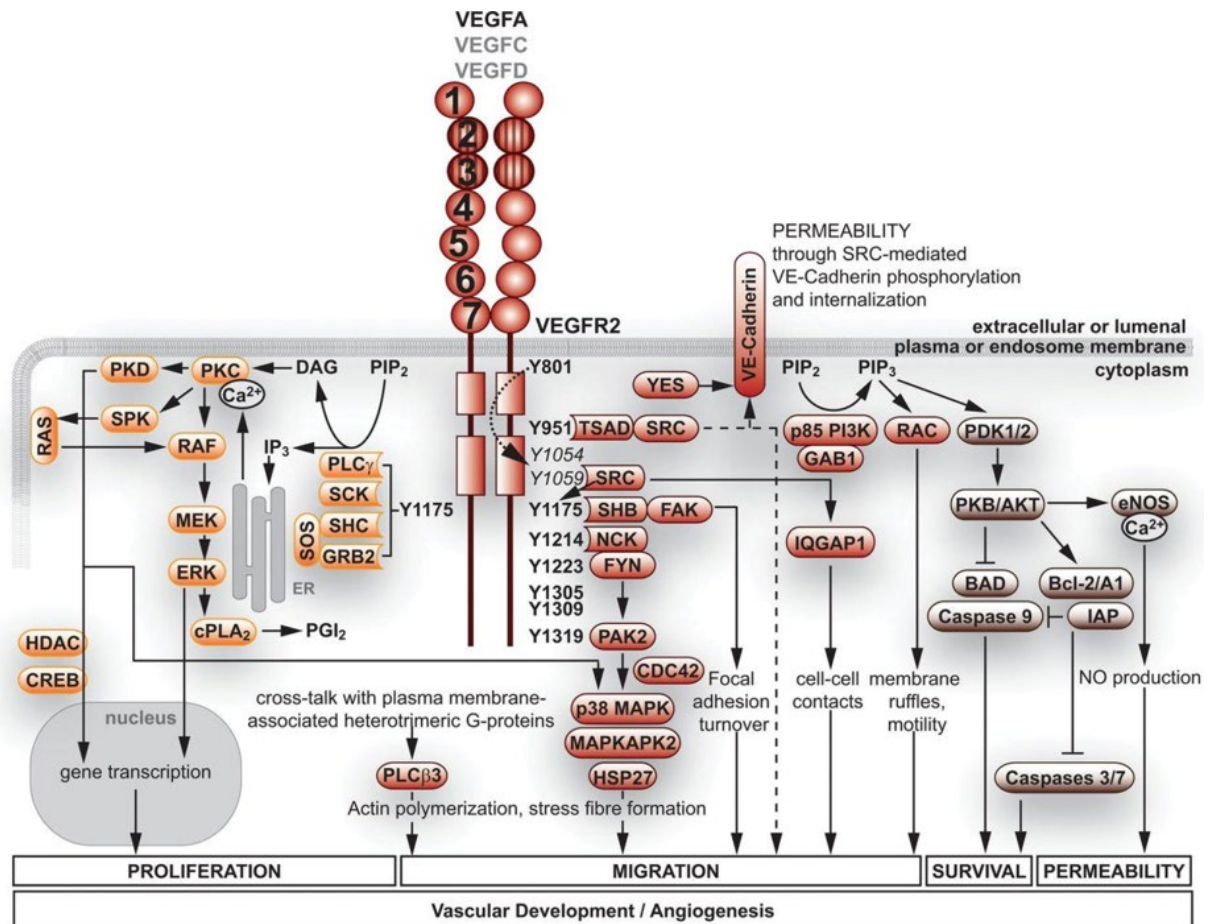


Figure 2.10 VEGF-mediated signal transduction of VEGFR2. Schematic outlining the intracellular signaling pathways of dimeric and activated VEGFR2. VEGF-A, VEGF-C and VEGF-D after proteolytic processing, binds to the extracellular Ig-like domains 2 and 3 of VEGFR2 (hatched circles). Signaling molecules ('rocket' shapes) bind to respective tyrosine phosphorylation sites (indicated by numbers) in the intracellular domain of VEGFR2 and activate downstream mediators (ovals). Tyr 1054 and Tyr 1059 are crucial for VEGFR2 kinase activity (italics). The complex network of intracellular signal transduction pathways results in biological responses such as proliferation, migration, survival and permeability (bottom boxes), which are all required for the coordinated arrangement of endothelial cells in three dimensions to form and maintain vascular tubes. See the main text for details. CDC42, cell division cycle 42; DAG, diacylglycerol; FAK, focal adhesion kinase; HSP27, heat-shock protein-27; IP3, inositol 1,4,5-trisphosphate; MAPK, mitogen-activated protein kinase; MEK, MAPK/ERK kinase; PIP₂, phosphatidylinositol 4,5-bisphosphate; PI3K, phosphatidylinositol 3' kinase; PKC, protein kinase C; PLC γ , phospholipase C- γ ; Shb, SH2 and β -cells; SOS, Son of sevenless; TSAd, T-cell-specific adaptor. Adopted from (Koch & Claesson-Welsh, 2012).

acts upon endoplasmic reticulum (E.R.) receptors to increase intercellular Ca²⁺ levels (Bjorge et al., 2000; Holmes et al., 2007; Wang et al., 2020). Calcium-dependent PKC mediates the activation of the MAPK/ERK (extracellular signal-regulated kinases) pathway, a classical signaling pathway common to VEGFR2 and other RTKs (Bjorge et al., 2000; Fearnley et al., 2015; Holmes et al., 2007; Wang et al., 2020). Through VEGF-induced activation of VEGFR2, signals transduced via the PLC γ -PKC-MAPK/ERK signaling cascade regulate the activities of several transcription factors to enhance gene expression changes associated with cellular proliferation (Takahashi et al., 1999). Cytoplasmic increase of Ca²⁺

is also important for the activation of other signaling molecules, such as endothelial nitric oxide synthase (eNOS). VEGF-induced cell permeability requires Ca^{2+} or PKB/Akt-mediated eNOS generation of nitric oxide (NO) (Fearnley et al., 2015; Yamamoto et al., 2016).

The split kinase domain within the C-terminal tail of VEGFR2 is the main hub for the integration and transduction of VEGF-induced signaling (Wang et al., 2020). The targeted pathway activation as well as the intensity and duration of VEGFR2 kinase activity is regulated by Y801, located within the receptor JMD (Koch & Claesson-Welsh, 2012; Wang et al., 2020). This tyrosine residue is critical to the autophosphorylation rate of VEGFR2 as unphosphorylated Y801 autoinhibits receptor kinase activity (Koch & Claesson-Welsh, 2012; Wang et al., 2020). However, autophosphorylation of tyrosine residues Y1054 and Y1059 greatly enhances VEGFR2 kinase activity upon Y801 phosphorylation (Koch & Claesson-Welsh, 2012; Wang et al., 2020). The significance of the VEGFR2 kinase activity in regulating development angiogenesis is highlighted by the fact that a knock-in point mutation of Y1173 is embryonically lethal at E8.5 in mice due to defects in hematopoietic and endothelial cells (Sakurai et al., 2005). These observed developmental defects are like that of full VEGFR2^{-/-} mice (Ferrara et al., 1996; Hiratsuka et al., 2005).

2.6.6 Endocytic trafficking and signaling of VEGFR2

VEGFR2 has highly fine-tuned signaling properties through its relative binding affinities to VEGF ligands and co-receptors (Fearnley et al., 2015; Lampugnani et al., 2006; Peach et al., 2018; Sarabipour et al., 2023). VEGF-VEGFR2 binding induces receptor dimerization and autophosphorylation to activate downstream signaling cascades. It was initially thought that the signals transduced by the cell surface activation of VEGFR2 were terminated by receptor internalization and lysosomal degradation (Simons et al., 2016). However, it is now understood that VEGF-induced VEGFR2 internalization is required for the selective activation of intercellular signaling cascades, a process regulated by co-receptors such as vascular endothelial cadherin (VEC), NRP1, and ephrinB2 (Horowitz & Seerapu, 2012; Lampugnani et al., 2006; Sarabipour et al., 2023; Sawamiphak et al., 2010). Thus, the cellular dynamics of receptor endocytic trafficking and internalization contribute to the intensity, duration, and pathway activation specificity of intercellular VEGFR2 signaling.

VEGFR2 signaling can occur at the cell surface and within endosomes upon receptor internalization, of which the rate of receptor internalization-recycling-degradation determines signaling amplitude and duration (Basagiannis et al., 2016; Horowitz & Seerapu, 2012; Lampugnani et al., 2006). The endocytic trafficking of VEGFR2 highly depends on its membrane domain localization and surface interacting proteins (Figure 2.11) (Horowitz &

Seerapu, 2012; Nakayama et al., 2013; Simons et al., 2016; Tahir et al., 2009). In the presence and absence of VEGF, VEGFR2 participates in rapid constitutive recycling, a form

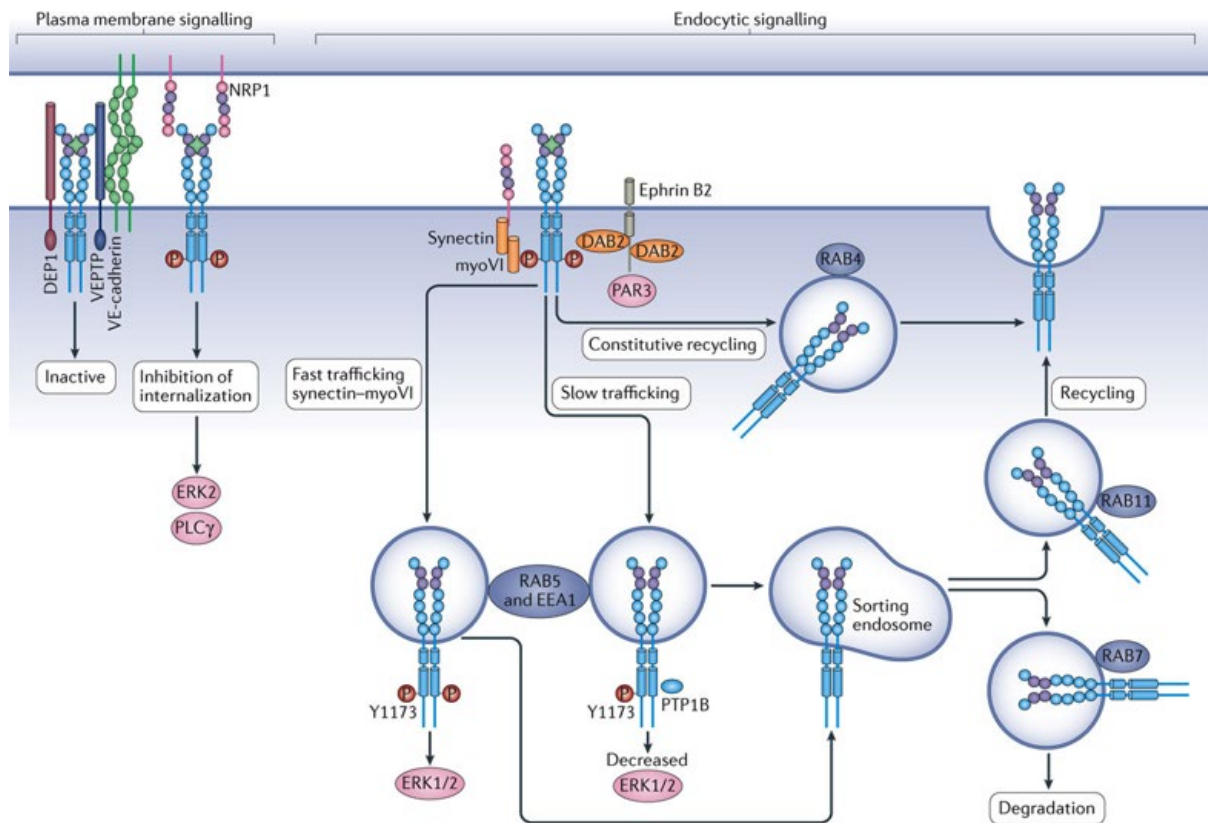


Figure 2.11 Plasma membrane versus endocytic VEGFR2 signaling. VEGFR2 signaling can occur both at the plasma membrane and within endosomes. When in complex with VE-cadherin–VEPTP–DEP1 at endothelial cell junctions, VEGFR2 is maintained at the cell surface in a dephosphorylated state and signaling is inactive. Furthermore, VEGFR2 internalization is inhibited by NRP1 binding in trans, which leads to the activation of ERK2 and PLC γ rather than alternative downstream signaling occurring within endosomes. This results in decreased angiogenic signaling. When VEGFR2 forms a complex with NRP1 in cis, VEGFR2 is internalized and trafficked to RAB5-positive and EEA1-positive endosomes by an NRP1–synectin–myoVI complex. Internalization of the activated VEGFR2 is further mediated by an ephrin B2–DAB2–PAR3 complex, which promotes movement of VEGFR2 from the plasma membrane into the cell. Signaling continues within endosomes until VEGFR2 is dephosphorylated by PTP1B, which is localized on the endoplasmic reticulum but clustered close to endosomes. VEGFR2 can then be degraded by RAB7 endosome shuttling or recycled back to the cell surface via RAB11 endosomes. VEGFR2 may also undergo ligand-independent, constitutive recycling via RAB4 endosomes. DAB2, disabled homologue 2; DEP1, density-enhanced phosphatase 1; EEA1, early endosome antigen 1; myoVI, myosin VI; NRP1, neuropilin 1; PAR3, partitioning defective 3 homologue; PLC γ , phospholipase C γ ; PTP1B, protein tyrosine phosphatase 1B; VE-cadherin, vascular endothelial cadherin; VEGFR2, vascular endothelial growth factor receptor 2; VEPTP, vascular endothelial protein tyrosine phosphatase; Y1173, Tyr1173. Adopted from (Simons et al., 2016).

of steady-state internalization with cell surface reinsertion, largely via RAB4+ endosomes (Simons et al., 2016). At endothelial cell junctions, VEGFR2 is spatially tethered and maintained at the cell surface in a dephosphorylated, inactive state within VEC-protein phosphatase complexes, inhibiting VEGF-induced VEGFR2 signaling (Lampugnani et al.,

2006). In the presence of VEGF, the *trans*-binding of NRP1 to VEGFR2 inhibits the internalization of the activated receptor, which is selectively permissive to PLC γ and ERK signaling pathway activation (Simons, 2012). The *cis*-binding of NRP1 allows for the rapid internalization of VEGFR2 into RAB5-EEA1 positive endosomes with the aid of cytoplasmic synectin-myoVI adaptor proteins (Simons, 2012). However, the process of VEGFR2 internalization is regulated by ephrinB2 as NRP1 is dispensable for VEGFR2 internalization, while ephrinB2 is not (Horowitz & Seerapu, 2012; Sarabipour et al., 2023; Sawamiphak et al., 2010). Endothelial cell deletion of ephrinB2 completely disrupts VEGFR2 internalization resulting in higher cell surface receptor expression and impairing vascular angiogenesis (Sawamiphak et al., 2010). Additionally, this mechanism of reverse signaling by ephrinB2 ligands can occur independently of EphB4 receptor binding (Bochenek et al., 2010). The cytoplasmic recruitment of disable homolog 2 (DAB2) and partitioning defective 3 homolog (PAR3) adaptor proteins to the PDZ-domain of ephrinb2 forms a signaling complex that interacts with the activated kinase domains of VEGFR2 to promote receptor internalization (Nakayama et al., 2013). The ephrinB2-DAB2-PAR3 complex traffics VEGFR2 back to the cell surface in RAB4+ endosomes or into RAB5+ endosomes for continued intercellular signaling (Simons et al., 2016). VEGFR2 signaling persists until dephosphorylated by protein tyrosine phosphatase 1B (PTP1B). Upon signaling termination, endosomal sorting shuffles VEGFR2 back to the cell surface in RAB11+ endosomes or targets VEGFR2 for lysosomal degradation in RAB7+ endosomes (Simons, 2012). The mechanisms of VEGFR2 endocytic tracking and intercellular signaling in vascular endothelial cells are highly diverse. However, whether these mechanisms are similarly exploited by other VEGFR2-expressing cell types, such as neurons, and their associated functional outputs remain to be fully explored.

3 Results

3.1 VEGF-induced VEGFR2 signaling in neurons requires ephrinB2

Intercellular communication at the neurovascular interface depends on the 3-dimensional organization and proximity of cellular structures as well as the relative expression of receptor-ligand interaction partners. In sprouting endothelial tip cells, the *in vivo* activation of VEGFR2 requires not only the expression of the receptor in a VEGF-enriched extracellular environment but also the co-localization of VEGFR2 and ephrinB2 in neurons (Sawamiphak et al., 2010). To investigate if VEGF had a similar functional role during neuronal dendritic development, the relative *in vivo* spatial expression of VEGFR2 and ephrinB2 in hippocampal tissue was characterized. The VEGF-induced VEGFR2-ephrinB2 interaction at neuronal surfaces was also examined.

3.1.1 VEGFR2 colocalizes with ephrinB2 in CA3 hippocampal neurons *in vivo*

It has been shown in the embryonic mouse brain that VEGFR2 is highly expressed in vessels (Millauer et al., 1993). VEGFR2 was also found to be upregulated in the axonal projections of the subiculum in the late embryonic mouse brain (Bellon et al., 2010). However, little was known about the neuronal localization of VEGFR2 in the postnatal mouse brain. Immunohistochemical analysis of VEGFR2 expression was performed at different stages in

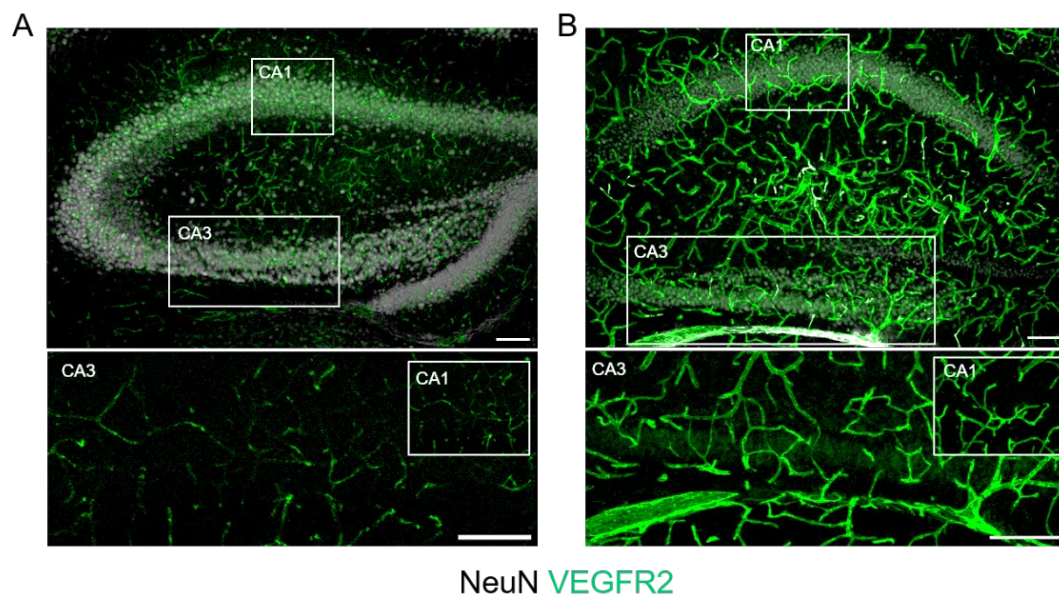


Figure 3.1 VEGFR2 is spatially and temporally expressed in CA3 neurons in the developing, early postnatal hippocampus. Representative images of VEGFR2 immunohistochemistry in the postnatal hippocampus of P1 (A) and P10 mice (B). A VEGFR2 is expressed in vessels at P1 with little no detectable expression in neurons. B by P10, VEGFR2 is additionally expressed in the neurons within the CA3, but not the CA1 region. Scale bars: 100 μ m.

the developing postnatal mouse brain to determine the *in vivo* spatial-temporal expression (Figure 3.1) At P1, VEGFR2 is expression localized within the vessels of the hippocampus, with no detectable expression outside of the vasculature through the first postnatal week (Figure 3.1A). By the second postnatal week, VEGFR2 remains highly expressed in the developing vasculature, but expression was now upregulated in neurons which was spatially confined to the CA3 region. At this time point, neuronal VEGFR2 expression is strongest in CA3 neurons proximal to the hilus, with a gradient decline in expression from proximal CA3 neurons to those more distally located near the CA2-CA3 field of the hippocampus (Figure 3.1B). Notably, VEGFR2 expression is absent from the neurons located in the CA1 field of the hippocampus.

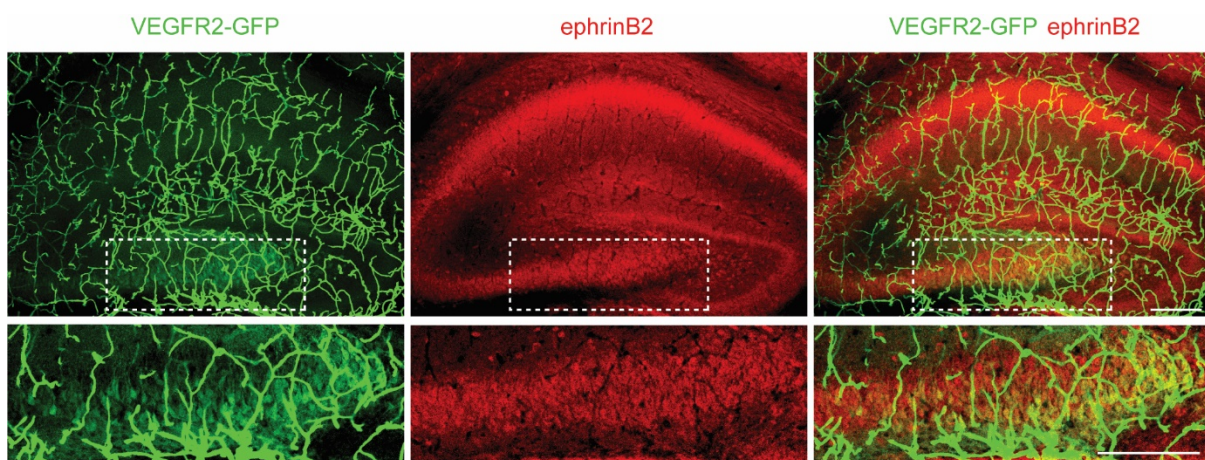


Figure 3.2 VEGFR2 is co-expressed with ephrinB2 in CA3 pyramidal cells in the postnatal hippocampus. ephrinB2 expression was detected by immunohistochemistry staining in the P8 hippocampus of VEGFR2-GFP knock-in mice. ephrinB2 is expressed in CA1, CA2, and CA3 pyramidal cells as well as the granule cells of the dentate gyrus. In higher magnification confocal images, VEGFR2 is co-expressed ephrinB2 in CA3 pyramidal neurons. Scale bar: 200 μm (10x), 100 μm (20x). [This experiment was performed by Dr. Eva Harde, in the laboratory of Amparo Acker-Palmer, University of Frankfurt.]

In endothelial cells in the postnatal retina, there is a dynamic interaction between ephrinB2 and VEGFR2 at membrane surfaces, contributing to VEGFR2 cellular signaling (Sawamiphak et al., 2010). As vessels and neurons share similar signaling cascades, it is plausible for ephrinB2 to be co-expressed in VEGFR2-expressing neurons, having the potential to facilitate VEGFR2 receptor signaling. Neuronal VEGFR2 expression was observed to be highest in CA3 hippocampal neurons during the 1st postnatal week in mouse brain tissues (P8-P10). Therefore, the spatial expression of ephrinB2 proteins was compared to that of VEGFR2 at P10. A VEGFR2-GFP mouse was also used to further validate the localized expression of VEGFR2 in CA3 neurons, outside of the observed expression in the hippocampal vasculature (Figure 3.2). In these mice, exon 1 of the VEGFR2 gene is replaced by GFP, mimicking the endogenous expression of VEGFR2. At P10, VEGFR2-GFP expression was highly observed in the vasculature, while a lower level

of expression was spatially restricted to CA3 neurons. In these same tissues, ephrinB2 expression is detected in all CA hippocampal fields, but not in the vasculature. There was also colocalized ephrinB2 expression in the VEGFR2-GFP positive CA3 pyramidal neurons.

Results from these experiments show that VEGFR2 is transiently expressed within the CA fields of the hippocampus. While expression can be detected in all CA fields in the adult mouse brain (data not shown), VEGFR2 expression is confined to the CA3 regions during the first two postnatal weeks. Within this same time frame, the expression of ephrinB2 is colocalized with that of the spatially restricted expression of VEGFR2 in CA3 neurons. The transient expression of VEGFR2 as well as its co-localization with ephrinB2 in CA3 pyramidal neurons indicates a potential functional role of these two proteins in the postnatal development of these neurons.

3.1.2 VEGF induces VEGFR2-ephrinB2 interaction in neurons *in vitro*

Our lab previously reported that VEGFR2 was spatially expressed at endothelial tip cells and that internalization of the receptor was required for downstream signaling events that lead to the extension of these specialized structures (Sawamiphak et al., 2010). It was also found that, in vessels, VEGF induced VEGFR2 activation and internalization in a process mediated by ephrinB2. In endothelial cells genetically lacking ephrinB2, not only was there a decrease in VEGFR2 phosphorylation upon VEGFA stimulation, but the receptor also failed to become internalized, remaining at the cell surface (Sawamiphak et al., 2010). Immunohistochemical experiments showed that VEGFR2 colocalized with ephrinB2 in CA3 pyramidal neurons of the P10 mouse hippocampus (Figure 3.2). Vessels and neurons share a physiological connection, which is facilitated by signaling molecules and mechanisms common to both cell systems (Elorza Ridaura et al., 2021). Based on our previous findings in vessels, we investigated whether a signaling interaction exists between VEGFR2 and ephrinB2 in neurons. However, it was not known if VEGF could induce the activation of VEGFR2 or ephrinB2 in cultured hippocampal neurons. Therefore, the activation potential of these two proteins was explored in cultured neurons *in vitro* using two different VEGF stimulation assays (Figure 3.3): 1) a co-immunoprecipitation assay of proteins isolated from VEGF stimulated cultures and 2) an ELISA assay of surface-bound VEGFR2 and ephrinB2 using biotinylated VEGF. Activation of ephrinB2 can occur through autophosphorylation upon direct binding to its cognate receptor EphB4 (Kania & Klein, 2016; Pitulescu & Adams, 2010). ephrinB2 can also be cross-phosphorylation by co-receptor interactions with other Eph receptor-bound ligands as well as by other activated RTKs (Kania & Klein, 2016). VEGF does not directly bind to ephrinB2. Therefore, an increase in ephrinB2 phosphorylation in the presence of VEGF would indicate a signaling interaction with VEGFR2.

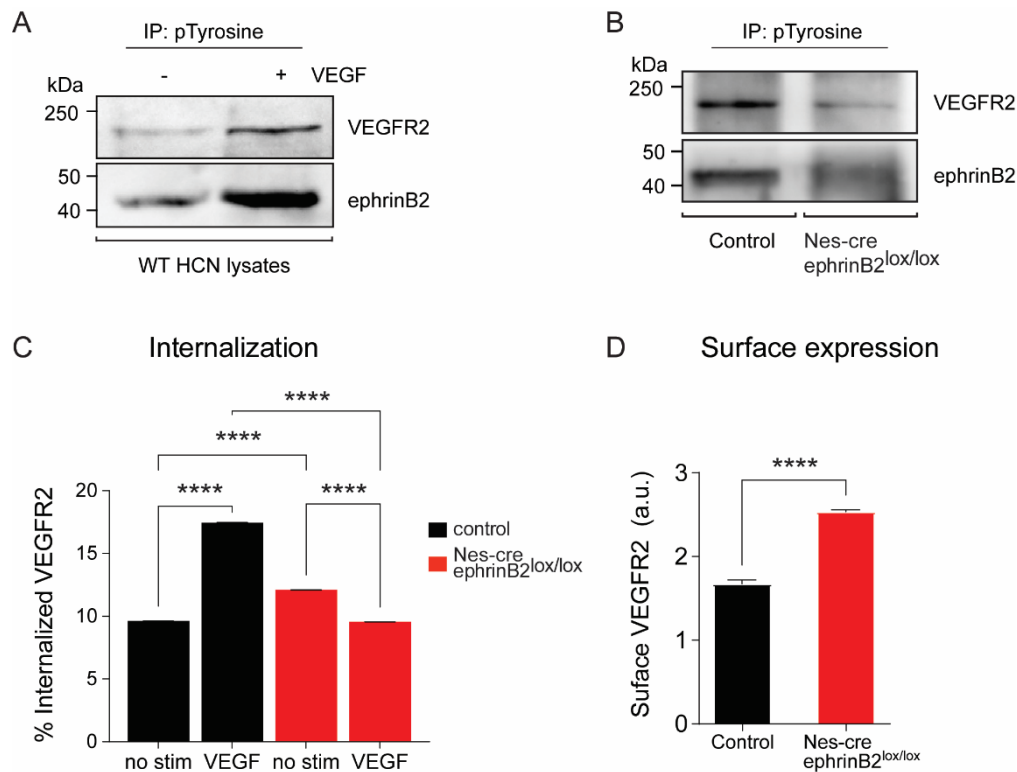


Figure 3.3 VEGF-induced VEGFR2 activation and internalization is impaired in Nes-cre ephrinB2^{lox/lox} mice. **A-B**) Western Blots of primary DIV14 neuronal cultures stimulated with and without VEGF for 30 mins *in vitro*. Protein extracts of **(A)** WT hippocampal neurons or **(B)** Control or Nes-cre ephrinB2^{lox/lox} cell lysates were immunoprecipitated against anti-phospho-tyrosine then analyzed via western blot for co-immunoprecipitation VEGFR2 and ephrinB2. **A)** WT neurons exhibit increased VEGFR2 and ephrinB2 phosphorylation upon VEGF stimulation. **B)** Immunoprecipitation of phosphorylated VEGFR2 is abolished in VEGF stimulated cultured Nes-cre ephrinB2^{lox/lox} neurons. **C-D)** Primary DIV14 neuronal cultures stimulated with and without biotinylated VEGF for 30 mins at 4

Therefore, we first determined if VEGF stimulation could directly activate VEGFR2 and ephrinB2 in neurons based on the respective tyrosine phosphorylation signals. A co-immunoprecipitation assay was performed using antibodies bound to sucrose beads against phosphorylated tyrosine. First, WT neurons were isolated from the hippocampal tissues of E16-17.5 mouse embryos of time-pregnant female mice. In cultured neurons, there is a temporal expression of VEGFR2 mRNAs with an initial peak after 1 day *in vitro* (DIV1) followed by a sustained peak in expression beginning at DIV14 (unpublished data from Eva Harde). Therefore, neurons were cultured for 14 days and then stimulated with and without VEGF for 30 minutes. Lysates from cultured neurons, containing equal amounts of protein, were immunoprecipitated against α -phospho-tyrosine and analyzed by western

blot (Figure 3.3A). In non-stimulated neurons, low levels of phosphorylated VEGFR2 and ephrinB2 are detected. Upon VEGF stimulation, there was an increased immunoprecipitation of both phosphorylated VEGFR2 and ephrinB2. This indicates that VEGF ligands can directly induce the activation of neuronally expressed VEGFR2. VEGF-induced VEGFR2 activation also leads to the activation of ephrinB2. VEGFR2 signaling can occur at the cell surface or intracellularly within internalized endosomes (Horowitz & Seerapu, 2012; Lampugnani et al., 2006; Simons et al., 2016). Depending on the biological context, VEGFR2 may remain dephosphorylated at the cell membrane even in the presence of VEGF, due to the action of membrane-bound phosphatases (Simons et al., 2016). As a result, full receptor activation and signal transduction may only occur after the internalization of VEGFR2, which can be triggered by co-receptor interactions. Therefore, we tested if VEGF-induced VEGFR2 activation required the presence of ephrinB2 using the same immunoprecipitation approach in neurons isolated from Nes-cre ephrinB2^{lox/lox} mice and Nes-cre negative littermate controls. In Nes-cre ephrinB2^{lox/lox} mice, the Nestin promoter selectively drives Cre expression to recombinantly delete ephrinB2 expression neuronal cell populations while Cre negative control neurons express ephrinB2 normally. Results from this assay show that there is activated VEGFR2 and ephrinB2 in stimulated control neurons (Figure 3.3B). However, in VEGF-stimulated cultured neurons isolated from Nes-cre ephrinB2^{lox/lox} mice, the immunoprecipitation of phosphorylated VEGFR2 as well as ephrinB2 was reduced when compared to non-stimulated controls. This confirms that the VEGF-induced activation of VEGFR2 requires the presence of ephrinB2.

Next, it was investigated if VEGF could induce the internalization of VEGFR2 in neurons in a manner that was mechanistically mediated by ephrinB2. Using two-week cultured neurons isolated from Nes-cre ephrinB2^{lox/lox} with biotinylated VEGF followed by a VEGFR2 capture ELISA to determine the surface versus internalized VEGFR2 (Figure 3.3C, D). For measuring the surface levels of VEGFR2, cells were washed to remove excess biotinylated VEGF and then immediately lysed. For internalization events, followed by an acetic acid wash to remove all non-internalized biotinylated VEGF. The basal levels of internalized VEGFR2 are different between Nes-cre ephrinB2^{lox/lox} neurons and control neurons in the absence of VEGF (Figure 3.3C). However, upon VEGF stimulation there is a two-fold increase in the internalization of VEGFR2 in control neurons, which is abolished in Nes-cre ephrinB2^{lox/lox} neurons (Figure 3.3C). Moreover, at the neuronal membrane surface, there is an increase in the basal level of membrane-bound VEGFR2 in Nes-cre ephrinB2^{lox/lox} when compared to control neurons (Figure 3.3D). These

series of *in vitro* experiments suggest that the activation and internalization of VEGFR2 induced by VEGF stimulation require the presence of ephrinB2.

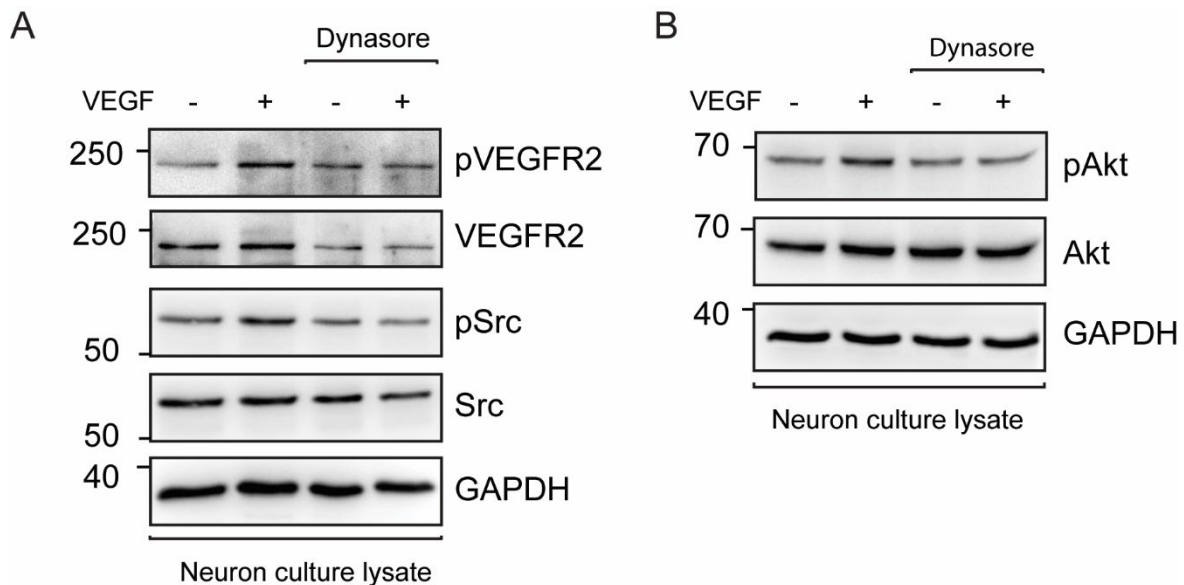


Figure 3.4 VEGFR2 internalization is required for downstream signaling in neurons. Wildtype hippocampal neurons cultured until DIV14 were pre-treated for 2 hours with PBS or with Dynasore, a dynamin-specific inhibitor to block internalization of VEGFR2, then stimulated with VEGF to activate downstream intracellular signaling. In Dynasore-untreated neurons, 30 mins of VEGF stimulation led to increased VEGFR2 and Src phosphorylation (**A**) as well as an increased in Akt phosphorylation (**B**) while treatment with Dynasore impaired the phosphorylation of VEGFR2 and its downstream signaling partners. *These results are published in Harde et al., 2019*

In endothelial cells, VEGF stimulation leads to the activation of downstream signaling partners that are phosphorylated by activated VEGFR2, such as Src and Akt (Sawamiphak et al., 2010). Both Src and Akt have been shown to contribute to angiogenic processes in vessels (Holmqvist et al., 2003; Wang et al., 2010; Yang et al., 2015), as well as having functional roles in migrating newborn neurons in the cerebellum and synaptic plasticity in the adult hippocampus (Meissirel, Ruiz de Almodovar, et al., 2011; Ruiz de Almodovar et al., 2011). However, it was unknown if a similar downstream cascade would be triggered by VEGF-VEGFR2 signaling in neurons. We also questioned if internalization for VEGFR2 would also be required for the activation. The internalized trafficking and signaling of VEGFR2 involves the clathrin-based endocytosis of the receptor in a process that is mediated by dynamin (Zhang & Simons, 2014). The GTPase dynamin plays a critical role in the formation of clathrin-coated vesicles by surrounding and constricting the neck of clathrin-coated pits during endocytosis, facilitating membrane internalization and vesicle formation. Conversely, Dynasore is a small molecule inhibitor that blocks the GTPase activity of dynamin, thereby preventing clathrin-mediated endocytosis, including that of VEGFR2 (Basagiannis et al., 2017).

Therefore, we investigated if VEGF-induced activation of VEGFR2 leads to phosphorylation of Src and Akt in cultured wildtype (WT) neurons, then assessed whether blocking the internalization of activated VEGFR2 with Dynasore inhibits this phosphorylation (Figure 3.4). DIV14 cultured WT neurons were incubated for 2 hours in the absence or presence of Dynasore, followed by another 30 min with or without VEGF stimulation. We then compared phosphorylated and total protein levels of VEGFR2, Src, and Akt using the cultured cell lysates via Western Blot. In line with our previous results, VEGF stimulation induces the phosphorylation of VEGFR2 in neurons, which was diminished when endocytic events were blocked by Dynasore. There was also a corresponding increase in the phosphorylation of Src and Akt in VEGF-treated neurons, which was also similarly diminished when endocytosis is inhibited by Dynasore (Figure 3.4A, B). Interestingly, while the total protein levels for Src and Akt remained relatively similar, there appears to be a decrease in total VEGFR2 protein levels in neurons cultured with Dynasore. This observed reduction could be due to the inhibitory functions of Dynasore which might indirectly create an imbalance in the membrane recycling and degradation processes of VEGFR2, causing a decrease in total protein levels over time.

Here we demonstrate that VEGF-induced activation of VEGFR2 also triggers the activation of downstream signaling molecules, Src and Akt, and this activation is dependent upon VEGFR2 internalization. This process is modulated by ephrinB2 at neuronal cell surfaces, as the presence of ephrinB2 is required for the receptor activation and internalization induced by VEGF stimulation. These results collectively suggest that VEGF induces a cooperative signaling mechanism between VEGFR2 and ephrinB2, which is mechanistically similar to VEGF-VEGFR2 signaling observed in vessels.

3.2 ephrinb2 modulates VEGFR2 function *in vivo* to promote the morphological development of CA3 pyramidal cells.

VEGFR2 plays a critical role in vascular development, in which its early deletion is embryonically lethal. To specifically explore the postnatal functional significance of VEGFR2 in the *in vivo* nervous system, we generated a conditional knockout mouse model using *Cre/loxP* genetic editing, as depicted in

Figure 3.5. VEGFR2-floxed mice (Mühlner et al., 1999) were crossed with a Nestin-Cre mouse line that carried one allelic copy of a Nestin promoter-driven Cre-recombinase (Dubois et al., 2006; Mignone et al., 2004). Through this breeding strategy, we attained a targeted deletion of VEGFR2 in the nervous system, resulting in offspring that were

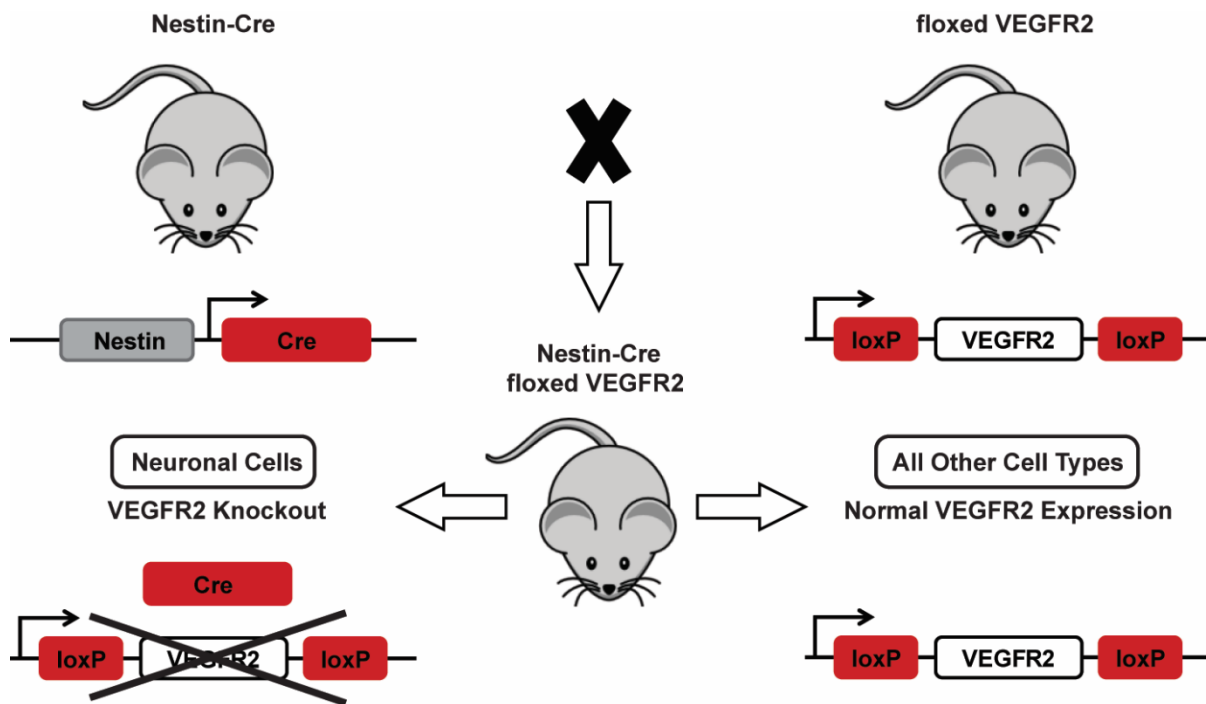


Figure 3.5 Schematic of mouse crossing to generate a nervous system specific VEGFR2 mouse line. The nervous system specific removal of VEGFR2 as achieved by crossing VEGFR2-floxed mice with a Nestin-cre mouse line. As the Nestin promoter is active in neuronal precursor cells, cre-recombinease deletion of VEGFR2 is achieved only in the system whereas it is expressed normally in non-neuronal cell types. [This mouse line was generated for this study by Dr. Eva Harde, laboratory of Amparo Acker-Palmer, University of Frankfurt.]

heterozygous for Nestin-cre and carried one conditional "floxed" allele and one null *Vegfr2* allele, referred to as Nes-cre $VEGFR2^{lox/-}$. To examine the functional consequences, these mice were always compared to Nestin-cre negative littermates, $VEGFR2^{lox/-}$, now referred to as control. We selected the Nestin-cre mouse line to establish this model as the Nestin promoter is specifically upregulated in neuronal precursor cells starting from E10 (Dubois et al., 2006; Liang et al., 2012; Mignone et al., 2004). This breeding approach enabled us to delete VEGFR2-floxed genes in the nervous system while preserving normal receptor expression in all other cell types. Moreover, it allowed us to directly investigate the role of VEGFR2 in the nervous system without impairing VEGFR2 signaling in the vasculature.

The experiments presented in this chapter were performed together with Eva Harde within the research group of Prof. Amparo Acker-Palmer.

3.2.1 Neuronal-specific VEGFR2 deletion impairs the dendritic arborization and spine formation of CA3 neurons

In the mouse hippocampus, the first two weeks after birth coincides with the phase in which hippocampal neurons undergo extensive dendritic arborization and spine formation (Dailey & Smith, 1996). The stabilization of dendritic arbors occurs through synaptogenesis and

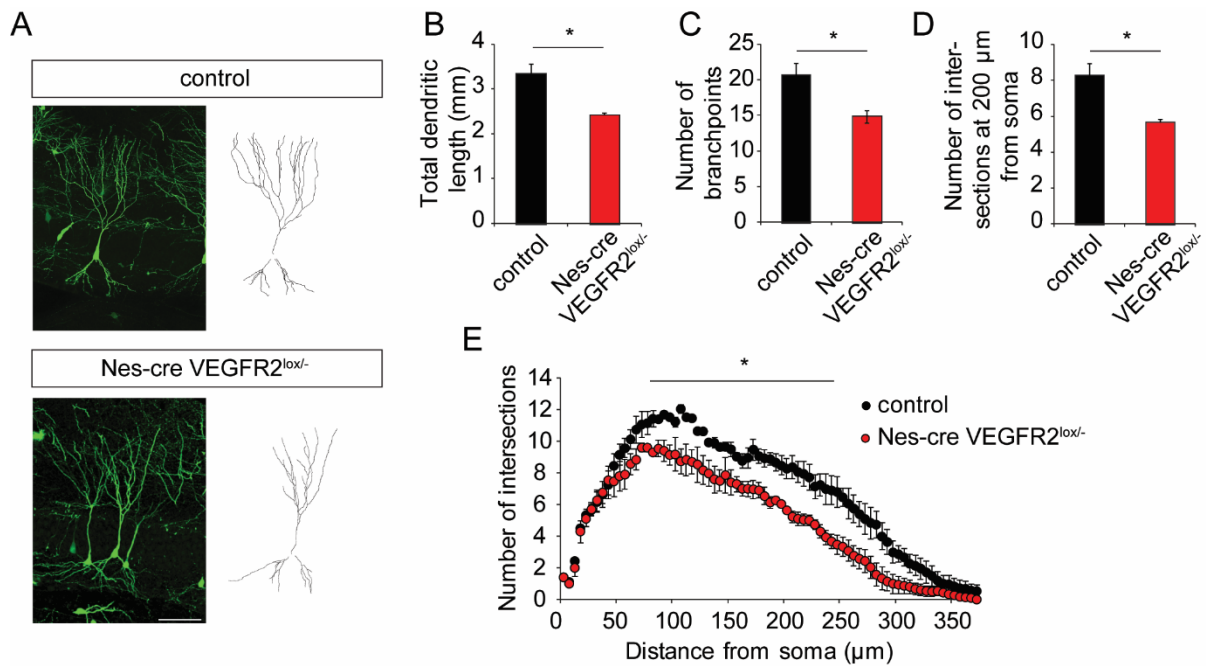


Figure 3.6 Neuronal specific VEGFR2 deletion results in defects in the dendritic branching of CA3 pyramidal neurons. A-C, Nes-cre VEGFR2^{lox/-} mice were cross crossed to Thy1-GFP transgenic mice to visualize the whole cell morphology of pyramidal cell neurons. **A)** Z-projections of confocal images taken and corresponding neurite tracings from CA3 neurons of P10 Nes-cre VEGFR2^{lox/-} mice and Nes-cre littermate controls. Nes-cre VEGFR2^{lox/-} mice exhibit a reduction in **(B)** total dendritic length and **(C)** total number of branch points. **D)** A quantitative analysis showing a reduction in the number neuronal dendrites 200 μm from the soma. **E)** 3D Sholl analysis of confocal z-stacks showing a reduction in branching and dendritic complexity in the CA3 pyramidal neurons of Nes-cre VEGFR2^{lox/-} mice. Scale bar = 100 μm. n= 3 mice per genotype; SEM *p<0.05. [This experiment was performed in collaboration with Dr. Eva Harde, laboratory of Amparo Acker-Palmer, University of Frankfurt. These results are published in Harde et al., 2019]

ongoing synaptic remodeling, processes that are essential for the establishment and strengthening of hippocampal circuitry (Koleske, 2013; Sorra & Harris, 2000; Valnegri et al., 2015). Our findings show that outside of the vasculature, VEGFR2 expression is spatially confined to CA3 pyramidal cells during the second postnatal week (Figure 3.1, Figure 3.2), suggesting a potential role in the development of these neurons during that time. Therefore, we examined CA3 dendritic morphologies in the hippocampus of P10 mice. To visualize and analyze the full dendritic tree structures of CA3 neurons, generated Nes-Cre VEGFR2^{lox/-} and control mice further crossbred with the Thy1-GFP M line (Feng et al., 2000; Vlachos et al., 2013). In this mouse line, a sparse number of neurons are labeled with GFP, which allows for the visualization of the whole-cell morphology of individual neurons within the hippocampus. Neuronal dendritic trees in the hippocampus are highly branched, spanning 200-300 μm in size. Therefore, coronal sections of 350 μm thickness were obtained from the brains of Nes-cre VEGFR2^{lox/-} mice and control littermates to capture complete tree structures. To analyze the dendritic tree structures and branch complexity of CA3 neurons, three-dimensional (3D) tracing and reconstruction were performed using

confocal z-stack images of GFP-positive cells (Figure 3.6A). The results show that CA3 neurons in Nes-cre VEGFR2^{lox/-} mice had less complex dendritic arbors compared to control mice, with significant reductions in total length and branch points (Figure 3.6B,C). Scholl analysis was then conducted on each 3D reconstruction by quantifying the number of traced dendrites that intersect incremental concentric spheres around the cell body (Figure 3.6E). The reduction in dendritic arborization was most pronounced in areas located 100-250 μm from the cell soma (Figure 3.6E). Especially at 200 μm , in the region of *stratum radiatum* where only apical dendrites are present, the number of branching intersections was reduced by 25% (Figure 3.6D).

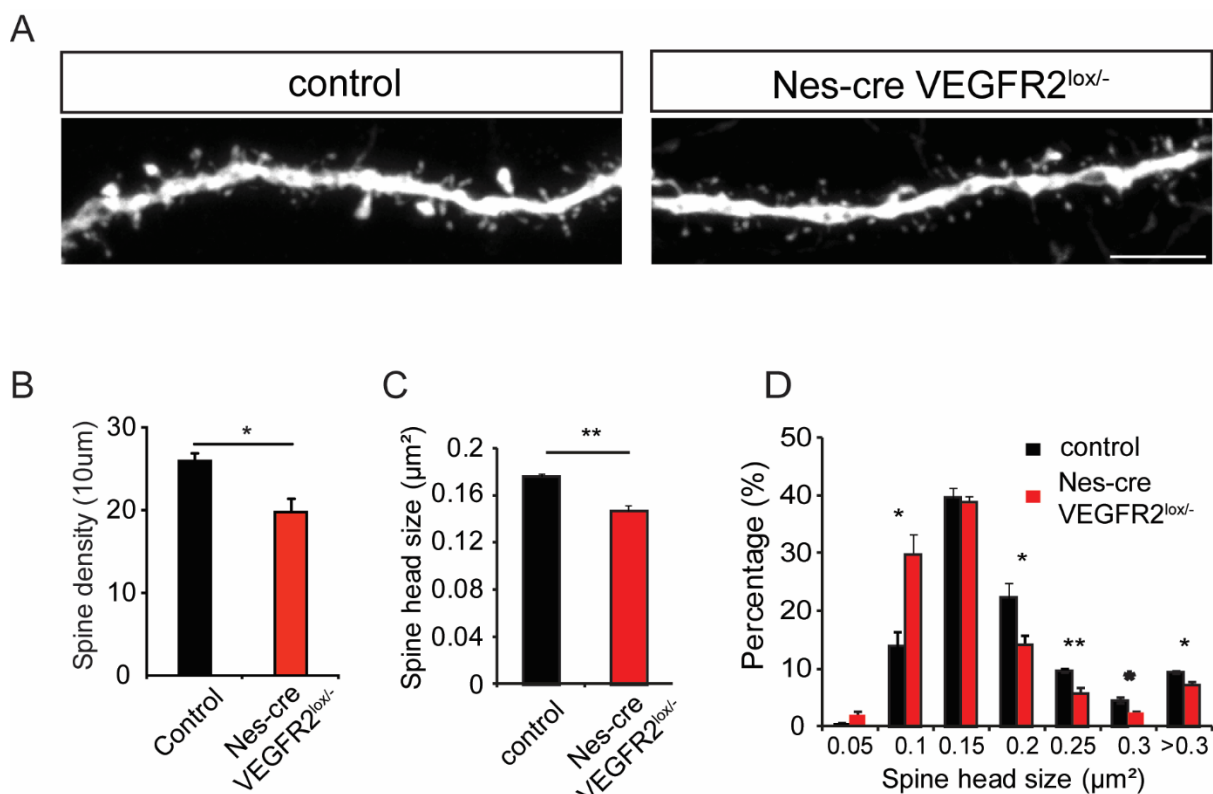


Figure 3.7 Nestin-cre VEGFR2^{lox/-} have an increased proportion of immature spines. **A**, Representative images of dendritic segments acquired within the CA3 *stratum radiatum* of P15 Nes-cre VEGFR2^{lox/-} mice and littermate control mice crossed to Thy1-GFP transgenic animals. Scale bar: 5 μm . The spine density (**B**) and head size (**C**) is reduced in Nes-cre VEGFR2^{lox/-} mice as compared to controls. **D**) The distribution of the spine head area is also proportionately smaller ($<0.15 \mu\text{m}^2$) in Nes-cre VEGFR2^{lox/-} mice, whereas control mice have a higher percentage of larger spine heads ($>0.15 \mu\text{m}^2$). $n=3$ mice per genotype; SEM, * $p<0.05$, ** $p<0.01$. [This experiment was performed in collaboration with Dr. Eva Harde, laboratory of Amparo Acker-Palmer, University of Frankfurt. These results are published in Harde et al., 2019]

In the CA3 region of the hippocampus, the *stratum radiatum* receives input from associational/commissural fibers (Ishizuka et al., 1990; Li et al., 1994; Vago et al., 2014). Therefore, investigating spine morphologies in this region is informative as to how these neuronal connections are established and refined during this critical period of circuit formation in the hippocampus. By P15, dendritic arborization has largely occurred, with

neurons primarily undergoing synapse formation and maturation. Therefore, we imaged spines on the apical dendritic branches of CA3 pyramidal neurons in the *stratum radiatum* region at P15 using Nes-cre VEGFR2^{lox/-} and control mice with GFP-labeled neurons (Figure 3.7A). Spine morphologies were analyzed by measuring the spine head size and spine length (see Figure 2.4B) as well as quantifying the overall spine density using the maximum intensity z-projections of confocal z-stacks. Nes-cre VEGFR2^{lox/-} mice exhibited a significant decrease in spine density (Figure 3.7B), accompanied by an approximate 20% reduction in spine head size compared to littermate controls (Figure 3.7C). Additionally, the distribution of spine head area was altered in Nes-cre VEGFR2^{lox/-} mice compared to controls. Nes-cre VEGFR2^{lox/-} mice had a higher proportion of small spine heads and a lower proportion of larger spines, as shown in Figure 3.7D.

These findings imply that VEGFR2 is crucial to the proper development of CA3 dendrites and spines during the early postnatal weeks.

3.2.2 VEGFR2 and ephrinB2 genetic interaction is functionally required for the dendritic arborization and spine morphogenesis of CA3 hippocampal neurons.

Our *in vitro* analysis demonstrated that VEGF stimulation induces a signaling interaction between VEGFR2 and ephrinB2 in cultured hippocampal neurons. Moreover, the observed significant alterations in CA3 morphologies upon the conditional deletion of VEGFR2 in the nervous system further suggest a functional relevance of VEGFR2 during CA3 development. In light of these results, we investigated whether a genetic interaction between VEGFR2 and ephrinB2 is physiologically necessary for the proper development of CA3 neurons *in vivo*. Using the same breeding strategy described in section 3.2, we generated compound VEGFR2-ephrinB2 featuring conditional deletion of both proteins in the nervous system. For this experimental paradigm, double-heterozygous floxed, Nestin-cre positive compound mice (Nes-cre VEGFR2^{lox/+} ephrinB2^{lox/+}) were compared to VEGFR2^{lox/+} ephrinB2^{lox/+} mice (now referred to as control), which were negative for Nestin-cre. As before, Nes-cre VEGFR2^{lox/+} ephrinB2^{lox/+} and control mice were crossbred to the Thy1-GFP mouse line. Again, confocal z-stack images were acquired of GFP-labeled CA3 neurons and the 3D reconstructions of their dendritic morphologies were analyzed at P10 (Figure 3.8A). In Nes-cre VEGFR2^{lox/+} ephrinB2^{lox/+} mice, CA3 pyramidal neurons display a significant reduction in the number of dendritic branches as well as the total dendritic length as compared to control mice (Figure 3.8B,C). This observed phenotype contributes to an overall decrease in dendritic tree complexity as measured by Sholl analysis (Figure 3.8E,D). The branching defects observed in the CA3 pyramidal cells of compound Nes-cre

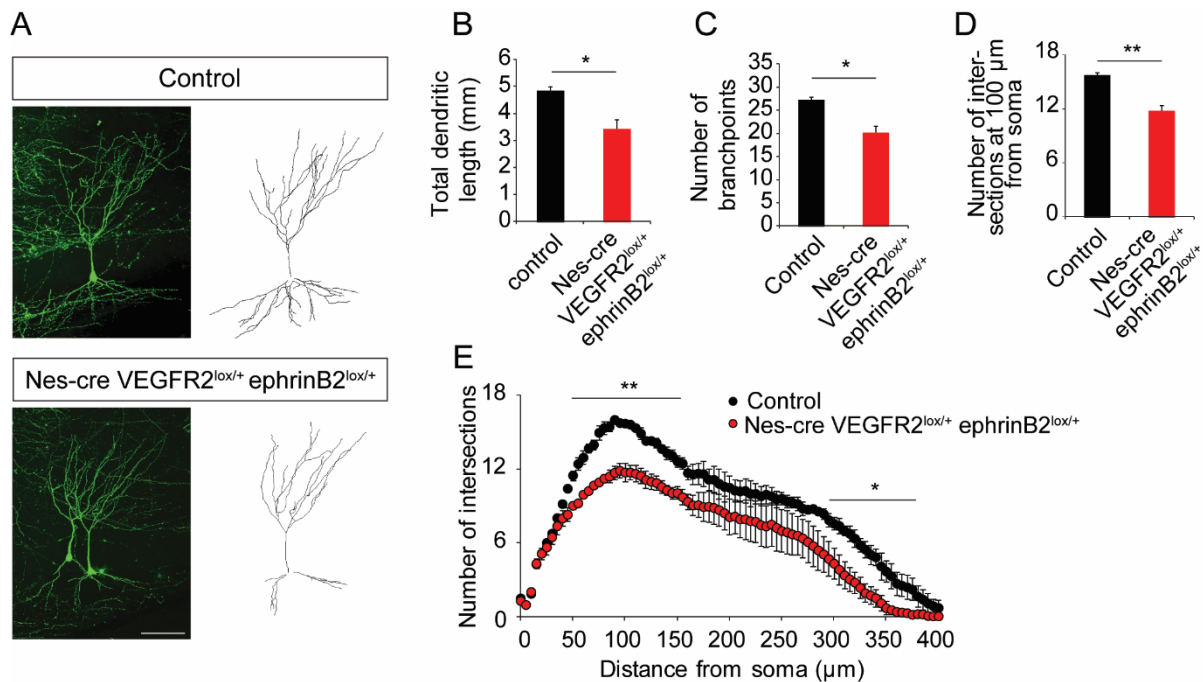


Figure 3.8 VEGFR2 interaction with ephrinB2 is required for proper dendritic arborization in CA3 pyramidal neurons. Nes-cre VEGFR2^{lox/-} ephrinB2^{lox/-} compound mice were crossed to Thy1-GFP transgenic mice to visualize the whole cell neuronal morphologies. **A)** Representative confocal Z-projection images of CA3 pyramidal neurons and corresponding neurite tracings of control and compound Nes-cre VEGFR2^{lox/-} ephrinB2^{lox/-} mice. Scale bar: 100 μm. **B)** The total dendritic length and **C)** number of branch points was significantly reduced in Nes-cre VEGFR2^{lox/-} ephrinB2^{lox/-} mice. **D)** Total number of neurite crossings was also reduced at 100 μm from the soma as quantified by 3D Sholl's analysis **E)** 3D Sholl's analysis also revealed that the CA3 pyramidal neurons in Nes-cre VEGFR2^{lox/-} ephrinB2^{lox/-} mice have truncated dendritic trees with reduced branch complexity. n= 3-4 mice per genotype; SEM; *p<0.05, **p<0.01). [This experiment was performed in collaboration with Eva Harde, laboratory of Amparo Acker-Palmer, University of Frankfurt. These results are published in Harde et al., 2019]

VEGFR2^{lox/+} ephrinB2^{lox/+} mice were comparable to the observations in Nes-cre VEGFR2^{lox/+} mice (Figure 3.6), albeit with a less pronounced phenotype. For Nes-cre VEGFR2^{lox/+} ephrinB2^{lox/+} mice, Cre-induced genetic recombination reduces the protein levels for VEGFR2 and ephrinB2 by half, as compared to the full knockdown of VEGFR2 expression in Nes-cre VEGFR2^{lox/+} mice, which could explain its stronger phenotype observed in the latter. To confirm that the branching defects in Nes-cre VEGFR2^{lox/+} mice are due to a genetic interaction between VEGFR2 and ephrinB2, as opposed to reduced VEGFR2 levels alone, we analyzed the dendritic morphologies of CA3 neurons in single heterozygous Nes-cre VEGFR2^{lox/+} and Nes-cre ephrinB2^{lox/+} and mice. Each of these single heterozygous mice and respective VEGFR2^{lox/+} and ephrinB2^{lox/+} Cre-negative controls were crossed to Thy1-GFP mice and CA3 dendritic morphologies similarly analyzed at P10. In each of these single heterozygous mice, there were no observed defects in CA3 dendritic arbors when compared to their corresponding control (data not shown). Collectively, these results suggest that VEGFR2 and ephrinB2 genetically interact, which is functionally required for the proper development of CA3 pyramidal cells *in vivo*.

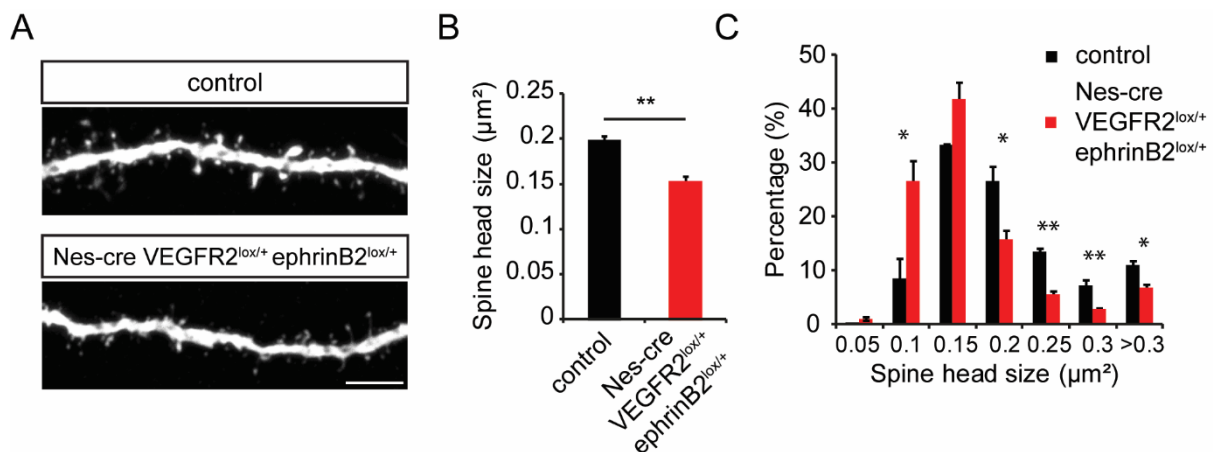


Figure 3.9 VEGFR2 interaction with ephrinB2 is required for spine maturation in CA3 pyramidal neurons. Spine morphological assessment of CA3 pyramidal neurons in P15 Nes-cre VEGFR2^{lox/+} ephrinB2^{lox/+} compound mice and Nes-cre littermate controls, both crossed to Thy1-GFP transgenic animals. **A)** Representative images of dendritic segments within the CA3 *stratum radiatum* regions of control and compound mice. Scale bar 5 μm. **B),** Compound mice exhibit a reduction in spine head size and **C)** reduced proportion of larger spines (>0.2 μm²) with a higher proportion of smaller immature spines (<0.2 μm²) as compared to controls. (n=3-4 mice per genotypes; ±SEM. *p<0.05, **p<0.01. [This experiment was performed in collaboration with Eva Harde, laboratory of Amparo Acker-Palmer, University of Frankfurt. These results are published in Harde et al., 2019]

We further investigated if a genetic interaction between VEGFR2 and ephrinB2 is similarly required for the dendritic spine development of CA3 neurons (Figure 3.9A-C). As done previously, the spines along stretches of apical dendritic branches were imaged within the *stratum radiatum* region of GFP-labeled CA3 pyramidal cells at P15. Nes-cre VEGFR2^{lox/+} ephrinB2^{lox/+} mice showed a reduction in both spine density and spine head size as compared to their littermate controls (Figure 3.9B-C). Likewise, the overall distribution of spine head size was also altered in Nes-cre VEGFR2^{lox/+} ephrinB2^{lox/+} compound mice (Figure 3.9C), with the proportion of smaller spine head size being significantly higher compared to littermate controls, which had a greater proportion of larger spine head sizes. To confirm that the spine defects in compound Nes-cre VEGFR2^{lox/+} ephrinB2^{lox/+} due to the combined reduction of VEGFR2 and ephrinB2, spine morphologies were also analyzed in single heterozygous mice for each protein as well as the corresponding controls. Like our dendritic branching analysis of these mice, there was also no measurable difference between control and single heterozygous mice (data not shown).

The spine phenotype observed in Nes-cre VEGFR2^{lox/+} ephrinB2^{lox/+} compound mice resembles that of Nes-cre VEGFR2^{lox/-} mice. These results, in conjunction with our *in vitro* analysis, indicates a functional involvement of ephrinB2 in mediating VEGFR2-dependent spine maturation in CA3 neurons. This developmentally required physiological interaction between ephrinB2 and VEGFR2 in CA3 neurons is also consistent with our previous finding demonstrating ephrinB2 mediates VEGFR2 signaling in vessels (Sawamiphak et al., 2010).

3.3 VEGF is expressed by multiple cell types in the early postnatal hippocampal

Our *in vitro* analysis demonstrated that VEGF-induced a VEGFR2-ephrinB2 signaling complex that leads to the activation of intercellular signaling molecules, Src and Akt (Figure 3.1, 3.2). Specifically, we found that ephrinB2 modulates VEGFR2 signaling response to VEGF stimulation, by regulating receptor internalization. We also found that VEGFR and ephrinB2 genetically interact to facilitate the development of CA3 neurons during the first postnatal weeks. This suggests that the *in vivo* function of VEGFR2 in CA3 neurons not only requires the co-localized of ephrinB2 but also a VEGF-enriched extracellular environment. As VEGFR2 has a direct functional role in the early development of CA3 pyramidal neurons, we also examined the spatial distribution of VEGF mRNAs and secreted proteins in postnatal hippocampal tissues.

3.3.1 Multiple VEGF mRNA splice variants were detected in the postnatal mouse hippocampus

Due to alternative splicing, mouse VEGF mRNA transcripts can be either 120, 164, or 188 amino acids in length (VEGF₁₂₀, VEGF₁₆₄, VEGF₁₈₈, respectively) (Peach et al., 2018). Splice variants are caused by alternative splicing of exons 6 and 7, which encode for the dual HSPG binding domains (Ferrara, 2010). These domains interact with the extracellular matrix, causing diffusion gradients in tissues, which can affect neurite outgrowth as well as

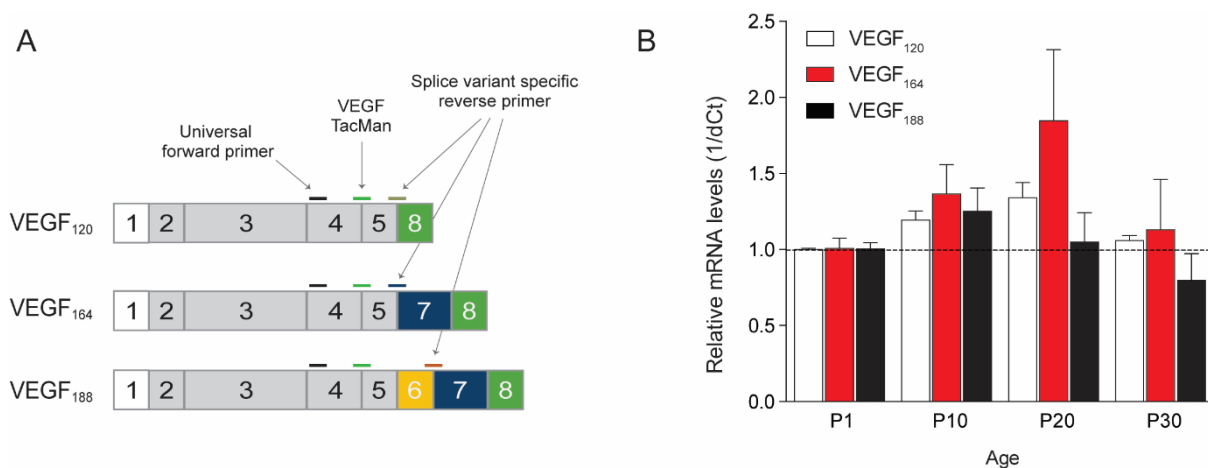


Figure 3.10 VEGF expression is elevated during early postnatal hippocampal development. **A**, Schematic of VEGF isoforms and corresponding binding location for the VEGF TaqMan probe, forward and reverse primers used for q-PCR assessment of hippocampal VEGF transcript levels. **B**, Relative mRNA transcript levels of VEGF₁₂₀, VEGF₁₆₄, and VEGF₁₈₈ mouse isoforms at P1 to P30 days of age in wildtype mice, normalized to P1 expression levels. All probed VEGF isoforms are detected within the hippocampus with VEGF levels upregulated within the first two weeks of postnatal development as compared to normalized expression values at birth (P1). n=3 independent experiments.

vessel sprouting (Meissirel, Ruiz de Almodovar, et al., 2011; Ruhrberg et al., 2002; Ruiz de Almodovar et al., 2010; Teran & Nugent, 2015; Yamamoto et al., 2016). Additionally, *in vitro* studies have shown that VEGF splice variants initiate signaling VEGFR2 at different activation strengths, inducing distinctive downstream signaling cascades in response to altered intercellular calcium release (Bergantino et al., 2015; Fearnley et al., 2015; King & Hristova, 2019). VEGF splice variants can also vary in their relative abundance depending on the developmental timepoint and tissue or organ type (Ng et al., 2001).

To determine if there was a developmentally dominant VEGF splice variant, qPCR analysis was performed on micro-dissected hippocampal tissues isolated from WT mice at P1, P10, and P20, P30 (Figure 3.10). Primers and FAM-tagged probes were designed to target specific VEGF transcript lengths (Figure 3.10A). Relative expression values of each VEGF transcript were normalized to that of β 2-microglobulin (B2m), a protein found in most nucleated cell types. VEGF transcript expression increases during the second and third weeks of mouse hippocampal development (Figure 3.10B). However, all three VEGF transcripts are detected in hippocampal tissues at P10 and therefore can contribute to VEGFR2 signaling in CA3 neurons at that time.

3.3.2 VEGF mRNA expression colocalizes with vessels, astrocytes, and neurons in mouse hippocampus.

As qPCR analysis of VEGF detected all major VEGFs splice variants in the postnatal hippocampus, (Figure 3.10B), we used fluorescence *in situ* hybridization (FISH) combined with immunohistochemistry to resolve the cellular location of VEGF mRNAs. Since VEGFR2 is locally expressed in CA3 neurons at P10, this same developmental timepoint was assessed for *in vivo* VEGF mRNA expression. Riboprobes were designed to target multiple regions of VEGF mRNA transcripts to amplify the expression signal for detection via confocal microscopy (Figure 3.11A). It has been reported that VEGF is expressed by multiple cell types, namely glia, neurons, and vessels in the brain (Chow et al., 2001; Jin et al., 2002; Ogunshola et al., 2000). Thus, VEGF FISH experiments were performed in combination with a GFAP riboprobe targeting astrocytes or protein antibodies labeling vessels (Pdx) or neurons (NeuN). In the hippocampus, *in situ* hybridization results show that VEGF mRNAs colocalize with neurons, vessels, and astrocytes throughout the P10 mouse hippocampus (Figure 3.11B).

The VEGF protein expression of each of these cell types was also investigated using an antibody that detects all VEGF isoforms (Figure 3.12). For vessels, there is a distinctive halo of VEGF signal within the proximal extracellular space (dotted line indicates signal border),

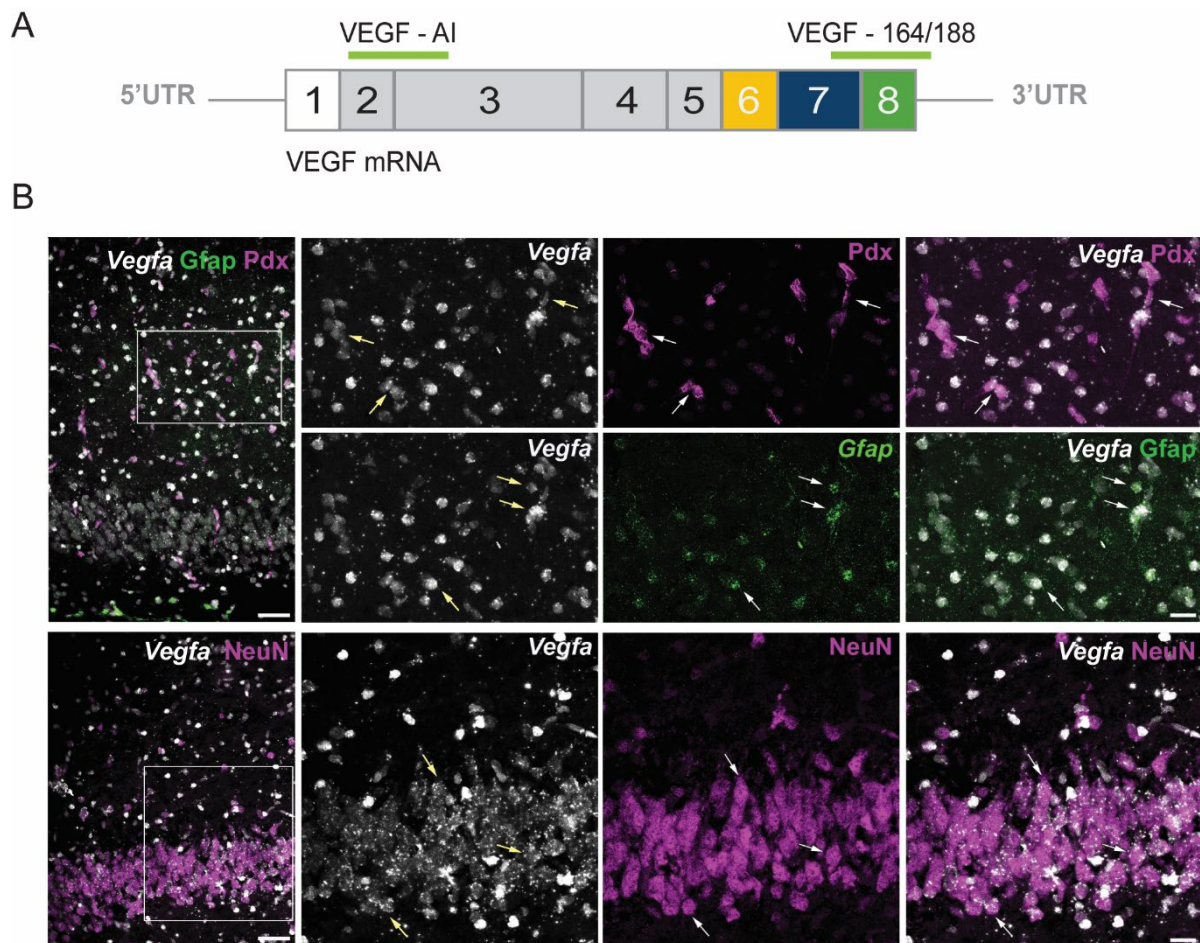


Figure 3.11 VEGF mRNA colocalize with neurons, astrocytes, and vessels within the early postnatal hippocampus. **A**, Schematic of *Vegfa* mRNA and the binding regions of *in situ* hybridization riboprobes used in combination to amplify the expression signal of VEGF mRNAs. **B**, Fluorescent *in situ* hybridization (FISH) of *Vegfa* co-labeled either riboprobed *Gfap* or immunolabeled Pdx (vascular maker) or NeuN (neuronal marker). *Vegfa* mRNAs detected in neuronal, vascular, and astrocytic cell types. Scale bar= 50 μ m (lower magnification), 25 μ m (higher magnification). Representative images of n=6 experiments.

while astrocytes have a more punctate signal located along individual processes (Figure 3.12A, next page). While in neurons, VEGF can be seen surrounding the somata of pyramidal neurons across all CA fields (Figure 3.12B, next page). VEGF₁₆₄ protein expression appears to be distinctly associated with each cell type, of which each produces micro domains VEGF diffusion gradients within their respective extracellular space.

3.3.3 Astrocytes secrete VEGF in response to cellular stimulation *in vitro*.

Results from this study show that VEGF mRNAs are expressed in hippocampal astrocytes *in vivo*. Although astrocytes reportedly secrete VEGF proteins, this has been associated with a hypoxia-induced upregulation of VEGF expression during BBB development or as apart of inflammatory signaling response (Argaw et al., 2012; Chow et al., 2001). Astrocytes participate in the uptake and release of extracellular metabolites that help to maintain the physiological microenvironments surrounding neuronal synapses. However, it is unclear if

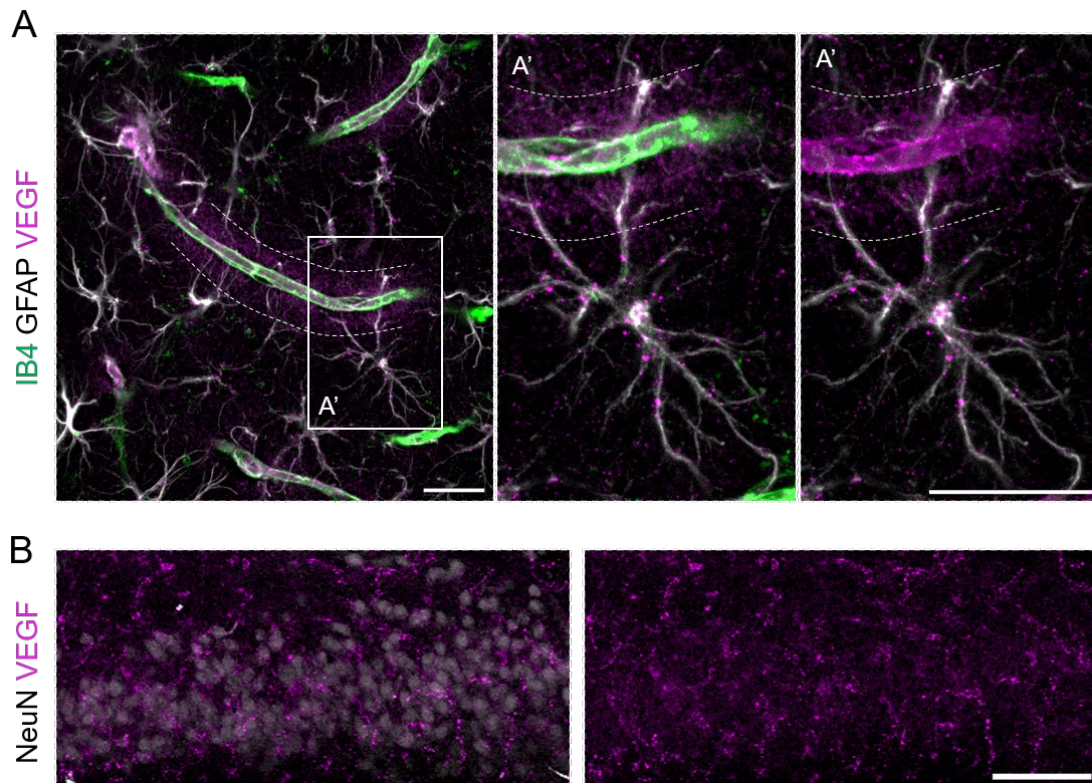


Figure 3.12 VEGF proteins surround vessels, astrocytes, and neurons within the CA3 hippocampal field. Representative images of VEGF immunohistochemistry in the postnatal hippocampus of the P10 mouse brain. **A)** A diffused VEGF signal surrounds IB4⁺ vessel (dotted line indicates the diffusion border), while VEGF⁺ punctate are located around astrocytes. **B)** VEGF proteins surround CA3 somata. Scale bars: 25 μ m.

there is neuro-astrocytic paracrine signaling between VEGFR2-expressing neurons and VEGF-releasing astrocytes in response to neuronal activity. Alternatively, astrocytes could participate in the extracellular removal of VEGF, reducing the activation potential of VEGFR2 in developing neurons independent of neuronal firing. To address these questions, the capacity of astrocytes to release VEGF in response to neuronal activity was tested *in vitro* (Figure 3.13).

For this purpose, astrocytes were isolated from pooled P4 wildtype mouse hippocampi and culture to >95% purity. Mimicking neuronal depolarization, astrocytes were stimulated for 30mins with or without 40mM KCl. Western blot analysis of cell lysates shows that there is an increase in astrocytic VEGF protein levels upon KCl stimulation (Figure 3.13A). VEGF mRNA levels in astrocytic cell lysates were also elevated upon stimulation with KCl (Figure 3.13B). Astrocytic cells were cultured on glass coverslips coated with PDL and laminin and processed immunocytochemically for cell surface VEGF labeling before cell permeabilization. Likewise, immuno-labeled cells showed an increase in VEGF upon KCl stimulation compared to non-stimulated controls (Figure 3.13C). Cells were immuno-labeled with a VEGF antibody which specifically targets VEGF₁₆₄. Due to its single HSPG

domain, VEGF₁₆₄ is weakly diffusible as compared to the highly diffusible, HSPG lacking VEGF₁₂₁ and the non-diffusible, membrane-bound VEGF₁₈₈, which contains two HSPG binding domains (Ferrara, 2010). Furthermore, VEGF₁₆₄, unlike VEGF₁₈₈, does not require proteolytic processing to bind to VEGFR2 (Koch & Claesson-Welsh, 2012). VEGFR2 is not expressed by astrocytes in the early postnatal *in vivo* mouse brain at P10 (Figure 3.1), nor in cultured astrocytes *in vitro* (data not shown). Taken together, the increase of VEGF₁₆₄ in KCl-stimulated culture astrocytes hints at the *in vivo* potential of astrocytes to locally release and activate neuronal expressing VEGFR2 at synapses in response to the physiological function of neurons.

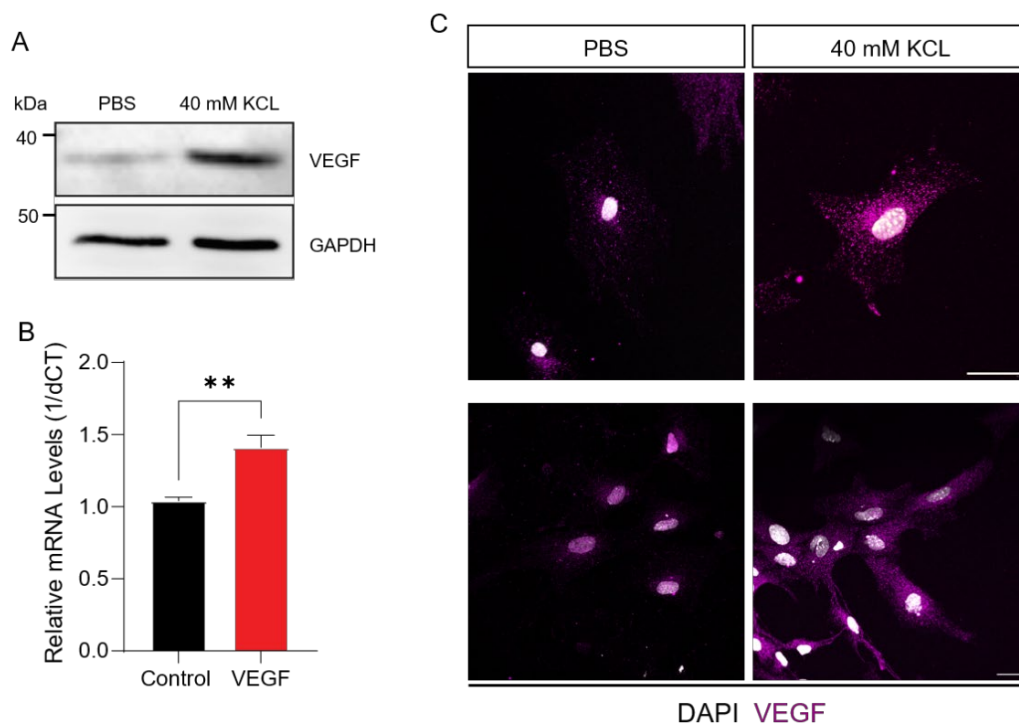


Figure 3.13 Astrocytes secrete VEGF in response to neuronal-like depolarizing stimulus *in vitro*. Primary cultured astrocytes isolated from P4 wildtype pooled mouse hippocampal tissues, cultured to >95% purity the stimulated with 40mM KCl to mimic activity induced neuronal polarization **A**) Western blot of astrocytic cell lysates showed an increased in VEGF protein levels after 30mins of 40mM KCl stimulation. **B**) KCl stimulation also induced an increase in astrocytic VEGF mRNA levels as detected by qPCR. n=4 wells per condition. \pm SEM, **p<0.01 **C**) Representative images of cultured astrocytes, with and without KCL stimulation, immunolabelled for surface VEGF. Top: Single cell, 63x Obj, Bottom: Cell cluster, 40x Obj. Scale bar= 25 μ m.

In summary, in the P10 mouse hippocampus VEGF is globally expressed by multiple cell types while VEGFR2 expression is confined to endothelial cells and CA3 hippocampal neurons at the same stage of development. There is a strong likelihood of a functional relationship between VEGF-secreting cells and the early postnatal development of CA3 hippocampal neurons. However, it is not clear if one specific cell type is critically involved in this process.

3.4 A mouse model for the targeted ablation of cell type-specific VEGF expression

During the first week of postnatal mouse brain development, VEGF is expressed by neurons, vessels, and astrocytes throughout the brain parenchyma. Alternative mRNA splicing of VEGF mRNAs produces localized chemo-attractive diffusion gradients within the extracellular matrix surrounding the ligand-secreting cell (Ambesi & McKeown-Longo, 2014; Egervari et al., 2016; Ng et al., 2001; Ruiz de Almodovar et al., 2010). This contrasts with the neuronal expression of the receptor for VEGF, VEGFR2, which is spatially restricted to CA3 pyramidal cells in the postnatal hippocampus. Therefore, we aim to identify the

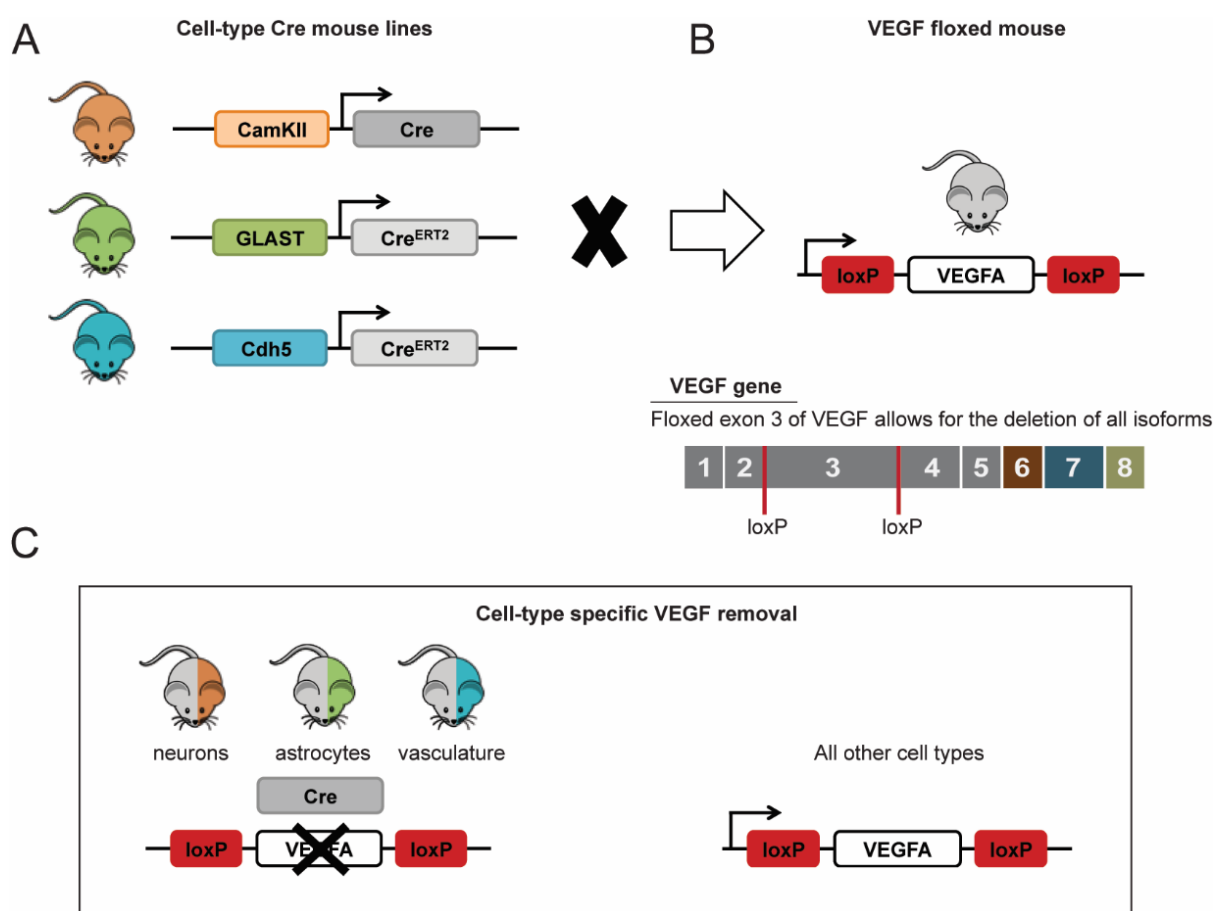


Figure 3.14 Schematic of mouse crossings for generating a cell specific VEGF deletion model using the Cre-LoxP gene modification technology. An overview of how to generate vascular, astrocytic, and neuronal cell specific knockdown mice of VEGF. A, Cre-LoxP is an established system to induced genomic editing using promoter driving Cre-recombinase cassettes that recognizes LoxP consensus cleavage sites. As VEGF expression is required for early embryonic development, Cre can be inserted downstream of late activated promoters such as the neuronal CaMKII promoter, which is turn on at P3-4. Alternatively, Cre-ER^{T2}, a tamoxifen-inducible modified Cre-cassette that unmasks Cre-recombinase activity when injectable tamoxifen molecules bind to the estrogen receptor (ER) binding motif of cytoplasmic sequestered Cre-enzymes, allowing nuclear translocation and genetic modification at LoxP sites. B, A VEGF-floxed mouse line carrying exon 3 flanked LoxP sites has been established (cite). C, Once each cell specific Cre mouse line is crossed with a VEGF-floxed mice, VEGF expression will be Cre-recombinantly knockdown in the targeted cell type upon induction while other cells would express VEGF normally.

potential functional relationship between VEGF-secreting cells and VEGF-VEGFR2 signaling facilitating the postnatal development of CA3 neurons.

A multi-mouse model with cell-specific targeted VEGF deletion would allow for the uncoupling of VEGF signaling at the neurovascular interface. Thus, allowing for the systematic analysis of neuro-vascular, neuroglial, and neuronal autocrine signaling of VEGF. Such an experimental mouse model system could be established using the *Cre/LoxP* system in genetically engineered mice (Figure 3.14), similar to the approach used in this study. Cre-LoxP mice are transgenic mice carrying the Cre-recombinase gene which recognizes and enzymatically cleaves LoxP sites resulting in the genetic alteration of genomic DNA strands (Branda & Dymecki, 2004). Cre expression could be driven in a cell-type specific matter if genetically inserted downstream of cell-type specific promoters (Figure 3.14A). Depending on the orientation of the LoxP sites, stretches of DNA can either be inverted or excised, resulting in the loss of gene function (Branda & Dymecki, 2004). If neuronal, astrocytic, or vascular-specific mouse Cre driver lines are then crossed with mice genetically modified with a VEGF gene containing paired LoxP sites (Figure 3.14B), VEGF gene expression could be knocked down in a cell-specific matter (Figure 3.14C). The resulting multi-modal VEGF deletion mouse model system would allow for the study of VEGF signaling at the neuro-vascular interface as a guidance molecule for neuronal circuitry formation.

To test the validity of this model, mice containing the *CaMKIIa* (neuronal), *GLAST* (astrocytic), or *Cdh5* (vascular) promoters directly upstream of Cre-recombinase were bred within the C57BL6/J mouse background as described (Figure 3.14A). Cre driver mice were then crossed with a (ROSA26)EYFP mouse (referred to as ROSA26 mice). These mice contain an Enhanced Yellow Fluorescent Protein (EYFP) gene inserted into the *Gt(ROSA)26Sor* locus (Srinivas et al., 2001). This strain serves as a reporter strain, with successful Cre excision being indicated by EYFP expression in Cre-expressing cells whereas all remaining cell types would be EYFP negative.

According to the Allen Developing Mouse Brain Atlas, *in situ* expression of *CaMKIIa* mRNA is detected in the mouse forebrain as early as postnatal day 3 (P3) (Thompson et al., 2014). Therefore, to assess the genetic onset of promoter activation, *CaMKIIa*-cre mice were crossed to ROSA26 mice, after which the off-spring were sacrificed at p5 and their brains underwent IHC analysis for YFP expression in the mouse hippocampus. At P5, *CaMKIIa*-cre ROSA26 mice exhibited induced YFP expression in all CA fields of the hippocampus (Figure 3.15). Whereas no YFP expression is observed in littermate control

mice. This induced expression is specific to neurons and is not observed in other cell types, as expression co-localizes only with NeuN⁺ somata. Furthermore, YFP expression levels are higher in homozygous CAMKIIa-cre ROSA26 mice as compared to heterozygous littermates. Thus, the expression level of YFP is dependent upon the level of CaMKIIa promoter-driven expression of Cre-recombinase. This indicates that the biologically induced Cre-recombinase activity is directly linked to the allelic activation of the CaMKII promoter.

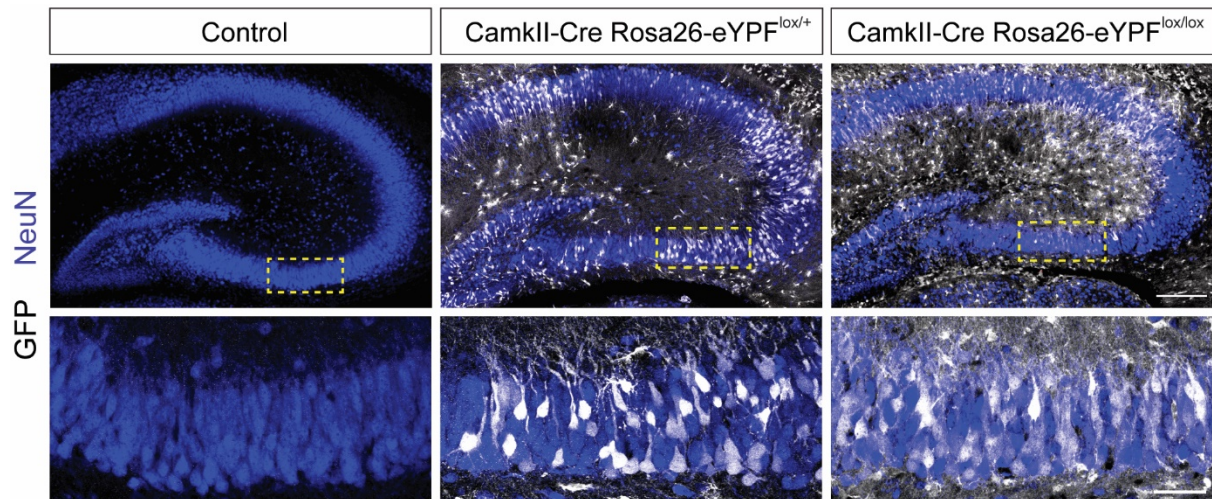


Figure 3.15 Validation of a neuronal cell targeted Cre mouse line. Mouse crossing of neuronal specific CaMKII-Cre mouse line with the ROSA26-eYFP^{lox/lox} reporter mouse line. Representative images of P5 mice are shown. ROSA26 mice have a LoxP-flanked stop codon that is downstream of YFP expression cassette. Cre expression is indicated by the YFP signal (white). In P5 mice, YFP expression is only detected in NeuN positive cells, but not in CaMKII-cre negative mouse controls. Homozygous, ROSA26-eYFP^{lox/lox} also have higher levels of YFP expression as compared to heterozygous mice, indicating a dependency upon Cre-recombinase expression level.

The *Cdh5* and *GLAST* promoters are active during the early stages of embryonic development. Therefore, this study utilized mice in which these respective promoters were fused to CreERT2, a tamoxifen-inducible variant of the Cre-recombinase gene. *Cdh5*-CreERT2 and the *Glast*-CreERT2 were crossed to the ROSA26 reporter mouse line and their respective offspring were assessed for the cell specificity of Cre activation. Postnatal mice were treated with 50 μ L of 1 mg/mL 4-OHT via intraperitoneal (i.p.) application, once every 24hrs, from P3-P5 in the case of *Glast*-CreERT2 mice. VEGF is highly expressed in the vasculature and critical to vascular development, which needs to be taken into consideration when one wants to investigate the effect of VEGF on neurons independent of the vasculature. Therefore, *Cdh5* CreERT2 Rosa26 mice were injected with tamoxifen from P5-P7 and assessed for YFP expression at P10, following the timeframe that would potentially be used in future *Cdh5*-cre VEGF-floxed mice. Brain tissues were excised for IHC processing of which representative images are shown in Figure 3.16 and Figure 3.17.

Cdh5-CreERT2 ROSA26 mice showed strong vascular-specific YFP expression upon 4-OHT induction when compared to control mice (Figure 3.16). Glst-CreERT2 ROSA26 mice required inbreeding to the F4 generation before sufficient YFP expression could be detected in a significant proportion of astrocytic cells (data not shown). In mice off-spring inbred beyond the F4 generation, three consecutive injections of 4-OHT were sufficient to effectively induce CreERT2 activity as shown by ROSA26 YFP expression (Figure 3.17). The ROSA26 signal, reflecting the cellular expression and activation of Cre-recombinase is restricted to and highly expressed in the astrocytic cell populations.

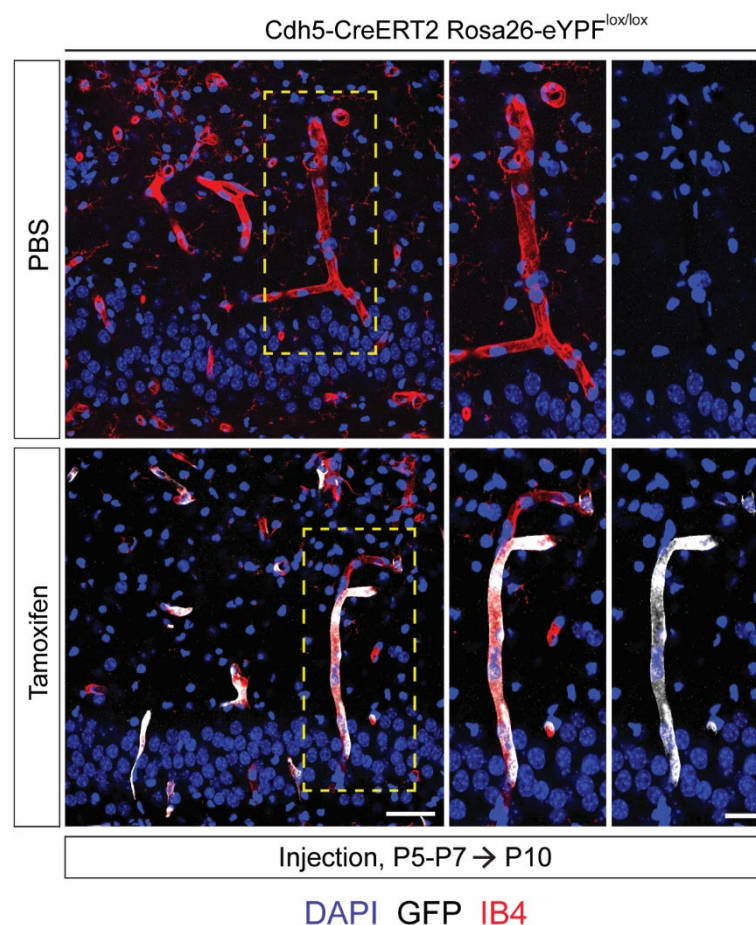


Figure 3.16 Validation of an endothelial cell targeted Cre mouse line. Mouse crossing of a vascular endothelial cell specific Cdh5-CreERT2 mouse line with the ROSA26-eYFP^{lox/lox} reporter mouse line. Representative images of P10 mice are shown. Vascular deletion of VEGF is embryonically lethal, therefore a mouse line with a tamoxifen inducible Cre-expression cassette was used. Tamoxifen was administered between P5-7 and by P10 YFP expression is strongly expressed in the vasculature in ROSA26-eYFP^{lox/lox} reporter mice while completely absent in Cdh5-CreERT2 only mice.

Once the specificity of each promoter was proven, mice were bred to VEGF-floxed mice (generously donated by the research group of Prof. Dr. Ralph Adams) for the analysis of autonomous and non-autonomous effects on the postnatal development of CA3 neurons.

Due to time constraints, the completion of this phase of the study was continued by another Ph.D. student in the lab of Prof. Dr. Amparo Acker-Palmer.

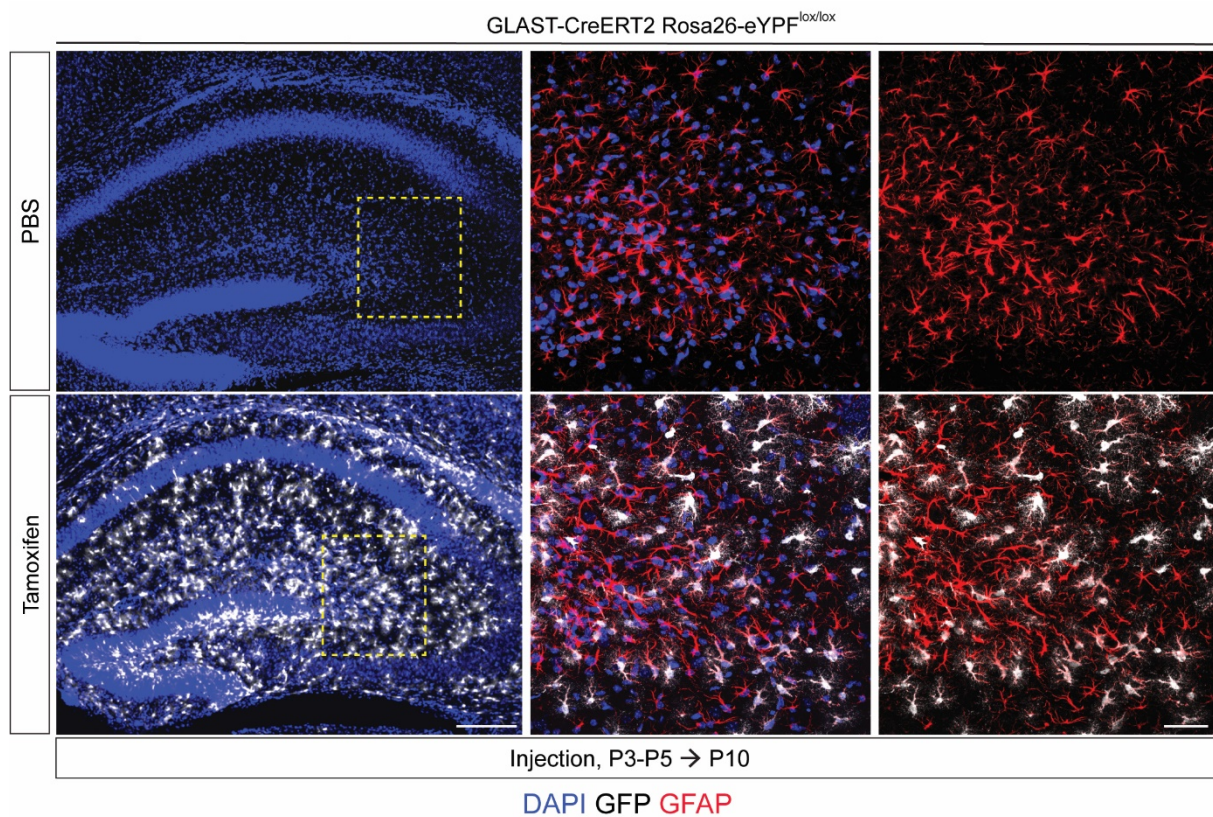


Figure 3.17 Validation of an astrocytic cell specific Cre mouse line. Mouse crossing of the astrocytic cell specific GLAST-CreERT2 mouse line with the ROSA26-eYFP^{lox/lox} reporter mouse line. Representative images of P10 mice are shown. Tamoxifen was administered between P3-5 and by P10 YFP expression is strongly expressed in the astrocytic cells throughout the hippocampal formation in ROSA26-eYFP^{lox/lox} reporter mice as compared to the null expression observed in GLAST-CreERT2 only mice.

However, the *Cre/LoxP* system is a versatile tool that allows for the reliable and reproducible genetic modification of targeted gene expression in a tissue- and cell-specific manner in mice (Branda & Dymecki, 2004; Gavériaux-Ruff & Kieffer, 2007). This enables one to precisely control the timing and location of gene expression, making it a valuable tool for evaluating the biological relevance of specific gene functions. As such, this type of multi-mouse model deletion system could be used to study the capacity in which VEGF-secreting cells can coordinate neuronal circuitry development via neuronal expressing VEGFR2 in the early postnatal hippocampus.

4 Discussion

The development of neurons and blood vessels is physiologically coupled through shared signaling molecules and mechanisms (Carmeliet & Tessier-Lavigne, 2005; Paredes et al., 2018; Tam & Watts, 2010; Walchli, Wacker, et al., 2015). At the neurovascular interface, cellular crosstalk via these dualistic signaling mechanisms facilitates the coordinated expansion and integration of neurons and vessels into complex cellular networks (Tata & Ruhrberg, 2018). This study investigated the localized expression and function of VEGFR2, a receptor for vascular endothelial growth factor (VEGF), during postnatal neuronal development in the mouse hippocampus. VEGF is a secreted guidance cue critical to developmental angiogenesis. VEGF has also been functionally linked to various aspects of neuronal development (Mackenzie & Ruhrberg, 2012), including neuronal migration (Ruiz de Almodovar et al., 2010; Schwarz et al., 2004), neurite outgrowth (Sondell et al., 2000), and synaptic plasticity (De Rossi et al., 2016; Licht et al., 2011). However, it was not clear if VEGF signaling had a direct effect on neuronal physiology and function through neuronal-expressing receptors. In this study, we describe a previously unknown function of VEGFR2, of which VEGF-induced signaling coordinates the development and circuitry integration of CA3 pyramidal neurons. We found that the VEGFR2 activation and signal transduction requires receptor endocytosis via a process modulated by interactive signaling with ephrinB2 at neuronal cell membranes. Furthermore, cooperative signaling between VEGFR2 and ephrinB2 is physiologically required for dendritic arborization and spine maturation of CA3 neurons. We previously identified a similar signaling mechanism that promoted angiogenic sprouting in retinal endothelial tip cells (Sawamiphak et al., 2010). Collectively, our findings demonstrate a conserved functional role of VEGF in neurovascular signaling, further highlighting how vascular signaling cues can coordinate nervous system development and physiology.

This study investigated the role of VEGF-VEGFR2 signaling in the dendritic development of CA3 neurons. The research was part of a collaborative effort with Carmen Ruiz de Almodovar's group, formally of the University of Heidelberg, which studied VEGF-VEGFR2 signaling in CA3 axonal development. By working together, we aimed to gain a comprehensive understanding of the complex interplay between VEGF-VEGFR2 signaling and the development of CA3 neurons. Our findings on CA3 dendritic development, some of which are discussed below, were published in Harde et al. (2019). The complementary work on CA3 axonal development from Ruiz de Almodovar's group was presented in the co-published manuscript, Luck et al. (2019). Although the totality of Ruiz de Almodovar's

group's work on CA3 axons is not fully discussed here, it is referenced where noted to provide biological context for our findings on CA3 dendritic development.

4.1 VEGF induces VEGFR2-ephrinB2 cooperative signaling in neurons

Many studies have pointed to a direct physiological role of VEGF, a pro-angiogenic mitogen, in CNS development (Ruiz de Almodovar et al., 2009). VEGFR2 was found to be expressed on cultured neural progenitor cells *in vitro*, however, receptor expression varied both spatiotemporally in neural progenitor cells *in vivo* (Javaherian & Kriegstein, 2009; Meissirel, de Almodovar, et al., 2011; Tata et al., 2016). Also, both VEGF and VEGFR2 are highly expressed by endothelial cells (Ogunshola et al., 2000; Okabe et al., 2014). Consequently, the initial observed neurotrophic effects of VEGF were closely associated with VEGF signaling within angiogenic niches (Meissirel, Ruiz de Almodovar, et al., 2011; Ruiz de Almodovar et al., 2009). Unsurprisingly, studies resulting in cortical abnormalities when using either global or endothelial-specific knockdown of VEGF expression also exhibited severely impaired vascular development (Li et al., 2013). Therefore, it was unclear if the physiological effect of VEGF on developing neurons was the result of direct VEGFR2 signaling activity in neurons or via an indirect angiogenic signaling axis. To answer this question, we investigated the nervous system-specific functional role of VEGFR2 expression *in vivo* as well as its mechanism of action on developing neurons using cultured primary hippocampal neurons.

A direct functional role of VEGFR2 in nervous system development was first investigated using a conditionally knockdown approach of either VEGF or VEGFR2 expression in neurons in a study conducted by Haigh et al. (2003). Deletion of neuronal VEGF in this model system resulted in embryonic lethality by E15.5 due to severe cortical degeneration resulting from hypoxia and poor CNS vascularization (Haigh et al., 2003). In contrast, mice deficient in neuronal VEGFR2 developed normally, leading Haigh and colleagues to conclude that angiogenic paracrine VEGF/VEGFR2 signaling was the key factor in determining the architectural organization and development of the CNS. However, in a later study conducted by Bellon et al. (2010), VEGFR2 was found to be expressed in the fimbria and postcommissural fornix along axons projecting from the subiculum of the hippocampus to the mamillary bodies of the hypothalamus in E17.5 mice. In collaboration with the C. Ruiz de Almodovar research group, formerly at the University of Heidelberg, we studied the temporal expression of VEGFR2 in the postnatal mouse brain. Our colleagues could show that by postnatal day 4 (P4), VEGFR2 mRNAs are specifically expressed in the CA3 region

of the WT mouse hippocampus (Luck et al., 2019). Using both the immunological detection of VEGFR2 and a GFP knock-in mouse model of VEGFR2 promoter activity, we found neuronal VEGFR2 protein expression to be spatially confined to CA3 pyramidal neurons (Figure 3.1, Figure 3.2). Within these neurons, expression was strongest within the first two postnatal weeks after birth (Figure 3.1, Figure 3.2) (Luck et al., 2019). Simultaneously, secreted VEGF proteins are also strongly expressed throughout entire the hippocampus (Figure 3.11).

In the first weeks after birth, neurons within the mouse hippocampus enter a phase of rapid outgrowth and maturation of neurite processes (Figure 2.2) (Dailey & Smith, 1996; Kirov et al., 2004). This process includes extensive dendritic arborization and the onset of synaptogenesis with ongoing synaptic remodeling. VEGF stimulation-induced neurite extension and spine formation has been demonstrated in cultured neurons (Böcker-Meffert et al., 2002; Jin et al., 2002; Rosenstein et al., 2003). Furthermore, a corresponding decrease in synapse formation was also observed in newborn neurons in the olfactory bulb when VEGF signaling is sequestered by soluble VEGFR1 injection (Licht et al., 2010). In this study, we observed that VEGFR2 is spatiotemporally expressed in CA3 pyramidal cells during a confined postnatal timeframe. As VEGF ligands primarily bind and activate VEGFR2, we hypothesized that VEGF-induced VEGFR2 signaling would control the morphological and functional development of these neurons at this time point.

VEGF ligand-induced VEGFR2 activation and signaling have been demonstrated in neurons, although the mechanism action has not been fully understood until now (De Rossi et al., 2016; Licht et al., 2010; Licht et al., 2011; Meissirel, Ruiz de Almodovar, et al., 2011; Sondell et al., 2000). VEGFR2 is a type IV RTK, which can transduce signals at the cell surface as well as undergo receptor internalization and trafficking by co-receptors to activate various intracellular signaling pathways (Basagiannis & Christoforidis, 2016; Nakayama et al., 2013; Zhang & Simons, 2014). As such, the interaction of VEGFR2 with co-receptors has been found to fine-tune VEGFR2 signaling in vessel angiogenesis. Type IV RTKs are involved in the downstream activation of Src and Akt signaling pathways to promote cell survival, proliferation, and migration in endothelial cells and fibroblasts (Holmqvist et al., 2003; Zhang et al., 2003). VEGF has also been shown to activate Src Kinase in migrating granule cells within the cerebellum (Meissirel, Ruiz de Almodovar, et al., 2011). In a previous study from our research group, we identified a signaling mechanism in vessels in which ephrinB2 regulates the internalization of VEGFR2 at endothelial tip cells upon VEGF stimulation (Sawamiphak et al., 2010). In this context, ephrinB2 facilitated the dynamin-mediated endocytosis of VEGFR2 into clathrin-coated vesicles. Internalized

VEGFR2 signaling led to the subsequent activation of the Akt signaling pathway to promote endothelial cell survival and proliferation. Additionally, the study showed that VEGFR2-ephrinB2 signaling phosphorylates Src and its downstream effector protein, FAK, to enhance endothelial cell sprouting. When probing for ephrinB2 *in vivo*, we found it to be expressed throughout the postnatal mouse hippocampus with colocalized expression with VEGFR2 in CA3 neurons (Figure 3.2). Collectively, this evidence suggested a VEGFR2-ephrinB2 signaling mechanism with a functional role in neurons and we explored this plausibility.

Our approach was to investigate if VEGF could induce the activation of VEGFR2 and its downstream signaling partners in the absence of ephrinB2. Our *in vitro* analysis using primary WT cultured neurons shows that VEGF stimulation increases the phosphorylation of both ephrinB2 and VEGFR2. Conversely, VEGF-induced VEGFR2 phosphorylation is greatly reduced in primary cultured neurons isolated from Nes-cre ephrinB2^{lox/lox} mice. While VEGF stimulation enhances VEGFR2 internalization, receptor endocytosis was blocked in Nes-cre ephrinB2^{lox/lox} neurons. Interestingly, in these same neurons, the surface expression of VEGFR2 was also increased (Figure 3.3D). These findings suggest that VEGFR2 recycling upon VEGF stimulation is impaired with less receptor internalization resulting in the increased cell surface insertion of VEGFR2 in the absence of ephrinB2. It further indicates the potential for ephrinB2 to facilitate the degradation of VEGFR2 and reduced its cell surface availability, which has been an observed feature of VEGFR2 signaling (Horowitz & Seerapu, 2012; Nakayama et al., 2013; Sawamiphak et al., 2010; Wang et al., 2010). Upon activation, type IV RTK can transduce signals at the cell surface and can also continue to signal within endocytic vesicles (Basagiannis et al., 2016; Lampugnani et al., 2006; Nakayama et al., 2013). Therefore, we examined if VEGFR2 internalization was required for downstream signaling. When dynamin-dependent endocytosis was blocked, VEGF stimulation failed to induce the phosphorylation of VEGFR2 as well as Src and Akt. Thus, receptor internalization is required for activation and downstream signaling. ephrinB2 may mediate VEGFR2 activation signal transduction by promoting receptor internalization for proper signaling. Similarly, it has been shown that Nrp1 binding orients VEGFR2 to enable VEGF-induced dimerization and receptor activation (Horowitz & Seerapu, 2012; Koch & Claesson-Welsh, 2012; Sarabipour et al., 2023; Teran & Nugent, 2015). Alternatively, VEGFR2 could be maintained in a dephosphorylated state by cell surface protein phosphates as previously reported (Lampugnani et al., 2006; Sarabipour et al., 2023). Thereby requiring both VEGF stimulation and ephrinB2-mediated endocytosis for full receptor activation. Our findings do show that the *in vitro* activation of

VEGFR2 requires the presence of ephrinB2. However, due to the experimental limitations of this study, it is unclear if ephrinB2 participates in the phosphorylation of VEGFR2, for example via ephrinB2 reverse signaling by EphB4. It has been demonstrated that ephrinB2 reverse signaling can activate Src, leading to increased spine formation in hippocampal neurons (Essmann et al., 2008). ephrinB2 has also been shown to regulate the outgrowth and repulsion motility of axons via Src and Akt signaling (Davy & Soriano, 2005; Palmer et al., 2002). Similar roles of ephrinB2 involvement in Src and Akt activation have also been described in endothelial cells (Davy & Soriano, 2005; Sawamiphak et al., 2010; Wang et al., 2010). To establish if there is a direct signaling interaction with VEGFR2, one could truncate the extracellular or intercellular domains of ephrinB2 and assess if these downstream signaling partners are still activated upon VEGF stimulation of VEGFR2. Additionally, one could assess if EphB4 stimulation of ephrinB2 either enhances or abolishes VEGFR2 function in neurons.

However, although not presented here, there is strong evidence that VEGF induces the formation of a signaling complex between VEGFR2 and ephrinB2. In collaboration with Eva Harde, of which our findings are reported in Harde et al. (2019), we could show that ephrinB2 physically interacts with VEGFR2 in neurons. In hippocampal neuronal cell lysates, VEGFR2 co-immunoprecipitation occurs when ephrinB2 is pulled down using the ectodomain of its associated receptor, EphB4, fused to Fc (Harde et al., 2019). VEGFR2 also colocalizes with ephrinB2 in EEA1 positive endosomes in WT neurons, which is enhanced by VEGF stimulation but is diminished in the absence of ephrinB2 (Harde et al., 2019). Most significantly, it was found that VEGF-ephrinB2 complexes are spatially localized to synaptic puncta and are required for VEGF-mediated spine morphogenesis (Branda & Dymecki, 2004). Collectively, these findings show that ephrinB2 co-operatively interacts with VEGFR2, thereby modulating VEGF-induced signal transduction. In conclusion, VEGFR2-ephrinB2 signaling is not limited to angiogenesis, having a conserved role in neuronal signaling and functional development.

4.2 VEGF signaling promotes the development and circuitry formation of CA3 pyramidal neurons.

In this study, we have described the mechanism by which VEGF stimulation induces VEGFR2 activation and downstream signaling responses in hippocampal neurons *in vitro*. Our findings corroborate those of other *in vitro* studies that have shown increased neurite outgrowth in cortical explants and primary cortical neurons treated with VEGF (Böcker-

Meffert et al., 2002; Jin et al., 2002; Rosenstein et al., 2003). Furthermore, our findings demonstrate the underlying functional mechanism for VEGF-induced synapse formation observed in hippocampal neuron cultures (Harde et al., 2019; Jin et al., 2002; Meissirel, Ruiz de Almodovar, et al., 2011). *In vivo* expression of VEGF and VEGFR2 has been observed in the adult hippocampus, although VEGF expression was found to be downregulated over time (De Rossi et al., 2016; Licht et al., 2011; Ogunshola et al., 2000; Wang et al., 2005). However, studies have reported that increased VEGF levels coincide with spine formation and enhanced potentiation or functional activation of hippocampal neurons *in vivo* (Huang et al., 2012; Licht et al., 2010). Despite the proposed functional role of VEGF ligands in dendrite development and spine morphogenesis *in vivo*, little was known about the localization of VEGFR2 during hippocampal development at that time. Nor had it been fully established that VEGFR2 was the neuronal receptor that played a direct role in these processes as signaling at the neurovascular has direct and indirect physiological effects on the nervous system. VEGF and VEGFR2 are highly expressed in the brain vasculature, in which their respective targeted downregulation indirectly impairs CNS development (Carmeliet et al., 1996; Li et al., 2013; Ng et al., 2001; Yang et al., 2013). VEGF/VEGFR2 signaling has also been functionally linked to BDNF expression in endothelial cells (Chen et al., 2005), of which endothelial expressions of both VEGF and BDNF are upregulated in neurorestorative treatments used in stroke models (Chen et al., 2002; Matsuno et al., 2004). BDNF is a well-known neurotrophic factor and cognate receptor for TrkB with extensively studied effects on neuronal development, including dendritic arborization and synaptogenesis as well as their maturation and maintenance (Cohen-Cory et al., 2010). Neuronal expressing VEGFR2 was shown to directly coordinate the pathfinding of subiculo-mamillary axons, albeit through the mechanistic association with co-receptors Plexin/Nrp1 as a binding complex for Sema3E in a process independent of VEGF (Bellon et al., 2010). In this study, we present experimental evidence that there is a colocalized expression of VEGFR2 and ephrinB2 in CA3 pyramidal cells in the first weeks after birth in the mouse hippocampal (Figure 3.2). During the postnatal development of the hippocampus, the growth and stabilization of dendritic trees are strongly coupled to spine formation and maturation (Dailey & Smith, 1996; Fischer et al., 1998; Li et al., 2011). In a signaling mechanism analogous to that in the vasculature, we also show that VEGF induces a VEGFR2-ephrinB2 signaling complex that is required for spine morphogenesis *in vitro* (Figure 3.3, Figure 3.4, corresponding spine morphogenesis results are published in Harde et al. (2019)). We therefore proposed that a similar signaling mechanism was responsible for the early postnatal development of CA3 dendrites *in vivo*.

First, we verified the *in vivo* functional role of VEGFR2 in CA3 neurons through targeted genetic deletion from the nervous system. VEGFR2 is expressed in the vasculature and neurons throughout CNS development and into adulthood (Bellon et al., 2010; Meissirel, Ruiz de Almodovar, et al., 2011; Nowacka & Obuchowicz, 2012; Okabe et al., 2020). Reportedly, VEGFR2 is also upregulated in Schwann cells/oligodendrocytes, pericytes, and astrocytes (Hayakawa et al., 2011; Scott et al., 2010; Sweeney et al., 2016). To understand the importance of postnatal upregulation of VEGFR2 in CA3 pyramidal neurons, we pursued a nervous system deletion of VEGFR2 using the *Cre/loxP* system. Cre-mediated recombination is a broadly used tool that selectively modifies gene expression through the enzymatic targeting of loxP consensus binding sites (Branda & Dymecki, 2004). Here we used genetically modified mice containing in-frame *loxP* sites flanking exon 1 of the genomic VEGFR2 sequence (Mühlner et al., 1999). Mice were bred to generate VEGFR2^{lox/-} mice, which possess both a VEGFR2-floxed allele and a non-functional allelic expression of VEGFR2 resulting from parental Cre-recombinant knockdown. In the experimental paradigm used in this study, VEGFR2^{lox/-} mice were crossed with mice expressing Cre-recombinase under the control of the Nestin promoter, resulting in a reduction of VEGFR2 specifically in the nervous system as previously described (Dubois et al., 2006; Haigh et al., 2003; Petersen et al., 2002). The offspring of these mice were further crossbred with the Thy1-GFP M1 mouse line, which sparsely expresses GFP in neurons allowing for the unimpaired visualization of full dendritic tree structures (Feng et al., 2000; Vlachos et al., 2013). In mice, Nestin expression is observed in neural progenitor cells and detected as early as E11 in the neurogenic niches of various tissues and organs (Kamei et al., 1998; Lendahl et al., 1990; Mignone et al., 2004). Thus, the promoter-driven upregulation of Nestin coincides with late embryonic and early postnatal stages of neurogenesis. Although greatly reduced in the adult brain (Kamphuis et al., 2012), Nestin expression persists in the subventricular zone and hippocampus (Encinas et al., 2011; Kokoeva et al., 2007). Nestin-Cre mouse models are also ideal for studying neuronal development because the targeted genetic recombination event is maintained in the progeny of Nestin-expressing cells (Bernal & Arranz, 2018; Dubois et al., 2006; Mignone et al., 2004). Crossbreeding VEGFR2^{lox/-} with Nestin-cre mice allows for the assessment of neuronal VEGFR2 function during postnatal development independent of its functional role in the vasculature.

In our Nestin-cre VEGFR2^{lox/-} mouse model, the dendritic trees of CA3 neurons exhibited stunted growth with decreased branch complexity coupled with a strong reduction in spine head size (Figure 3.6, Figure 3.7). Additionally, there was also an overall reduction in spine density. Our findings indicate that the *in vivo* dendritic development and spine

morphogenesis of CA3 pyramidal cells depend on neuronal VEGFR2 signaling. To corroborate our *in vitro* results showing ephrinB2 regulates VEGF-induced VEGFR2 signaling, we extended our *in vivo* analysis to Nestin-cre VEGFR2^{lox/+} ephrinB2^{lox/+} mice crossbred into the same Thy1-GFP neuronal reporter line. Nestin-cre VEGFR2^{lox/+} ephrinB2^{lox/+} mice allowed for the simultaneous conditional knockdown of VEGFR2 and ephrinB2 expression within the same Nestin-expressing cells. Consistent with the phenotypical observations in Nestin-cre VEGFR2^{lox/-} mice, compound Nestin-cre VEGFR2^{lox/+} ephrinB2^{lox/+} mice also showed impaired dendritic arborization and synapse maturation. However, in correspondence with VEGFR2 and ephrinB2 protein levels in Nestin-cre VEGFR2^{lox/+} ephrinB2^{lox/+} mice, the overall developmental defects were reduced as compared to Nestin-cre VEGFR2^{lox/+}. Furthermore, single Nestin-cre VEGFR2^{lox/+} Nestin-cre ephrinB2^{lox/+} develop normally with no neuronal or vascular defects (unpublished data produced by Eva Harde). The requirement of both VEGFR2 and ephrinB2 for proper dendritic development and spine morphogenesis of CA3 neurons *in vivo* suggests a genetic interaction between these two proteins. Our *in vitro* experiments demonstrate that VEGFR and ephrinB2 interact, as a VEGF-induced signaling complex, to promote spine formation and maturation through the activation of Src and Akt signaling pathways (Figure 3.4, corresponding spine morphogenesis results are published in Harde et al. (2019)). These congruent findings strongly suggest that VEGF also induces a developmentally required VEGFR2-ephrinB2 signaling complex *in vivo*.

Our investigation primarily focused on identifying the functional role of VEGFR2 in the dendritic development of CA3 pyramidal cells, which exhibit localized expression of this receptor during the first two postnatal weeks (Figure 3.2). However, VEGFR2 expression is not spatially restricted to the somatodendritic compartment of neurons; it is also expressed in axons and plays a functional role in axonal pathfinding (Ruiz de Almodovar et al., 2011; Tillo et al., 2015). Moreover, VEGF stimulates axonal development and promotes axonal migration through chemoattractive signaling at axonal growth cones (Böcker-Meffert et al., 2002). Therefore, it was highly plausible that VEGFR2 signaling is also functionally involved in the outgrowth and development of CA3 axonal arbors. CA3 pyramidal cells project their axons, the Schaffer collaterals, to the CA1 region of the hippocampus (Szirmai et al., 2012). In mice, the initial formation of Schaffer collateral projections from CA3 pyramidal cells is observed around P3-P4 (Li et al., 1994), with the axons beginning to form synaptic contacts with target cell dendrites in the CA1 region between P5-P10 (Li et al., 1994; O'Brien et al., 1999). These initial synapses are relatively weak and undergo extensive remodeling and strengthening over the following weeks and into adulthood, as the animal matures and

experiences various learning and memory tasks (Dumas, 2005; Fischer et al., 1998; Kirov et al., 2004). Overall, the formation and maturation of Schaffer collateral projections is a dynamic process that coincides with the upregulation of VEGFR2 expression in CA3 pyramidal cells.

As a complementary investigation, our colleagues in the research group of C. Ruiz de Almodovar studied the physiological role of VEGFR2 during the axonal development of CA3 pyramidal cells in the early postnatal hippocampus. For their experimental analysis, they utilized the same Nestin-cre VEGFR2^{lox/-} and compound Nestin-cre VEGFR2^{lox/+} ephrinB2^{lox/+} mice, of which the totality of their findings are reported in (Luck et al., 2019). In summary, our colleagues found that VEGF-induced VEGFR2 signaling also regulates axonal branching in developing CA3 neurons. In their approach, they used a primary hippocampal neuron culture system to determine if VEGFR2 is mechanistically required for axonal branching dynamics. Cultured neurons undergo well-defined developmental stages with axon specification and outgrowth beginning at DIV3 (Goslin & Banker, 1989). VEGFR2 expression is localized at axonal branch points and within the filopodial structures of axonal growth cones in culture neurons (unpublished data from Eva Harde). Our colleagues observed VEGFR2 internalization and its subsequent association with activated Src in F-actin-rich patches within the growth cone and along the axon shaft, particularly at subsequent branch points, in neurons stimulated with VEGF (Luck et al., 2019). This is consistent with a previously reported role of VEGF in regulating Src-dependent guidance of commissural axonal fibers (Ruiz de Almodovar et al., 2011). In endothelial cells, F-actin is highly enriched within the filopodia of endothelial tip cells, in which VEGFR2 signaling controls tip cell behavior through the probing and navigation towards VEGF within ECM environments (Fraccaroli et al., 2012; Gerhardt et al., 2003; Nakayama et al., 2013). In one study, knockdown of VEGFR2 expression in human umbilical vein endothelial cells (HUVECs) resulted in shorter less complex cellular networks with excessive filopodia productions (Simmons et al., 2018). It is interesting to note that disrupted VEGFR2 signaling similarly leads to hyperactive production of immature filopodial protrusions along the axons of Nestin-cre VEGFR2^{lox/-} cultured neurons and *in vivo* CA3 pyramidal cells, resulting in shortened yet highly branched axonal arbors (Luck et al., 2019). Thus, VEGFR2 is not involved in the formation of axonal branches of CA3 Schaffer collaterals but instead is required for their stabilization and maturation. This contrasts with our findings, where the loss of VEGFR2 leads to a reduction in the number of dendritic branches and spine density as well as impaired spine maturation of CA3 neurons. In further divergent findings, CA3 axons of Nestin-cre VEGFR2^{lox/+} ephrinB2^{lox/+} mice develop normally, while dendritic

development is impaired (Figure 3.8) (Harde et al., 2019; Luck et al., 2019). The observations suggest that the VEGF-induced VEGFR2 signaling had distinct physiological roles in the axons and dendrites of CA3 neurons.

Compartmentalized functions have been reported for other neuronal guidance molecules such as Sema3A, which inhibits axonal growth while promoting dendritic outgrowth (Schwarz et al., 2004). Likewise, BDNF signaling through TrkB activates calcium-dependent and calcium-independent signaling cascades in cell dendrites and axons, respectively (Cohen-Cory et al., 2010). However, in conjunction with our colleagues' findings, we have determined that VEGFR2 signaling supports the development and maturation of both CA3 axons and dendrites. This suggests that there may be a difference in the intracellular trafficking of VEGFR2 between these two cellular compartments. In cultured neurons transfected with VEGFR2-GFP, VEGF stimulation enhances VEGFR motility and migration towards actin-rich patches at the base of filopodia protrusion, promoting branch development and outgrowth (Luck et al., 2019). This dynamic actin-associated process involves the signaling of activated VEGFR2 and Src, independent of the ephrinB2 function (Luck et al., 2019). Antibody blockade of Nrp1 signaling demonstrates that Nrp1 does not act as a co-receptor for VEGFR2 in hippocampal neurons, as it has no impact on the axonal branching of hippocampal neurons (Luck et al., 2019). Nor does Nrp1 participate in compensatory VEGF signal transduction in Nestin-cre VEGFR2^{lox/-} neurons to counteract the increased production of immature filopodial in axons (Luck et al., 2019). Therefore, there is an unidentified mechanism that modulates VEGF-VEGFR2 signaling in CA3 axons that is independent of both Nrp1 and ephrinB2. One potential class of candidate molecules is the Ras homologous (Rho) family of GTPases, a group of membrane-associated intracellular signaling G proteins, reviewed by (Govek et al., 2005). Rho GTPases are considered 'molecular switches' that regulate cellular processes, such as axonal outgrowth and cell motility, by controlling cytoskeletal and cell adhesion dynamics (Govek et al., 2005). Guanine nucleotide exchange factors (GEFs) and GTPase-activating proteins (GAPs) are regulators of Rho GTPase activity, respectively catalyzing conversion between the active and inactive states of Rho (Govek et al., 2005). Additionally, a third class of regulator proteins, guanine nucleotide dissociation inhibitors (GDIs), forms a membrane anchoring complex to spatially control Rho activity (Govek et al., 2005). Activated Src can interact with the Rho GTPase signaling pathway depending on the biological context and adaptor proteins involved (Su et al., 2004; Wang et al., 2010). For example, Src can regulate Rho activity through the phosphorylation of GEFs, such as Vav2 which is reportedly involved in axon and spine morphogenesis (Cowan et al., 2005; Hale et al., 2011). Separate studies

involving VEGF stimulation and stimulation of Eph receptors have induced Vav2 activity (Cowan et al., 2005; Garrett et al., 2007). ephrins have also been shown to mediate spine formation and maturation via Rho signaling (Yoshihara et al., 2009). The exact mechanism for VEGF-induced VEGFR2 internalized signaling in the CA3 axon remains unclear. However, considering these points, there is a strong possibility that Rho GTPase activity is involved, possibly through Eph receptor reverse signaling.

Together with our collaboration partners, we have presented evidence demonstrating that VEGF/VEGFR2 signaling plays a crucial role in the postnatal development of axonal and dendritic compartments of CA3 pyramidal cells. For the transduction of VEGF signals, internalization of VEGFR2 is required for both cellular compartments. In dendrites, ephrinB2 regulates VEGFR2 activity, which promotes dendritic arborization, spine morphogenesis, and spine maturation. However, this regulator function of ephrinB2 does not facilitate axonal development. Synaptic connections within the hippocampus are established and refined through the formation and activity-dependent maturation of synapses (Echegoyen et al., 2007; Grove & Tole, 1999; Turrigiano et al., 1998). The refinement process is highly dynamic, involving the removal of weaker spines while others are simultaneously stabilized and potentiated. Complementary assessments of the LTP responses of CA3-CA1 Schaffer collaterals and CA3-CA3 associated/commissural synaptic connections were conducted in Nestin-cre VEGFR2^{lox/-} mice (Harde et al., 2019; Luck et al., 2019). Impaired LTP was observed in Nestin-cre VEGFR2^{lox/-} mice; CA3-CA1 presynaptic responses were altered whereas CA3-CA3 presynaptic responses were not significantly affected (Harde et al., 2019; Luck et al., 2019). This indicates that VEGFR2 signaling is specific to CA3 pyramidal neurons, and deletion of the receptor blocks the ability of CA3 neurons to receive synaptic transmission inputs. Our findings shed light on the circuitry formation of CA3 neurons, which leverages the compartmentalization of VEGFR2 signaling modalities to separately control the synapse formation and integration of dendritic and axonal branches.

4.3 Future directions: A comparative mouse model strategy to identify the cellular source of VEGF guidance cues coordinating the wiring of CA3 neurons

In this study and that of our collaboration partners, we investigated the mechanism by which VEGF-VEGFR2 signaling facilitates the structural and physiological development of CA3 neurons. As a potent neurovascular guidance molecule, VEGF participates in the growth and remodeling of both neurons and vessels through complex signaling

mechanisms (Ruiz de Almodovar et al., 2009; Simons et al., 2016). These signaling mechanisms help to coordinate the development and maintenance of these interdependent cell systems, thus the precision of VEGF signaling is critical for tissue and organ development. Here, we have described a process essential for the development of CA3 neurons in which the modulation of VEGF signals is achieved through the spatiotemporal expression and cellular trafficking of its cognate receptor, VEGFR2. Consequently, the timing of VEGF availability as well as the expression and cellular dynamics of VEGFR2 in CA3 pyramidal cells are critical steps for insuring the proper wiring of hippocampal circuitry. This is not a unique biological phenomenon limited to VEGF-directed VEGFR2 signaling in CA3 neurons. As demonstrated by (Mauceri et al., 2011), VEGF-D signaling through VEGFR3 regulates the geometric morphology and synaptic plasticity of CA1 basal dendrites (Mauceri et al., 2011). Similarly, as VEGF is secreted into the extracellular environment, the cell source of these molecules also plays a significant role in the proper geometric orientation and synaptic formations of CA3 neurite arbors.

The fine-tuning of VEGF signaling occurs at various cellular levels, beginning with the transcriptional regulation of VEGF expression. The primary physiological regulator of VEGF gene expression is oxygen tension (Ramakrishnan et al., 2014). In hypoxic, or low oxygen tension environments, the transcription factor HIF1- α accumulates and binds to the HRE sites located within the 5' and 3' UTRs of VEGF, resulting in the upregulation of VEGF transcription. Various growth factors and cytokines, such as PDGFs, FGFs, and ILs, can also act synergistically to upregulate VEGF gene expression in hypoxic environments (Ramakrishnan et al., 2014). The bioavailability of VEGF is further controlled through alternative mRNA splicing, resulting in the production of splice variants that differ in their abilities to bind to HSPGs within the ECM and thereby altering their localization (Ruhrberg et al., 2002; Ruiz de Almodovar et al., 2010; Teran & Nugent, 2015). This spatial modulation of VEGF influences the stimulatory signals that can trigger a wide range of cellular responses. For example, gradient variations of VEGF within the ECM alter the responsive behavior of endothelial tip cells to influence angiogenic sprouting, elongation, and overall vascular patterning (Carmeliet et al., 1996; Haigh et al., 2003; Nakayama et al., 2013). VEGF splice variants also differ in their binding efficiencies and activation strength of VEGFR2, as with VEGF_{164/165} inducing a stronger downstream signaling response than VEGF_{121/122} (Bergantino et al., 2015; Fearnley et al., 2015; King & Hristova, 2019). Differential VEGF binding to VEGFR2 aids in the fine-tuning of the receptor's signaling, leading to variations in intercellular calcium levels and activation specificity of downstream signaling cascades (Bergantino et al., 2015; Gabhann & Popel, 2004; King & Hristova,

2019; Yamamoto et al., 2016). Considering the impact of alternative VEGF splicing on cellular responses, we investigated the global mRNA transcript levels of the major mouse VEGF splice variants, VEGF₁₂₀, VEGF₁₆₄, and VEGF₁₈₈, in the hippocampus during the first four postnatal weeks (Figure 3.10). In line with previous studies, hippocampal VEGF level increases in the days after birth, peaking during the third week, then declines with age (Ogunshola et al., 2000). During the ten days after birth, all three splice variants are equally upregulated in their potential bioavailability for VEGFR2 signaling in CA3 neurons. In addition to its role in CA3 neuronal development, VEGF signaling is involved in other cellular processes as this is also a highly dynamic stage of hippocampal development. This includes the angiogenic invasion of vessels, glial cell infiltration, and the establishment of the BBB (Dumont et al., 1995). Therefore, tight regulation of VEGF signaling at various cellular levels, including the source of cellular release into the ECM, is necessary for the proper orchestration of hippocampal development. As multiple cells express VEGF, we decided to probe for the cellular localization of VEGF transcripts using RNA FISH. In the CA3 region of the hippocampus, VEGF mRNAs are found in vessels, neurons as well as astrocytes (Figure 3.11). Unfortunately, due to the overlapping sequence homology of the VEGF splice variants, we were not able to determine if one cell type preferentially expressed one variant over others (Holmes & Zachary, 2005; Peach et al., 2018; Takahashi & Shibuya, 2005). However, the expression patterning of VEGF surrounding astrocytes, vessels, and neurons is distinctly different between cell types (Figure 3.12), indicating differential expression of VEGF splice variants.

Notably, each of these cell types has the potential to influence the geometric and synaptic development of CA3 neurons through the cellular release of VEGF. Such interactions have been described in coordinating vascular patterning. For example, during the early postnatal development in the retina, neurons expressing VEGFR2 titrate VEGF to control vascular patterning, while astrocytes simultaneously act as a physical barrier to segregate the layers of vessel networks (Dorrell et al., 2002; Okabe et al., 2014; Scott et al., 2010). Notably, retinal astrocytes do not express VEGFR2 and dispensable amounts of VEGF, they only participate in the spatial separation of their signaling interactions (Okabe et al., 2014; Scott et al., 2010). In this study, we did not observe colocalized expression of VEGFR2 astrocytes in the mouse postnatal hippocampus (Figure 3.1, Figure 3.2) (Harde et al., 2019; Luck et al., 2019). Therefore, we can conclude that astrocytes do not regulate VEGF signaling through direct regulation of VEGFR2 expression. In CNS injury models, it has been reported that reactive astrocytes within the brain express both VEGF and VEGFR1, potentially allowing VEGF to exert direct autocrine and/or paracrine signaling via VEGFR1 to promote

astrocytic recruitment and proliferation (Krum & Rosenstein, 1998; Wang et al., 2005). It is plausible that astrocytes can also express VEGFR1, potentially regulating VEGF bioavailability for VEGFR2 signaling during early postnatal brain development. To address this, one could immunohistochemically assess VEGFR1 colocalization with astrocytes in postnatal mouse brain tissues. Astrocytes have also been shown to spatially limit the bioavailability of VEGF through the phagocytosis of VEGF molecules from the ECM (Eddleston & Mucke, 1993; Krum & Rosenstein, 1998; Rosenstein et al., 2003). Astrocytic release of VEGF increased BBB permeability, contributing to the BBB breakdown observed in neuroinflammatory diseases such as multiple sclerosis and Alzheimer's disease (Argaw et al., 2012; Eddleston & Mucke, 1993; Stackhouse & Mishra, 2021). Although astrocytes are known to play important roles in various aspects of neuronal development and function, their role in VEGF release under non-pathological conditions remains unclear. We therefore tested whether astrocytes would release VEGF using a KCL stimulation to mimic neuronal activity. In our *in vitro* experiments, we found that astrocytes express VEGF, and the expression was further increased after KCL stimulation, indicating the potential for astrocytes to modulate VEGF release in support of neuronal function.

As we found that astrocytes, neurons, and vessels all express VEGF (Figure 3.11, Figure 3.12). Thus, it is plausible that one or more of these cell types could titrate the VEGF signals that are necessary for the development of CA3 neurons. Therefore, we established a comparative mouse model strategy for deleting VEGF in specific cell types using the *Cre/loxP* system. Numerous studies have utilized both VEGF and VEGFR2 deletion models to investigate the effects of VEGF-VEGFR2 signaling on neurovascular development. Knockout and knockdown mouse models of VEGF or VEGFR2 expression have aided our understanding of vasculogenesis and angiogenesis during early embryonic development, as well as the impact of neurovascular signaling on CNS development (Carmeliet et al., 1996; Millauer et al., 1993; Okabe et al., 2020). Single splice variant deletion models of VEGF have highlighted the significant role that VEGF gradients play in vessel development (Maes et al., 2004; Ruhrberg et al., 2002). More recent studies have used cell-specific deletion models to better distinguish paracrine and autocrine VEGF-VEGFR2 signaling on neuronal and vascular development (Haigh et al., 2003). These models have greatly contributed to our understanding of the VEGF/VEGFR2 signaling system in coordinating the developmental process of these cell systems. However, these studies did not fully consider the temporal and cell-specific expression pattern of VEGF and VEGFR2, which can significantly alter their perceived biological impact during neurovascular development. For example, using the same Nestin-Cre VEGFR2 deletion model, Haigh et al. (2003) reported

that VEGFR2 had no functional role in CNS development by E15.5. However, two days later at E17.5, Bellon et al. (2010) found that VEGFR2 was critical for the development of subiculo-mamillary axonal projections. In this study, again using a Nestin-cre VEGFR2 deletion model, we found that a VEGF-induced VEGFR2-ephrinB2 signaling complex is necessary for the postnatal dendritic development of CA3 neurons. Conversely, in the (Bellon et al., 2010) study, it was found that Sema3A, not VEGF, was the ligand partner for VEGFR2 signaling. Therefore, we wanted to exploit the versatility of the *Cre/loxP* system to precisely time the cell-specific knockdown of VEGF to when VEGFR2 is required for the development of CA3 neurons. By leveraging the upregulation of cell-type-specific promoters, it is possible to temporally induced Cre-recombinase expression in targeted cell populations (Gavériaux-Ruff & Kieffer, 2007). The timed translocation of Cre into the nucleus for gene editing can be further controlled using CreERT2, a modification in which Cre is fused with a mutated estrogen receptor that selectively accepts synthetic tamoxifen ligands (Pitulescu et al., 2010). In our purposed VEGF deletion model system, we selected the CamkIIa-Cre mice line for selective recombination activity in neurons (Brinkmann et al., 2008). For targeted VEGF knockdown in vessels and astrocytes, we opted for the inducible Cdh5-CreERT2 and GLAST-CreERT2 mouse lines, respectively. In mice, the CamKIIa promoter is upregulated just after birth, with gene transcripts detected in hippocampal neurons as early as P4 (Thompson et al., 2014). GLAST expression has been reported to begin between E11 and E13 (Regan et al., 2007). Therefore, the P3-5 tamoxifen induction paradigm used for GLAST-CreERT2 mice was chosen as the optimal window for the conditional postnatal deletion of VEGF in astrocytes. As VEGF is critical for vessel development and is highly expressed in endothelial cells, as compared to astrocytes, we choose the P5-7 timeframe to induce Cdh5-CreERT2 activity in vessels with tamoxifen injections. These promoters driving Cre expression in conjunction with tamoxifen-inducible systems were specifically chosen to minimize any potential effects of VEGF on the vasculature while studying the impact of VEGF on CA3 development. To assess the effectiveness of conditionally induced Cre expression, we crossed each mouse line with a Rosa26-EYFP reporter stain to examine the cell selectivity of Cre activity. For each mouse model, Cre activity was only detected in the targeted cell populations. In GLAST-CreERT2 and Cdh5-CreERT2 mice, Cre activity was observed in tamoxifen, but not PBS-treated animals. In the case of CamkIIa-Cre mice, the YFP reporter expression levels of Cre activity were higher in homozygous mice as compared to heterozygous mice. Our results indicate that *Cre* activity is selectively driven by its corresponding promoter and can be tightly regulated in a time-dependent manner.

In the next phase of this project, we plan to crossbreed each of these Cre mouse lines with VEGF-floxed mice. This will enable us to identify the specific paracrine or autocrine VEGF signals that contribute to the development of CA3 pyramidal cells. Unfortunately, due to time constraints we were unable to carry this step out in the present study. However, in a study by Okabe et al. (2020), the functional relationship between neuronal VEGF and neuronal VEGFR1/2 was examined during the first two postnatal weeks of mouse brain development, also using the *Cre/loxP* system. In their study, a hGFAP-Cre mouse line, with a human GFAP promoter (hGFAP), was used for the selective removal of floxed VEGF, VEGFR1 and VEGFR2 expression neurons. The authors established that, surprisingly hGFAP driven Cre expression recombined floxed genes in cortical and hippocampal neurons, but hGFAP-cre was minimally express in brain astrocytes (Okabe et al., 2020). Using this model system, the authors claimed that indirect angiogenic signaling of neuronal VEGF contributes to postal neuronal development as opposed to cell autonomous signaling via neuronal VEGFR1/2 (Okabe et al., 2020). However, there are some critical issues with their experimental design, which may have impacted their conclusions. For example, the authors state that they could not detect a significant role of VEGFR2 expression in the hippocampal neurons, but they do not experimentally show VEGFR2 expression patterns in neurons (Okabe et al., 2020). In our study, we clearly show the localized expression of VEGFR2 in CA3 neurons, of which VEGFR2 signaling is required for proper development (Figure 3.1, Figure 3.2, Figure 3.6, Figure 3.7). The authors do report minimally hGFAP-cre expression in brain astrocytes, therefore the contribution of astrocytic VEGF cannot be fully mitigated. Astrocytes are a highly diverse cell type, exhibiting a wide range of functional roles and cellular associations (Argaw et al., 2012; Barker et al., 2008; Barker & Ullian, 2008; Chow et al., 2001; Scott et al., 2010). Despite having overlapping physiological roles, GFAP and GLAST-positive astrocytes differ in their distribution in the cortex and hippocampus. GFAP-positive astrocytes are more closely associated with blood vessels, forming more cellular contacts with vessels as compared to GLAST-positive cells (Bushong et al., 2002; Jurga et al., 2021). On the other hand, the glutamate transporter slc1a3 (GLAST), is expressed in astrocytes located near glutamatergic synapses, which participate in glutamate uptake and release (Jurga et al., 2021; Regan et al., 2007; Shibata et al., 1997). Therefore, the use of a GFAP versus a GLAST promoter to drive Cre recombinant deletion of VEGF may present with a stronger vascular or neuronal phenotype, respectively. Considering the points mentioned, the exact role of VEGF signaling during neuronal development in the postnatal hippocampus remains inconclusive using the model system approach employed by (Okabe et al., 2020). Our purposed experimental design for cell-type-specific VEGF deletion is a better mouse model system to address this question.

In conclusion, VEGF/VEGFR2 signaling pathway plays a critical role in regulating various cellular processes, which is essential for coordinating organ development (Hogan et al., 2004; Li et al., 2013; Paredes et al., 2018; Zhang et al., 2003). This process involves the modulation of VEGFR2 activation by ligand binding and co-receptor interactions, which allows for the selective downstream of signaling and the fine-tuning of cellular responses (Bellon et al., 2010; Harde et al., 2019; Nakayama et al., 2013; Sarabipour et al., 2023; Sawamiphak et al., 2010; Wang et al., 2010). Additionally, the spatiotemporal expression of both ligand and receptor also influences orientation and patterning through cellular crosstalk (Greenberg et al., 2008; Hayakawa et al., 2011; Lee et al., 2007; Li et al., 2013; Yamamoto et al., 2016). Our proposed VEGF deletion mouse model system takes into consideration all these factors, thus enabling a rigorous investigation of the cellular source of VEGF that coordinates the integration of CA3 pyramidal neurons into the hippocampal circuitry.

4.4 Clinical implications

This study investigated the molecular mechanisms of the VEGF-induced VEGFR2 signaling and its role in the physiological processes governing neuronal development. Within the CNS, VEGF signaling mainly occurs in neurovascular niches, specialized environments comprised of neural progenitor cells, vessels as well as supporting cells such as pericytes, astrocytes, and microglia. Neurovascular niches serve as a signaling platform for interactive cellular communication as VEGF has dualistic functions in both vessel and nervous system development (Ruiz de Almodovar et al., 2009). As such, signaling mechanisms within the VEGF/VEGFR2 signaling pathway involves both opposing and complementary functions that aid in the coordinated development of both systems (Di Marco et al., 2015; Paredes et al., 2018; Ruiz de Almodovar et al., 2009; T. Wada et al., 2006). Thus, identifying the molecules and signaling events underlying neuronal guidance is essential for understanding how neuronal connectivity is established during development and regulated in adulthood. Furthermore, the signaling mechanisms that guide the development of the central nervous system have commonalities with regenerative processes that occur in the CNS after injury (Almodovar et al., 2009; Dumpich & Theiss, 2015; Paredes et al., 2018; Ruiz de Almodovar et al., 2009). By investigating the molecular basis of VEGF/VEGFR2 signaling, this study provides valuable insights into the cellular responses not only in neuronal development but also in neurodegenerative diseases, which often use the same mechanisms for repair (Carmeliet & Storkebaum, 2002; Paredes et al., 2018; Shim & Madsen, 2018; Takahashi & Shibuya, 2005).

VEGF/VEGFR2 signaling has been linked to several neurodegenerative diseases, such as amyotrophic lateral sclerosis (ALS), Parkinson's (PD), and Alzheimer's Disease (AD) (Marti et al., 2000; Sathasivam, 2008; Shim & Madsen, 2018). Neurodegenerative diseases are CNS disorders characterized by age-progressive neuronal loss that results in cognitive decline or, as in the case of ALS and multiple sclerosis (MS), a loss in motor functions. These disorders have different underlying pathologies that contribute to their distinct clinical presentations. Nevertheless, they do share a common feature in that there is a pathophysiological disruption in both the vascular and nervous systems, which contributes to their neurodegenerative phenotypes (Di Marco et al., 2015; Raz et al., 2016; Sweeney et al., 2018). This is also the case for vascular disease, such as stroke, in which a disruption in the blood supply of oxygen and nutrients severely and acutely alters the metabolic state of neurons causing rapid cell death (Zhang et al., 2000). According to the CDC, stroke is the 5th leading cause of death in the US. Dementias, such as PD and AD, rank number 7th, of which AD makes up 70-80% of the reported cases (Xu et al., 2022). These diseases have a profound impact on patient's lives and that of their families and caregivers as commercially available disease-modifying therapies are limited or lacking altogether.

The effects of VEGF signaling on the brain in the context of neurodegenerative diseases have been extensively reviewed (Lange et al., 2016; Nelson et al., 2016; Zlokovic, 2008). Properly regulated VEGF signaling is neuroprotective, promotes neurogenesis, and modulates synaptic plasticity changes in neurons (Licht et al., 2010; Meissirel, Ruiz de Almodovar, et al., 2011; Ruiz de Almodovar et al., 2010; Sondell et al., 2000). However, under pathological conditions, altered VEGF levels can have deleterious effects on BBB integrity causing neurotoxic effects that contribute to disease progression (Lange et al., 2016; Nelson et al., 2016; Sathasivam, 2008). ALS is characterized by chronic neuroinflammation due to the neural damage caused by proinflammatory signals from activated immune cells (Robberecht & Philips, 2013; Sathasivam, 2008). Although the mechanisms are not yet well understood, dysregulated VEGF expression can lead to the disruption of the BBB and infiltration of CNS immune cells, which contributes to the neuroinflammatory aspects of ALS (Just et al., 2007; Nagata et al., 2007; Oosthuysen et al., 2001; Robberecht & Philips, 2013). In ALS patients, the rapid degeneration of motor neurons has been linked to low VEGF levels, possibly due to chronic CNS ischemia from poor vascular perfusion (Devos et al., 2004). Furthermore, a signal nucleotide polymorphism in the VEGF gene (-2578C/A) is a clinical risk factor for the disease and is also associated with lower VEGF levels (Lambrechts et al., 2003). The pathological hallmark of PD is a loss of dopaminergic neurons within the substantia nigra. There are conflicting reports as to

whether VEGF levels are up or downregulated in PD, mostly due to the stage and severity of the disease and method of analysis (Ohlin et al., 2011; K. Wada et al., 2006). However, dopamine may regulate VEGFR2 activity by enhancing receptor endocytosis to limit VEGF signaling in dopaminergic neurons (Ohlin et al., 2011). Abnormal capillary densities have also been observed in the substantia nigra of PD brains, with a leaky BBB due to VEGF upregulation in GFAP-positive astrocytes (Cabezas et al., 2014; Ohlin et al., 2011). Neuroinflammatory signaling from astrocytes and other immune cells further exacerbates the disease as proinflammatory signals lead to both full BBB breakdown and increase cell death (Cabezas et al., 2014; Ohlin et al., 2011; K. Wada et al., 2006; Zlokovic, 2008). AD pathology results from the extracellular accumulation of amyloid beta oligomers (A β) and tau neurofibrillary tangles in the brain parenchyma (Tzioras et al., 2023). Mechanistically, A β induces cellular prion protein (PrPC) binding at mGluR5, triggering aberrant mGluR5 signaling which leads to glial-mediate synapse loss and impaired LTP (Spurrier et al., 2022; Stoner et al., 2023). AD pathology is highly complex with VEGF and VEGFR2 signaling having both neurotoxic and neurotrophic effects. In 80% of AD patients, A β deposits are also detected in the arterial walls of vessels before any neural defects or cognitive decline occur, and this vascular A β deposition can damage BBB integrity, resulting in cerebral hypoperfusion, which is a preclinical indicator for AD onset (Sweeney et al., 2018). BBB breakdown also impairs the glymphatic clearance of A β and other toxic substances which causes neurotoxicity (Nation et al., 2019; Sweeney et al., 2018). It has been shown that A β plaque formations generate a hypoxic microenvironment that induces astrocytic VEGF expression, promoting the hyperactive sprouting of leaky, poorly formed vessels (Alvarez-Vergara et al., 2021). Conversely, reportedly A β can interact with VEGF molecules to prevent VEGFR2 activation, triggering structural and functional changes in synapses that are reversed by VEGF treatment (Martin et al., 2021). VEGF-induced VEGFR2 signaling participates in synapse formation and synaptic plasticity by enhancing NMDAR and AMPAR activity (De Rossi et al., 2016). Therefore, increased VEGF levels reduce A β -induced AMPAR loss in AD, reducing synapse loss (Martin et al., 2021). Although a direct link between VEGFR2 signaling and the aberrant activation of mGluR5 has not been established, these findings suggest that there is a complex interplay between VEGF-VEGFR2 signaling and the progression of AD pathology.

Dysregulated VEGF/VEGFR2 signaling plays diverse roles in neurodegenerative diseases, contributing to altered disease progression and pathological outcomes, thereby requiring corresponding treatment strategies. For instance, studies have found a correlation between higher levels of VEGF in cerebrospinal fluids and improved age-associated cognitive decline

(Devos et al., 2004; Just et al., 2007). VEGF treatment may be clinically beneficial for ALS or AD patients who present with cerebral hypoperfusion (Sathasivam, 2008; Shim & Madsen, 2018). On the other hand, VEGF treatment in AD patients with vascular risk factors like stroke or diabetes may result in adverse outcomes (Lange et al., 2016; Yang et al., 2013). In mouse models of PD, low levels of VEGF have been shown to have neurotrophic effects, whereas high levels of VEGF accelerate the loss of dopaminergic neurons (Ohlin et al., 2011; K. Wada et al., 2006). This suggests that there is a narrow therapeutic window for VEGF in PD, which limits its clinical application for disease treatment due to the variable expression levels of VEGF in PD patients (Ohlin et al., 2011; Shim & Madsen, 2018; K. Wada et al., 2006).

In conclusion, VEGF/VEGFR2 signaling under both development and pathological conditions is highly complex yet variable due to the involved signaling partners and biological context. Therefore, clinical strategies aimed at countering VEGF/VEGFR2 signaling should consider the spatiotemporal changes in ligand and receptor expression, as well as the methods for modulating their respective signaling.

4.5 Concluding remarks

In this study, we describe a previously unknown function of VEGFR2 signaling during dendritic arborization and spine formation in the development of CA3 pyramidal neurons. Mechanistically, we found that VEGF-induced VEGFR2 signaling requires receptor internalization in a process that is mediated by ephrinB2. We also show that VEGF induces the formation of a signaling complex between VEGFR2 and ephrinB2, the internalization of which can lead to downstream signaling events. VEGF-induced cooperative signaling between VEGFR2 and ephrinB2 is functionally required for the dendritic development, spine morphogenesis, and maturation processes of CA3 neurons. This study was part of a research collaboration that investigated the role of VEGF-induced VEGFR2 signaling in CA3 axonal development. It was found that, unlike the branch and spine development of CA3 dendrites, VEGF-VEGFR2 signaling promotes axonal development through mechanisms that are independent of ephrinB2. Collectively, our findings show that VEGF signaling coordinates the development and circuitry formation of CA3 neurons through a differential trafficking mechanism of VEGFR2 within the axonal and somatodendritic compartment. The signaling mechanism that regulates VEGF-VEGFR2 signaling in CA3 axons, as well as the cellular source titrating VEGF signals, thereby coordinating the development of CA3 neurons, remains to be further investigation.

5 Materials & Methods

5.1 Materials

5.1.1 Chemicals & reagents

Table 5.1: Chemicals, enzymes, and reagents.

Chemical	Supplier	Article Number
2-Mercaptoethanol	Sigma	M7522
Acrylamide/Bisacrylamid (29:1) 30%	AppliChem	A0951
Agarose	Sigma	A9414
Ammonium persulfate (APS)	Bio-Rad	161-0700
Amphotericin B	Millipore	A 2612
Ampicillin sodium salt	Roth	HP62.1
B27 - supplement (50x)	Life Technologies	17504-044
Borax (sodium tetraborate decahydrate)	Sigma	B3545
Boric Acid	Merck	203667
Bovine serum albumin powder	Sigma	7906
Bromophenol blue, sodium salt	Roth	A512.1
Calcium chloride dihydrate	Roth	HN04.1
Complete EDTA-free Protease Inhibitor Cocktail Tablets	Roche	11873580001
Collagenase Type II (CLS II)	Roche	C2-28
DAPI	Roth	6335,1
D(+) - Glucose (cell cultured tested)	Sigma	G7021
D(+) - Sucrose	AppliChem	A3935-1000
Dimethyl sulfoxide (DMSO)	Roth	6335,1
Distilled water, endotoxin screened	Life Technologies	15230-089
DMEM (1x) with Glutamaxx	ThermoFisher, Gibco	61965-026
DNA Ladder Gene Ruler Ladder Mix	Fermentas	M0331
dNTP	NEB	40447
DPBS [+CA ⁺⁺ , +Mg ⁺⁺]	Life Technologies	14040-174
DPBS [-CA ⁺⁺ , -Mg ⁺⁺]	Life Technologies	14190-169
Dynabeads Sheep anti-Rat IgG	Invitrogen	11035
E. Coli One Shot TOP 10 competent cells	Life Technologies	C4040-52

ECL Western blotting detection reagents	GE Healthcare	RPN 2134
ECL Western blotting detection reagents	VWR/Healthcare	RPN 2209
Endothelial Cell Growth Supplement / Heparin (ECGS-H)	Promo Cell	C-30210
Ethanol, extra pure	Roth	5054,1
Ethylenediaminetetraacetic acid (EDTA)	Roth	X986.2
Ethidium bromide solution (1%)	Roth	2218,1
EZ-Link™ Sulfo-NHS-SS-Biotin	Thermo Scientific	21330
Fetal Bovine Serum (FBS)	Invitrogen	F-7524
Gelatin (from porcine skin)	Sigma	G2500-100G
Glutamax	Life Technologies	35050-038
Glutaraldehyde 25% solution in water	Roth	3778,1
Glutathione reduced (cell culture tested)	Sigma	G6013
Glycerol, insect cultured tests, 99%	Sigma	G2025
Glycine	Sigma	G7403
GoTaq® Green Master Mix	M7122	Promega
HBSS [+CA ⁺⁺ , +Mg ⁺⁺], with Phenol red	Life Technologies	24020-091
HBSS [+CA ⁺⁺ , +Mg ⁺⁺], without Phenol red	Life Technologies	14025-050
Heparin sodium salt	Sigma	H3149
HEPES	Life Technologies	15630-056
High-capacity cDNA reverse transcription kit	Life Technologies	4368814
Hydrochloride (HCl) 4M	Roth	N076.1
Isopropanol	Roth	7343,2
Ketamine	Henry Schein VET	799760
L-Glutamine	Life Technologies	H25030-024
Laminin - natural mouse laminin	Sigma	L2020
LB-Agar	Roth	X965.2
LB-Medium (Luria/Miller)	Roth	X964.2
Liquid Nitrogen	Air Liquide	1007754
Magnesium chloride hexahydrate	Sigma	HN03.1
Methanol (molecular biology)	Roth	7342,2
MITO+ serum extender	Becton Dickerson	35 50 06
Milk powder (blotting grade)	Roth	T145.2
Mounting medium (fluorescence)	Dako	S2302380-2
Neurobasal medium (1x), liquid	ThermoFisher, Gibco	21103-049

Normal donkey serum	Dianova	017-00-121
NeutrAvidin Agarose Resins	Pierce	29200
O.C.T Compound	4583	Tissue-Tek
Orange G (60%)	Sigma	O1625
Paraformaldehyde (PFA)	Polyscience	104018
Penicillin-Streptomycin	Life Technologies	15140-122
Poly-D-lysine hydrobromide	Sigma	P7886
Ponceau S staining solution	Sigma	9198
Potassium chloride	Sigma	HN02.3
Protein A Sepharose™ CL-4B	GE Healthcare	17-0780-01
Protein B Sepharose™ Fast Flow	GE Healthcare	17-0618-07
Protein ladder high range	Thermo Scientific	26625
Protein ladder page ruler	Thermo Scientific	26616
Proteinase K	Roth	7528,2
RNaseZAP™	Sigma	R2020-250ML
Saline	Braun	0.9% NaCl Solution
Sodium azide	Sigma	71289
Sodium chloride	Roth	HN00.2
Sodium dodecyl sulfate	Roth	4360,2
Sodium Fluoride (NaF), crystalline	Sigma	S1504
Sodium hydrogen carbonate	Roth	HN01.1
Sodium Orthovanadate (NO ₃ VO ₄)	NEB	S-6508
Sodium Pyrophosphate decahydrate (NaPP)	Sigma	221368
Sodium pyruvate	Life Technologies	11360-039
Taq DNA polymerase	NEB	M0267 L
TEMED Electrophoresis buffer	Roth	2367,1
Trans-Blot® Turbo™ 5x Transfer Buffer	Bio-Rad	10026938
Trichloromethane/Chloroform	Roth	Y015.1
TRIS - Base	Roth	4855,3
TRIS - Hydrochloride	Roth	9090,3
TripLE Select	Gibco	A12177-01
Triton-X-100	Roth	3051,1
TRIzol Reagent	Life Technologies	15596-018
Trypan Blue	Invitrogen	15250061

Trypsin-EDTA (0.25%)	Life Technologies	15090046
TWEEN 20	Roth	9127,1
Water, distilled, UltraPure DNase/RNase free	Invitrogen	10977035
Western Chemiluminescent HRP Substrate	Millipore	WBKL S0050
Xylazine	Rompun	2% solution

5.1.2 Reagents for tri-color fluorescent *in situ* (FISH)Table 5.2: Reagents for *in situ* hybridization.

Chemical	Supplier	Article Number
10x PBS pH 7.4 for pretreatment steps	Sigma	P5493-1L
5 M NaCl	Ambion	AM9760G
Acetic anhydride, 250 ml (now 1L)	Fluka	45830
Anti-dinitrophenyl-KLH, rabbit IgG fraction	Molecular Probes	A6430
Anti-fluorescein-HRP conjugate	Perkin Elmer	NEF710
Blocking reagent	Perkin Elmer	FP1012 (10 g)
Denhardt's solution, 5 ml	Sigma	D2532
Dextran sulfate	Sigma	31395-50G
DNP-11-UTP	Perkin Elmer	NEL555
EDTA pH 8.0 0.5M 100ml	Ambion	AM9261
Ethyl alcohol	Sigma	32205-1L
Fluorescein RNA labeling mix, 10x conc.	Roche	11685619910
Formamide for hybridization and wash steps, 500 ml	Roche	11814320001
HNPP fluorescent detection set	Roche	11758888001
Hydrochloric acid, 500 ml	Sigma	320331
Hydrogen peroxide (30% solution), 100 ml	Sigma	21676-3
Lithium chloride 7.5 M solution	Ambion	AM9480
Nuclease-free water, 50 ml	Ambion	AM9937
pGEM-T Easy Vector System I	Promega	A1360
Proteinase K, 5ml	Roche	3115828001
RIBONUCLEASE A SOLUTION (Molecular biology)	Sigma	R4642-50MG
Ribonucleoside triphosphate set	Roche	11277057001
SDS, 20%, 250 ml	Ambion	AM9820
Triethanolamine, 500 ml	Sigma	T58300-1

Tris (pH8.0) for the hybridization step, 500 ml	Ambion	AM9856
TSA Plus Fluorescein System, for 50-150 slides	Perkin Elmer	NEL741001KT
Water, for molecular biology, DNase, RNA, 1L	Fisher Scientific	327390010
Wizard SV Gel and PCR Clean-up System	Promega	A9281
Yeast RNA, 10 mg/ml, 10 tubes	Ambion	AM7118

5.1.3 Commercial kits

Table 5.3: Commercial kits

Kit	Supplier	Article Number
DuoSet ELISA, msVEGF	R&D Systems	DY493-05
Hydroxyprobe™ kit	Hydroxprobe, Inc.	HP1-100
NucleoSpin® Tissue	Macherey-Nagel	740952,10
Pierce™ BCA Protein Assay Kit	Thermo Scientific	23227
EndoFree Plasmid Maxi Kit	Qiagen	12362
Substrate Reagent Pack	R&D Systems	DY999
Stop solution	R&D Systems	DY994
TransBlot® Turbo™ RTA Transfer Kit, Nitrocellulose	Bio-Rad	1704271
Wizard SV Gel and PCR Clean-Up System	Promega	A9280

5.1.4 Consumables

Table 5.4: Consumables.

Materials	Model or Type	Supplier
8-strip flat caps	Atk-Nr# 65 1998 400	Sarstedt
96-well plate (Cell culture)	Falcon™ Polystyrene Microplate REF 353072	Thermo Scientific
96-well plate (ELISA)	Nunc Immuno Maxisorp, Atk-Nr# 442404	Thermo Scientific
96-well plate (PCR, genotyping)	Atk-Nr# 72 1978 202	Sarstedt
Cell scraper	Atk-Nr# 83.183	Sarstedt
Cellstrainer	BD Falcon 40 µm Nylon	NeoLab
Eppendorf Combi-tips plus	2 mL, 5 mL, 10 mL	NeoLab
Filter pipette tips	10 µL, 40 µL, 200 µL, 1000 µL	Biozym
GasPaK™ EZ	Atk-Nr# 206683	BD Biosciences

Gene Pulser Cuvettes	0.2 cm, Atk-Nr# 1652089	RioRad
Glass coverslips, 12/13 mm Ø	Atk-Nr# 01 115 30	Marienfeld
Glass coverslips, 24 x 32 mm	Atk-Nr# 01 021 72	Marienfeld
Glass coverslips, 24 x 60 mm	Atk-Nr# 01 072 42	Marienfeld
Gel-Saver-Tip II, (Western blot)	1 - 200 µL, Atk-Nr# GSII 054B	G. Kisker
Hypodermic needles	26G x 23 mm	Terumo
Hypodermic needles	27G x 3/4"	Terumo
Hypodermic needles	30G x 1/2"	Henry Schein
Latex gloves, powder-free	Atk-Nr# GSII054	G. Kisker
Multi-well culture plates	6-, 12-, 24-, 96-well plates	TPP
Nitrile gloves, powder-free	Size S	SempreGuard
Nitrile gloves, powder-free	Size S	VWR
Nunc EasyFlask (angled, filter)	25 cm ² , 75 cm ²	VWR
Parafilm	"M" laboratory film	Pechiney Plastic Packaging
Pasture pipette, glass	Atk-Nr# 4518	Roth
Pasture pipette, plastic	1 mL, 3 mL, 5 mL	Alpha laboratories limited
Petri dishes	60 cm, 10 cm	Nunc
Plastic pipette tips	10 µL, 200 µL, 1000 µL	Sarstedt
Polypropylene conical tube	15 mL, 50 mL	Becton Dickinson
Reaction tube, safe lock	0.5 mL, 1.5 mL, 2 mL	Eppendorf
Steritop bottle top filter unit	Atk-Nr# SCGPU01RE	Milipore
Storage box (Microscopy slides)	50 slides	Rother
Superfrost® Plus Microscopy slides	J1800AZMNZ	Thermo Scientific
Surgical disposable scalpel	Atk-Nr# BA210, BA211 or BA222	Braun
Serological pipette	2 mL, 5 mL, 10 mL, 25mL 50mL	Sarstedt
Syringe (for injections, tissue titration)	1 mL	Braun
Syringe (for filter unit)	5 mL, 10 mL, 50mL	Becton Dickinson
Syringe-driven filter unit	0.22 µm, 0.45 µm	TPP
Weighing dishes	41 x 41 mm, 89 x 89 mm	Roth
Weighing paper	9 x 11.5 cm	Roth
Whatman Protran nitrocellulose transfer membrane	Atk-Nr# 10401196	GE Healthcare

5.1.5 Equipment

Table 5.5: Equipment.

Equipment	Model or Type	Supplier
Fridge,	Premium	Liebherr
Freezer, -	ComfortGS-5203	Liebherr
Freezer, -	Ultra-low freezer	Thermo Scientific
Bunsen Berner	Gasprofi 1 SCS micro	WLD-TEC
Centrifuge, mini	Sprout	Biozym
Centrifuge, conical tubes	Hettich Rotanta 460 R	Thermo Scientific
Centrifuge, microtubes strip	5424 R	Eppendorf
CO2 incubator	Heraeus HERAcell 240	Thermo Scientific
Cryostat	SuperFrost	Thermo Scientific
Electroporation system	MicroPulser™	Bio-Rad
Gel chamber, electrophoresis	Compact XL	Biometra
Gel documentation system	UVP GelStudio Plus, Felix CCD Camera	Analytik Jena
Gel system, Western blot	Mini PROTEAN® 3 cell	BioRad
ImageQuant Blot Developer	LAS 4000 system	GE Healthcare
Laminar flow hood	Heraeus HERAguard	Thermo Scientific
Magnetic separation rack	15 mL tube rack	Invitrogen
Magnetic stirrer, heating	MSH-20A	IDL GmbH
Microplate absorbance reader	iMark	Bio-Rad
Microscope, brightfield	CKX31	Olympus
Microscope, dissection	SZX10	Olympus
Microscope, laser scanning Confocal	TCS SP-5 (405 Diode, Argon, DPSS 561, and HeNe 633 lasers)	Leica
Microwave	Severin 700	Severin
Multi-channel pipette	0.5 – 10 µL	Eppendorf
Multi-channel pipette	20 – 200 µL	Brand
Multi-pipette	Multipipette® Plus	Eppendorf
Neubauer Chamber	0.100 mm Depth, 0.0025 mm ²	Marienfeld
PCR machine	Flex cycler	Analytic Jena
Peristaltic Pump	Minipulse™ 3	Gilson
pH meter	Lab 850	Schott Instruments

Pipetteman	2 μ L, 10 μ L, 20 μ L, 200 μ L, 1000 μ L	Gilson
Pipette boy	Pipetteboy acu	Integra Biosciences
Power supply, gel electrophoresis	EPS 301	Amersham Pharmacia Biotech
Power supply, Western blot	PowerPac™ HC	Bio-Rad
Shaker, plates	DRS-12	NeoLab
Shaker, tube rotator	Rotator 2-1175	NeoLab
Spectrophotometer	PeqLab NanoDrop 2000	Thermo Scientific
Thermal heating block	Dri-Block DB-2D	Techne
Thermomixer compact	25 x 1.5 mL wells	Eppendorf
ThermoShaker	96 x 0.2mL MTP	Biometra (Analytik Jena)
Semi-dry blotting apparatus	Trans-blot SD Cell	Bio-Rad
Ultrasonic bath	USC-TH	VWR
Vacuum pump	VNC 2	Vacuubrand
Vibratome	VT1200S	Leica Instruments
Vortex	Top-Mix 11118	Fisher Scientific
Vortex	Sprout	Biozym
Water bath	Polystat 24	Fisher Scientific
Water purification system	Mili-QBiocel A10	Milipore
Weight balance, coarse	EMB I000-2	Kern
Weight balance, fine	SI-234	Denver Instrument

5.1.6 Surgical tools

Specialized surgical tools (Fine Science Tools, FST) were used for organ and tissue dissections for primary cell isolation for cell culture experiments as well as for experiments performed on fixed tissues.

Table 5.6: Surgical Tools.

Tool	Article Number
Cover glass forceps	11074-02
Curved forceps	11271-30
Dumont 5 forceps	11295-00
Hippocampal dissecting tool	10099-15

Mirror finished forceps	11252-23
Scissors-curved	15004-08
Scissors-large	14001-14
Scissors-Marco	14088-10
Scissors-straight	15024-10

5.1.7 Drugs, injectable probes, and stimulants

All drugs were prepared following the respective manufacturer's protocol.

Table 5.7: Drugs, injectables probes, and stimulants.

Drugs	Working Concentration	Supplier	Article Number
hVEGF-165, biotinylated	50 µg/mL	R&D Systems	NFVE0
msVEGFA-164	50 µg/mL	R&D Systems	493-MV-O25
msVEGFA-164	50 µg/mL	Cell Signaling	5211
Dynasore	40mM	Biozol	S8047
4-Hydroxytamoxifen	1mg/mL (Postnatal mice) 2mg/mL (Adult mice)	Sigma	T176-50mg
Pimondazole HCl	50mg/mL	Hydroxyprobe, Inc.	HP1-100

5.1.8 Primary Antibodies

Table 5.8: Primary antibodies. Abbreviations: WB (Western Blot), IHC (immunohistochemistry), IP (Immunoprecipitation).

Primary Antibody	Host Species	Dilution	Supplier	Article Number
-Akt	rabbit	1:1000 WB	Cell Signaling	9272
-(phospho)-Akt	rabbit	1:1000 WB	NEB	9275
-CD31	rat	66:1000 IP	BD Biosciences	553370
-cleaved Caspase3	rabbit	1:200 IHC	NEB	9661
-ephrinB2	goat	1:500 WB	R&D Systems	AF496
-ephrinB2	rabbit	1:100 IHC	Sigma	HPA008999

-GAPDH	mouse	1:1000 WB	Millipore	MAB374
-GFAP	mouse	1:500 IHC	Sigma	G3893
-GFAP	rabbit	1:500 IHC	Dako Cytomation	Z0335
-GFP	chicken	1:500 IHC	Abcam	Ab13970
-GFP	rabbit	1:500 IHC	Fitzgerald	20R-GF011
-GLUT-1	rabbit	1:200 IHC	Millipore	07-1401
-NeuN	mouse	1:200 IHC	Chemicon	MAB377
-NeuN	rabbit	1:200 IHC	Millipore	ABN78
-Pan-cadherin	mouse	1:1000 WB	Sigma	C1821
-Podocalyxin	goat	1:200 IHC	R&D Systems	AF1556
-(phospho)-tyrosine	clone 4G10	1:500 IP	Millipore	05-321
-Src	rabbit	1:1000 WB	Cell Signaling	2123
-(phospho)-Src	rabbit	1:1000 WB	Cell Signaling	2101
-VEGF	goat	1:100 IHC	R&D Systems	AF-493-NA
-VEGF	mouse	1:1000 WB 1:500 ELISA	Abcam	ab1316
-VEGF	rabbit	1:100 IHC	Santa Cruz	sc-152
-VEGFR2	goat	1:100 IHC 1:500 ELISA	R&D Systems	AF644
-VEGFR2	rabbit	1:1000 WB 1:100 IP	Cell Signaling	2479
-(phospho) VEGFR2 (Tyr1175)	rabbit	1:1000 WB	Cell Signaling	2478

5.1.9 Secondary Antibodies

Table 5.9: Secondary and conjugated fluorescent antibodies. Abbreviations: WB (Western Blot), IHC (Immunohistochemistry), IF (Immunofluorescence).

Secondary Antibody	Dilution	Supplier	Article Number
Donkey -chicken Alexa 488	1:500 IF	Dianova	703-546-155
Donkey -goat Alexa 488	1:200 IF	Molecular Probes	A11055
Donkey -goat Alexa 568	1:200 IF	Molecular Probes	A11057

Donkey -goat Alexa 647	1:200 IF	Molecular Probes	A21447
Donkey -mouse Alexa 488	1:200 IF	Molecular Probes	A21202
Donkey -mouse Alexa 568	1:200 IF	Molecular Probes	A10037
Donkey -mouse Alexa 647	1:200 IF	Molecular Probes	A31571
Donkey -rabbit Alexa 488	1:200 IF	Molecular Probes	A21206
Donkey -rabbit Alexa 555	1:200 IF	Molecular Probes	A31572
Donkey -rabbit Alexa 647	1:200 IF	Molecular Probes	A31573
Donkey -goat HRP	1:3000 WB	Dianova	705-035-003
Goat -mouse HRP	1:3000 WB	Dianova	115-035-146
Isolectin GS-IB4 Alexa Fluor 488	1:200 IF	Life Technologies / Invitrogen	I21411
Isolectin GS-IB4 Alexa Fluor 568	1:200 IF	Life Technologies / Invitrogen	I21411
Isolectin GS-IB4 Alexa Fluor 647	1:200 IF	Life Technologies / Invitrogen	I32450
Goat -rabbit HRP	1:3000 WB	Dianova	111-035-003

5.1.10 Primer sequences for genotyping

Table 5.10: Oligonucleotide sequences and pairings for genotyping PCR.

Gene Target	Primer Name	Primer Orientation	Sequence (5' 3')
Cre- Recombinase	Cre-1	Forward	GCCTGCATTACCGGTCGATGCAACGA
	Cre-2	Reverse	GTGGCAGATGGCGCGGCAACACCATT
ephrinB2	B2Cs1	Forward	CTTCAGCAATATACACAGGATG
	B2Cas1	Reverse	TGCTTGATTGAAACGAAGCCCGA
	B2del	Reverse	AATACTGTTACTACAGGGTCC
(Rosa26)EYFP	Rosa-1	Forward	AAA GTC GCT CTG AGT TGT TAT
	Rosa-1	Reverse	GCG AAG AGT TTG TCC TCA ACC
	Rosa-1	Reverse	GGA GCG GGA GAA ATG GAT ATG
(Thy1)EGFP	Thy1-GFP-F	Forward	TCT GAG TGG CAA AGG ACC TTA GG
	Thy1-GFP-R	Reverse	CGC TGA ACT TGT GGC CGT TTA CG
VEGF	mVEGF-loxP-fwd	Forward	CCT GGC CCT CAA GTA CAC CTT

	mVEGF-loxP-rev	Reverse	TCC GTA CGA CGC ATT TCT AG
VEGFR2	VR2del-F2	Forward	CAA CAG CAC GGA GTG ATT GAT GCC AGC
	VR2del-R3	Reverse	GGC CTG CAG GTT CTG GTT TGT ATT AGA GG
	Fkiflox-rev1	Reverse	GCT GTG ACA TCT GGG TAG AG

5.1.11 Primers & Probes for Quantitative Real-Time PCR

Commercial TaqMan[®] gene expression assay probes were used for the detection of relative expression levels of Vegfa mRNA transcripts.

Table 5.11: TaqMan[®] probes for quantitative Real-Time PCR.

TaqMan [®] Assay Probe [Target Region]	Article Number	Fluorophore	Supplier
Vegfa [exon 1/3]	Mm00437304_m1	FAM	Applied Biosystems
Vegfa [exon 2/3]	Mm01281447_m1	FAM	Applied Biosystems
Vegfa [exon 3/4]	Mm00437306_m1	FAM	Applied Biosystems
B2M [exon 1/2]	Mm00437762_m1	FAM	Applied Biosystems

Custom oligonucleotide primers and a targeted DNA transcript probe were designed to detect the relative expression levels of VEGF splice variants in hippocampal tissues as well as in individual cell types.

Table 5.12: Oligonucleotides for detecting VEGF splice variants by quantitative Real-Time PCR.

Name [Target Region]	Type	Sequence (5' 3')
VEGF universal [exon 4]	Universal Forward Primer	GCC AGC ACA TAG GAG AGA TGA GC
VEGF_120 [exon 5/8]	Reverse Primer	GGC TTG TCA CAT TTT TCT GGC TTT G
VEGF_164 [exon 5/7]	Reverse Primer	CAA GGC TCA CAG TGA TTT TCT GG
VEGF_188 [exon 6/7]	Reverse Primer	AAC AAG GCT CAC AGT GAA CG CT
VEGF FAM-BHQ1 [exon 4/5]	Probe	ACA GCA GAT GTG AAT GCA GAC CAA AGA AAG

5.1.12 Riboprobes

Table 5.13: Riboprobes for in situ hybridizations.

Transcript Target	NCBI Accession Number	Region	Riboprobe size (bp)
<i>Vegf</i> [164/188]	NM_001025250.3	1431 - 1922	422
<i>Vegf</i> [120/164/188]	NM_001025250.3	488 - 1440	504
<i>Gfap</i>	NM_001131020.1	624 - 1238	615

5.1.13 Mouse lines

The mouse lines used in this study were bred in a C57BL6/J background. All animal experiments were conducted in accordance with the German institutional guidelines and ethical committees.

Table 5.14: Mouse lines.

Mouse Line	Source	MGI ID	Reference
CaMKIIa-Cre	Prof. Dr. Ruediger Klein (MPI for Neurobiology, Martinsried)	J:145464	(Brinkmann et al., 2008)
Cdh5-CreERT2	Prof. Dr. Ralf Adams (MPI for molecular Biomedicine, Muenster)	J:161965	(Sorensen et al., 2009)
ephrinB2 ^{lox/lox}	Prof. Dr. Ruediger Klein (MPI for Neurobiology, Martinsried)	3026687	(Grunwald et al., 2004)
GLAST-CreERT2 [<i>Slc1a3-cre/ERT</i>]	Prof. Dr. Carmen Almodovar (University of Heidelberg, Heidelberg)	J:157151	
VEGFR2-GFP (<i>Kdr-GFP</i>)	Jackson Laboratories #01006	3629041	(Ema et al., 2006)
Nestin-Cre	Prof. Dr. Ruediger Klein (MPI for Neurobiology, Martinsried)	2176173	(Tronche et al., 1999)
(Rosa26)EYFP	Jackson Laboratories #006148	104735	(Srinivas et al., 2001)
(Thy1)EGFP, <i>M-line</i>	Jackson Laboratories #007788	3766828	(Feng et al., 2000)
VEGFR2 ^{lox/lox}	Prof. Dr. Ruediger Klein (MPI for Neurobiology, Martinsried)	4422101	(Haigh et al., 2003)
Wildtype C57BL6/J	Jackson Laboratories #000664	5755427	

5.1.14 Standard solutions

Phosphate-buffered saline (10x PBS)

137 mM NaCl	80.0 g
2.7 mM KCl	20.0 g
8 mM Na ₂ HPO ₄	14.4 g
1.5 mM KH ₂ PO ₄	0.24 g

Ingredients were dissolved in 800 ml of sterile water and pH adjusted to 7.4 with HCl. Water was added to a total volume of 1 L and the buffer was stored at RT.

Tris-buffered saline (10x TBS)

150 mM NaCl	88.0 g
25 mM Tris base	3.0 g

The ingredients were dissolved in 800 ml of distilled water and the pH was adjusted to 7.6 with HCl. Distilled water was added until a total volume of 1 L was reached. The buffer was stored at RT.

5.1.15 Solutions for genotyping and agarose gel electrophoresis

1.5 M Tris-HCl, pH 8.8

Tris-base	18.2 g
-----------	--------

Tris-base was dissolved in 80 ml of distilled water, then the pH was adjusted to 8.8 and the solution was filled up to a final volume of 100 ml and stored at RT.

0.5 M EDTA, pH 8.0

EDTA x 2 H ₂ O	186.1 g
---------------------------	---------

EDTA was added to 800 ml of distilled water. After adjusting the pH to 8.0, the EDTA was dissolved. Finally, distilled water was added to a total volume of 1 L. The solution was stored at RT.

50 mM NaOH

NaOH	1.0 g
------	-------

1 g of NaOH pellets was dissolved in 500 ml distilled water and stored at RT

50x Tris-acetate-EDTA (TAE) electrophoresis buffer

Tris base	242.0 g
Acetic acid	57.1 mL
EDTA	100 mL 0.5 EDTA, pH 8.0

For the stock solution, distilled water was added to the chemicals with a total volume of 1 L, and the pH was adjusted to ~8.3. The buffer was stored at RT. To prepare 1x TAE for gel electrophoresis usage, 40 ml of 50x TAE was mixed with distilled water to a final volume of 1 L.

6x Agarose gel-loading buffer

50 % Glycerol (v/v)	50 mL Glycerol
1x TAE buffer	2 mL 50x TAE
0.2 % Orange G (w/v)	0.2 g Orange G

Add distilled water to 100 ml total volume and store at room temperature (RT).

2% Agarose gel

1x TAE buffer	2 mL 50x TAE
2% Agarose	6 g Agarose
0.01 % Ethidium bromide	3 μ L

The agarose was dissolved in 300 mL 1x TAE buffer by heating up in the microwave and then cooled down to approximately 40 °C before adding 3 μ L ethidium bromide (0.01%). The solution was poured into a gel chamber, combs were inserted, and the solution was allowed to polymerize and the combs were removed.

5.1.16 Media and supplements for primary cell culture**0.2% Gelatin**

PBS	50 mL 10x PBS	\
Gelatin	1.0 g	
Distilled water	q.s. 500 mL	

Autoclaved at 165°C then stored at RT. The amount need for coating cell culture plates and Petri dishes was filtered-sterilized through a 0.22 μ m syringe filter unit just before use.

Borate buffer

Boric acid	1.55 g
Borax	2.375 g

Ingredients were dissolved in 400 mL of distilled water. pH was adjusted to 8.5. Water was added to a final volume of 500 ml and the buffer was stored at 4°C.

Collagenase

Collagenase CLS II	75 mg
PBS	10mL 1x PBS

Mixed well and stored in 1 mL aliquots at -20°C.

Coupling Buffer

HBSS (w/o phenol red)	50 mL
2% BSA	1.0 g

Filtered sterilized with 0.22 µm syringe filter unit, then stored at 4°C.

Cell culture media, Astrocytes

DMEM	500 mL
10% FBS	50.0 mL
200 mM Glutamaxx	5.0 mL
1% Penicillin-streptomycin	5.0 mL
MitoSerum extender	500 µL

Media was stored at 4°C.

Laminin

PBS	10 mL
Laminin	50 µL 1 mg/mL Laminin

Diluted 1 mg/mL laminin stock solution 1:20 in PBS⁺⁺ to a final concentration of 5 µg/mL.

Made fresh before each use.

Poly-D-Lysine

Diluted 1 mg/mL poly-D-lysine (pre-warmed to RT) in borate buffer, filtered-sterilized with a 0.22 µm syringe tip filter. Made fresh before each use.

MLEC medium

DMEM	400 mL
20% FBS	100 mL
1% P/S	5.0 mL
0.4% EHCS	2.0 mL

0.7% Amphotericin 3.5 mL

Culture media was stored at 4°C and pre-heated to 37°C prior to use.

Neurobasal medium (NB)

Neurobasal medium 500 mL

1% Penicillin-streptomycin 5.0 mL

200 mM Glutamaxx 5.0 mL

D-Glucose 7.0 g

To adjust the NB medium to 290 mOsm/L, 7 g of D-glucose was added to the medium.

The medium was filtered-sterilized using a 0.45 µm filter unit system. NB medium was stored at 4°C. B-27 supplement, 1:50 dilution, was added just before use.

Serum medium (SM)

DMEM 500 mL

10% FBS 50 mL

Medium was sterilized by filtration and stored at 4°C.

Dissection media (DM), serum-free, astrocytes (Astro)

DMEM 500 mL

200 mM Glutamaxx 5.0 mL

1% Penicillin-streptomycin 5.0 mL

DM-Astro Media was stored at 4°C.

Dissection medium (DM), endothelial cells (EC)

HBSS (with phenol red) 500 mL

10% FBS 50.0 mL

DM-EC media was stored at 4°C.

Dissection medium (DM), neurons

HBSS 500 mL

Penicillin-streptomycin 5.0 mL

1 M Hepes 3.5 mL

200 mM Glutamaxx 5.0 mL

DM medium was stored at 4°C.

5.1.17 Solutions for VEGF biotinylation assay

Biotin solution

Prepared 3 mL per 60 cm petri dish. EZ-Link™ Sulfo-NHS-SS-Biotin was diluted in 1x PBS to a final working concentration of 1 mg/mL. The solution was prepared fresh directly before use.

Biotin inactivation solution, 3 mL per 60 cm petri dish

200 mM Glycine was prepared in DPBS [+CA⁺⁺, +Mg⁺⁺] at a final concentration of 0.0147 g / mL, which was made fresh directly before use.

Biotin stripping solution, 3 mL per 60 cm petri dish

NaCl 0.0087 g/mL

Glutathione 0.046 g/mL

Solution was prepared with distilled water at the final concentration listed, which was made fresh before use.

VEGF Stimulation Solution

DPBS [+CA⁺⁺, +Mg⁺⁺] 500 µL

0.1% BSA 5.0 µg

Recombinant msVEGF-164 25 µg

Recombinant msVEGF-164 (493-MV-025, R&D systems) was prepared in a 1xPBS solution containing 0.1% BSA to a final stock concentration of 50 µg/mL. A working concentration of 50 ng/mL was prepared by diluting the stock solution 1:1000 in DPBS [+CA⁺⁺, +Mg⁺⁺].

Acid Wash

0.2M Acetic Acid 100 mL

0.5M NaCl 14.61 gm

The solution was prepared in water and adjusted to pH 2.9 using 1N HCL, then q.s. to 500mL. The solution was stored at RT and the pH was measured and adjusted to 2.9 before each use.

5.1.18 Solutions for animal perfusion and tissue fixation

Anesthesia

Saline (0.9% NaCl) 9.0 mL

Ketamine (10%) 2.0 mL (final concentration 17.4 mg/mL)

Xylazine (2%) 0.5 mL (final concentration 0.87 mg/mL)

Administration dose: 50-100 μ L of the anesthetic mixture was given to the postnatal and juvenile mice via intraperitoneal (i.p.) injection to ensure a minimal dose of 100 mg/kg body weight of Ketamine and 10 mg/kg body weight of Xylazine.

4 % Paraformaldehyde (PFA)

4% PFA 40 mL 10% PFA

1x PBS 10 mL 10xPBS

VE Water was added to a final volume of 100 mL and the solution was always prepared fresh.

5.1.19 Solutions for immunohistochemistry and immunocytochemistry

0.05% PBS-T

PBS 50 mL 10x PBS

0.05% Tween20 250 μ L

Distilled water q.s. 500 mL

50 mN NH_4Cl

PBS 50 mL 10x PBS

NH_4Cl 1.35 g

Distilled water was added up to a total volume of 500 mL and the buffer was stored at 4°C.

Blocking Buffer, ICC

PBS 12 mL 1x PBS

2% BSA 0.24 g

4% Donkey serum 480 μ L

Made fresh before use.

Blocking Buffer, IHC

PBS 12 mL 1x PBS

2% BSA 0.24 g

4% Donkey serum 480 μ L

Made fresh before use.

5.1.20 Solutions and buffers for western blot

LBA lysis buffer

50 mM Tris-HCl, pH 7.5	25 mL 1 M Tris, pH 7.5
150 mM NaCl	4.4 g
1% Triton X-100	2.5 mL

Distilled water was added up to a total volume of 500 mL and the buffer was stored at 4°C. Before usage for cell lysis, the following reagents were added fresh to 5 mL LBA lysis buffer:

1 mM Sodium orthovanadate	50 µL
10 mM NaPPi	0.022 g
20 mM Sodium Fluoride	0.004 g
Proteinase inhibitor cocktail	50 µL (tablet was dissolved in 500 µL distilled water)

4x SDS sample buffer

8% (w/v) SDS	2.4 g
200 mM Tris-HCl	4 mL 1.5 M Tris-HCL
400 mM DTT	1.85 g
0.4% Bromphenol blue	0.12 g
40% Glycerol	12 mL Glycerol

Distilled water was added up to a total volume of 30 ml. The buffer was stored in aliquots at -20°C. For reducing conditions 50 µL β-mercaptoethanol was added to 1 mL of 4x buffer.

5x Laemmli electrophoresis buffer

Tris-base	154.5 g
Glycerin	721.0 g
SDS	50.0 g

Distilled water was added to 10 l total volume and the buffer was stored at RT.

SDS separation gel

The recipe for make either a 10% or 12% SDS separation gel for western blots is shown in Table 5.15. APS and TEMED were added directly before pouring the gel into the casting unit. An overlay of Isopropanol is used to level the gel during polymerization.

Table 5.15: SDS separation gel.

SDS separation gel	10 %	12 %
30% (w/v) Acrylamide/bisacrylamide	3.3 mL	4 mL
1.5 M Tris-HCl pH 8.8, 0.4 % SDS	2.6 mL	2.6 mL
H ₂ O	4.05 mL	3.5 mL
10% APS	50.0 µL	50.0 µL
TEMED	5.0 µL	5.0 µL

SDS stacking gel (4%, 10 ml)

30% (w/v) Acrylamide/bisacrylamide	1.3 mL
0.5 M Tris-HCl pH 6.8, 0.4 % SDS	2.6 mL
H ₂ O	6.1 mL
10% APS	6.1 mL
TEMED	10 µL

APS and TEMED were added directly before pouring the gel into the casting unit, over the SD separation gel, and a multi-well comb was immediately inserted. Once the stacking gel solidified, the comb was removed, and samples were loaded as described in section 5.2.21.

10x Transfer buffer

Tris-base	60.5 g
Glycerin	281.5 g
SDS	25.0 g

Distilled water was added to a final volume of 2.5 L. Before usage, 20% methanol was added to the 1x transfer buffer.

Trans-Blot Turbo transfer buffer

5x Trans-Turbo transfer buffer	200 mL
Distilled water	600 mL
Ethanol	200 mL

Solution was made and stored at RT.

TBST

1x TBS	1000 mL
0.1% Tween-20	1 mL

Solution was made and stored at RT.

Blocking solution

Depending on the requirements of the primary antibody, TBST with 5% milk powder or 5% BSA was used as a blocking solution, which was always prepared fresh.

0.5 M Tris-HCl, pH 6.8

Tris-base	6.06 g
-----------	--------

Tris-base was dissolved in 60 ml of distilled water, then the pH was adjusted to 6.8 and the solution was filled up to a final volume of 100 mL and stored at 4°C.

Stripping buffer (100 mL), harsh

0.5 M Tris pH 6.8	12.5 mL
10% SDS	20.0 mL
Distilled water	67.5 mL
β-Mercaptoethanol	0.8 mL

Solution was made fresh before use.

Stripping buffer (100 mL), Mild

5 N NaCl	20 mL
Glycine	7.5 g

Distilled water was added to a total volume of 1 L and the pH was adjusted to 2.3 with HCl.

5.1.21 Solutions for fluorescent *in situ* hybridization (FISH)

(Dinitrophenyl) DNP-Labeling Mixture

100 mM GTP	1.0 μL (final 10 mM)
100 mM ATP	1.0 μL (final 10 mM)
100 mM CTP	1.0 μL (final 10 mM)
100 mM UTP	0.65 μL (final 6.5 mM)
10 mM DNP-UTP	3.5 μL (final 3.5 mM)
H ₂ O (Ambion)	2.85 μL

The DNP-labeling mixture can be kept at -20°C.

DEPC H₂O

1 mL of DEPC solution was added to 1L of distilled water, then incubated overnight at 37°C.

15% Sucrose

Sucrose	4.5 g
DEPC H ₂ O	q.s. 30 mL

Vortexed to mix, stored at 4°C

30% Sucrose

Sucrose	9.0 g
DEPC H ₂ O	q.s. 30 mL

Vortexed to mix, stored at 4°C.

Hybridization solution (Hyb+), ~40 slides

Formamide	4.0 mL
10 mM Tris-HCl, pH 8.8	80 µL
200 ug/mL Yeast tRNA	200 µL
10% Dextran	2.0 mL
Denhardt	160 µL
600 mM NaCl	960 µL
0.25% SDS	100 µL
1mM EDTA, pH 8.0	16.0 µL
DEPC H ₂ O	484 µL

Yeast tRNA and dextran were pre-warmed at 37°C and the thick solution was added last, directly to the tube (no pipette) to achieve a final volume of 8 mL. Before use, the solution was pre-thawed at 37°C, then the required amount (1:1 ratio to RNA probe mix) was pre-aliquoted in a 1.5 mL Eppendorf tube.

Wash solution 1

Formamide	100 mL
20x SSC, pH4.5	40 mL
10% SDS	20 mL
RNAse/DNase free ddH ₂ O	q.s 40 mL

Vortexed to mix, stored at 4°C.

Wash solution 2

Formamide	100 mL
20x SSC, pH4.5	20 mL
RNAse/DNase free ddH ₂ O	q.s 80 mL

Vortexed to mix, stored at 4°C.

TBST

50mM Tris HCl, pH7.5 (1M)	25 mL
15mM NaCl (5M)	15 mL
10mM KCl (1M)	5.0 mL
1% Triton (100%)	5.0 mL
2mM Levamisol (200mM)	5.0 mL
RNAse/DNase free ddH ₂ O	q.s. 500 mL

Vortexed to mix, stored at 4°C.

4% PFA:0.2% Glutaraldehyde

PFA	5 mL
Glutaraldehyde	40 uL

Vortexed to mix, stored at 4°C.

NTMT Staining Buffer

Tris HCl, pH9.5 (1M)	10 mL
MgCl ₂ (1M)	5.0 mL
NaCl (5M)	2.0 mL
Tween-20 (20%)	0.5 mL
2mM Levamisol (200mM)	5.0 mL
RNAse/DNase free ddH ₂ O	q.s. 500 mL

Vortexed to mix, stored at 4°C.

5.2 Methods

5.2.1 Mouse care and husbandry

All mouse lines were housed and bred in the animal facility of the Goethe University Frankfurt and maintained in accordance with EU regulatory guidelines. For this study, wild-type mice were obtained from C57BL6/J breedings, in which all transgenic mouse lines were bred in the C57BL6/J background. All mice were weaned around 3 weeks after birth

(P20-22), with males and females housed separately. Experimental postnatal mice (P10 and under) were labeled with a number, while adult mice were ear-tagged, and tail biopsies were obtained for genotyping. The day of birth for all animals was recorded as postnatal day 0 (P0). All mouse lines used in this study are listed in Table 5.14.

5.2.2 Strategy for generating a cell-type specific Rosa26 reporter mice

To assess the cell-specific promoter activity of the CaMKIIa-Cre, GLAST-CreRT2, and Cdh5-CreRT mouse lines, mice from these lines were crossbred to the (Rosa26)EYFP reporter line. In each case, Cre-positive males were crossed with (Rosa26)EYFP^{lox/lox} females. The Cre-positive, (Rosa26)EYFP^{lox/+} males were further crossed with (Rosa26)EYFP^{lox/lox} females to generate homozygous (Rosa26)EYFP mice that were either Cre-positive or Cre-negative. Post-fixation mouse brain tissues were collected at P5 from CaMKIIa-Cre (Rosa26)EYFP^{lox/lox} mice, or at P10 from GLAST-Cre (Rosa26)EYFP^{lox/lox} mice and Cdh5-Cre (Rosa26)EYFP^{lox/lox} mice, post tamoxifen induction regimen, then qualitatively assessed for cell-specific promoter activity by immunohistochemistry.

5.2.3 Tamoxifen applications of inducible knockout mouse lines

GLAST-CreRT2 and Cdh5-CreRT2 mice required the administration of tamoxifen to induce the activity of Cre-recombinase, expressed exclusively under the GLAST and VE-Cadherin promoters, respectively. Therefore, mice were treated with 4-hydroxytamoxifen (4-OHT), an active metabolite of tamoxifen generated in the liver. A 10mg/mL stock solution was prepared by first dissolving 4-OHT in 200 μ L 99% ethanol with the aid of an ultrasonic water bath. Once completely dissolved, peanut oil was added to not exceed a maximal concentration of 20% ethanol in the stock solution and further mixed in with the aid of water bath sonication. The 4-OHT 10mg/mL stock solution was aliquoted and stored, protected from light, at -20°C. Before administration, a 4-OHT working solution was freshly prepared by further dilution of the stock solution with peanut oil and brief water bath sonication. Postnatal mice were treated with 50 μ L of 1 mg/mL 4-OHT via intraperitoneal (i.p.) application, once every 24hrs, from P5-P7 or P8-P9. Adolescent GLAST-CreRT2 mice received an i.p. injection of 50 μ L, 2 gm/mL 4-OHT, once every 24hr from P15-17.

5.2.4 Breeding for embryonic neuronal cultures

Primary hippocampal neurons were isolated from the mouse embryos of either wild-type or Nes-cre VEGFR2^{lox/-}, or compound Nes-cre VEGFR2^{lox/} ephrinB2^{lox/-} mice. Time-pregnant breedings were established for these mouse lines in which the formation of vaginal plugs on female mice was monitored daily from the first day of breeding. The day of the plug detection was recorded as embryonic day 0.5 (E0.5). Embryos were removed according to

experimental procedures between E16.5 - E18.5.

5.2.5 Coverslip pre-treatment for primary cell cultures

Coverslips were treated with nitric acid in a glass beaker at RT overnight then washed 3-4 times, in 15 min intervals while gently rotating, to remove the acid. Washed coverslips were spread separately on WhatMann paper to dry, then transferred to a glass petri dish and baked at 165 °C to sterilize.

5.2.6 Coating of coverslips and culture dishes

For astrocytic cell cultures. Acid-treated coverslips were placed into 24-well plates and coated with 1 mg/ml poly-D-lysine (PDL) in borate buffer (400 µL/well) at 37 °C for a minimum of 5 hours. Then coverslips were washed 3 times with distilled sterile water, left in the hood to dry for 20 minutes, and coated with 5 µg/ml laminin in DPBS [+CA⁺⁺, +Mg⁺⁺] (400 µL/well) for at least 2 hours at 37 °C. Excessive laminin was removed by washing coverslips 3 times with DPBS [+CA⁺⁺, +Mg⁺⁺], then stored in DPBS at 4 °C until further use. Before cell seeding, the wells were filled with 400 µL NB medium and placed at 37 °C, 5% CO₂ incubation for pH and temperature equilibration.

For neuronal cell cultures. For biochemistry and molecular biology experiments, primary hippocampal neurons were seeded in 60 mm and 100 mm Petri dishes. Before cell seeding, dishes were coated overnight at 37 °C with 1 mg/mL PDL in borate buffer. Plates were washed 3 times with distilled water, air dried for 20 min, then coated with 5 µg/mL laminin in DPBS [+CA⁺⁺, +Mg⁺⁺] for a minimum of 2 hours. Coated plates were stored in DPBS [+CA⁺⁺, +Mg⁺⁺] until further use.

5.2.7 Isolation of primary hippocampal neuron cultures

Time-pregnant female mice were sacrificed by cervical dislocation and their E16.5 to E17.5 embryos were collected in a pre-chilled petri dish. Embryos were separated from their decidua and placenta, their heads decapitated, and placed in the wells of a 24-well plate filled with pre-chilled dissection medium (DM). The corresponding tails were cut for genotyping. Brains were dissected from the head tissues and skull, then placed in a petri dish containing chilled DM. Underneath a dissection microscope, the surrounding meninges were removed from the brain, and the brain split into two cortical halves and separated from the brain stem. The hippocampal tissues were micro-dissected from each cortical half and collected, on ice, in a 15mL conical tube (per animal genotype) containing 1 mL of DM. Once all hippocampi tissues were collected, the DM was replaced with 1 mL pre-warmed 0.25% trypsin-EDTA and samples were water bath incubated at 37 °C for 15 min. Post incubation, the trypsin-EDTA was discarded, and the tissue samples were washed 3

times with serum-containing medium (SM), followed by 3 washes with neurobasal medium (NB). Tissues were dissociated with gentle titration in 2 mL NB medium via 20-30 repetitive passages through a fire-polished glass Pasteur pipette. To pellet the dissociated cells, the total NB medium volume was adjusted to 5 mL and samples were centrifuged at 71 x g for 5 min. The debris containing supernatant was removed and the remaining cell pellet was resuspended in 1 mL warm NB medium using the fire-polished Pasteur pipette. A sub-sample of cells was mixed 1:1 with trypan blue to determine the number of viable cells using a Neubauer chamber. In Petri dishes pre-coated with PDL and laminin, cells were seeded at 600,000 cells per 60 mm plate, or 1.5 million cells per 100 mm plate, in NB medium supplemented with B27. Cells were cultured for 14 days at 37°C in the presence of 5% CO₂.

5.2.8 Isolation of primary Astrocytic cultures

Primary astrocytes were harvested from hippocampal brain tissues isolated from P10 wild-type mice. Mice were deeply anesthetized with an i.p. administered Ketamine/Xylazine cocktail, then decapitated. Brains were removed from their skulls and placed in cold serum-free dissection media (DM-Astro). Under a dissection microscope, in cold DM-Astro, the brain tissues were separated into left, and right cortices and the meninges were removed. Hippocampal tissues were dissected from each cortical half and placed in 15 mL conical tubes per genotype. Tissues were digested for 25 min at 37°C in 2 mL 0.25% trypsin-EDTA, diluted 1:1 with DPBS [-CA⁺⁺, -Mg⁺⁺]. The digestion was stopped by adding 3 mL pre-warmed serum-containing medium (SM) and gently inverting the tubes to mix. Tissues were washed by twice removing and replacing the medium with SM using a Pasteur pipette. In 1 mL SM, the cells were gently dissociated via 20 - 30 repetitive passages through a fire-polished glass Pasteur pipette. The cell suspension was adjusted to a total volume of 5 mL with SM, then centrifuged at 71 x g for 5 minutes. The debris containing supernatant was removed, cells resuspended in SM, and centrifuged again. The cell pellet was resuspended in 5 mL culture media and transferred to a T-25 flask and incubated at 37°C in the presence of 5% CO₂. Once cell colonies started to form, 1 - 2 days post seeding, the culture medium was replaced. After reaching 90% confluence, cells underwent 3 days of 220 rpm orbital shaking at 37°C with 5% CO₂ to obtain greater than 95% cell purity. The medium was replaced after 1.5 days and 3 days of shaking. Cells were maintained in cell culture media at 37°C with 5% CO₂ for a maximum of 3 weeks before experimental use.

5.2.9 Plasmid DNA preparations

Large-scale plasmid preparation was performed via bacterial electroporation of stock plasmid DNO. A 30 μL aliquot of *E. coli*/One Shot TOP10 competent cells was co-incubated on ice with 1 μL plasmid DNA stock (50 ng/ μL) and 20 μL distilled water for 30 min. The mixture was transferred to a 0.2 cm electroporation cuvette, stimulated with a 5.5 ms pulse of 1.5 V, and immediately resuspended in 500 μL of SOC media in a 1.5 mL Eppendorf tube. Following a 1 h 37°C incubation period, 50-100 μL of the transformant bacteria were plated on LB-agar plates containing the appropriate selection antibiotic. Bacterial cultures were generated by single bacteria colony inoculation of a 5 ml LB-medium starter culture containing 100 $\mu\text{g}/\text{ml}$ kanamycin or 50 $\mu\text{g}/\text{ml}$ Ampicillin. The culture was grown over night at 37°C, then used to inoculate 200 mL LB-media with selection antibiotics. Bacteria were harvested by centrifugation at 6000 x g for 15 minutes at 4°C. Plasmid DNA preparation was carried out using the QIAGEN EndoFree Plasmid Maxi Kit in accordance with the manufacturer's protocol. The precipitated DNA was resuspended in 500 μL Tris-EDTA (kit provided) and concentration was measured with a spectrophotometer, NanoDrop 2000.

5.2.10 Genomic DNA extraction

From mouse tail biopsies. 0.1 - 0.5 cm long mouse tail biopsies were obtained using heat-sterilized surgical scissors. DNA was extracted by boiling biopsies at 95 °C in 100 μL 50 mM NaOH for 2 h. The lysates were neutralized by adding 10 μL of 1.5 M Tris pH 8.8 and vortexed. For genotyping PCR reactions, 2 μL of the lysate was used.

From primary cell cultures. Genomic DNA was extracted from primary cell cultures using the Macherey-Nagel NucleoSpin® Tissue kit. Cells were washed twice with cold DPBS [+CA⁺⁺, +Mg⁺⁺] to remove cell culture media. Cells were then collected in 500 μL DPBS [+CA⁺⁺, +Mg⁺⁺] using a cell scraper, pelleted at 71 g for 5 min at 4 °C, then lysed using the kit provided lysis buffer ATL and proteinase K digestion. Genomic DNA extraction was performed according to the kit-provided manufacturer's protocol. DNA concentration was measured with a spectrophotometer, NanoDrop 2000.

5.2.11 Genotyping PCR

Per genetic sample, a 25 μL PCR-master mix was prepared as indicated in Table 5.16. Taq polymerase was added to the reaction mix directly before use and briefly vortexed. Primers used for the different PCR reactions are listed in Table 5.10.

Table 5.16: PCR master mix, amount per reaction.

Component	Amount
Distilled Water	q.s. 25 μ L
10x Taq polymerase buffer (NEB)	2.5 μ L
dNTP cocktail (25 mM each)	0.2 μ L
Primer (forward and reverse primer, 100mM each)	0.25 μ L
Taq Polymerase (NEB)	0.25 μ L

The reaction mixture was combined with 2 μ L of extracted DNA sample per well in a 0.2 ml 96-well plate. Samples were amplified using the appropriate PCR program for the respective genotype as listed in Table 5.17.

Table 5.17: Genotyping PCR programs.

Target Gene	Cre	ephrinB 2	(Thy1)EGF P	(Rosa26)EYF P	VEGF	VEGFR2-del	
Initial Denature	94 °C, 3 min	94 °C, 1 min	95 °C, 2 min	94 °C, 2 min	95 °C, 1 min	94 °C, 2 min	
Denature	94 °C, 1 min	94 °C, 45 sec	95 °C, 30 sec	94 °C, 45 sec	95 °C, 1 min	94 °C, 1 min	35x cycles
Annealing	67 °C, 1 min	62 °C, 45 sec	60 °C, 45 sec	65 °C, 45 sec	60 °C, 55 sec	65 °C, 1 min	
Extension	72 °C, 1 min	72 °C, 45 sec	72 °C, 40 sec	72 °C, 1 min	72 °C, 2 min	72 °C, 3 min	
Final Extension	72 °C, 5 min	72 °C, 5 min	72 °C, 5 min	72 °C, 5 min	72 °C, 5 min	72 °C, 5 min	
Final Hold	4 °C, ∞	4 °C, ∞	4 °C, ∞	4 °C, ∞	4 °C, ∞	4 °C, ∞	
Product Size (bp)	Positive: 720	WT: 240 Lox: 320	Positive: 300	WT: 650 Tg: 350	WT: 105 Lox: 149	WT: 121 Lox: 149 Deletion: 400	

5.2.12 DNA size discrimination by agarose gel electrophoresis

Agarose (2%, w/v) was heat dissolved in a 1x TAE solution using a microwave. After cooling, 1 μ L EtBr per 100 mL gel volume was added and the solution was poured into a gel cast.

DNA products were mixed with loading buffer (1:6), loaded in the gel, and separated for 30 - 45 min at 200 V at 400 amp together with a DNA ladder reference. After electrophoresis, the DNA fragments were visualized using the UVP GelStudio Plus gel documentation system.

5.2.13 RNA extraction from primary tissue and cell samples

From hippocampal brain tissue. Whole hippocampal brain tissue was isolated from P1, P10, P20, and P30 mice for RNA extraction. Mice were deeply anesthetized with an i.p. administered Ketamine/Xylazine cocktail, then decapitated. Brains were removed from their skulls and placed in cold dissection media (DM). Under a dissection microscope, in cold DM, the brain tissues were separated into left and right cortices, and the meninges were removed. Hippocampal tissues were dissected from each cortical half and placed in 1.5 mL Eppendorf tubes, then snap-frozen in liquid nitrogen and stored at -80°C until further used.

For RNA extraction, tissue samples were resuspended in 1 mL TRIzol reagent and triturated by repetitive passage through a 27G x 3/4" hypodermic needle docked to a 1 mL syringe. The homogenized samples were incubated at RT for 5 min to ensure the complete dissociation of nucleoprotein complexes. Samples were treated with 200 µL cold chloroform, vigorously shaken for 15 seconds, and then further incubated at RT for 2-3 min. To induce the phase separation of RNA molecules, samples were centrifuged at 12,000 g for 15 minutes at 4°C. The RNA containing the upper aqueous phase was transferred to a new 1.5 mL Eppendorf tube containing 500 µL cold 100% isopropanol and incubated overnight at 4°C with gentle mixing to enhance RNA precipitation. Next, the RNA precipitant was pelleted by centrifugation at 12,000 g for 10 min at 4°C. The supernatant was removed, and the remaining pellet was washed by briefly vortexing in 1 mL 75% ethanol. Again, the sample was pelleted with a 7,500 g centrifugation for 5 min at 4°C, after which the ethanol wash was discarded, and the remaining pellet was left to air dry at RT for 10-15min then resuspended in RNase-free distilled water. Samples were boiled in a heating block at 55°C for 10 minutes and RNA concentration was measured with a spectrophotometer, NanoDrop 2000. Aliquoted RNA samples were stored at -80°C until further use.

From primary cell cultures. Hippocampal neurons and astrocytes were isolated and cultured as described in Section 5.2.7. Dishes containing 90% confluent culture cells were placed on ice, the culture medium was removed, and cells were washed twice with PBS. After discarding the PBS, cells were treated with 1 ml TRIzol reagent. Cell samples were

incubated at RT for 5 minutes and gently homogenized, via trituration with a pipette docked with a 1.5mL tip, then transferred into 1.5 mL Eppendorf tubes. The homogenized samples were processed for RNA isolation as described above.

5.2.14 Reverse transcriptase PCR

Single-stranded cDNA was synthesized from total RNA samples using the High Capacity cDNA Reverse Transcription Kit (Applied Biosystems). On ice, equal amounts of total RNA were prepared in RNase-free distilled water in a total volume of 10 μ L per sample. A 2x reverse transcriptase master mix was prepared as shown in Table 5.18 of which 10 μ L was to each RNA sample and gently mixed.

Table 5.18: RT-PCR master mix, amount per reaction. Cocktail mix for generating cDNAs.

Component	Amount
10x RT Buffer	2.0 μ L
25X dNTP Mix (100mM)	0.8 μ L
10x RT Random Primers	2.0 μ L
MultiScribe™ Reverse Transcriptase	1.0 μ L
RNase Inhibitor	1.0 μ L
Nuclease-free H ₂ O	3.2 μ L
Total reaction volume	10 μ L

Using a thermo cycler, the reverse transcriptase PCR was conducted under the programmed settings displayed in Table 5.19.

Table 5.19: Reverse transcription PCR program.

	Step 1	Step 2	Step 3	Step 4
Temperature	25 °C	37 °C	85 °C	4 °C
Time	10 min	120 min	5 min	∞

5.2.15 Quantitative Real-Time PCR

Synthesized cDNA was used for quantitative real-time PCR to determine the expression levels of VEGF in primary tissue and cell samples (Table 5.18). As described in section

5.3.5, the relative VEGF mRNA levels were normalized to those of the housekeeping gene, beta-actin, measured in the same cDNA sample. Quantitative real-time PCR assay primer and TaqMan[®] probe mixtures used in this study for each targeted gene are listed in Table 5.20. All samples were prepared and measured in triplicates per gene target.

Table 5.20: TaqMan[®] quantitative real-time PCR mix, amount per reaction.

Component	Amount
2x TaqMan Master Mix	10 μ L
Primer & Probe (FAM-MGB) Mix	1.0 μ L
cDNA	1.0 μ L
Nuclease-free H ₂ O	8.0 μ L
Total reaction volume	20 μ L

Due to alternative splicing, mouse VEGF mRNA transcripts can be either 120, 164, or 188 amino acids in length. To determine the relative expression levels of VEGF splice variants in cells isolated from primary hippocampal tissues, primers, and FAM-tagged probes were designed (Table 5.12, Figure 3.10) to target each transcript splice variant as described in section 3.3.1. Total RNA was isolated from each cultured cell-type (section 5.2.13) and reverse transcribed into cDNA (section 5.2.14). The synthesized cDNA was combined with a primer-probe cocktail mix for each targeted splice variant (Table 5.12). Using quantitative real-time PCR, the relative expression levels were quantified, in triplicate, in reference to that of beta-actin in the same sample.

Table 5.21: Custom quantitative real-time PCR mix, amount per reaction.

Component	Amount
2x TaqMan Master Mix	10 μ L
VEGF universal forward primer [exon 4] (10 pmol)	1.8 μ L
VEGF reverse primer (10 pmol)	1.8 μ L
VEGF FAM-BHQ1 (10 pmol)	0.5 μ L
cDNA	1.0 μ L
Nuclease-free H ₂ O	4.9 μ L
Total reaction volume	20 μ L

The program settings for performing all quantitative real-time PCR reactions are shown in Table 5.22 and the analysis is described in section 5.3.5.

Table 5.22: Quantitative real-time PCR program.

Step	Temperature	Time	
First Strand Synthesis	50 °C	2min	
RT Inactivation	95 °C	10 min	
Denaturation	95 °C	15 sec	<i>40x cycles</i>
Annealing / Extension	60 °C	1 min	

5.2.16 VEGF stimulation assay of primary neuronal cultures

Recombinant VEGF was added at a final concentration of 50 ng/mL to the culture medium. A stimulation duration of 30 minutes was used for the biochemical analysis of VEGFR2 activation and downstream signaling, as well as receptor internalization in neurons. The experimental details for each assay are described below.

5.2.17 KCl stimulation assay of primary astrocytic cultures

Primary astrocytes were harvested from WT mice, purified, and cultured on coated 60 mm Petri dishes or glass coverslips in 24-well plates as previously described (see section 5.2.8). Cultured cells were grown until 80% confluence (~48 hrs) at 37 °C with 5% CO₂, then switched to minimum medium (FBS-free DMEM with 5% PenStrep) and further incubated for another 24 hrs. Just before stimulation, cells were washed 3 times with minimum media, then stimulated with 40 mM KCL diluted in DMEM or DMEM only for 30mins at 37 °C with 5% CO₂. Cells grown on 60 mm petri dishes were placed on ice, washed twice with PBS then immediately lysed and processed for protein expression analysis by Western Blot. Cells grown on glass coverslips were fixed and immunolabeled for imaging (section 5.2.8).

5.2.18 VEGFR2 receptor internalization assay

VEGFR2 membrane dynamics in neurons were assessed by stimulating cells with biotinylated VEGF, followed by a VEGFR2 capture ELISA, to determine the amount of surface vs internalized receptor. As described in section 5.2.7, hippocampal neurons were isolated from E17.5 mouse embryos, and cells were seeded at a density of 5 x 10⁶ cells per 60 cm petri dish. Neuronal cells were cultured for 2 weeks at 37 °C in the presence of 5% CO₂. One day prior to the biotinylation assay, the wells of a flat-bottom Maxisorp Nunc-Immuno ELISA plate were coated with either 100 µL per well of 1:500 -VEGFR2 (R&D Systems) in PBS, 3 wells per treatment condition, or PBS only, 2 wells per treatment condition as a negative control. The ELISA plate was incubated over night at 4 °C. The next

day, the coated ELISA plate was washed 3 times for 5 min with PBS, then incubated at RT for 2 hr in a PBS-blocking solution containing 5% FBS. During the incubation period, cultured neuronal cells were placed on ice for 5 mins and washed 2 times with DPBS [+CA⁺⁺, +Mg⁺⁺], then incubated on ice with a final concentration of 50 ng/mL biotin-VEGF (R&D systems, Atk-Nr# NFVE0) for 20mins at 4 °C to allow for the maximum binding of VEGF to membrane-bound VEGFR2.

For measuring surface VEGFR2. A subset of cultured cells remained on ice for an additional 30 min and then were washed 2 times with DPBS [+CA⁺⁺, +Mg⁺⁺]. The cell supernatant was aspirated for each, then cells were treated with 250 µL lysis buffer and transferred to a 1.5 mL Eppendorf tube using a cell scraper.

For measuring internalized VEGFR2. The remaining cell samples were incubated at 37 °C for 30 min to promote receptor internalization. Following the incubation period, the cells were washed with a pH 2.9 acetic acid solution for 6 mins on ice to remove all non-internalized biotinylated VEGF molecules. Plates were then washed 2 times with DPBS [+CA⁺⁺, +Mg⁺⁺], the supernatant aspirated, then the cells were lysed and transferred to a 1.5 mL Eppendorf tube.

For capture ELISAs. All collected samples were incubated at 4 °C with end-over-end rotation for 20min to complete the lysis process. Next, the samples were centrifuged at 16,000 x g at 4 °C for 15 min to pellet the cellular debris. The protein-containing supernatants were transferred to fresh tubes and their concentration was determined via Bradford assay (described in section 5.2.19). ELISA plates were washed 3 times for 5 min in PBS to remove the excess blocking buffer. Equal amounts of protein samples, or lysis buffer only as a background control, were added to the -VEGFR2, or PBS, coated wells and incubated overnight at 4 °C with gentle rocking. The following day, the plate was washed at RT 3 times with 0.05% PBS-Tween and then treated with 100 µL per well horse radish peroxidase (HRP, 1:200 in 1% FBS-PBS, R&D systems msVEGF DuoSet kit, Atk-Nr# DY493-05) for 30 min at RT. Again, the plate was washed 3 times for 5 mins with 0.05% PBS-Tween at RT. Following the washing steps, the wells were treated with 100 µL of a kit to provide substrate to induce HRP chemiluminescence and incubated for 20 min in the dark at RT. The reaction was stopped by adding 50 µL of a kit-provided stop solution and absorbance was measured at 450 nm wavelength using a microplate reader.

5.2.19 Protein concentration measurements of cell lysates

Cultured cells (neurons, astrocytes, or endothelial cells) were placed on ice and washed twice with pre-chilled DPBS [+CA⁺⁺, +Mg⁺⁺] and then aspirated. The remaining adherent

cells were collected in pre-chilled 250 μ L LBA lysis buffer using cell scrapers and transferred to 1.5 mL Eppendorf tubes. Samples were incubated at 4 $^{\circ}$ C for 20 min with end-over-end rotation to complete the cell lysis process. To remove insoluble material (nuclei, cytoskeletal, and insoluble membrane components), the lysate was centrifuged at 14,000 x g for 15 min at 4 $^{\circ}$ C. The supernatants were placed in fresh Eppendorf tubes and stored at -80 $^{\circ}$ C if not immediately used for downstream assays. Sample protein concentration was measured directly before the experimental procedure with the aid of the Pierce[™] BCA Protein Assay Kit. BSA protein standard series was prepared in LBA lysis buffer with a final working range of 20 - 20,000 μ g/mL. A working reagent of bicinchoninic acid was prepared by mixing 50 parts of BCA Reagent A with 1 part of BCA Reagent B (50:1, Reagent A:B). Samples and BSA standards were assayed together in triplicates, in a Falcon[™] 96-well flat bottom plate, by mixing 25 μ L volume of each with 200 μ L of the working reagent per well. Next, the plate was covered and incubated at 37 $^{\circ}$ C for 30min. The colorimetric detection and quantification of the protein amounts were achieved by measuring the absorbance at 562 nm wavelength with a microplate reader. Sample total protein concentration was determined with respect to the BSA standard and equal amounts of sample protein were used for subsequent assays.

5.2.20 Immunoprecipitation and pull-down assays

Protein A or protein G sepharose[™] beads were used, depending on the species in which the antibody for immunoprecipitation was produced. The beads were kept in a 1:1 PBS suspension with 50% ethanol to avoid contamination. For co-immunoprecipitation assays, 40 μ L of bead suspension was washed three times with PBS by centrifugation at 2,500 rpm for 2.5 min in a 1.5 mL Eppendorf tube. After washing, the sepharose[™] beads were coupled to the desired IP antibody by co-incubation at the appropriate antibody dilution (see 5.2.20) for 45 minutes at RT with end-over-end rotation. Controls were performed using non-antibody coupled sepharose[™] beads. For pulldown assays, lysates from VEGF-stimulated neuronal cultures were used (see section 5.2.16). As described in section 5.2.19, cells were lysed and protein concentrations were determined. Equal amounts of protein (200 μ g to 800 μ g) were added to pre-antibody coupled or non-coupled sepharose[™] beads and incubated overnight at 4 $^{\circ}$ C with end-over-end rotation. On the following day, the beads were washed 3 times by centrifugation at 600 x g for 3 min with pre-chilled LBA lysis buffer containing vanadate to remove unbound proteins. After the last washing step, the supernatant was completely removed using gel saver tips. Samples were boiled at 95 $^{\circ}$ C for 5 min in 20 μ L 2x SDS sample buffer containing 50 μ L of 2-

mercaptoethanol to denature the proteins. The samples were kept and stored at RT or directly separated on SDS gels for western blot analysis.

5.2.21 SDS polyacrylamide gel electrophoresis and Immunoblotting

For the separation and detection of desired proteins in the cell and tissue lysates, sodium dodecyl sulfate-polyacrylamide gel electrophoresis (SDS-PAGE) and Western blotting were performed. Depending on the size of the proteins, different concentrations of SDS-PAGE gels were used (Table 5.15). Sample protein concentrations were determined (see section 5.2.19) and equivalent amounts of protein were loaded onto the gel with a pre-stained protein marker as a reference. Gels were run at a voltage of 80 V until the proteins entered the separating gel. Then the voltage was increased to 120 V for 60-90 min. After separation via gel electrophoresis the proteins were transferred to a nitrocellulose membrane using a semi-dry blotting chamber (~5.5 mA/cm², 10-15 V for 60 min) in transfer buffer containing 20% methanol or with the Trans-Blot Turbo transfer system (~21.8 mA/cm², 15-25 V for 10 min) from Bio-Rad in Trans-Blot Turbo transfer buffer. After transfer blotting, membranes were stained for 5 min at RT with Ponceau protein detection solution as a quality control check for equivalent protein loading. The Ponceau stain was gently removed membranes by brief rinsing with 0.1 N NaOH followed by several water rinses. The membrane was blocked in the blocking solution (3-5% milk powder or BSA in TBS-T) for 1 hour at RT, then incubated with a 1:1000 dilution of primary antibody in blocking solution overnight at 4°C. The following day, the membrane was washed 3 times for 10 min in TBS-T before incubation with 1:1000 dilution HRP conjugated secondary antibody in blocking solution for 2 hours at RT. The membrane was again washed 3 times for 10 min in TBS-T and the respective protein was visualized by adding an enhanced chemiluminescence detection reagent (ECL). The chemiluminescent exposure coincided with a white light exposure (30 sec to 2 min) for simultaneous protein band and marker detection with the ImageQuant LAS 4000 system.

5.2.22 Stripping and re-blotting

After immunoblotting, some membranes were stripped of bound antibodies in order to reprobe for alternative proteins. The membranes were washed in TBS-T for 10 min and then incubated with stripping buffer for 5 min at RT. The buffer was discarded, and fresh stripping buffer was applied for an additional 5 min. The membrane was then washed twice with distilled water for 5 min, followed by 2 further TBS-T washes for 10 min. The efficiency of stripping was confirmed by incubation with ECL and detection imaging. The membrane was then rinsed several times with distilled water and TBS-T. Hereafter, a second round of membrane immunoblotting was performed as described above.

5.2.23 Perfusion and fixations

Postnatal or Juvenile mice were first deeply anesthetized with Xylazine/Ketamine as confirmed by a limb reflex test. Mice were perfused transcardially under anesthesia first with pre-chilled PBS for 5 to 8 min and then with pre-chilled 4% PFA in PBS for 7 to 15 min. After perfusion, brains were dissected from the skull and post-fixed overnight in 4% PFA at 4°C or for 4 hr at RT, depending on primary antibody requirements. Brains were washed several times in PBS then either embedded directly for sectioning or stored in 0.01% sodium azide PBS solution at 4°C.

5.2.24 Immunocytochemistry

Astrocytic cells, cultured on glass coverslips in 24-well plates, were washed twice with PBS and then placed on ice. Cells were fixed with a solution of pre-chilled 4% PFA-Sucrose in PBS for 12 min then washed twice with pre-chilled PBS. Excessive PFA was removed by incubating fixed cells with pre-chilled 50 mM NH₄Cl in PBS for 10 minutes. Fixed cell samples were washed twice with PBS and then permeabilized with 0.1% Triton X-100 in PBS for 5 min. Next, cells were further washed 3 times in PBS for 5 min followed by 30 min incubation at RT in blocking solution (2% BSA / 4% donkey serum in PBS). Primary antibody incubation (see **Error! Reference source not found.** for dilutions) in blocking solution was carried out overnight at 4°C. The following day, samples were washed three times for 5 min with PBS and then incubated at RT for 2hr in secondary antibody (all 1:500, see 5.1.9) diluted in blocking solution. Cell fixed coverslips were washed three times for 5 minutes with PBS, dipped in water, and mounted upside down onto microscope slides using Dako mounting medium. Images were acquired using a digital camera attached to a laser scanning confocal microscope SP5 (Leica, SP5).

5.2.25 Embedding and cutting of vibratome sections

Brains were embedded in 4% agarose, which was heat dissolved in water, then allowed to polymerize at RT. Embedded brains were directly mounted on a flat metal block using super glue, docked onto a vibratome (Leica), and immersed in 1% PBS for cutting. Depending on the experimental requirements, brains were sliced into either coronal or transverse sections (see Table 5.23). Cut sections were serially collected in 24-well plates containing 0.1% sodium azide in PBS and stored at 4°C until processed for immunohistochemistry.

Table 5.23: Tissue sectioning parameters.

Tissue Samples		Vibratome settings		
Analysis Type	Section Type	Section Thickness	Speed	Amplitude
Dendritic Branching & Spines	Coronal	300 μm	0.34 $\mu\text{m/s}$	0.90 μm
Protein Expression	Coronal	80 - 100 μm	0.2 $\mu\text{m/s}$	0.90 μm

5.2.26 Immunohistochemistry of free-floating sections

For thin sections (50-100 μm). Free-floating vibratome sections of postnatal mice brains were first permeabilized with 0.4% PBS-Triton X-100 for 30 minutes, then blocked with 10% PBS-DS for 1 hr with gentle rocking. Alternatively, brain sections from juvenile mice were permeabilized in blocking solution (0.4% Triton X-100 and 10% donkey serum in PBS) for 2 hrs at RT. After blocking, sections were incubated at 4°C with primary antibodies (see 5.1.8 for dilutions) in 1% donkey serum in PBS. Sections were thrice washed in PBS for 10 min and then incubated with fluorescent-labeled secondary antibodies (all 1:250, see **Error! Reference source not found.**) in 1% PBS-DS for 2 hr at RT. Sections were further 3 washes in PBS followed by a 10 min incubation of 1:1000 DAPI in PBS to stain all cellular nuclei. After a final 10 min PBS wash, sections were mounted and dried on glass slides, then preserved in fluorescent mounting medium (Dako) and coverslipped.

For thick sections (300 μm). Thick coronal brain sections, of transgenic (Thy1)EGFP crossed-breed mouse lines, were used for analyzing the spines and complete dendritic tree structures of hippocampal neurons. Sections were initially permeabilized in 1% PBS-Triton X-100 for 30 min at RT, then further permeated in 1% PBS-BSA/Triton-X-100 blocking solution for 1 hr. Permeabilized sections were incubated in primary antibody (1:500 ck - GFP in blocking solution) at RT overnight. The following day, sections were thrice washed at RT in PBS and then incubated for 2hrs at RT in secondary antibody (1:500 dk -Chicken 488 in blocking solution). After three final 10 min PBS washes, sections were mounted on glass slides, dried, and preserved in fluorescent mounting medium (Dako).

5.2.27 *In situ* hybridization probe design

Riboprobes were designed using the FASTA database of annotated mRNA coding sequence entries of the NCBI Nucleotide database. FASTA sequences were entered into the http://biotools.umassmed.edu/bioapps/primer3_www.cgi, which generated probe sequence options based on product size, primer melting points, and other parameters. Riboprobes were crossed check for target specificity using the NCBI BLASTn search tool. Probes that targeted the introns or intron/exon regions were not used. Selected probe design sequencings were synthesized as primer oligos and used to amplify RNA isolated from WT mice tissues with known expression of the target gene. The resulting cDNA product was gel separated on a 1% agarose gel and then underwent gel exaction and amplicon product purification using a PCR clean-up kit (Promega). The final cDNA product was then inserted into the pGEM-T Easy Vector System (Promega) which has a T7/SP6 dual promoter for RNA synthesis for long-term storage and repeat use. For *in situ* experiments, the plasmid vector was linearized and then processed for *in vitro* transcription, using either the T7 or SP6 promoter to generate a sense (target probe) and anti-sense (negative control) riboprobe from the same probes sequence. The amplicon products were treated with DNase1 to remove any DNA contaminants and purified using a Qiagen RNaseay Kit. Riboprobes were assessed for quality and concentration using a NanoDrop nucleic meter. Probes with a 260/280 ratio of 2.0-2.2 and also higher than the 260/230 ratio were considered of good quality. Final riboprobes products were stored in hybridization buffer (Hyb⁺) at -80 C in 10 uL aliquots at a concentration of 30 ng/uL. For *in situ* experiments, a final riboprobe concentration of 200-400ng (0.2-0.4 µg) per mL Hyb⁺ was used.

5.2.28 Fluorescence *In situ* hybridization (FISH)

FISH experiments were performed over three days using cryo-fixed brain tissues, sliced into 10 µm thick sections.

Day 1: Proteinase K treatment & In situ Hybridization. Mounted sections were washed 3 times briefly in PBT at RT. Next slides were treated at 20°C in the proteinase K solution for 20 mins to permeabilize the tissues. The tissues were then treated with 4% PFA:0.2% glutaraldehyde for 10 mins at RT followed by two 5 min washes in PBT solution. Samples were then pre-treated at 60°C-70°C for 1-3 hrs with Hyb⁺ buffer. Separately, riboprobes were diluted to 0.2-0.4 ng/mL in Hyb⁺ buffer and pre-incubated for 1 hr between 60-70°C. Tissues were then transferred to the pre-warmed Riboprobe/Hyb⁺ solution and incubated overnight at 60-70°C.

Day 2: Immuno-staining for anti-dig (for Digoxigenin coupled RNA probes). Overnight riboprobe-treated samples were washed twice for 30 min each in wash solution 1 at 65°C. Next, samples were washed three times in wash solution 2 for 5 min at RT, followed by three 15 min washes in the same solution at 65°C. Then samples were washed three times in TBST containing 2 mM levamisole for 10 mins each at RT. Samples were then pre-incubated with TBST containing 10% sheep serum to block the non-specific binding of the anti-digoxigenin-AP probe. Finally, samples were placed in a 1:2000 dilution of anti-digoxigenin-AP in 10% lamb serum at 4°C overnight.

Day 3 of in situ: Development of probed mRNA signal. Overnight samples were washed for 20 min in TBST (with 2mM levamisole) at RT followed by two 15 min washes in NTMT buffer. Probe signals were developed in NTMT buffer containing 20uL per mL NBT/BCIP stock solution. Depending on the probe, development took 2-4 hrs at RT to several days at 4°C. Samples stayed in the developing solution until the desired signal strength is achieved, which could take several days. Signal intensity (red) was checked periodically under a light source using a white background. The NTMT buffer used for the developing solution is of high pH. To stop the signal development process, samples were washed several times in 1x PBS solution to lower the pH which stops the NTMT reaction.

5.3 Data analysis

5.3.1 bodyweight measurements of endothelial-specific VEGF deletion mice

The body weights of tamoxifen-induced Cdh5-CreRT2 VEGF^{lox/lox} mice, and their littermate controls, were measured across 3 mouse litters, and the values were pooled per genotype to determine a mean value. The statistical analysis was performed with GraphPad Prism (Student's t-test; two-tailed, unpaired).

5.3.2 Image acquisition

Images were obtained with a Leica SP5 confocal Laser Scanning microscope equipped with a 10x/0.3 NA dry objective, a 20x/0.5 NA dry as well as a 40x/1.3 NA and a 63x/1.4 NA Plan Apo oil immersion objective for high-resolution imaging. Z-stack images were exported as TIF files and modified to increase contrast and intensity with the use of ImageJ. Image analysis was performed using animals of each genotype from 2 to 3 independent litters. Animal numbers used for analyses are indicated in the respective figure legends and were directly compared between littermates.

5.3.3 Dendrite branching and Sholl analysis

For dendritic branching analysis images were obtained as stacks from 300 μm thick brain sections using a laser scanning confocal microscope (Leica TCS SP5, 20x objective, X:1024 x Y:024 x Z:2). Dendrites were traced in 3D using the Simple Neurite Tracer plugin from ImageJ. Sholl analysis was performed by counting the intersections of concentric spheres around the cell body with the traced dendrites at various distances from the soma. Additionally, dendritic parameters, like total dendritic length and number of branch points were assessed.

5.3.4 Dendritic spine density and morphology analysis

For *in vivo* dendritic spine analysis, images were obtained using a laser scanning confocal microscope (Leica TCS SP5, 63x objective, 1.4 NA, 4x zoom, X:1024 x Y:256 x Z:0.13). Secondary dendrite stretches in the *stratum radiatum* were acquired as image stacks and the 2D maximum intensity projection images were used for subsequent spine morphology quantification. Quantification of spine morphology was performed using ImageJ. Spines were defined as protrusions with clearly visible heads and filopodia as thin protrusions without a spine head. Spine head size was assessed by measuring the spine head area and spine length was defined as the length from the dendritic shaft to the protrusion tip. Spine density was determined as the number of protrusions within a minimum dendritic stretch of 30 μm . At least 2-3 dendritic stretches were measured per individual neuron. Intra-animal means of spine density and morphological parameters were calculated using at least 10-15 neurons, with a minimum of 30 dendritic stretches, per mouse brain.

5.3.5 Quantification of mRNA levels using qRT-PCR

The expression levels of VEGF mRNA were quantified using C_T (cycle threshold) values obtained from real-time PCR. All samples were run in triplicates and C_T values compared to that of beta-2-microglobulin (B2M), measured in the corresponding sample, to account for cDNA input. VEGF mRNA levels were calculated as a log ratio where the target gene is normalized to the reference gene using the following formula for each sample:

$$2^{-(CT(VEGF) - CT(B2M))}$$

where $C_T(VEGF)$ is the mean cycle threshold value for VEGF and $C_T(B2M)$ is the mean cycle threshold value for B2M of the same sample.

5.3.6 Statistical analysis

The statistical analysis was performed with the GraphPad Prism software to compare the values between genotypes as described in the figure legends. The arithmetic average, the

standard deviation, and the standard error of the mean (SEM) were calculated. The SEM is indicated in the graphs as error bars. The data of all experiments were pooled from at least 2-3 liters per genotype and the p-value was calculated with the unpaired student's t-test (two-tailed) with GraphPad Prism. When * p-value < 0.05, ** p-value < 0.01, *** p-value ≤ 0.001. n= number of animals.

6 References

- Abbott, N. J. (2002). Astrocyte-endothelial interactions and blood-brain barrier permeability. *J Anat*, *200*(6), 629-638.
- Adams, R. H., & Eichmann, A. (2010). Axon guidance molecules in vascular patterning. *Cold Spring Harb Perspect Biol*, *2*(5), a001875.
- Al-Bassam, S., Xu, M., Wandless, T. J., & Arnold, D. B. (2012). Differential trafficking of transport vesicles contributes to the localization of dendritic proteins. *Cell Rep*, *2*(1), 89-100.
- Almodovar, C. R. d., Lambrechts, D., Mazzone, M., & Carmeliet, P. (2009). Role and Therapeutic Potential of VEGF in the Nervous System. *Physiological Reviews*, *89*(2), 607-648.
- Alvarez-Vergara, M. I., Rosales-Nieves, A. E., March-Diaz, R., Rodriguez-Perinan, G., Lara-Ureña, N., Ortega-de San Luis, C., Sanchez-Garcia, M. A., Martin-Bornez, M., Gómez-Gálvez, P., Vicente-Munuera, P., Fernandez-Gomez, B., Marchena, M. A., Bullones-Bolanos, A. S., Davila, J. C., Gonzalez-Martinez, R., Trillo-Contreras, J. L., Sanchez-Hidalgo, A. C., del Toro, R., Scholl, F. G., . . . Pascual, A. (2021). Non-productive angiogenesis disassembles Aβ plaque-associated blood vessels. *Nature Communications*, *12*(1), 3098.
- Ambesi, A., & McKeown-Longo, P. J. (2014). Conformational remodeling of the fibronectin matrix selectively regulates VEGF signaling. *J Cell Sci*, *127*(Pt 17), 3805-3816.
- Apte, R. S., Chen, D. S., & Ferrara, N. (2019). VEGF in Signaling and Disease: Beyond Discovery and Development. *Cell*, *176*(6), 1248-1264.
- Araque, A., Parpura, V., Sanzgiri, R. P., & Haydon, P. G. (1999). Tripartite synapses: glia, the unacknowledged partner. *Trends Neurosci*, *22*(5), 208-215.
- Arcondeguy, T., Lacazette, E., Millevoi, S., Prats, H., & Touriol, C. (2013). VEGF-A mRNA processing, stability and translation: a paradigm for intricate regulation of gene expression at the post-transcriptional level. *Nucleic Acids Res*, *41*(17), 7997-8010.
- Argaw, A. T., Asp, L., Zhang, J., Navrazhina, K., Pham, T., Mariani, J. N., Mahase, S., Dutta, D. J., Seto, J., Kramer, E. G., Ferrara, N., Sofroniew, M. V., & John, G. R. (2012). Astrocyte-derived VEGF-A drives blood-brain barrier disruption in CNS inflammatory disease. *J Clin Invest*, *122*(7), 2454-2468.
- Ashwell, K. (1991). The distribution of microglia and cell death in the fetal rat forebrain. *Brain Res Dev Brain Res*, *58*(1), 1-12.

- Bączyńska, E., Pels, K. K., Basu, S., Wodarczyk, J., & Ruszczycki, B. (2021). Quantification of Dendritic Spines Remodeling under Physiological Stimuli and in Pathological Conditions. *International Journal of Molecular Sciences*, *22*(8), 4053.
- Bagri, A., Cheng, H.-J., Yaron, A., Pleasure, S. J., & Tessier-Lavigne, M. (2003). Stereotyped pruning of long hippocampal axon branches triggered by retraction inducers of the semaphorin family. *Cell*, *113*(3), 285-299.
- Barker, A. J., Koch, S. M., Reed, J., Barres, B. A., & Ullian, E. M. (2008). Developmental control of synaptic receptivity. *J Neurosci*, *28*(33), 8150-8160.
- Barker, A. J., & Ullian, E. M. (2008). New roles for astrocytes in developing synaptic circuits. *Commun Integr Biol*, *1*(2), 207-211.
- Barnes, A. P., Lilley, B. N., Pan, Y. A., Plummer, L. J., Powell, A. W., Raines, A. N., Sanes, J. R., & Polleux, F. (2007). LKB1 and SAD kinases define a pathway required for the polarization of cortical neurons. *Cell*, *129*(3), 549-563.
- Basagiannis, D., & Christoforidis, S. (2016). Constitutive Endocytosis of VEGFR2 Protects the Receptor against Shedding. *Journal of Biological Chemistry*, *291*(32), 16892-16903.
- Basagiannis, D., Zografou, S., Galanopoulou, K., & Christoforidis, S. (2017). Dynasore impairs VEGFR2 signalling in an endocytosis-independent manner. *Sci Rep*, *7*, 45035.
- Basagiannis, D., Zografou, S., Murphy, C., Fotsis, T., Morbidelli, L., Ziche, M., Bleck, C., Mercer, J., & Christoforidis, S. (2016). VEGF induces signalling and angiogenesis by directing VEGFR2 internalisation through macropinocytosis. *Journal of Cell Science*, *129*(21), 4091-4104.
- Bellon, A., Luchino, J., Haigh, K., Rougon, G., Haigh, J., Chauvet, S., & Mann, F. (2010). VEGFR2 (KDR/Flk1) Signaling Mediates Axon Growth in Response to Semaphorin 3E in the Developing Brain. *Neuron*, *66*(2), 205-219.
- Bergantino, F., Guariniello, S., Raucci, R., Colonna, G., De Luca, A., Normanno, N., & Costantini, S. (2015). Structure-fluctuation-function relationships of seven pro-angiogenic isoforms of VEGFA, important mediators of tumorigenesis. *Biochim Biophys Acta*, *1854*(5), 410-425.
- Bernal, A., & Arranz, L. (2018). Nestin-expressing progenitor cells: function, identity and therapeutic implications. *Cell Mol Life Sci*, *75*(12), 2177-2195.
- Bjorge, J. D., Jakymiw, A., & Fujita, D. J. (2000). Selected glimpses into the activation and function of Src kinase [Research Journal]. *Oncogene*, *19*(49), 5620-5635.

- Blinder, P., Shih, A. Y., Rafie, C., & Kleinfeld, D. (2010). Topological basis for the robust distribution of blood to rodent neocortex. *Proceedings of the National Academy of Sciences*, *107*(28), 12670-12675.
- Bliss, T. V., & Collingridge, G. L. (1993). A synaptic model of memory: long-term potentiation in the hippocampus. *Nature*, *361*(6407), 31-39.
- Bochenek, M. L., Dickinson, S., Astin, J. W., Adams, R. H., & Nobes, C. D. (2010). ephrin-B2 regulates endothelial cell morphology and motility independently of Eph-receptor binding. *J Cell Sci*, *123*(Pt 8), 1235-1246.
- Böcker-Meffert, S., Rosenstiel, P., Röhl, C., Warneke, N., Held-Feindt, J., Sievers, J., & Lucius, R. (2002). Erythropoietin and VEGF promote neural outgrowth from retinal explants in postnatal rats. *Invest Ophthalmol Vis Sci*, *43*(6), 2021-2026.
- Bortolotto, Z. A., Anderson, W. W., Isaac, J. T., & Collingridge, G. L. (2001). Synaptic plasticity in the hippocampal slice preparation. *Curr Protoc Neurosci*, *Chapter 6*, Unit 6 13.
- Bourne, J. N., & Harris, K. M. (2011). Coordination of size and number of excitatory and inhibitory synapses results in a balanced structural plasticity along mature hippocampal CA1 dendrites during LTP. *Hippocampus*, *21*(4), 354-373.
- Bower, N. I., Vogrin, A. J., Le Guen, L., Chen, H., Stacker, S. A., Achen, M. G., & Hogan, B. M. (2017). Vegfd modulates both angiogenesis and lymphangiogenesis during zebrafish embryonic development. *Development*, *144*(3), 507-518.
- Branda, C. S., & Dymecki, S. M. (2004). Talking about a Revolution: The Impact of Site-Specific Recombinases on Genetic Analyses in Mice. *Developmental Cell*, *6*(1), 7-28.
- Brinkmann, B. G., Agarwal, A., Sereda, M. W., Garratt, A. N., Mueller, T., Wende, H., Stassart, R. M., Nawaz, S., Humml, C., Velanac, V., Radyushkin, K., Goebbels, S., Fischer, T. M., Franklin, R. J., Lai, C., Ehrenreich, H., Birchmeier, C., Schwab, M. H., & Nave, K. A. (2008). Neuregulin-1/ErbB signaling serves distinct functions in myelination of the peripheral and central nervous system. *Neuron*, *59*(4), 581-595.
- Bushong, E. A., Martone, M. E., & Ellisman, M. H. (2004). Maturation of astrocyte morphology and the establishment of astrocyte domains during postnatal hippocampal development. *Int J Dev Neurosci*, *22*(2), 73-86.
- Bushong, E. A., Martone, M. E., Jones, Y. Z., & Ellisman, M. H. (2002). Protoplasmic astrocytes in CA1 stratum radiatum occupy separate anatomical domains. *J Neurosci*, *22*(1), 183-192.

- Cabezas, R., Ávila, M., Gonzalez, J., El-Bachá, R. S., Báez, E., García-Segura, L. M., Jurado Coronel, J. C., Capani, F., Cardona-Gomez, G. P., & Barreto, G. E. (2014). Astrocytic modulation of blood brain barrier: perspectives on Parkinson's disease [Review]. *Frontiers in Cellular Neuroscience*, *8*.
- Carmeliet, P., Ferreira, V., Breier, G., Pollefeyt, S., Kieckens, L., Gertsenstein, M., Fahrig, M., Vandenhoek, A., Harpal, K., Eberhardt, C., Declercq, C., Pawling, J., Moons, L., Collen, D., Risau, W., & Nagy, A. (1996). Abnormal blood vessel development and lethality in embryos lacking a single VEGF allele. *Nature*, *380*(6573), 435-439.
- Carmeliet, P., & Storkebaum, E. (2002). Vascular and neuronal effects of VEGF in the nervous system: implications for neurological disorders. *Semin Cell Dev Biol*, *13*(1), 39-53.
- Carmeliet, P., & Tessier-Lavigne, M. (2005). Common mechanisms of nerve and blood vessel wiring. *Nature*, *436*(7048), 193-200.
- Castets, M., Coissieux, M. M., Delloye-Bourgeois, C., Bernard, L., Delcros, J. G., Bernet, A., Laudet, V., & Mehlen, P. (2009). Inhibition of endothelial cell apoptosis by netrin-1 during angiogenesis. *Developmental Cell*, *16*(4), 614-620.
- Castets, M., & Mehlen, P. (2010). Netrin-1 role in angiogenesis: to be or not to be a pro-angiogenic factor? *Cell Cycle*, *9*(8), 1466-1471.
- Chauvet, S., Cohen, S., Yoshida, Y., Fekrane, L., Livet, J., Gayet, O., Segu, L., Buhot, M. C., Jessell, T. M., Henderson, C. E., & Mann, F. (2007). Gating of Sema3E/PlexinD1 signaling by neuropilin-1 switches axonal repulsion to attraction during brain development. *Neuron*, *56*(5), 807-822.
- Chen, J., Zhang, C., Jiang, H., Li, Y., Zhang, L., Robin, A., Katakowski, M., Lu, M., & Chopp, M. (2005). Atorvastatin Induction of VEGF and BDNF Promotes Brain Plasticity after Stroke in Mice. *Journal of Cerebral Blood Flow & Metabolism*, *25*(2), 281-290.
- Chen, X., Li, Y., Wang, L., Katakowski, M., Zhang, L., Chen, J., Xu, Y., Gautam, S. C., & Chopp, M. (2002). Ischemic rat brain extracts induce human marrow stromal cell growth factor production. *Neuropathology*, *22*(4), 275-279.
- Chow, J., Ogunshola, O., Fan, S. Y., Li, Y., Ment, L. R., & Madri, J. A. (2001). Astrocyte-derived VEGF mediates survival and tube stabilization of hypoxic brain microvascular endothelial cells in vitro. *Brain Res Dev Brain Res*, *130*(1), 123-132.
- Cohen-Cory, S., Kidane, A. H., Shirkey, N. J., & Marshak, S. (2010). Brain-derived neurotrophic factor and the development of structural neuronal connectivity. *Dev Neurobiol*, *70*(5), 271-288.

- Cowan, C. W., Shao, Y. R., Sahin, M., Shamah, S. M., Lin, M. Z., Greer, P. L., Gao, S., Griffith, E. C., Brugge, J. S., & Greenberg, M. E. (2005). Vav family GEFs link activated Ephs to endocytosis and axon guidance. *Neuron*, *46*(2), 205-217.
- Craig, A. M., & Banker, G. (1994). Neuronal polarity. *Annu Rev Neurosci*, *17*, 267-310.
- Dailey, M. E., & Smith, S. J. (1996). The dynamics of dendritic structure in developing hippocampal slices. *J Neurosci*, *16*(9), 2983-2994.
- Daneman, R., Agalliu, D., Zhou, L., Kuhnert, F., Kuo, C. J., & Barres, B. A. (2009). Wnt/-catenin signaling is required for CNS, but not non-CNS, angiogenesis. *Proceedings of the National Academy of Sciences*, *106*(2), 641-646.
- Darling, T. K., & Lamb, T. J. (2019). Emerging Roles for Eph Receptors and ephrin Ligands in Immunity [Review]. *Frontiers in Immunology*, *10*.
- Davy, A., & Soriano, P. (2005). ephrin signaling in vivo: look both ways. *Dev Dyn*, *232*(1), 1-10.
- De Almodovar, C. R., Lambrechts, D., Mazzone, M., & Carmeliet, P. (2009). Role and Therapeutic Potential of VEGF in the Nervous System. *Physiological Reviews*, *89*(2), 607-648.
- De Roo, M., Klausner, P., & Muller, D. (2008). LTP promotes a selective long-term stabilization and clustering of dendritic spines. *PLoS Biol*, *6*(9), e219.
- De Rossi, P., Harde, E., Dupuis, J. P., Martin, L., Chounlamountri, N., Bardin, M., Watrin, C., Benetollo, C., Pernet-Gallay, K., Luhmann, H. J., Honnorat, J., Malleret, G., Groc, L., Acker-Palmer, A., Salin, P. A., & Meissirel, C. (2016). A critical role for VEGF and VEGFR2 in NMDA receptor synaptic function and fear-related behavior. *Mol Psychiatry*, *21*(12), 1768-1780.
- Demas, J. A., Payne, H., & Cline, H. T. (2012). Vision drives correlated activity without patterned spontaneous activity in developing *Xenopus* retina. *Dev Neurobiol*, *72*(4), 537-546.
- Dent, E. W., & Gertler, F. B. (2003). Cytoskeletal dynamics and transport in growth cone motility and axon guidance. *Neuron*, *40*(2), 209-227.
- Dent, E. W., Gupton, S. L., & Gertler, F. B. (2011). The growth cone cytoskeleton in axon outgrowth and guidance. *Cold Spring Harb Perspect Biol*, *3*(3).
- Devos, D., Moreau, C., Lassalle, P., Perez, T., De Seze, J., Brunaud-Danel, V., Destee, A., Tonnel, A., & Just, N. (2004). Low levels of the vascular endothelial growth factor in CSF from early ALS patients. *Neurology*, *62*(11), 2127-2129.

- Di Marco, L. Y., Venneri, A., Farkas, E., Evans, P. C., Marzo, A., & Frangi, A. F. (2015). Vascular dysfunction in the pathogenesis of Alzheimer's disease--A review of endothelium-mediated mechanisms and ensuing vicious circles. *Neurobiol Dis*, *82*, 593-606.
- Dixelius, J., Makinen, T., Wirzenius, M., Karkkainen, M. J., Wernstedt, C., Alitalo, K., & Claesson-Welsh, L. (2003). Ligand-induced vascular endothelial growth factor receptor-3 (VEGFR-3) heterodimerization with VEGFR-2 in primary lymphatic endothelial cells regulates tyrosine phosphorylation sites. *J Biol Chem*, *278*(42), 40973-40979.
- Dorrell, M. I., Aguilar, E., & Friedlander, M. (2002). Retinal vascular development is mediated by endothelial filopodia, a preexisting astrocytic template and specific R-cadherin adhesion. *Invest Ophthalmol Vis Sci*, *43*(11), 3500-3510.
- Downward, J. (2004). PI 3-kinase, Akt and cell survival. *Seminars in cell & developmental biology*,
- Dubois, N. C., Hofmann, D., Kaloulis, K., Bishop, J. M., & Trumpp, A. (2006). Nestin-Cre transgenic mouse line Nes-Cre1 mediates highly efficient Cre/loxP mediated recombination in the nervous system, kidney, and somite-derived tissues. *Genesis*, *44*(8), 355-360.
- Dumas, T. C. (2005). Developmental regulation of cognitive abilities: modified composition of a molecular switch turns on associative learning. *Prog Neurobiol*, *76*(3), 189-211.
- Dumont, D. J., Fong, G. H., Puri, M. C., Gradwohl, G., Alitalo, K., & Breitman, M. L. (1995). Vascularization of the mouse embryo: a study of flk-1, tek, tie, and vascular endothelial growth factor expression during development. *Dev Dyn*, *203*(1), 80-92.
- Dumpich, M., & Theiss, C. (2015). VEGF in the nervous system: an important target for research in neurodevelopmental and regenerative medicine. *Neural Regen Res*, *10*(11), 1725-1726.
- Echegoyen, J., Neu, A., Graber, K. D., & Soltesz, I. (2007). Homeostatic plasticity studied using in vivo hippocampal activity-blockade: synaptic scaling, intrinsic plasticity and age-dependence. *PLoS One*, *2*(8), e700.
- Eddleston, M., & Mucke, L. (1993). Molecular profile of reactive astrocytes--implications for their role in neurologic disease. *Neuroscience*, *54*(1), 15-36.
- Egea, J., & Klein, R. (2007). Bidirectional Eph-ephrin signaling during axon guidance. *Trends in Cell Biology*, *17*(5), 230-238.
- Egervari, K., Potter, G., Guzman-Hernandez, M. L., Salmon, P., Soto-Ribeiro, M., Kastberger, B., Balla, T., Wehrle-Haller, B., & Kiss, J. Z. (2016). Astrocytes spatially

- restrict VEGF signaling by polarized secretion and incorporation of VEGF into the actively assembling extracellular matrix. *Glia*, *64*(3), 440-456.
- Elorza Ridaura, I., Sorrentino, S., & Moroni, L. (2021). Parallels between the Developing Vascular and Neural Systems: Signaling Pathways and Future Perspectives for Regenerative Medicine. *Advanced Science*, *8*(23), 2101837.
- Ema, M., Takahashi, S., & Rossant, J. (2006). Deletion of the selection cassette, but not cis-acting elements, in targeted Flk1-lacZ allele reveals Flk1 expression in multipotent mesodermal progenitors. *Blood*, *107*(1), 111-117.
- Encinas, J. M., Michurina, T. V., Peunova, N., Park, J. H., Tordo, J., Peterson, D. A., Fishell, G., Koulakov, A., & Enikolopov, G. (2011). Division-coupled astrocytic differentiation and age-related depletion of neural stem cells in the adult hippocampus. *Cell Stem Cell*, *8*(5), 566-579.
- Essmann, C. L., Martinez, E., Geiger, J. C., Zimmer, M., Traut, M. H., Stein, V., Klein, R., & Acker-Palmer, A. (2008). Serine phosphorylation of ephrinB2 regulates trafficking of synaptic AMPA receptors. *Nature Neuroscience*, *11*(9), 1035-1043.
- Farmer, W. T., Abrahamsson, T., Chierzi, S., Lui, C., Zaelzer, C., Jones, E. V., Bally, B. P., Chen, G. G., Theroux, J. F., Peng, J., Bourque, C. W., Charron, F., Ernst, C., Sjöström, P. J., & Murai, K. K. (2016). Neurons diversify astrocytes in the adult brain through sonic hedgehog signaling. *Science*, *351*(6275), 849-854.
- Favia, A., Desideri, M., Gambarà, G., D'Alessio, A., Ruas, M., Esposito, B., Del Bufalo, D., Parrington, J., Ziparo, E., Palombi, F., Galione, A., & Filippini, A. (2014). VEGF-induced neoangiogenesis is mediated by NAADP and two-pore channel-2-dependent Ca²⁺ signaling. *Proc Natl Acad Sci U S A*, *111*(44), E4706-4715.
- Fearnley, G. W., Bruns, A. F., Wheatcroft, S. B., & Ponnambalam, S. (2015). VEGF-A isoform-specific regulation of calcium ion flux, transcriptional activation and endothelial cell migration. *Biology Open*, *4*(6), 731-742.
- Feldman, D. E. (2012). The spike-timing dependence of plasticity. *Neuron*, *75*(4), 556-571.
- Fellin, T. (2009). Communication between neurons and astrocytes: relevance to the modulation of synaptic and network activity. *J Neurochem*, *108*(3), 533-544.
- Feng, G. P., Mellor, R. H., Bernstein, M., Keller-Peck, C., Nguyen, Q. T., Wallace, M., Nerbonne, J. M., Lichtman, J. W., & Sanes, J. R. (2000). Imaging neuronal subsets in transgenic mice expressing multiple spectral variants of GFP. *Neuron*, *28*(1), 41-51.
- Ferrara, N. (2001). Role of vascular endothelial growth factor in regulation of physiological angiogenesis. *Am J Physiol Cell Physiol*, *280*(6), C1358-1366.

- Ferrara, N. (2010). Binding to the Extracellular Matrix and Proteolytic Processing: Two Key Mechanisms Regulating Vascular Endothelial Growth Factor Action. *Molecular Biology of the Cell*, 21(5), 687-690.
- Ferrara, N., Carver-Moore, K., Chen, H., Dowd, M., Lu, L., O'Shea, K. S., Powell-Braxton, L., Hillan, K. J., & Moore, M. W. (1996). Heterozygous embryonic lethality induced by targeted inactivation of the VEGF gene. *Nature*, 380(6573), 439-442.
- Fischer, M., Kaech, S., Knutti, D., & Matus, A. (1998). Rapid actin-based plasticity in dendritic spines. *Neuron*, 20(5), 847-854.
- Fraccaroli, A., Franco, C. A., Rognoni, E., Neto, F., Rehberg, M., Aszodi, A., Wedlich-Söldner, R., Pohl, U., Gerhardt, H., & Montanez, E. (2012). Visualization of endothelial actin cytoskeleton in the mouse retina. *PLoS One*, 7(10), e47488.
- Gabhann, F. M., & Popel, A. S. (2004). Model of competitive binding of vascular endothelial growth factor and placental growth factor to VEGF receptors on endothelial cells. *American Journal of Physiology-Heart and Circulatory Physiology*, 286(1), H153-H164.
- Garrett, T. A., Van Buul, J. D., & Burridge, K. (2007). VEGF-induced Rac1 activation in endothelial cells is regulated by the guanine nucleotide exchange factor Vav2. *Experimental cell research*, 313(15), 3285-3297.
- Gavériaux-Ruff, C., & Kieffer, B. L. (2007). Conditional gene targeting in the mouse nervous system: Insights into brain function and diseases. *Pharmacol Ther*, 113(3), 619-634.
- Gerhardt, H., Golding, M., Fruttiger, M., Ruhrberg, C., Lundkvist, A., Abramsson, A., Jeltsch, M., Mitchell, C., Alitalo, K., Shima, D., & Betsholtz, C. (2003). VEGF guides angiogenic sprouting utilizing endothelial tip cell filopodia. *J Cell Biol*, 161(6), 1163-1177.
- Gianni-Barrera, R., Burger, M., Wolff, T., Heberer, M., Schaefer, D. J., Gürke, L., Mujagic, E., & Banfi, A. (2016). Long-term safety and stability of angiogenesis induced by balanced single-vector co-expression of PDGF-BB and VEGF164 in skeletal muscle. *Scientific Reports*, 6(1), 21546.
- Goldie, L. C., Nix, M. K., & Hirschi, K. K. (2008). Embryonic vasculogenesis and hematopoietic specification. *Organogenesis*, 4(4), 257-263.
- Goslin, K., & Banker, G. (1989). Experimental observations on the development of polarity by hippocampal neurons in culture. *J Cell Biol*, 108(4), 1507-1516.
- Götz, M., Hartfuss, E., & Malatesta, P. (2002). Radial glial cells as neuronal precursors: a new perspective on the correlation of morphology and lineage restriction in the developing cerebral cortex of mice. *Brain Res Bull*, 57(6), 777-788.

- Govek, E. E., Newey, S. E., & Van Aelst, L. (2005). The role of the Rho GTPases in neuronal development. *Genes Dev*, *19*(1), 1-49.
- Greenberg, J. I., Shields, D. J., Barillas, S. G., Acevedo, L. M., Murphy, E., Huang, J., Scheppeke, L., Stockmann, C., Johnson, R. S., Angle, N., & Cheresch, D. A. (2008). A role for VEGF as a negative regulator of pericyte function and vessel maturation. *Nature*, *456*(7223), 809-813.
- Grove, E. A., & Tole, S. (1999). Patterning events and specification signals in the developing hippocampus. *Cerebral Cortex*, *9*(6), 551-561.
- Grunwald, I. C., Korte, M., Adelman, G., Plueck, A., Kullander, K., Adams, R. H., Frotscher, M., Bonhoeffer, T., & Klein, R. (2004). Hippocampal plasticity requires postsynaptic ephrinBs. *Nature Neuroscience*, *7*(1), 33-40.
- Haigh, J. J., Morelli, P. I., Gerhardt, H., Haigh, K., Tsien, J., Damert, A., Miquerol, L., Muhliner, U., Klein, R., Ferrara, N., Wagner, E. F., Betsholtz, C., & Nagy, A. (2003). Cortical and retinal defects caused by dosage-dependent reductions in VEGF-A paracrine signaling. *Dev Biol*, *262*(2), 225-241.
- Hale, C. F., Dietz, K. C., Varela, J. A., Wood, C. B., Zirlin, B. C., Leverich, L. S., Greene, R. W., & Cowan, C. W. (2011). Essential role for vav Guanine nucleotide exchange factors in brain-derived neurotrophic factor-induced dendritic spine growth and synapse plasticity. *Journal of Neuroscience*, *31*(35), 12426-12436.
- Harde, E., Nicholson, L., Furones Cuadrado, B., Bissen, D., Wigge, S., Urban, S., Segarra, M., Ruiz De Almodóvar, C., & Acker-Palmer, A. (2019). ephrinB2 regulates VEGFR2 during dendritogenesis and hippocampal circuitry development. *eLife*, *8*.
- Hatami, M., Conrad, S., Naghsh, P., Alvarez-Bolado, G., & Skutella, T. (2018). Cell-Biological Requirements for the Generation of Dentate Gyrus Granule Neurons. *Front Cell Neurosci*, *12*, 402.
- Hayakawa, K., Pham, L. D., Som, A. T., Lee, B. J., Guo, S., Lo, E. H., & Arai, K. (2011). Vascular endothelial growth factor regulates the migration of oligodendrocyte precursor cells. *J Neurosci*, *31*(29), 10666-10670.
- Herculano-Houzel, S., Mota, B., & Lent, R. (2006). Cellular scaling rules for rodent brains. *Proceedings of the National Academy of Sciences*, *103*(32), 12138-12143.
- Hicklin, D. J., & Ellis, L. M. (2005). Role of the Vascular Endothelial Growth Factor Pathway in Tumor Growth and Angiogenesis. *Journal of Clinical Oncology*, *23*(5), 1011-1027.
- Himanen, J.-P., Henkemeyer, M., & Nikolov, D. B. (1998). Crystal structure of the ligand-binding domain of the receptor tyrosine kinase EphB2. *Nature*, *396*(6710), 486-491.

- Hiratsuka, S., Kataoka, Y., Nakao, K., Nakamura, K., Morikawa, S., Tanaka, S., Katsuki, M., Maru, Y., & Shibuya, M. (2005). Vascular endothelial growth factor A (VEGF-A) is involved in guidance of VEGF receptor-positive cells to the anterior portion of early embryos. *Mol Cell Biol*, *25*(1), 355-363.
- Hiratsuka, S., Minowa, O., Kuno, J., Noda, T., & Shibuya, M. (1998). Flt-1 lacking the tyrosine kinase domain is sufficient for normal development and angiogenesis in mice. *Proceedings of the National Academy of Sciences*, *95*(16), 9349-9354.
- Ho, V. M., Lee, J. A., & Martin, K. C. (2011). The cell biology of synaptic plasticity. *Science*, *334*(6056), 623-628.
- Hogan, K. A., Ambler, C. A., Chapman, D. L., & Bautch, V. L. (2004). The neural tube patterns vessels developmentally using the VEGF signaling pathway. *Development*, *131*(7), 1503-1513.
- Holmes, D. I., & Zachary, I. (2005). The vascular endothelial growth factor (VEGF) family: angiogenic factors in health and disease. *Genome Biology*, *6*(2), 209.
- Holmes, K., Roberts, O. L., Thomas, A. M., & Cross, M. J. (2007). Vascular endothelial growth factor receptor-2: Structure, function, intracellular signalling and therapeutic inhibition. *Cellular Signalling*, *19*(10), 2003-2012.
- Holmqvist, K., Cross, M., Riley, D., & Welsh, M. (2003). The Shb adaptor protein causes Src-dependent cell spreading and activation of focal adhesion kinase in murine brain endothelial cells. *Cellular Signalling*, *15*(2), 171-179.
- Horowitz, A., & Seerapu, H. R. (2012). Regulation of VEGF signaling by membrane traffic. *Cell Signal*, *24*(9), 1810-1820.
- Huang, Y.-F., Yang, C.-H., Huang, C.-C., & Hsu, K.-S. (2012). Vascular Endothelial Growth Factor-dependent Spinogenesis Underlies Antidepressant-like Effects of Enriched Environment*. *Journal of Biological Chemistry*, *287*(49), 40938-40955.
- Ishizuka, N., Weber, J., & Amaral, D. G. (1990). Organization of intrahippocampal projections originating from CA3 pyramidal cells in the rat. *J Comp Neurol*, *295*(4), 580-623.
- James, J. M., & Mukoyama, Y. S. (2011). Neuronal action on the developing blood vessel pattern. *Semin Cell Dev Biol*, *22*(9), 1019-1027.
- Janssen, B. J., Malinauskas, T., Weir, G. A., Cader, M. Z., Siebold, C., & Jones, E. Y. (2012). Neuropilins lock secreted semaphorins onto plexins in a ternary signaling complex. *Nat Struct Mol Biol*, *19*(12), 1293-1299.

- Javaherian, A., & Kriegstein, A. (2009). A Stem Cell Niche for Intermediate Progenitor Cells of the Embryonic Cortex. *Cerebral Cortex*, *19*, 170-177.
- Jin, K., Zhu, Y., Sun, Y., Mao, X. O., Xie, L., & Greenberg, D. A. (2002). Vascular endothelial growth factor (VEGF) stimulates neurogenesis in vitro and in vivo. *Proc Natl Acad Sci U S A*, *99*(18), 11946-11950.
- Jinno, S., Klausberger, T., Marton, L. F., Dalezios, Y., Roberts, J. D., Fuentealba, P., Bushong, E. A., Henze, D., Buzsáki, G., & Somogyi, P. (2007). Neuronal diversity in GABAergic long-range projections from the hippocampus. *J Neurosci*, *27*(33), 8790-8804.
- Jurga, A. M., Paleczna, M., Kadluczka, J., & Kuter, K. Z. (2021). Beyond the GFAP-Astrocyte Protein Markers in the Brain. *Biomolecules*, *11*(9).
- Just, N., Moreau, C., Lassalle, P., Gosset, P., Perez, T., Brunaud-Danel, V., Wallaert, B., Destée, A., Defebvre, L., Tonnel, A. B., & Devos, D. (2007). High erythropoietin and low vascular endothelial growth factor levels in cerebrospinal fluid from hypoxic ALS patients suggest an abnormal response to hypoxia. *Neuromuscular Disorders*, *17*(2), 169-173.
- Kaipainen, A., Korhonen, J., Mustonen, T., Van Hinsbergh, V., Fang, G.-H., Dumont, D., Breitman, M., & Alitalo, K. (1995). Expression of the fms-like tyrosine kinase 4 gene becomes restricted to lymphatic endothelium during development. *Proceedings of the National Academy of Sciences*, *92*(8), 3566-3570.
- Kalil, K., & Dent, E. W. (2014). Branch management: mechanisms of axon branching in the developing vertebrate CNS. *Nature Reviews Neuroscience*, *15*(1), 7-18.
- Kamei, Y., Inagaki, N., Nishizawa, M., Tsutsumi, O., Taketani, Y., & Inagaki, M. (1998). Visualization of mitotic radial glial lineage cells in the developing rat brain by Cdc2 kinase-phosphorylated vimentin. *Glia*, *23*(3), 191-199.
- Kamphuis, W., Mamber, C., Moeton, M., Kooijman, L., Sluijs, J. A., Jansen, A. H., Verveer, M., de Groot, L. R., Smith, V. D., Rangarajan, S., Rodríguez, J. J., Orre, M., & Hol, E. M. (2012). GFAP isoforms in adult mouse brain with a focus on neurogenic astrocytes and reactive astrogliosis in mouse models of Alzheimer disease. *PLoS One*, *7*(8), e42823.
- Kania, A., & Klein, R. (2016). Mechanisms of ephrin-Eph signalling in development, physiology and disease. *Nat Rev Mol Cell Biol*, *17*(4), 240-256.
- Keleman, K., & Dickson, B. J. (2001). Short- and long-range repulsion by the Drosophila Unc5 netrin receptor. *Neuron*, *32*(4), 605-617.

- Kennedy, T. E., Serafini, T., de la Torre, J. R., & Tessier-Lavigne, M. (1994). Netrins are diffusible chemotropic factors for commissural axons in the embryonic spinal cord. *Cell*, *78*(3), 425-435.
- Kennedy, T. E., Wang, H., Marshall, W., & Tessier-Lavigne, M. (2006). Axon guidance by diffusible chemoattractants: a gradient of netrin protein in the developing spinal cord. *J Neurosci*, *26*(34), 8866-8874.
- Kettenmann, H., & Ransom, B. R. (2004). The Concept of Neuroglia: A Historical Perspective. In *Neuroglia* (pp. 0). Oxford University Press.
- King, C., & Hristova, K. (2019). Direct measurements of VEGF-VEGFR2 binding affinities reveal the coupling between ligand binding and receptor dimerization. *Journal of Biological Chemistry*, *294*(23), 9064-9075.
- Kirov, S. A., Goddard, C. A., & Harris, K. M. (2004). Age-dependence in the homeostatic upregulation of hippocampal dendritic spine number during blocked synaptic transmission. *Neuropharmacology*, *47*(5), 640-648.
- Klein, R. (2009). Bidirectional modulation of synaptic functions by Eph/ephrin signaling. *Nature Neuroscience*, *12*(1), 15-20.
- Koch, S., & Claesson-Welsh, L. (2012). Signal transduction by vascular endothelial growth factor receptors. *Cold Spring Harb Perspect Med*, *2*(7), a006502.
- Kokoeva, M. V., Yin, H., & Flier, J. S. (2007). Evidence for constitutive neural cell proliferation in the adult murine hypothalamus. *J Comp Neurol*, *505*(2), 209-220.
- Koleske, A. J. (2013). Molecular mechanisms of dendrite stability. *Nature Reviews Neuroscience*, *14*(8), 536-550.
- Krum, J. M., & Rosenstein, J. M. (1998). VEGF mRNA and its receptor flt-1 are expressed in reactive astrocytes following neural grafting and tumor cell implantation in the adult CNS. *Experimental Neurology*, *154*(1), 57-65.
- Lambrechts, D., Storkebaum, E., Morimoto, M., Del-Favero, J., Desmet, F., Marklund, S. L., Wyns, S., Thijs, V., Andersson, J., & van Marion, I. (2003). VEGF is a modifier of amyotrophic lateral sclerosis in mice and humans and protects motoneurons against ischemic death. *Nature genetics*, *34*(4), 383-394.
- Lampugnani, M. G., Orsenigo, F., Gagliani, M. C., Tacchetti, C., & Dejana, E. (2006). Vascular endothelial cadherin controls VEGFR-2 internalization and signaling from intracellular compartments. *J Cell Biol*, *174*(4), 593-604.

- Lange, C., Storkebaum, E., de Almodóvar, C. R., Dewerchin, M., & Carmeliet, P. (2016). Vascular endothelial growth factor: a neurovascular target in neurological diseases. *Nat Rev Neurol*, *12*(8), 439-454.
- Lee, J., Ku, T., Yu, H., Chong, K., Ryu, S. W., Choi, K., & Choi, C. (2012). Blockade of VEGF-A suppresses tumor growth via inhibition of autocrine signaling through FAK and AKT. *Cancer Lett*, *318*(2), 221-225.
- Lee, S., Chen, T. T., Barber, C. L., Jordan, M. C., Murdock, J., Desai, S., Ferrara, N., Nagy, A., Roos, K. P., & Iruela-Arispe, M. L. (2007). Autocrine VEGF signaling is required for vascular homeostasis. *Cell*, *130*(4), 691-703.
- Lemmon, M. A., & Schlessinger, J. (2010). Cell signaling by receptor tyrosine kinases. *Cell*, *141*(7), 1117-1134.
- Lendahl, U., Zimmerman, L. B., & McKay, R. D. (1990). CNS stem cells express a new class of intermediate filament protein. *Cell*, *60*(4), 585-595.
- Li, J., Erisir, A., & Cline, H. (2011). In vivo time-lapse imaging and serial section electron microscopy reveal developmental synaptic rearrangements. *Neuron*, *69*(2), 273-286.
- Li, S. Y., Haigh, K., Haigh, J. J., & Vasudevan, A. (2013). Endothelial VEGF Sculpts Cortical Cytoarchitecture. *Journal of Neuroscience*, *33*(37), 14809-14815.
- Li, X. G., Somogyi, P., Ylinen, A., & Buzsáki, G. (1994). The hippocampal CA3 network: an in vivo intracellular labeling study. *J Comp Neurol*, *339*(2), 181-208.
- Liang, H., Hippenmeyer, S., & Ghashghaei, H. T. (2012). A Nestin-cre transgenic mouse is insufficient for recombination in early embryonic neural progenitors. *Biology Open*, *1*(12), 1200-1203.
- Licht, T., Eavri, R., Goshen, I., Shlomai, Y., Mizrahi, A., & Keshet, E. (2010). VEGF is required for dendritogenesis of newly born olfactory bulb interneurons. *Development*, *137*(2), 261-271.
- Licht, T., Goshen, I., Avital, A., Kreisel, T., Zubedat, S., Eavri, R., Segal, M., Yirmiya, R., & Keshet, E. (2011). Reversible modulations of neuronal plasticity by VEGF. *Proceedings of the National Academy of Sciences of the United States of America*, *108*(12), 5081-5086.
- Liebner, S., Corada, M., Bangsow, T., Babbage, J., Taddei, A., Czupalla, C. J., Reis, M., Felici, A., Wolburg, H., & Fruttiger, M. (2008). Wnt/ β -catenin signaling controls development of the blood-brain barrier. *The Journal of cell biology*, *183*(3), 409-417.

- Liu, X.-B., Low, L. K., Jones, E. G., & Cheng, H.-J. (2005). Stereotyped axon pruning via plexin signaling is associated with synaptic complex elimination in the hippocampus. *Journal of Neuroscience*, *25*(40), 9124-9134.
- Lowery, L. A., & Vactor, D. V. (2009). The trip of the tip: understanding the growth cone machinery. *Nature Reviews Molecular Cell Biology*, *10*(5), 332-343.
- Lu, X., Le Noble, F., Yuan, L., Jiang, Q., De Lafarge, B., Sugiyama, D., Bréant, C., Claes, F., De Smet, F., Thomas, J. L., Autiero, M., Carmeliet, P., Tessier-Lavigne, M., & Eichmann, A. (2004). The netrin receptor UNC5B mediates guidance events controlling morphogenesis of the vascular system. *Nature*, *432*(7014), 179-186.
- Luck, R., Urban, S., Karakatsani, A., Harde, E., Sambandan, S., Nicholson, L., Haverkamp, S., Mann, R., Martin-Villalba, A., Schuman, E. M., Acker-Palmer, A., & Ruiz de Almodóvar, C. (2019). VEGF/VEGFR2 signaling regulates hippocampal axon branching during development. *eLife*, *8*, e49818.
- Luo, L., & O'Leary, D. D. (2005). Axon retraction and degeneration in development and disease. *Annu. Rev. Neurosci.*, *28*, 127-156.
- Mac Gabhann, F., & Popel, A. S. (2008). Systems biology of vascular endothelial growth factors. *Microcirculation*, *15*(8), 715-738.
- Mackenzie, F., & Ruhrberg, C. (2012). Diverse roles for VEGF-A in the nervous system. *Development*, *139*(8), 1371-1380.
- Maes, C., Stockmans, I., Moermans, K., Van Looveren, R., Smets, N., Carmeliet, P., Bouillon, R., & Carmeliet, G. (2004). Soluble VEGF isoforms are essential for establishing epiphyseal vascularization and regulating chondrocyte development and survival. *113*(2), 188-199.
- Majewska, A. K., Newton, J. R., & Sur, M. (2006). Remodeling of Synaptic Structure in Sensory Cortical Areas *In Vivo*. *The Journal of Neuroscience*, *26*(11), 3021-3029.
- Malenka, R. C. (1994). Synaptic plasticity in the hippocampus: LTP and LTD. *Cell*, *78*(4), 535-538.
- Malinow, R. (2003). AMPA receptor trafficking and long-term potentiation. *Philos Trans R Soc Lond B Biol Sci*, *358*(1432), 707-714.
- Mancuso, M. R., Kuhnert, F., & Kuo, C. J. (2008). Developmental angiogenesis of the central nervous system. *Lymphat Res Biol*, *6*(3-4), 173-180.
- Marti, H. J., Bernaudin, M., Bellail, A., Schoch, H., Euler, M., Petit, E., & Risau, W. (2000). Hypoxia-induced vascular endothelial growth factor expression precedes neovascularization after cerebral ischemia. *Am J Pathol*, *156*(3), 965-976.

- Martin, L., Bouvet, P., Chounlamountri, N., Watrin, C., Besançon, R., Pinatel, D., Meyronet, D., Honnorat, J., Buisson, A., Salin, P.-A., & Meissirel, C. (2021). VEGF counteracts amyloid- β -induced synaptic dysfunction. *Cell Reports*, *35*(6), 109121.
- Matsuno, H., Takei, M., Hayashi, H., Nakajima, K., Ishisaki, A., & Kozawa, O. (2004). Simvastatin enhances the regeneration of endothelial cells via VEGF secretion in injured arteries. *J Cardiovasc Pharmacol*, *43*(3), 333-340.
- Mauceri, D., Freitag, H. E., Oliveira, A. M., Bengtson, C. P., & Bading, H. (2011). Nuclear calcium-VEGFD signaling controls maintenance of dendrite arborization necessary for memory formation. *Neuron*, *71*(1), 117-130.
- McCaslin, A. F., Chen, B. R., Radosevich, A. J., Cauli, B., & Hillman, E. M. (2011). In vivo 3D morphology of astrocyte-vasculature interactions in the somatosensory cortex: implications for neurovascular coupling. *J Cereb Blood Flow Metab*, *31*(3), 795-806.
- Meissirel, C., de Almodovar, C. R., Knevels, E., Coulon, C., Chounlamountri, N., Segura, I., de Rossi, P., Vinckier, S., Anthonis, K., Deleglise, B., de Mol, M., Ali, C., Dassonville, K., Loyens, E., Honnorat, J., Michotte, Y., Rogemond, V., Smolders, I., Voets, T., . . . Carmeliet, P. (2011). VEGF modulates NMDA receptors activity in cerebellar granule cells through Src-family kinases before synapse formation. *Proceedings of the National Academy of Sciences of the United States of America*, *108*(33), 13782-13787.
- Meissirel, C., Ruiz de Almodovar, C., Knevels, E., Coulon, C., Chounlamountri, N., Segura, I., de Rossi, P., Vinckier, S., Anthonis, K., Deleglise, B., de Mol, M., Ali, C., Dassonville, K., Loyens, E., Honnorat, J., Michotte, Y., Rogemond, V., Smolders, I., Voets, T., . . . Carmeliet, P. (2011). VEGF modulates NMDA receptors activity in cerebellar granule cells through Src-family kinases before synapse formation. *Proc Natl Acad Sci U S A*, *108*(33), 13782-13787.
- Mel, B. W. (1993). Synaptic integration in an excitable dendritic tree. *J Neurophysiol*, *70*(3), 1086-1101.
- Mignone, J. L., Kukekov, V., Chiang, A.-S., Steindler, D., & Enikolopov, G. (2004). Neural stem and progenitor cells in nestin-GFP transgenic mice. *Journal of Comparative Neurology*, *469*(3), 311-324.
- Millauer, B., Wizigmann-Voos, S., Schnürch, H., Martinez, R., Møller, N. P., Risau, W., & Ullrich, A. (1993). High affinity VEGF binding and developmental expression suggest Flk-1 as a major regulator of vasculogenesis and angiogenesis. *Cell*, *72*(6), 835-846.
- Mody, M., Cao, Y., Cui, Z., Tay, K. Y., Shyong, A., Shimizu, E., Pham, K., Schultz, P., Welsh, D., & Tsien, J. Z. (2001). Genome-wide gene expression profiles of the developing mouse hippocampus. *Proc Natl Acad Sci U S A*, *98*(15), 8862-8867.

- Molofsky, A. V., & Deneen, B. (2015). Astrocyte development: A Guide for the Perplexed. *Glia*, *63*(8), 1320-1329.
- Mühlner, U., Möhle-Steinlein, U., Wizigmann-Voos, S., Christofori, G., Risau, W., & Wagner, E. F. (1999). Formation of transformed endothelial cells in the absence of VEGFR-2/Flk-1 by Polyoma middle T oncogene. *Oncogene*, *18*(29), 4200-4210.
- Murai, K. K., & Pasquale, E. B. (2011). Eph Receptors and ephrins in Neuron-Astrocyte Communication at Synapses. *Glia*, *59*(11), 1567-1578.
- Nagata, T., Nagano, I., Shiote, M., Narai, H., Murakami, T., Hayashi, T., Shoji, M., & Abe, K. (2007). Elevation of MCP-1 and MCP-1/VEGF ratio in cerebrospinal fluid of amyotrophic lateral sclerosis patients. *Neurological research*, *29*(8), 772-776.
- Nakayama, M., Nakayama, A., van Lessen, M., Yamamoto, H., Hoffmann, S., Drexler, H. C., Itoh, N., Hirose, T., Breier, G., Vestweber, D., Cooper, J. A., Ohno, S., Kaibuchi, K., & Adams, R. H. (2013). Spatial regulation of VEGF receptor endocytosis in angiogenesis. *Nat Cell Biol*, *15*(3), 249-260.
- Nation, D. A., Sweeney, M. D., Montagne, A., Sagare, A. P., D'Orazio, L. M., Pachicano, M., Sepeshband, F., Nelson, A. R., Buennagel, D. P., Harrington, M. G., Benzinger, T. L. S., Fagan, A. M., Ringman, J. M., Schneider, L. S., Morris, J. C., Chui, H. C., Law, M., Toga, A. W., & Zlokovic, B. V. (2019). Blood-brain barrier breakdown is an early biomarker of human cognitive dysfunction. *Nature Medicine*, *25*(2), 270-276.
- Nelson, A. R., Sweeney, M. D., Sagare, A. P., & Zlokovic, B. V. (2016). Neurovascular dysfunction and neurodegeneration in dementia and Alzheimer's disease. *Biochim Biophys Acta*, *1862*(5), 887-900.
- Ng, Y. S., Rohan, R., Sunday, M. E., Demello, D. E., & D'Amore, P. A. (2001). Differential expression of VEGF isoforms in mouse during development and in the adult. *Developmental Dynamics*, *220*(2), 112-121.
- Nowacka, M. M., & Obuchowicz, E. (2012). Vascular endothelial growth factor (VEGF) and its role in the central nervous system: a new element in the neurotrophic hypothesis of antidepressant drug action. *Neuropeptides*, *46*(1), 1-10.
- O'Brien, R. J., Xu, D., Petralia, R. S., Steward, O., Huganir, R. L., & Worley, P. (1999). Synaptic Clustering of AMPA Receptors by the Extracellular Immediate-Early Gene Product Narp. *Neuron*, *23*(2), 309-323.
- Ogunshola, O. O., Antic, A., Donoghue, M. J., Fan, S. Y., Kim, H., Stewart, W. B., Madri, J. A., & Ment, L. R. (2002). Paracrine and autocrine functions of neuronal vascular endothelial growth factor (VEGF) in the central nervous system. *J Biol Chem*, *277*(13), 11410-11415.

- Ogunshola, O. O., Stewart, W. B., Mihalcik, V., Solli, T., Madri, J. A., & Ment, L. R. (2000). Neuronal VEGF expression correlates with angiogenesis in postnatal developing rat brain. *Brain Res Dev Brain Res*, *119*(1), 139-153.
- Ohlin, K. E., Francardo, V., Lindgren, H. S., Sullivan, S. E., O'Sullivan, S. S., Luksik, A. S., Vassoler, F. M., Lees, A. J., Konradi, C., & Cenci, M. A. (2011). Vascular endothelial growth factor is upregulated by L-dopa in the parkinsonian brain: implications for the development of dyskinesia. *Brain*, *134*(Pt 8), 2339-2357.
- Okabe, K., Fukada, H., Tai-Nagara, I., Ando, T., Honda, T., Nakajima, K., Takeda, N., Fong, G. H., Ema, M., & Kubota, Y. (2020). Neuron-derived VEGF contributes to cortical and hippocampal development independently of VEGFR1/2-mediated neurotrophism. *Dev Biol*, *459*(2), 65-71.
- Okabe, K., Kobayashi, S., Yamada, T., Kurihara, T., Tai-Nagara, I., Miyamoto, T., Mukoyama, Y. S., Sato, T. N., Suda, T., Ema, M., & Kubota, Y. (2014). Neurons Limit Angiogenesis by Titrating VEGF in Retina. *Cell*, *159*(3), 584-596.
- Okamoto, K. I., Nagai, T., Miyawaki, A., & Hayashi, Y. (2004). Rapid and persistent modulation of actin dynamics regulates postsynaptic reorganization underlying bidirectional plasticity. *Nature Neuroscience*, *7*(10), 1104-1112.
- Olsson, A.-K., Dimberg, A., Kreuger, J., & Claesson-Welsh, L. (2006). VEGF receptor signalling ? in control of vascular function. *Nature Reviews Molecular Cell Biology*, *7*(5), 359-371.
- Olsson, A. K., Dimberg, A., Kreuger, J., & Claesson-Welsh, L. (2006). VEGF receptor signalling - in control of vascular function. *Nature Reviews Molecular Cell Biology*, *7*(5), 359-371.
- Oosthuysen, B., Moons, L., Storkebaum, E., Beck, H., Nuyens, D., Brusselmans, K., Dorpe, J. V., Hellings, P., Gorselink, M., & Heymans, S. (2001). Deletion of the hypoxia-response element in the vascular endothelial growth factor promoter causes motor neuron degeneration. *Nature genetics*, *28*(2), 131-138.
- Palmer, A., Zimmer, M., Erdmann, K. S., Eulenburg, V., Porthin, A., Heumann, R., Deutsch, U., & Klein, R. (2002). ephrinB phosphorylation and reverse signaling: regulation by Src kinases and PTP-BL phosphatase. *Molecular Cell*, *9*(4), 725-737.
- Paredes, I., Himmels, P., & de Almodovar, C. R. (2018). Neurovascular Communication during CNS Development. *Developmental Cell*, *45*(1), 10-32.
- Paridaen, J. T., & Huttner, W. B. (2014). Neurogenesis during development of the vertebrate central nervous system. *EMBO reports*, *15*(4), 351-364.
- Parker, K. K., Brock, A. L., Brangwynne, C., Mannix, R. J., Wang, N., Ostuni, E., Geisse, N. A., Adams, J. C., Whitesides, G. M., & Ingber, D. E. (2002). Directional control of

- lamellipodia extension by constraining cell shape and orienting cell tractional forces. *The FASEB Journal*, 16(10), 1195-1204.
- Peach, C., Mignone, V., Arruda, M., Alcobia, D., Hill, S., Kilpatrick, L., & Woolard, J. (2018). Molecular Pharmacology of VEGF-A Isoforms: Binding and Signalling at VEGFR2. *International Journal of Molecular Sciences*, 19(4), 1264.
- Peters, A., & Kaiserman-Abramof, I. R. (1970). The small pyramidal neuron of the rat cerebral cortex. The perikaryon, dendrites and spines. *The American journal of anatomy*, 127 4, 321-355.
- Petersen, J. D., Kaech, S., & Banker, G. (2014). Selective Microtubule-Based Transport of Dendritic Membrane Proteins Arises in Concert with Axon Specification. *The Journal of Neuroscience*, 34(12), 4135-4147.
- Petersen, P. H., Zou, K., Hwang, J. K., Jan, Y. N., & Zhong, W. (2002). Progenitor cell maintenance requires numb and numbl like during mouse neurogenesis. *Nature*, 419(6910), 929-934.
- Pitulescu, M. E., & Adams, R. H. (2010). Eph/ephrin molecules--a hub for signaling and endocytosis. *Genes Dev*, 24(22), 2480-2492.
- Pitulescu, M. E., Schmidt, I., Benedito, R., & Adams, R. H. (2010). Inducible gene targeting in the neonatal vasculature and analysis of retinal angiogenesis in mice. *Nat Protoc*, 5(9), 1518-1534.
- Quaegebeur, A., Lange, C., & Carmeliet, P. (2011). The neurovascular link in health and disease: molecular mechanisms and therapeutic implications. *Neuron*, 71(3), 406-424.
- Rajasekharan, S., & Kennedy, T. E. (2009). The netrin protein family. *Genome Biol*, 10(9), 239.
- Rama, N., Dubrac, A., Mathivet, T., RA, N. C., Genet, G., Cristofaro, B., Pibouin-Fragner, L., Ma, L., Eichmann, A., & Chédotal, A. (2015). Slit2 signaling through Robo1 and Robo2 is required for retinal neovascularization. *Nat Med*, 21(5), 483-491.
- Ramakrishnan, S., Anand, V., & Roy, S. (2014). Vascular Endothelial Growth Factor Signaling in Hypoxia and Inflammation. *Journal of Neuroimmune Pharmacology*, 9(2), 142-160.
- Raz, L., Knoefel, J., & Bhaskar, K. (2016). The neuropathology and cerebrovascular mechanisms of dementia. *J Cereb Blood Flow Metab*, 36(1), 172-186.
- Regan, M. R., Huang, Y. H., Kim, Y. S., Dykes-Hoberg, M. I., Jin, L., Watkins, A. M., Bergles, D. E., & Rothstein, J. D. (2007). Variations in Promoter Activity Reveal a

- Differential Expression and Physiology of Glutamate Transporters by Glia in the Developing and Mature CNS. *The Journal of Neuroscience*, 27(25), 6607-6619.
- Risau, W., & Wolburg, H. (1990). Development of the blood-brain barrier. *Trends in Neurosciences*, 13(5), 174-178.
- Robberecht, W., & Philips, T. (2013). The changing scene of amyotrophic lateral sclerosis. *Nat Rev Neurosci*, 14(4), 248-264.
- Rosenstein, J. M., Mani, N., Khaibullina, A., & Krum, J. M. (2003). Neurotrophic effects of vascular endothelial growth factor on organotypic cortical explants and primary cortical neurons. *J Neurosci*, 23(35), 11036-11044.
- Ruhrberg, C., Gerhardt, H., Golding, M., Watson, R., Ioannidou, S., Fujisawa, H., Betsholtz, C., & Shima, D. T. (2002). Spatially restricted patterning cues provided by heparin-binding VEGF-A control blood vessel branching morphogenesis. *Genes & Development*, 16(20), 2684-2698.
- Ruiz de Almodovar, C., Coulon, C., Salin, P. A., Knevels, E., Chounlamountri, N., Poesen, K., Hermans, K., Lambrechts, D., Van Geyte, K., Dhondt, J., Dresselaers, T., Renaud, J., Aragones, J., Zacchigna, S., Geudens, I., Gall, D., Stroobants, S., Mutin, M., Dassonville, K., . . . Meissirel, C. (2010). Matrix-Binding Vascular Endothelial Growth Factor (VEGF) Isoforms Guide Granule Cell Migration in the Cerebellum via VEGF Receptor Flk1. *Journal of Neuroscience*, 30(45), 15052-15066.
- Ruiz de Almodovar, C., Fabre, P. J., Knevels, E., Coulon, C., Segura, I., Haddick, P. C. G., Aerts, L., Delattin, N., Strasser, G., Oh, W. J., Lange, C., Vinckier, S., Haigh, J., Fouquet, C., Gu, C., Alitalo, K., Castellani, V., Tessier-Lavigne, M., Chedotal, A., . . . Carmeliet, P. (2011). VEGF Mediates Commissural Axon Chemoattraction through Its Receptor Flk1. *Neuron*, 70(5), 966-978.
- Ruiz de Almodovar, C., Lambrechts, D., Mazzone, M., & Carmeliet, P. (2009). Role and therapeutic potential of VEGF in the nervous system. *Physiol Rev*, 89(2), 607-648.
- Sakurai, Y., Ohgimoto, K., Kataoka, Y., Yoshida, N., & Shibuya, M. (2005). Essential role of Flk-1 (VEGF receptor 2) tyrosine residue 1173 in vasculogenesis in mice. *Proceedings of the National Academy of Sciences*, 102(4), 1076-1081.
- Salvucci, O., & Tosato, G. (2012). Essential roles of EphB receptors and ephrinB ligands in endothelial cell function and angiogenesis. *Adv Cancer Res*, 114, 21-57.
- Sarabipour, S., Kinghorn, K., Quigley, K. M., Kovacs-Kasa, A., Annex, B. H., Bautch, V. L., & Gabhann, F. M. (2023). Trafficking dynamics of VEGFR1, VEGFR2, and NRP1 in human endothelial cells. *bioRxiv*, 2022.2009.2030.510412.
- Sathasivam, S. (2008). VEGF and ALS. *Neuroscience Research*, 62(2), 71-77.

- Sawamiphak, S., Seidel, S., Essmann, C. L., Wilkinson, G. A., Pitulescu, M. E., Acker, T., & Acker-Palmer, A. (2010). ephrin-B2 regulates VEGFR2 function in developmental and tumour angiogenesis. *Nature*, *465*(7297), 487-491.
- Schwarz, Q., Gu, C., Fujisawa, H., Sabelko, K., Gertsenstein, M., Nagy, A., Taniguchi, M., Kolodkin, A. L., Ginty, D. D., Shima, D. T., & Ruhrberg, C. (2004). Vascular endothelial growth factor controls neuronal migration and cooperates with Sema3A to pattern distinct compartments of the facial nerve. *Genes & Development*, *18*(22), 2822-2834.
- Scott, A., Powner, M. B., Gandhi, P., Clarkin, C., Gutmann, D. H., Johnson, R. S., Ferrara, N., & Fruttiger, M. (2010). Astrocyte-derived vascular endothelial growth factor stabilizes vessels in the developing retinal vasculature. *PLoS One*, *5*(7), e11863.
- Segura, I., De Smet, F., Hohensinner, P. J., Almodovar, C. R. d., & Carmeliet, P. (2009). The neurovascular link in health and disease: an update. *Trends in Molecular Medicine*, *15*(10), 439-451.
- Segura, I., Essmann, C. L., Weinges, S., & Acker-Palmer, A. (2007). Grb4 and GIT1 transduce ephrinB reverse signals modulating spine morphogenesis and synapse formation. *Nature Neuroscience*, *10*(3), 301-310.
- Sennino, B., Kuhnert, F., Tabruyn, S. P., Mancuso, M. R., Hu-Lowe, D. D., Kuo, C. J., & McDonald, D. M. (2009). Cellular source and amount of vascular endothelial growth factor and platelet-derived growth factor in tumors determine response to angiogenesis inhibitors. *Cancer Res*, *69*(10), 4527-4536.
- Shibata, T., Yamada, K., Watanabe, M., Ikenaka, K., Wada, K., Tanaka, K., & Inoue, Y. (1997). Glutamate transporter GLAST is expressed in the radial glia-astrocyte lineage of developing mouse spinal cord. *J Neurosci*, *17*(23), 9212-9219.
- Shim, J. W., & Madsen, J. R. (2018). VEGF Signaling in Neurological Disorders. *Int J Mol Sci*, *19*(1).
- Simmons, A. B., Bretz, C. A., Wang, H., Kunz, E., Hajj, K., Kennedy, C., Yang, Z., Suwanmanee, T., Kafri, T., & Hartnett, M. E. (2018). Gene therapy knockdown of VEGFR2 in retinal endothelial cells to treat retinopathy. *Angiogenesis*, *21*(4), 751-764.
- Simons, M. (2012). An Inside View: VEGF Receptor Trafficking and Signaling. *Physiology*, *27*(4), 213-222.
- Simons, M., Gordon, E., & Claesson-Welsh, L. (2016). Mechanisms and regulation of endothelial VEGF receptor signalling. *Nature Reviews Molecular Cell Biology*, *17*(10), 611-625.

- Singh, N., Tiem, M., Watkins, R., Cho, Y. K., Wang, Y., Olsen, T., Uehara, H., Mamalis, C., Luo, L., Oakey, Z., & Ambati, B. K. (2013). Soluble vascular endothelial growth factor receptor 3 is essential for corneal alymphaticity. *Blood*, *121*(20), 4242-4249.
- Sivaraman Siveen, K., Prabhu, K., Krishnankutty, R., Kuttikrishnan, S., Tsakou, M., Q Alali, F., Dermime, S., M Mohammad, R., & Uddin, S. (2017). Vascular endothelial growth factor (VEGF) signaling in tumour vascularization: potential and challenges. *Current vascular pharmacology*, *15*(4), 339-351.
- Smith, G. A., Fearnley, G. W., Tomlinson, D. C., Harrison, M. A., & Ponnambalam, S. (2015). The cellular response to vascular endothelial growth factors requires co-ordinated signal transduction, trafficking and proteolysis. *Bioscience Reports*, *35*.
- Sondell, M., Sundler, F., & Kanje, M. (2000). Vascular endothelial growth factor is a neurotrophic factor which stimulates axonal outgrowth through the flk-1 receptor. *European Journal of Neuroscience*, *12*(12), 4243-4254.
- Song, A. H., Wang, D., Chen, G., Li, Y., Luo, J., Duan, S., & Poo, M. M. (2009). A selective filter for cytoplasmic transport at the axon initial segment. *Cell*, *136*(6), 1148-1160.
- Sorensen, I., Adams, R. H., & Gossler, A. (2009). DLL1-mediated Notch activation regulates endothelial identity in mouse fetal arteries. *Blood*, *113*(22), 5680-5688.
- Sorra, K. E., & Harris, K. M. (2000). Overview on the structure, composition, function, development, and plasticity of hippocampal dendritic spines. *Hippocampus*, *10*(5), 501-511.
- Spurrier, J., Nicholson, L., Fang, X. T., Stoner, A. J., Toyonaga, T., Holden, D., Siegert, T. R., Laird, W., Allnutt, M. A., Chiasseu, M., Brody, A. H., Takahashi, H., Nies, S. H., Pérez-Cañamás, A., Sadasivam, P., Lee, S., Li, S., Zhang, L., Huang, Y. H., . . . Strittmatter, S. M. (2022). Reversal of synapse loss in Alzheimer mouse models by targeting mGluR5 to prevent synaptic tagging by C1Q. *Science Translational Medicine*, *14*(647), eabi8593.
- Srinivas, S., Watanabe, T., Lin, C.-S., William, C. M., Tanabe, Y., Jessell, T. M., & Costantini, F. (2001). Cre reporter strains produced by targeted insertion of EYFP and ECFP into the ROSA26 locus. *BMC Developmental Biology*, *1*(1), 4.
- Stackhouse, T. L., & Mishra, A. (2021). Neurovascular Coupling in Development and Disease: Focus on Astrocytes [Review]. *Frontiers in Cell and Developmental Biology*, *9*.
- Stenman, J. M., Rajagopal, J., Carroll, T. J., Ishibashi, M., McMahon, J., & McMahon, A. P. (2008). Canonical Wnt signaling regulates organ-specific assembly and differentiation of CNS vasculature. *Science*, *322*(5905), 1247-1250.

- Stone, J., Itin, A., Alon, T., Pe'er, J., Gnessin, H., Chan-Ling, T., & Keshet, E. (1995). Development of retinal vasculature is mediated by hypoxia-induced vascular endothelial growth factor (VEGF) expression by neuroglia. *J Neurosci*, *15*(7 Pt 1), 4738-4747.
- Stoner, A., Fu, L., Nicholson, L., Zheng, C., Toyonaga, T., Spurrier, J., Laird, W., Cai, Z., & Strittmatter, S. M. (2023). Neuronal Transcriptome Disruption, Tau Accumulation and Synapse Loss in Alzheimer's Knock-in Mice Require Cellular Prion Protein. *bioRxiv*, 2023.2002.2015.528700.
- Stuttfield, E., & Ballmer-Hofer, K. (2009). Structure and function of VEGF receptors. *IUBMB Life*, *61*(9), 915-922.
- Su, Z., Xu, P., & Ni, F. (2004). Single phosphorylation of Tyr304 in the cytoplasmic tail of ephrin B2 confers high-affinity and bifunctional binding to both the SH2 domain of Grb4 and the PDZ domain of the PDZ-RGS3 protein. *Eur J Biochem*, *271*(9), 1725-1736.
- Supèr, H., Martínez, A., R'ó, J. A. D., & Soriano, E. (1998). Involvement of Distinct Pioneer Neurons in the Formation of Layer-Specific Connections in the Hippocampus. *The Journal of Neuroscience*, *18*(12), 4616-4626.
- Sweeney, M. D., Ayyadurai, S., & Zlokovic, B. V. (2016). Pericytes of the neurovascular unit: key functions and signaling pathways. *Nature Neuroscience*, *19*(6), 771-783.
- Sweeney, M. D., Sagare, A. P., & Zlokovic, B. V. (2018). Blood–brain barrier breakdown in Alzheimer disease and other neurodegenerative disorders. *Nature Reviews Neurology*, *14*(3), 133-150.
- Swinnen, N., Smolders, S., Avila, A., Notelaers, K., Paesen, R., Ameloot, M., Brône, B., Legendre, P., & Rigo, J. M. (2013). Complex invasion pattern of the cerebral cortex by microglial cells during development of the mouse embryo. *Glia*, *61*(2), 150-163.
- Szebenyi, G., Callaway, J. L., Dent, E. W., & Kalil, K. (1998). Interstitial branches develop from active regions of the axon demarcated by the primary growth cone during pausing behaviors. *J Neurosci*, *18*(19), 7930-7940.
- Szirmai, I., Buzsáki, G., & Kamondi, A. (2012). 120 years of hippocampal Schaffer collaterals. *Hippocampus*, *22*(7), 1508-1516.
- Tahir, S. A., Park, S., & Thompson, T. C. (2009). Caveolin-1 regulates VEGF-stimulated angiogenic activities in prostate cancer and endothelial cells. *Cancer Biol Ther*, *8*(23), 2286-2296.
- Takahashi, H., & Shibuya, M. (2005). The vascular endothelial growth factor (VEGF)/VEGF receptor system and its role under physiological and pathological conditions. *Clin Sci (Lond)*, *109*(3), 227-241.

- Takahashi, T., Svoboda, K., & Malinow, R. (2003). Experience strengthening transmission by driving AMPA receptors into synapses. *Science*, *299*(5612), 1585-1588.
- Takahashi, T., Ueno, H., & Shibuya, M. (1999). VEGF activates protein kinase C-dependent, but Ras-independent Raf-MEK-MAP kinase pathway for DNA synthesis in primary endothelial cells. *Oncogene*, *18*(13), 2221-2230.
- Takeuchi, S., Katoh, H., & Negishi, M. (2015). Eph/ephrin reverse signalling induces axonal retraction through RhoA/ROCK pathway. *J Biochem*, *158*(3), 245-252.
- Tam, S. J., & Watts, R. J. (2010). Connecting Vascular and Nervous System Development: Angiogenesis and the Blood-Brain Barrier. *Annual Review of Neuroscience*, *Vol 33*, *33*, 379-408.
- Tammela, T., Zarkada, G., Wallgard, E., Murtomäki, A., Suchting, S., Wirzenius, M., Waltari, M., Hellström, M., Schomber, T., Peltonen, R., Freitas, C., Duarte, A., Isoniemi, H., Laakkonen, P., Christofori, G., Ylä-Herttuala, S., Shibuya, M., Pytowski, B., Eichmann, A., . . . Alitalo, K. (2008). Blocking VEGFR-3 suppresses angiogenic sprouting and vascular network formation. *Nature*, *454*(7204), 656-660.
- Tata, M., & Ruhrberg, C. (2018). Cross-talk between blood vessels and neural progenitors in the developing brain. *Neuronal Signaling*, *2*(1).
- Tata, M., Wall, I., Joyce, A., Vieira, J. M., Kessar, N., & Ruhrberg, C. (2016). Regulation of embryonic neurogenesis by germinal zone vasculature. *Proceedings of the National Academy of Sciences of the United States of America*, *113*(47), 13414-13419.
- Teran, M., & Nugent, M. A. (2015). Synergistic Binding of Vascular Endothelial Growth Factor-A and Its Receptors to Heparin Selectively Modulates Complex Affinity. *J Biol Chem*, *290*(26), 16451-16462.
- Thion, M. S., & Garel, S. (2017). On place and time: microglia in embryonic and perinatal brain development. *Current Opinion in Neurobiology*, *47*, 121-130.
- Thompson, Carol L., Ng, L., Menon, V., Martinez, S., Lee, C.-K., Glattfelder, K., Sunkin, Susan M., Henry, A., Lau, C., Dang, C., Garcia-Lopez, R., Martinez-Ferre, A., Pombero, A., Rubenstein, John L. R., Wakeman, Wayne B., Hohmann, J., Dee, N., Sodt, Andrew J., Young, R., . . . Jones, Allan R. (2014). A High-Resolution Spatiotemporal Atlas of Gene Expression of the Developing Mouse Brain. *Neuron*, *83*(2), 309-323.
- Tillo, M., Erskine, L., Cariboni, A., Fantin, A., Joyce, A., Denti, L., & Ruhrberg, C. (2015). VEGF189 binds NRP1 and is sufficient for VEGF/NRP1-dependent neuronal patterning in the developing brain. *Development*, *142*(2), 314-319.

- Tillo, M., Ruhrberg, C., & Mackenzie, F. (2012). Emerging roles for semaphorins and VEGFs in synaptogenesis and synaptic plasticity. *Cell Adh Migr*, 6(6), 541-546.
- Tønnesen, J., Katona, G., Rózsa, B., & Nägerl, U. V. (2014). Spine neck plasticity regulates compartmentalization of synapses. *Nature Neuroscience*, 17(5), 678-685.
- Tronche, F., Kellendonk, C., Kretz, O., Gass, P., Anlag, K., Orban, P. C., Bock, R., Klein, R., & Schutz, G. (1999). Disruption of the glucocorticoid receptor gene in the nervous system results in reduced anxiety. *Nat Genet*, 23(1), 99-103.
- Tsai, P. S., Kaufhold, J. P., Blinder, P., Friedman, B., Drew, P. J., Karten, H. J., Lyden, P. D., & Kleinfeld, D. (2009). Correlations of neuronal and microvascular densities in murine cortex revealed by direct counting and colocalization of nuclei and vessels. *Journal of Neuroscience*, 29(46), 14553-14570.
- Tsay, D., & Yuste, R. (2004). On the electrical function of dendritic spines. *Trends Neurosci*, 27(2), 77-83.
- Turrigiano, G. G. (2017). The dialectic of Hebb and homeostasis. *Philos Trans R Soc Lond B Biol Sci*, 372(1715).
- Turrigiano, G. G., Leslie, K. R., Desai, N. S., Rutherford, L. C., & Nelson, S. B. (1998). Activity-dependent scaling of quantal amplitude in neocortical neurons. *Nature*, 391(6670), 892-896.
- Tzioras, M., McGeachan, R. I., Durrant, C. S., & Spires-Jones, T. L. (2023). Synaptic degeneration in Alzheimer disease. *Nature Reviews Neurology*, 19(1), 19-38.
- Vago, D. R., Wallenstein, G. V., & Morris, L. S. (2014). Hippocampus. In M. J. Aminoff & R. B. Daroff (Eds.), *Encyclopedia of the Neurological Sciences (Second Edition)* (pp. 566-570). Academic Press.
- Valnegri, P., Puram, S. V., & Bonni, A. (2015). Regulation of dendrite morphogenesis by extrinsic cues. *Trends Neurosci*, 38(7), 439-447.
- Vasistha, N. A., & Khodosevich, K. (2021). The impact of (ab)normal maternal environment on cortical development. *Prog Neurobiol*, 202, 102054.
- Vetter, P., Roth, A., & Häusser, M. (2001). Propagation of action potentials in dendrites depends on dendritic morphology. *J Neurophysiol*, 85(2), 926-937.
- Vetter, P., Roth, A., & Häusser, M. (2001). Propagation of Action Potentials in Dendrites Depends on Dendritic Morphology. *Journal of Neurophysiology*, 85(2), 926-937.

- Vlachos, A., Ikenberg, B., Lenz, M., Becker, D., Reifenberg, K., Bas-Orth, C., & Deller, T. (2013). Synaptopodin regulates denervation-induced homeostatic synaptic plasticity. *Proceedings of the National Academy of Sciences*, *110*(20), 8242-8247.
- Wada, K., Arai, H., Takanashi, M., Fukae, J., Oizumi, H., Yasuda, T., Mizuno, Y., & Mochizuki, H. (2006). Expression levels of vascular endothelial growth factor and its receptors in Parkinson's disease. *Neuroreport*, *17*(7), 705-709.
- Wada, T., Haigh, J. J., Ema, M., Hitoshi, S., Chaddah, R., Rossant, J., Nagy, A., & Kooy, D. v. d. (2006). Vascular Endothelial Growth Factor Directly Inhibits Primitive Neural Stem Cell Survival But Promotes Definitive Neural Stem Cell Survival. *The Journal of Neuroscience*, *26*(25), 6803-6812.
- Walchli, T., Mateos, J. M., Weinman, O., Babic, D., Regli, L., Hoerstrup, S. P., Gerhardt, H., Schwab, M. E., & Vogel, J. (2015). Quantitative assessment of angiogenesis, perfused blood vessels and endothelial tip cells in the postnatal mouse brain. *Nat Protoc*, *10*(1), 53-74.
- Walchli, T., Wacker, A., Frei, K., Regli, L., Schwab, M. E., Hoerstrup, S. P., Gerhardt, H., & Engelhardt, B. (2015). Wiring the Vascular Network with Neural Cues: A CNS Perspective. *Neuron*, *87*(2), 271-296.
- Wang, W. Y., Dong, J. H., Liu, X., Wang, Y., Ying, G. X., Ni, Z. M., & Zhou, C. F. (2005). Vascular endothelial growth factor and its receptor Flk-1 are expressed in the hippocampus following entorhinal deafferentation. *Neuroscience*, *134*(4), 1167-1178.
- Wang, X., Bove, A. M., Simone, G., & Ma, B. (2020). Molecular Bases of VEGFR-2-Mediated Physiological Function and Pathological Role. *Front Cell Dev Biol*, *8*, 599281.
- Wang, Y., Nakayama, M., Pitulescu, M. E., Schmidt, T. S., Bochenek, M. L., Sakakibara, A., Adams, S., Davy, A., Deutsch, U., Luthi, U., Barberis, A., Benjamin, L. E., Makinen, T., Nobes, C. D., & Adams, R. H. (2010). ephrin-B2 controls VEGF-induced angiogenesis and lymphangiogenesis. *Nature*, *465*(7297), 483-486.
- Xu, J., Murphy, S. L., Kochanek, K. D., & Arias, E. (2022). *Mortality in the United States, 2021* [Report].
- Yamamoto, H., Rundqvist, H., Branco, C., & Johnson, R. S. (2016). Autocrine VEGF Isoforms Differentially Regulate Endothelial Cell Behavior [Original Research]. *Frontiers in Cell and Developmental Biology*, *4*.
- Yang, G., Pan, F., & Gan, W.-B. (2009). Stably maintained dendritic spines are associated with lifelong memories. *Nature*, *462*(7275), 920-924.

- Yang, W.-J., Hu, J., Uemura, A., Tetzlaff, F., Augustin, H. G., & Fischer, A. (2015). Semaphorin-3C signals through Neuropilin-1 and PlexinD1 receptors to inhibit pathological angiogenesis. *EMBO Molecular Medicine*, *7*(10), 1267-1284.
- Yang, Y., Zhang, Y., Cao, Z., Ji, H., Yang, X., Iwamoto, H., Wahlberg, E., Länne, T., Sun, B., & Cao, Y. (2013). Anti-VEGF- and anti-VEGF receptor-induced vascular alteration in mouse healthy tissues. *Proceedings of the National Academy of Sciences*, *110*(29), 12018-12023.
- Yasuda, M., Johnson-Venkatesh, E. M., Zhang, H., Parent, J. M., Sutton, M. A., & Umemori, H. (2011). Multiple forms of activity-dependent competition refine hippocampal circuits in vivo. *Neuron*, *70*(6), 1128-1142.
- Ye, B., Zhang, Y., Song, W., Younger, S. H., Jan, L. Y., & Jan, Y. N. (2007). Growing dendrites and axons differ in their reliance on the secretory pathway. *Cell*, *130*(4), 717-729.
- Yoshihara, Y., De Roo, M., & Muller, D. (2009). Dendritic spine formation and stabilization. *Current Opinion in Neurobiology*, *19*(2), 146-153.
- Yuste, R., & Bonhoeffer, T. (2004). Genesis of dendritic spines: insights from ultrastructural and imaging studies. *Nature Reviews Neuroscience*, *5*, 24-34.
- Zelzer, E., McLean, W., Ng, Y. S., Fukai, N., Reginato, A. M., Lovejoy, S., D'Amore, P. A., & Olsen, B. R. (2002). Skeletal defects in VEGF(120/120) mice reveal multiple roles for VEGF in skeletogenesis. *Development*, *129*(8), 1893-1904.
- Zhang, H., Vutskits, L., Pepper, M. S., & Kiss, J. Z. (2003). VEGF is a chemoattractant for FGF-2-stimulated neural progenitors. *J Cell Biol*, *163*(6), 1375-1384.
- Zhang, L., Conejo-Garcia, J. R., Yang, N., Huang, W., Mohamed-Hadley, A., Yao, W., Benencia, F., & Coukos, G. (2002). Different effects of glucose starvation on expression and stability of VEGF mRNA isoforms in murine ovarian cancer cells. *Biochem Biophys Res Commun*, *292*(4), 860-868.
- Zhang, X., & Simons, M. (2014). Receptor tyrosine kinases endocytosis in endothelium: biology and signaling. *Arterioscler Thromb Vasc Biol*, *34*(9), 1831-1837.
- Zhang, Z. G., Zhang, L., Jiang, Q., Zhang, R., Davies, K., Powers, C., Bruggen, N., & Chopp, M. (2000). VEGF enhances angiogenesis and promotes blood-brain barrier leakage in the ischemic brain. *J Clin Invest*, *106*(7), 829-838.
- Zhao, Z., Nelson, A. R., Betsholtz, C., & Zlokovic, B. V. (2015). Establishment and Dysfunction of the Blood-Brain Barrier. *Cell*, *163*(5), 1064-1078.

Zlokovic, B. V. (2008). The blood-brain barrier in health and chronic neurodegenerative disorders. *Neuron*, 57(2), 178-201.

7 Appendix

7.1 Publications

Nicholson L, Gervasi N, Falières T, Leroy A, Miremont D, Zala D, Hanus C. ***Whole-Cell Photobleaching Reveals Time-Dependent Compartmentalization of Soluble Proteins by the Axon Initial Segment***. Front Cell Neurosci. 2020 Jul 10;14:180. doi: 10.3389/fncel.2020.00180.

Harde E, Nicholson L, Furones Cuadrado B, Bissen D, Wigge S, Urban S, Segarra M, Ruiz de Almodóvar C, Acker-Palmer A. ***ephrinB2 regulates VEGFR2 during dendritogenesis and hippocampal circuitry development***. Elife. 2019 Dec 23;8:e49819. doi: 10.7554/eLife.49819.

Luck R, Urban S, Karakatsani A, Harde E, Sambandan S, Nicholson L, Haverkamp S, Mann R, Martin-Villalba A, Schuman EM, Acker-Palmer A, Ruiz de Almodóvar C. ***VEGF/VEGFR2 signaling regulates hippocampal axon branching during development***. Elife. 2019 Dec 23;8:e49818. doi: 10.7554/eLife.49818.

7.2 Acknowledgment

As an American and a first-generation college graduate, the opportunity to pursue my Ph.D. in Germany has truly been a life-changing experience. My journey began unexpectedly while working as a technician in a coastal research lab for Prof. Dr. Armin Blesch at the University of California, San Diego. It was Dr. Blesch who extended an invitation to join his new lab in Heidelberg, Germany, and two years later, he encouraged me to pursue my master's degree and Ph.D. Little did I know that my initial decision to move would lead me to spend the next ten years of my life living abroad, traveling, and ultimately pursuing my doctoral degree. It is incredible how unforeseen opportunities can shape our lives in such significant ways. For that, and the countless experiences and cherished memories that followed, I am forever grateful.

The pursuit of my Ph.D. has been a deeply personal journey, filled with both challenges and excitement. However, no one embarks on such a journey alone. Therefore, I would like to express my gratitude to the following individuals:

First and foremost, I want to thank Prof. Amparo Acker-Palmer for providing me with the opportunity to conduct my Ph.D. in her research lab. The Buchmann Institute for Molecular Life Sciences was a beautiful place to work, with its panoramic views of Frankfurt. In this environment, I worked on an exciting project that has greatly influenced my current postdoctoral research. I am also grateful for her trust, which allowed me the freedom and independence to pursue my interests both within and outside the lab. Working in such a research environment enabled me to maximize my graduate student experience while making a lasting impact on the Frankfurt neuroscience community.

I would also like to express my appreciation to my colleagues with whom I had the pleasure of working during my time in the lab. Special thanks go to our administrator, Nathalie Bataille, and lab manager, Ursula Bauer, as well as animal caretakers Denis Schmelzer and Tarek Belefkih. I am also grateful to Marta Segarra, Eva Harde, Franziska Foss, Laura Mohr, Dewi Husainie, Anna Derrico, Maria Rodriguez Aburto, Angel Cuesta, Bettina Kirchmaier, Jennifer Stefani, Beatriz Furones, Cecilia Llaó Cid, Marta Parilla Monge, Blanca Peguerra, Olga Tschesnokowa, Jasmin Hefendehl, Sylvia Pfennig, Ricarda Härtl, and Florian Cop. Working with all of you in such a fun-filled and pleasant environment made my life in Frankfurt so much more enjoyable.

Special thanks go out to my office mates, Laura Mohr and Olga Tschesnokowa, who have provided unwavering support, positivity, and friendship since the day I joined the lab. A heartfelt thank you goes to Dewi Husainie, a truly special person and friend whom I deeply admire. Her kindness and unwavering support have been invaluable throughout my journey. The friendship of these ladies made the lab feel like a second home.

I also want to express my gratitude to Anna Derrica for the unforgettable fun times we shared and our shared passion for science outreach. Your enthusiasm has been contagious and inspiring.

Angel Cuesta, you have been a ray of sunshine in the lab. I am grateful for your constant positivity and for always remembering my birthday, even to this day.

To my "lab husbands," Tark and Denis, I cannot thank you enough for the tremendous support and care gave our mice and me while working on this project.

Marta Segarra, with her ever-present smile, deserves a special mention for her help, guidance, and advice throughout my time in the lab and while writing this thesis. Your positivity has been a constant source of motivation.

I would like to extend my thanks to Prof. Dr. Erin Schuman, in whose lab I completed my master's thesis. The experience in her lab, as well as her encouragement to pursue my Ph.D. in the IMPRS for Neural Circuits program, has had a profound impact on my academic journey.

A heartfelt thank you goes to Dr. Arjan Vink, our IMPRS coordinator, for wholeheartedly supporting my work both inside and outside of the lab during my Ph.D. Your enthusiasm and guidance have been invaluable.

I want to express my gratitude to the ever-growing family members of my Mosaic Church Community, particularly Pastor Stephen and Susan Beck, for making everyone feel at home. The support and sense of belonging I have found within this community have been truly immeasurable. I also want to thank my amazing sisters in Christ, Maria Agbur and Juanita Cheek, for their kindness and generosity throughout my journey. I want to thank you even more for the joy and laughter we have shared. Your unwavering support has been both refreshing and a source of strength.

Lastly, I want to dedicate a very special thank you to my late grandmother, Velma James, and my aunt, Janice James. Their love, encouragement, and continuous support have been a guiding light throughout my life and my Ph.D. journey, particularly during my time abroad.

Finally, it is my personal belief that regardless of where we are in the world, we should strive to contribute positively to the communities in which we live. Carrying this philosophy with me throughout my time in Frankfurt, I dedicated a significant amount of time and effort to establishing various programs within the local neuroscience community. It was a massive undertaking and a very personal passion. Thus, I would like to express my heartfelt gratitude to the individuals who supported me along this journey:

Deutsche Neurowissenschaften Olympiade e.V. (DNO e.V.) is a non-profit neuroscience outreach and educational platform for high school students. Originally known as the German Brain Bee, this organization started as a single annual event in Heidelberg, Germany. Through the collective support of countless individuals, my friends and I were able to expand this initiative to four locations: Berlin, Bonn, Frankfurt, and Heidelberg. DNO e.V. is now officially recognized as the national neuroscience Olympiad for high school students in Germany, with the backing of the German Society for Neuroscience. I am grateful to the DNO-Frankfurt team, both former and current members, for their creativity and contributions to our program in Frankfurt. Many thanks to the Department of Anatomy

at Goethe University and the director, Prof. Dr. Thomas Deller, for their material support. I would also like to extend my appreciation to the MPI for Brain Research for hosting our events in Frankfurt, and to Dr. Arjan Vink for his assistance with logistics. The Hertie Foundation deserves thanks for their financial support and belief in our organization. A special mention goes to Astrid Eberhart from the International Brain Bee (IBB), with whom I had the pleasure of working while organizing the IBB 2018 event in Berlin. Most importantly, I would like to express my deepest gratitude to the team leaders and the 60+ team members of the entire DNO organization. This brief paragraph does not do justice to the extent of my gratitude. Working alongside so many individuals who were excited to share their passion for neuroscience with young people has been an incredibly rewarding experience. I am immensely thankful to witness the growth and improvement of the organization year after year.

In addition to DNO e.V., I was also involved in GRADE Brain, NeuroXP (self-founded), and Science Innovation Union (SIU). Through these organizations, I had the opportunity to establish, curate, and organize career development training programs tailored to the needs of myself and my peers within the Frankfurt neuroscience community. Many thanks to Dr. Axel Kohler and Dr. Anna Derrico for sharing my passion for creating an enriching and unique neuroscience environment outside of traditional lab spaces. Lastly, I want to express my profound appreciation to my Ph.D. supervisor, Prof. Dr. Amparo Acker-Palmer, for granting me the freedom to explore my creativity and pursue my passions in various domains, both within and beyond the lab.

Each of these individuals, and many more, have played a significant role in shaping my experience in Germany and contributing to my growth as a researcher. I am truly thankful for their support, fellowship, and friendship, as well as joining in my passion for science.

7.3 Curriculum Vitae

LaShae K. Nicholson

Date of birth | 20.04.1982
Place of birth | Alabama, USA
Nationality | American

Professional Profiles

LinkedIn | www.linkedin.com/in/LaShaeNicholson

German Ministry of Education | <https://pageflow.daad.de/one-day-in-germany#766>

Education

2013 to 2019	Doctoral Student Goethe University Frankfurt, Frankfurt, Germany Buchmann Institute for Molecular Life Sciences Dissertation: "The Functional Role of VEGF Secretion During Neuronal Development"
Received 2013	Master's Degree University of Applied Sciences, Mannheim, Germany Master's program for Biomedical Sciences and Technology Master's Thesis: "Whole-cell dynamics of protein exchange in developing neurons"
Received 2006	Bachelor's Degree University of South Alabama, Alabama (USA) Bachelor's program for Biomedical Sciences Bachelor's Thesis: Characterization of the <i>StiC</i> gene locus involvement in the starvation stress response of <i>Salmonella enterica</i> serovar Typhimurium"

Research Experience

2020 to Present	Post Graduate Researcher Yale University, Dept. of Neuroscience, New Haven, USA Supervisor: Dr. Stephen Strittmatter, New Haven, USA Transcriptional profiling of BBB cellular components in Alzheimer's Disease.
2014 to 2019	Goethe University Frankfurt, Buchmann Institute for Molecular Life Sciences Supervisor: Prof. Dr. Amparo Acker-Palmer, Frankfurt, Germany Studied the functional role of vascular endothelial growth factor (VEGF) during early postnatal neuronal development.

2013 - 2014	<p>Goethe University Frankfurt, Neuroscience Center, IMPRS for Neural Circuits Fellowship Rotation</p> <p>Supervisor: Prof. Dr. Thomas Deller and Dr. Andreas Vlachos, Frankfurt, Germany</p> <p>Trained in culturing organotypic hippocampal slice cultures, performing entorhinal cortex lesions, and whole-cell patch clamping. Cloned a cell-type specific AAV library for targeting various neuronal cell subpopulations.</p>
Mar - Sept 2013	<p>Max Planck Institute for Brain Research, Dept. of Synaptic Plasticity</p> <p>Supervisor: Prof. Dr. Erin Schuman and Dr. Cyril Hanus, Frankfurt, Germany</p> <p>Developed a computational model to quantify and correlate protein mobility with respect to neuronal cell morphology in post-microscopy time-lapse images.</p>
2010 - 2013	<p>Heidelberg Universitätsklinikum, Klinik für Paraplegiologie</p> <p>Supervisor: Dr. Armin Blesch, Heidelberg, Germany</p> <p>Worked in an interdisciplinary environment to develop translational combinatorial approaches (gene therapy, biomaterials, physiotherapy) for treating spinal cord-injured clinical patients.</p>
2006—2010	<p>UC San Diego, School of Medicine, Dept. of Neurosciences</p> <p>Supervisors: Dr. Mark Tuszynski and Dr. Armin Blesch, San Diego, California USA</p> <p>Developed viral vector systems to regulate gene expression <i>in vivo</i> to study neuronal degeneration and promote axonal regeneration in a spinal cord injury model.</p>

Training

May 2012	<p>FELSA-B, Surgical Certification Animal injection, surgery, & postoperative care</p> <p>Tierschutz Ausnamegenehmigung Regierungspräsidium Karlsruhe, Baden-Württemberg, Germany</p>
2010	<p>FELSA-B Certification Laboratory animal science & methods of animal experimentation</p> <p>Interfakultäre Biomedizinische Forschungseinrichtung (IBF) Ruprecht-Karls-Universität Heidelberg, Germany</p>

Scientific Memberships

German Neuroscience Society | Hertie Foundation Alumni Association | FENS | Minerva FemmNet | Max Planck Society | SciMento | Young Entrepreneurs in Science (Falling Walls Organization) | Science Innovation Union | Deutsche Neurowissenschaften Olympiade e.V.